Roger Skjetne

The Maneuvering Problem

PhD-thesis 2005:1

Faculty of Information Technology,
Mathematics, and Electrical Engineering
Department of Engineering Cybernetics

NTNU

Norwegian University of Science and Technology
Faculty of Information Technology, Mathematics, and Electrical Engineering
Department of Engineering Cybernetics
NO-7491 Trondheim
Norway

NTNU Philosophiae Doctor 2005:1
ITK Report 2005:1-W

ISBN 82-471-6859-6 (electronic)
ISBN 82-471-6861-8 (printed)
ISSN 1503-8181

With appreciation and gratitude to my mentors,
Thor I. Fossen and Petar V. Kokotović.

Summary

The main contributions of this thesis is based on a new control problem statement called *The Maneuvering Problem*. This involves a desired path for the output of the system to follow and a speed assignment setting the desired motion along the path. This separation of tasks implies, on the one hand, that the design of the path and the desired motion along the path can be approached individually. On the other hand, this also introduces more flexibility in the development of the control law, since the desired motion along the path can be shaped by state feedback.

The main theoretical aspects are discussed in Chapters 2, 3, and 4. *The Maneuvering Problem* statement is presented in Chapter 2. A few application examples show how their respective control objectives can be conveniently set up as maneuvering problems by constructing a parametrized path and a speed assignment along the path. The last section of this chapter shows further that the problem statement implies the existence of a forward invariant manifold of the state space, represented by a desired noncompact set, to which all solutions must converge.

Chapter 3 presents a constructive control design solving the maneuvering problem. A feedback linearizable system is, for clarity of presentation, used in this section, and most of the involved theoretical aspects concerning the control objective with design are addressed. First the static part of the control law is developed, solving essentially the geometric part of the problem. Then the loop is closed by the design of an update law that shapes the motion along the path. The last section of Chapter 3 considers further one of the proposed update laws and show that this incorporates a gradient optimization algorithm that will improve transient performance in the system.

Uncertain systems are addressed in Chapter 4, and constructive designs based on ISS backstepping, adaptive backstepping, and sliding-mode are proposed for solving the maneuvering problem. In the backstepping designs, n design steps are first performed to derive the static part of the

control law. Then the dynamic update law is constructed to bridge the path following objective with the speed assignment. In the sliding-mode design, a maneuvering control law is first designed for the nominal part of the plant, and then traditional techniques are used to deal with the uncertain part and develop the overall control law.

Chapters 5 and 6 present applications of the theory, where the former chapter considers ships and the latter considers formation control. In Chapter 5, a fully actuated ship model is used, and specific maneuvering control laws are constructed based on adaptive backstepping, sliding-mode, and nonlinear PID techniques. Experimental results, using the model ship CyberShip II, are reported for each design. Experiments of both success and failure are discussed.

Chapter 6 proposes a maneuvering setup and design for formation control of r vessels. Two formation control designs are proposed. The first develops decentralized control laws and a centralized dynamic guidance law, which includes the dynamic update law, to solve the problem. In the second design, the guidance law is further decentralized in order to reduce communication demand.

Emphasis has been put on making the thesis coherent, starting with motivation and examples in the introduction, leading to the problem statement and its implications in Chapter 2, designs and analysis in Chapters 3 and 4, and finally applications with experimental results in Chapters 5 and 6. Moreover, Appendix A provides necessary background material on control theory, with emphasis on set-stability, and Appendix B reports an extensive work on modeling, system identification, and adaptive maneuvering with experiments performed for CyberShip II.

Preface

The research presented in this thesis is the result of my doctoral studies in the period August 2000 through July 2004, primarily at the Norwegian University of Science and Technology (NTNU), under the guidance of Professor Thor I. Fossen, and partly at the University of California, Santa Barbara (UCSB), under the guidance of Professor Petar V. Kokotović. My funding was provided by the Norwegian Research Council through the Strategic University Program in Marine Cybernetics, headed by Professor Olav Egeland at the Department of Engineering Cybernetics at NTNU.

The research leading to the thesis was initiated by the original working title "Ship operations in open seas," while the idea for the maneuvering problem was first conceived at UCSB in the summer of 2001. Since then it has matured into the product presented in this thesis through several publications on maneuvering control design and analysis.

I would most of all like to thank my advisor, Professor Thor I. Fossen, for choosing me as his doctoral student. He has been continuously supporting me through his great knowledge on marine control theory, by his constant flow of ideas, by his efficiency in dealing with practical issues such as financing and bureaucracy, and not the least by being a fantastic friend.

I would like to thank my co-advisor and mentor, Professor Petar V. Kokotović (PK), for inspiring me to start on a PhD study in the first place. I did my Bachelor and Master of Science studies at UCSB prior to my doctoral studies at NTNU. As a graduate student at UCSB, PK invited me to his research laboratory, and from that day on I became, in practice, a researcher. I would like to thank PK for always listening to my ideas, for adjusting my path through his exceptional knowledge in control theory, and for all our valuable discussions on textual formulations, control theory, control history, and life in general.

The material in this thesis on gradient optimization is based on a couple of joint papers with Professor Andrew R. Teel at UCSB. He was my nonlinear control professor in my graduate studies. Later it has been a pleasure

working with him professionally through valuable discussions on nonlinear control theory, discussions from which I have gained much understanding.

The working environment in which I have performed my research has been of utmost importance. At NTNU I was part of developing a new control theory laboratory, called the Lyapunov room, in which doctoral students and their professors can properly communicate and present ideas for the well-being of the entire group. The model was taken from PK's control lab at UCSB. In these research groups, both at NTNU and at UCSB, I would like to thank the students and other researchers for providing stimulating environments with a constant flow of theoretical challenges that made every day interesting. My research has, in particular, benefited from discussions with Lars Imsland, Bjørnar Vik, and Bjørnar Bøhagen at NTNU, and Dobrivoje Popović and Dragan B. Dačić at UCSB. In addition, I experienced much joy and understanding when advising several graduate students in their projects and diploma theses, in particular, Ivar-Andre Flakstad Ihle, Morten Breivik, and Dag Abel Sveen.

The material of the thesis has matured through many hours of improving the presentation according to reviewer comments, in particular, in the Automatica publications. These anonymous reviewers therefore have my appreciation for their constructive feedback.

The last part of my thesis has been put together after I was employed in the company, Marine Cybernetics AS. I am grateful to its founders and my collegues for giving me sufficient time and space for wrapping up the research.

I thank my girlfriend, Lillian, for her love and support, and last but not least, I would like to thank my parents, Reidar Skjetne and J. Sissel Bugge Skjetne, and the rest of my family for always being supportive in my choices, especially at important cross-roads in my academic education. They have given me great freedom for choosing my own path in life, and today I would like to partly dedicate this thesis to them as a token of my respect and gratitude.

Trondheim, February 6th, 2005 Roger Skjetne

Contents

Chapter 1

Introduction

"Space the final frontier. These are the voyages of the starship Enterprise, its continuing mission to explore strange new worlds, to seek out new life and new civilization, to boldly go where no one has gone before."

Star Trek - The Next Generation,
Gene Roddenberry (1921-1991)

1.1 Motivation

In many applications it is of primary importance to steer an object (robot arm, vehicle, ship, galaxy class starship, etc.) along a desired *path*. The speed or *dynamic behavior* along the path may be of secondary interest. Control problems for such applications are usually approached as two separate tasks. The first task, denoted the *Geometric task*, is for the output y of the system (usually the position) to reach and follow a desired path y_d designed as a function of an auxiliary *path variable* θ, left as an extra degree of freedom for the second task. In the second task, θ is used to satisfy an additional dynamic specification along the path. This task is denoted the *Dynamic task* and is usually specified as an assignment for the speed.

In the common *tracking problem* the path variable θ is assigned to a specific time function $\upsilon_t(t)$ constructed so that $\tilde{y}_d(t) := y_d(\upsilon_t(t))$ is a moving point that satisfies the tracking objective and the dynamic limitations of the system. In this case the two tasks, the geometric and dynamic parts of the problem, are merged into a single task with objectives often more stringent than required in applications. An example is to automatically drive a car

along a road. This can be achieved by making the car track a point that moves along the road with a certain speed. However, by instead emphasizing that the main task is to make the car stay on and follow the road, one can let the desired speed be of secondary interest and sacrificed if necessary.

A less restrictive control objective is to solve a pure *path following* problem. In this case the output y should merely converge to and follow the desired path $y_d(\theta)$ without any specific dynamic requirements along the path. Clearly, in many cases this problem statement is too flexible. When driving the car the primary importance is to follow the road. However, it is also important to keep up the speed to arrive at the destination in reasonable time.

The idea focused on in this thesis is to bridge the gap between tracking and path following, and the control concept will be called *maneuvering.* This is motivated by Hauser and Hindman (1995) who designed a *maneuver regulation* control law from a tracking algorithm by converting a time-parametrized desired output signal into a θ-parametrized desired output path and designing an *update law* to ensure proper motion for θ.

The class of systems considered in this thesis is represented by the ordinary differential equation (ODE)

$$\dot{x} = f(x, u, t) \tag{1.1}$$

where for each $t \geq 0$ the vector $x(t) \in \mathbb{R}^n$ is the state, $u(t) \in \mathbb{R}^p$ is an input vector that can be used to actively manipulate the state, $\dot{x} := \frac{d}{dt}x(t)$ is the time derivative of the state, and $f : \mathbb{R}^n \times \mathbb{R}^p \times \mathbb{R}_{\geq 0} \to \mathbb{R}^n$ is a nonlinear vector function that can be differentiated sufficiently many times. The state vector x can contain only the original states of the plant, or it can be augmented with some additional dynamic states necessary to solve a control problem.

To this equation belongs an output map

$$y = h(x) \tag{1.2}$$

where $y(t) \in \mathbb{R}^m$ is the system output that we wish to steer along a desired path.

1.1.1 The Tracking control problem

Let $y_d(t)$ be a bounded desired output for (1.2). Roughly speaking the *Tracking Problem* is then to design a function $\alpha(x, t)$ such that setting $u = \alpha(x, t)$ in (1.1) makes $y(t)$ converge to and eventually track $y_d(t)$, that is,

$$\lim_{t \to \infty} (y(t) - y_d(t)) = 0, \tag{1.3}$$

while keeping the internal states bounded. The desired output $y_d(t)$ is constructed *a priori* as a point in $\mathbb{R}^m$ that moves as a function of time. It traces out a trajectory corresponding to the desired path we want y to follow, and its velocity is given by the time derivative $\dot{y}_d(t)$. Tracking $y_d(t)$ will therefore satisfy both path following and the dynamic specification along the path in a single task.

Note that the terminology about the *tracking problem* is inconsistent. Some authors, Hauser and Hindman (1995); Ortega, Loría, Nicklasson and Sira-Ramírez (1998); Encarnação and Pascoal (2001b), call a desired output $y_d(t)$ a *desired trajectory* and the problem becomes a *trajectory tracking problem*. Other authors view a trajectory as a geometric curve and not a moving point, Anderson and Moore (1989); Åström and Wittenmark (1990), and refer to the same problem as a *trajectory following problem*. When the objective is to force the system output $y(t)$ to track a *desired output* $y_d(t)$, the problem is in this thesis referred to as *tracking* or a *tracking problem* in accordance with Athans and Falb (1966).

Example 1.1 *Suppose we want to automatically steer the position* $p = (p_x, p_y)$ *of a vehicle along a straight-line path. Solving this as a tracking problem, we need to design a desired time-parametrized trajectory. A straight-line can be parametrized by a path variable* θ *as*

$$p_d = \begin{bmatrix} a_1\theta + b_1 \\ a_2\theta + b_2 \end{bmatrix}$$

where a_1, a_2, b_1, b_2 *are constants. Suppose further that the car should move along the path with a constant speed reference* u_{ref}*. This means that* $|\dot{p}_d| = \sqrt{a_1^2 + a_2^2}|\dot{\theta}| = |u_{ref}|$*, and integration yields*

$$\theta(t) = \theta(0) + \int_0^t \frac{u_{ref}}{\sqrt{a_1^2 + a_2^2}} d\tau = \theta(0) + \frac{u_{ref}}{\sqrt{a_1^2 + a_2^2}} t =: \upsilon_t(t).$$

Setting $\theta(0) = 0$ *gives the desired position for the car as*

$$p_d(t) = \begin{bmatrix} u_{ref}\frac{a_1}{\sqrt{a_1^2+a_2^2}}t + b_1 \\ u_{ref}\frac{a_2}{\sqrt{a_1^2+a_2^2}}t + b_2 \end{bmatrix}$$

which satisfies both the path following and speed objectives in one package.

Numerous applications using various methods for solving the tracking problem is reported in the literature. For robotic manipulators some of

these references are Paden and Panja (1988); Zhao and Chen (1993); Zhang, Dawson, de Queiroz and Dixon (1997); Loría and Nijmeijer (1998); Song, Tarn and Xi (2000), for mobile robots there are Fierro and Lewis (1995); Jiang and Nijmeijer (1999); Aguiar and Hespanha (2003); Aguiar, Cremean and Hespanha (2003), and for different marine applications there are Yoerger and Slotine (1985); Fjellstad and Fossen (1994); Godhavn, Fossen and Berge (1998); Lefeber, Pettersen and Nijmeijer (2001); Behal, Dawson, Dixon and Fang (2002); Fossen, Lindegaard and Skjetne (2002); Lefeber, Pettersen and Nijmeijer (2003); Do, Jiang, Pan and Nijmeijer (2004).

Common for all these references was the use of a desired time-parametrized trajectory, either stated as a generic time function or generated by a reference model copying the dynamics of the plant. The time evolution of this trajectory is specified a priori and is not affected by the system state in any sense. What if the true system output y is not able to track the desired output $y_d(t)$, perhaps due to inherent limitations like unstable zero dynamics, exogenous disturbances, or a malfunction of some kind? Since $y_d(t)$ knows nothing of the status of the system it will continue unaffected on its path, the tracking performance will gradually degrade, and a failure is imminent. In such hypothetical cases, path following can be safer.

1.1.2 The Path Following control problem

In path following we consider the entire path rather than a point tracing out the path. If $y_d(\theta)$ is a continuous parametrization[1], the path can be represented by the set of points

$$\mathcal{P} := \{y \in \mathbb{R}^m : \ \exists \theta \in \mathbb{R} \text{ s.t. } y = y_d(\theta)\}. \tag{1.4}$$

For each $y \in \mathbb{R}^m$, let $d(y;\mathcal{P})$ be some function that measures the distance from y to the path $\mathcal{P}$ such that $d(y;\mathcal{P}) = 0$ for $y \in \mathcal{P}$ and $d(y;\mathcal{P}) > 0$ for $y \notin \mathcal{P}$. An example is the Euclidean distance $d(y;\mathcal{P}) = \inf_{z\in\mathcal{P}} |y - z|$ where $|\cdot|$ is the Euclidean norm. The *Path Following Problem* is to design a function $\alpha(x,t)$ such that setting $u = \alpha(x,t)$ in (1.1) makes $y(t)$ converge to and follow the path with nonzero motion, that is,

$$\lim_{t\to\infty} d(y(t);\mathcal{P}) = 0 \tag{1.5}$$

while $|\dot{y}(t)| > 0$ for most $t \geq 0$.

[1] A path can be parametrized continuously, discretely, or as a mix of both (hybridly); see Section 2.1.

In vehicle applications the practice is often to manually set the forward propulsion to a desired value, and then actively use the steering capacity of the vehicle to reach and stay on the path. Different solutions to this control problem for mobile robots and marine vessels have been presented by Micaelli and Samson (1993); Sarkar, Yun and Kumar (1993); Holzhter and Schultze (1996); Encarnação, Pascoal and Arcak (2000); Skjetne and Fossen (2001); Pettersen and Lefeber (2001); Do, Jiang and Pan (2002b).

1.1.3 From Tracking and Path Following to Maneuvering

In *Maneuvering* we will separate the problem into two tasks. The first and most important task is path following. The second and less important task is to satisfy a desired dynamic behavior along the path, for instance a desired speed. In a vehicle application this means that the speed should satisfy the desired *speed assignment* when tracing the path perfectly. However, if the vehicle experiences difficulties in tracing the path, it should if possible sacrifice the speed performance to achieve more accurate path following.

We will call the two tasks the *geometric task* and the *dynamic task*. The former is to force the system output to converge to the path, and the latter is to satisfy a desired dynamic behavior along the path.

Example 1.2 *For the robotic manipulator in Figure 1.1 (this could for instance be a cutting or welding tool), the control objective is for the tip of the tool, taken as the output y, to trace a desired triangular path. The further*

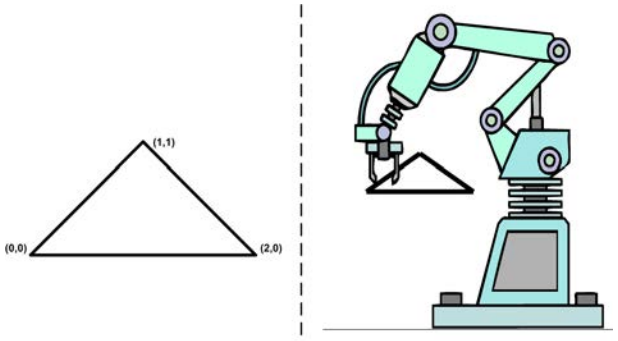

Figure 1.1: A robotic cutting tool.

requirement is to trace the path as fast as possible without exceeding a maximum speed constraint of about $m_s \approx 0.1\,\mathrm{m/s}$, and with the deviation from

the triangular path always kept less than 10^{-3} m. *This is a typical maneuvering application. The depicted triangle is the desired path in* $\mathbb{R}^2$. *Along this path a desired speed profile must be designed. This should conform to the maximum speed* m_s *along the edges, while it should slow down at the corners to avoid transients that could exceed the maximum deviation constraint.*

In its 30+ years of production, the Norwegian oil and gas industry has become a prime mover within Norwegian research by continuously setting new demands and standards to obtain cost effective, safe, and reliable operation in the North Sea. Control theory with applications have gotten strong focus in this research, leading to many new developments. The next two examples give some ideas to how maneuvering can be used to further enhance the performance of marine operations in the oil and gas industry.

Example 1.3 *In the oil industry the supply vessels are often equipped with a dynamical positioning (DP) system. This is an automatic control system*

Figure 1.2: The Oseberg South oil production platform of Norsk Hydro, and the supply vessel Far Star from Farstad Shipping. Courtesy: Norsk Hydro and Terje S. Knudsen.

that uses available measurements, like position and orientation, together with powerful thruster forces to position the vessel at a fixed point with a certain

heading (DP station-keeping) or move it slowly along a predetermined track (DP autotrack); see Strand (1999); Lindegaard (2003). DP station-keeping is a set-point regulation problem. However, suppose in the duration of a supply operation that the vessel needs to reposition itself at several different places around the platform. It would then be convenient to parametrize all those reference ponts in terms of a continuous path around the platform, as illustrated by the ellipsoid in Figure 1.2, and constraining the vessel to this path. The heading of the vessel could be taken as the direction of the tangent vector along the path, or simply as a constant heading, usually pointed against the environmental forces like waves and wind; see Fossen and Strand (2001). The desired dynamic behavior *along this path would be zero speed (fixed positioning) at the reference positions, and when moving along the path from one reference to the next the desired path speed should be commanded online by the pilot. This is a maneuvering problem.*

Example 1.4 *As the oil and gas industry moves production to greater depths, the need for more underwater autonomous control increases. One*

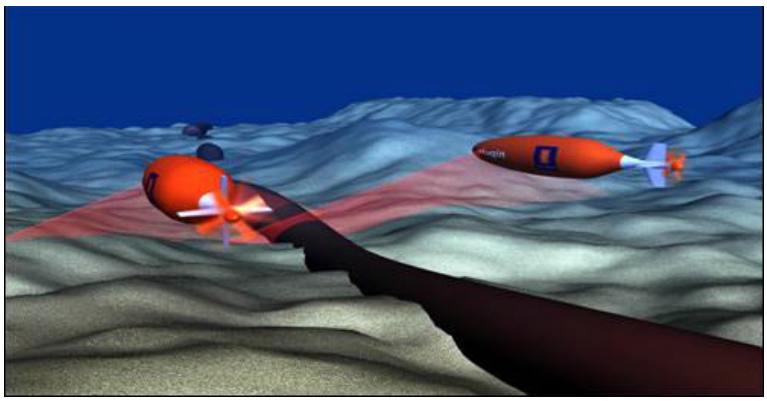

Figure 1.3: A formation of two Kongsberg Simrad Hugin AUVs scanning a pipeline for leakages or other abnormalities. Courtesy: Anders S. Wroldsen.

envisioned task is inspection of underwater pipelines. As depicted in Figure 1.3, it has been suggested to use a formation of autonomous underwater vehicles (AUVs) to perform such a task; see Chance, Kleiner and Northcutt (2000); Vestgård, Hansen, Jalving and Pedersen (2001). A formation of AUVs can be utilized to construct 3D images of the pipeline or even take time-synchronized snapshots covering a large spatial area of the seabed; see Pascoal (2003). This will increase the probability of discovering abnormal-

ities in, for instance, a pipeline. This formation control objective can also be solved as a maneuvering problem. Two parallel paths in 3D space, elevated from the seabed and offset from the pipeline, must be constructed. The speed along the paths should be a constant forward velocity. In addition an algorithm must ensure that the vehicles keep synchronized along the paths to stay in formation.

There are subtle differences in maneuvering as compared to tracking or path following. Maneuvering is by active control to achieve both convergence to the path and to satisfy the dynamic behavior along the path, approached as two separate tasks. Path following, on the other hand, is the same as solving the geometric task only (with a nonzero motion), whereas tracking is a method for strictly solving the geometric and dynamic tasks in a single task. The result is that tracking becomes a special case of maneuvering, and maneuvering becomes a special case of path following.

1.2 New developments

1.2.1 Background

Some of the results in this thesis were inspired by Hauser and Hindman (1995) who introduced a procedure to design a *maneuver regulation* controller. To determine the path variable θ, they used a numerical projection from the current state onto the path. An already available tracking controller was then converted into a maneuver regulation controller, and a quadratic Lyapunov function was employed to guarantee that the states converge to and move along the path. Their method applies to feedback linearizable systems, where the path is specified for the full state. The control structure is a mix of a continuous feedback law in conjunction with a numerical minimization algorithm. In Hindman and Hauser (1996) the auhors gave more insight into their methodology where they, among other things, showed that the desired path neither could have any sharp corners nor could it be self-intersecting for the projection algorithm to be locally well-defined. A nice extension of this procedure for nonminimum phase systems was proposed by Al-Hiddabi and McClamroch (2002). See also Gilbert and Kolmanovsky (2002) where a generalized reference governor is designed with state feedback so that constraints on state and control variables are satisfied.

Encarnação and Pascoal (2001b) proposed another extension of the maneuver regulation methodology for control of marine craft. By applying the above techniques, a maneuver regulation control law was designed for the

position kinematics. This control law was then stepped through the kinetic equations of motion using a *backstepping* design technique. Since the maneuver regulation "virtual" control law in the kinematic equation will be a function of the path variable θ, one step of backstepping will require the derivative $\dot{\theta}$ in the final control law. For systems of relative degree higher than two, this approach will require even higher order derivatives of θ. There is no mentioning from this reference how these derivatives are obtained from the projection algorithm.

Other references to what we in this thesis consider maneuvering systems are Hauser and Hindman (1997); Díaz del Río, Jiménez, Sevillano, Vicente and Civit Balcells (1999); Encarnação and Pascoal (2001c); Encarnação (2002); Do, Jiang and Pan (2002a); Fossen, Breivik and Skjetne (2003); Johansen, Skjetne and Sørensen (2003); Lapierre, Soetanto and Pascoal (2003). Most of these works solve the maneuvering problem differently than the methodology presented in this thesis. For instance, Fossen et al. (2003) uses a line-of-sight (LOS) algorithm to control the heading of an underactuated ship to ensure convergence to a straight-line path. The surge speed u of the ship is independently controlled to a desired surge speed $u_d(t)$. Together this means that both the geometric and dynamic tasks in a maneuvering problem are solved.

1.2.2 Contributions

The contributions of this thesis is focused around a problem statement we will call *The Maneuvering Problem.* The thesis includes designs for solving this objective together with analysis of the achieved performance and properties of the closed-loop systems. The results have been published in several international publications; the proper references are included in the introduction to each chapter. We summarize:

- *The Maneuvering Problem* is defined. We show that this is a convenient problem statement that can be used constructively to solve many problems of interest. In particular, choosing a suitable parametrization of the desired path and designing a dynamic assignment along the path, will show to be flexible tools for solving the problem at hand. The Maneuvering Problem implies the existence of an attractive, forward invariant manifold in the state space, to which all solutions must converge. This manifold is represented by a noncompact set for which the stability analysis of the closed-loop system is analyzed.

- Several constructive control designs are presented. These are based on

traditional nonlinear design methodologies such as *backstepping*, *feedback linearization*, and *sliding-mode control*, but extended to specifically solve the maneuvering problem. Stability of the resulting closed-loop systems are rigorously proved using tools from nonlinear set-stability theory; see Appendix A.

- The control designs are finalized by choosing an *update law* that will bridge the geometric task with the dynamic task. One such update law involves a dynamic gradient minimization algorithm that will continuously select the path variable θ that minimizes a cost function. An analysis is provided to show improved performance of the closed-loop system by using this update law, and several application scenarios are simulated and experimentally tested to illustrate these properties. Moreover, using this minimization property we define some new concepts called "*near forward invariance*" and "*near stability*" that will quantify this behavior.

- To test the maneuvering designs in a realistic environment, a model ship called CyberShip II (CS2) is used in the laboratory facility called the Marine Cybernetics Laboratory (MCLab) at the Norwegian University of Science and Technology (NTNU) in Trondheim, Norway. A nonlinear maneuvering model for a ship is derived, and system identification procedures have been performed on CS2 to obtain numerical values of the model. Several free-running experiments to automatically steer CS2 along a desired path have been performed. These are based on the different maneuvering designs presented in the thesis.

- An extension of the theory is developed for *formation control* of a group of vessels. First, a formation setup is suggested leading to the desired paths for the members of the formation. Then, designs based on the maneuvering theory are performed to solve the *formation maneuvering problem.* Different designs are presented, leading to both centralized and decentralized control structures.

1.2.3 Comparison to existing theory

In the works by Hauser and Hindman (1995); Hindman and Hauser (1996); Encarnação and Pascoal (2001b); Al-Hiddabi and McClamroch (2002) the authors always started with an already available tracking controller, and then converted this into a maneuver regulation controller. This is contrary to the designs presented here. We start with a parametrized path and a

dynamic assignment along the path, do the control designs, and ties together the geometric and dynamic objectives with the final pick of an update law. This is more flexible and has the advantage that the path variable can be a dynamic state integrated online in the controller to satisfy the dynamic assignment.

By using the gradient update law we obtain qualitatively the same performance as Hauser and Hindman using their projection algorithm. However, since the gradient minimization algorithm is dynamic, we relax the earlier restrictions imposed on the desired paths such as the "sharp corners" and "non-intersecting" conditions in Assumptions A and B in Hindman and Hauser (1996).

For a nonlinear system in *strict feedback form* (Krstić, Kanellakopoulos and Kokotović; 1995) of any relative degree, the proposed backstepping designs in this thesis will never require higher order derivatives of θ. This effectively overcomes the restriction in Encarnação and Pascoal (2001b) where a relative degree n plant will require up to the n'th derivative of θ in the control law. It should be mentioned, though, that since we design a dynamic update law for θ, higher order time derivatives may not pose a problem if accounted for properly in the design. All kinds of permutations in the design are possible based on the application at hand and the mathematical creativity of the designer.

1.2.4 Limitations

- This thesis will only deal with time-continuous plants. Clearly, the presented conceptual ideas are valid for discrete plants using parallel discrete design methods; however, such designs and analyses are not included here.

- All the presented designs assume full state measurements. This means that output feedback designs and controller/observer designs will not be considered. The reader is encouraged to confer with the extensive literature on such designs (Nijmeijer and Fossen; 1999) if a maneuvering application requires an output feedback control structure.

- All plant models considered are of known structure. The parameters of the models, however, may or may not be known.

- The applications considered in examples and experiments are all fully actuated systems. This means that all degrees-of-freedom (DOF) can be controlled simultaneously, implying that these systems are in some

sense "easy" to control. Nevertheless, we stress that this thesis will present conceptual ideas together with design tools for general classes of systems. For specific applications with specific limitations, like those that are nonholonomic or underactuated, the designs need to be modified in the same way as tracking designs are modified to fit the same applications.

1.3 Modularity in the closed-loop control system

It is convenient to systematize a closed-loop automatic control system by dividing it into subsystems or "blocks" that have specific input/output signals and inherent properties. This makes it easier to modify the overall system in case a task or objective changes, since only one or a few blocks need to be changed. For instance, if we want to change the desired trajectory in a tracking task, only the reference system needs to be adjusted, not the entire control system.

For most applications considered in this thesis, we propose to call the overall closed-loop system for an *Automatic Navigation System.* Such a system consists of the blocks called the *Plant*, the *Measurement system*, the *Control system*, and the *Guidance system*; see Figure 1.4.

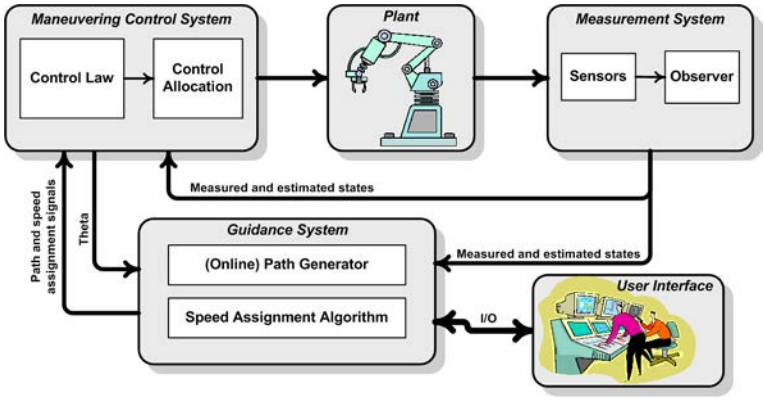

Figure 1.4: Closed-loop automatic navigation system.

This naming convention is motivated by the fact that this automatic feedback system performs *navigation* in this word's original meaning:

Navigation is "the art and science of maneuvering safely and efficiently from one point to another" (*MSN Learning and Research*; 2003). The word

navigation is derived from Latin where "navis" means boat and "agire" means to guide. It "traditionally meant the art or science of conducting ships and other watercraft from one place to another." Today we talk about navigating a car through a crowded city to get to the shopping mall, we navigate on foot through a forrest to get to our favorite fishing lake, or a space shuttle navigates from the earth to the moon. Speaking in terms of dynamical systems we propose:

We navigate the output from the initial condition to the final destination by maneuvering it safely and efficiently along a desired path with a desired dynamic behavior.

A description of the main components of an **Automatic Navigation System** follows:

- **Plant:** -the physical system under consideration, in this thesis represented by a set of differential equations describing its motion and behavior as a function of time. It is parametrized in terms of a set of *states*, usually taken as physical quantities such as position, velocity, accelerations, temperature, pressure, voltage, current, etc. In a control task, the states of the plant can be manipulated by a set of *control inputs* representing the *actuators*. These are, for instance, the propulsion and steering devices in a vehicle. To enable automatic feedback control, a subset (or function) of the states is measured by a sensory system.

- **Measurement system:** -the sensory system used to measure at least some of the physical states of the plant. It also includes filters and *observers* used to continuously estimate states that are not directly measured, but can be derived (statically or dynamically) from the measured states.

- **Guidance system:** -the planner (or supervisory decision maker) in the automatic navigation system, taking as input operator commands and, perhaps, the state of the system, and providing desired signals for the action to come. In a tracking task the guidance system is the same as a *reference system*, providing the desired trajectory with necessary derivatives to the control law. In a maneuvering task, the guidance system will provide information about the path and the desired dynamic assignment along the path.

- **Control system:** -a static or dynamic algorithm called a *control law* that continuously determines the actions of the actuators of the plant

in order for it to satisfy a certain *control objective*. Such objectives are usually stated as either set-point regulation, tracking, maneuvering, or path following. The control law will usually consist of *feedback* terms from the system states and *feedforward* terms provided by the guidance system.

Remark 1.1 *An* Automatic Navigation System*, as defined here, should not be confused with measurement systems such as an Inertial Navigation System (INS) or a Global Navigation Satellite System (GNSS) with the specific constellations GALILEO (European), GPS (American), and GLONASS (Russian). These are sensor systems aiding local or global navigation. In vehicle applications, a GNSS positioning system and an INS often constitutes the major part of the measurement system. The GNSS primary measurement is the absolute position, but it also provides translational velocity by a built-in Kalman filter, and orientation if several receivers are set up in a geometric architecture. The INS primary measurements are usually linear accelerations by built-in accelerometers and orientation angles by built-in gyrocompasses.*

1.4 Mathematical preliminaries

1.4.1 Notation

Table 1.1: Mathematical abbreviations

Symbol:	Meaning:
$\emptyset$	*empty set*
$\in$	*element of*
$\forall$	*for all*
$\exists$	*there exists*
$:=$	*defined as*
$=:$	*defines*
$\Rightarrow$	*implies*
$\Leftrightarrow$	*if and only if*
$\rightarrow$	*to* or *converge to*
$\mapsto$	*maps to*
$\nearrow$	*converge to from below*
$\searrow$	*converge to from above*

Table 1.2: Other abbreviations

Symbol:	Meaning:
US	*Uniformly Stable*
UGS	*Uniformly Globally Stable*
UGAS	*Uniformly Globally Asymptotically Stable*
UGES	*Uniformly Globally Exponentially Stable*
LAS	*Locally Asymptotically Stable*
LES	*Locally Exponentially Stable*
UA	*Uniformly Attractive*
UGA	*Uniformly Globally Attractive*
a.e.	*almost everywhere*
a.a.	*almost all*
s.t.	*such that*
w.r.t.	*with respect to*

- Total time derivatives of a function $x(t)$ are denoted $\dot{x}$, $\ddot{x}$, $x^{(3)}, \ldots, x^{(n)}$. A superscript with an argument variable will denote partial differentiation with respect to that argument, that is, $\alpha^t(x,\theta,t) := \frac{\partial \alpha}{\partial t}$, $\alpha^{x^2}(x,\theta,t) := \frac{\partial^2 \alpha}{\partial x^2}$, and $\alpha^{\theta^n}(x,\theta,t) := \frac{\partial^n \alpha}{\partial \theta^n}$, etc. The gradient $\alpha^x(x,\theta,t)$ with $x \in \mathbb{R}^n$ will always be a row vector.

- For a function $f : X \to Y$ we say that f is of class $\mathcal{C}^r$, and write $f \in \mathcal{C}^r$, if $f^{x^k}(x)$, $k \in \{0,1,\ldots,r\}$, is defined and continuous for all $x \in X$. f is *continuous* if $f \in \mathcal{C}^0$, f is *continuously differentiable* if $f \in \mathcal{C}^1$, and f is *smooth* if $f \in \mathcal{C}^\infty$.

- The p-norm of a vector is $|x|_p := (\sum_{i=1}^n |x_i|^p)^{1/p}$, where the most commonly used is the 2-norm, or the Euclidean vector norm, simply denoted $|x| := |x|_2 = (x^\top x)^{1/2}$. This reduces to the absolute value for a scalar.

- The signals norms are denoted by $||x||_p := \left(\int_{t_0}^\infty |x(t)|^p \, dt\right)^{1/p}$, where in particular $\|x\| := \|x\|_\infty = \operatorname{ess\,sup}\{|x(t)| : t \geq 0\}$. If a specific time-interval $[t_0, t_1]$ is of interest, we use the notation $\left\|x_{[t_0,t_1]}\right\| := \operatorname{ess\,sup}\{|x(t)| : t \in [t_0, t_1]\}$

- The *distance-to-the-set* function is denoted $|x|_{\mathcal{A}} := d(x;\mathcal{A}) =$

$\inf\{d(x,y):\ y\in\mathcal{A}\}$ where the point-to-point distance function is normally taken as $d(x,y)=|x-y|$. Note that for an equilibrium, $\mathcal{A}=\{0\}$, the distance-to-the-set function reduces to the norm, $|x|_{\mathcal{A}}=|x|_{\{0\}}=|x|$.

- A column vector is often stated as $\operatorname{col}(x,y,z):=\left[x^\top,y^\top,z^\top\right]^\top$, while a row vector is $\operatorname{row}(x,y,z):=[x^\top,y^\top,z^\top]$. For a vector $x=\operatorname{col}(x_1,x_2,\ldots,x_n)\in\mathbb{R}^{nm}$ we use the compact notation $\bar{x}_i:=\operatorname{col}(x_1,x_2,\ldots,x_i)$, $i=1,\ldots,m$. Whenever convenient (and clear from the context) the notation $|(x,y,z)|=|\operatorname{col}(x,y,z)|$ is used. A vector of only ones is denoted $\mathbf{1}=[1,1,\ldots,1]^\top$.

- The induced norm of a matrix A is denoted $||A||_p:=\max_{|x|_p=1}|Ax|_p$, where in particular $\|A\|:=\|A\|_2$.

- The minimum and maximum eigenvalues of a matrix A are given by $\lambda_{\min}(A)$ and $\lambda_{\max}(A)$.

- A diagonal matrix is often written as $\operatorname{diag}(a,b,c,\ldots)$, and the identity matrix is simply written I where its dimension should be clear from the context.

- In control design, the subscript 'd' as in $x_d(t)$ or $y_d(\theta)$ means 'desired.' It will always be used for a varying desired function. For constant set-points the subscript 'ref' is used as in x_{ref} or u_{ref}.

A remark on the notation

The partial derivative notation, for instance $\alpha^\theta(x,\theta,t)$, is a convenient compact notation. However, a superscript can be confused with some other mathematical operation, like taking the power of the function. This is solved by always keeping the argument list of the function. Partial derivatives will always come before the argument list, while other mathematical operations are indicated after the list (with partial differentiation as the primary operation). For example, $f^t(x,\theta,t)^2=\left(\frac{\partial f(x,\theta,t)}{\partial t}\right)^2$ and $\xi^{\theta^2}(\theta,t)^\top=\left(\frac{\partial^2\xi(\theta,t)}{\partial\theta^2}\right)^\top$. The only exception is $f^{-1}(x)$ which means the inverse map of the function f, while $f(x)^{-1}=1/f(x)$. If other ambiguous cases are encountered, they are solved using parentheses.

1.4.2 Stability of sets

Consider the *ordinary differential equation*

$$\dot{x} = f(x) \tag{1.6}$$

frequently referred to as the 'system,' where for each $t \geq 0$ the vector $x(t) \in \mathbb{R}^n$ is the state and $f : \mathbb{R}^n \to \mathbb{R}^n$ is a sufficiently smooth vector function. Let $x(t, x_0)$ denote the solution of (1.6) at time t with initial state $x(0) = x_0$. If there is no ambiguity from the context, the solution is simply written as $x(t)$. It is defined on some maximal interval of existence $(T_{\min}(x_0), T_{\max}(x_0))$ where $T_{\min}(x_0) < 0 < T_{\max}(x_0)$. The system (1.6) is said to be *forward complete* if $T_{\max}(x_0) = +\infty$ for all x_0, *backward complete* if $T_{\min}(x_0) = -\infty$ for all x_0, and *complete* if it is both forward and backward complete (Lin, Sontag and Wang; 1996).

In this thesis, stability for (1.6) will frequently be analyzed with respect to a closed, not necessarily bounded, set $\mathcal{A} \subset \mathbb{R}^n$. Such a set is said to be *forward invariant* for a forward complete system (1.6) if $\forall x_0 \in \mathcal{A}$ the solution $x(t, x_0) \in \mathcal{A}$, $\forall t \geq 0$. In order to measure the distance away from the set, the "distance to the set $\mathcal{A}$ function" is defined as

$$|x|_{\mathcal{A}} := d(x; \mathcal{A}) = \inf \{d(x, y) : \ y \in \mathcal{A}\} \tag{1.7}$$

where the point-to-point distance function is in this thesis simply taken as the Euclidean distance $d(x, y) = |x - y|$.

An example is given by an equilibrium. An equilibrium point $x_e \in \mathbb{R}^n$ of (1.6) is a point such that $f(x_e) = 0$. It can be represented by the compact set

$$\mathcal{A} := \{x \in \mathbb{R}^n : \ x = x_e\}.$$

The distance function is in this case $|x|_{\mathcal{A}} = \inf \{|x - y| : \ y = x_e\} = |x - x_e|$ showing that the distance function reduces to the traditional norm function.

Another example is the ε-ball given by the compact set

$$\mathcal{A}_\varepsilon = \{x \in \mathbb{R}^n : \ |x| \leq \varepsilon\},$$

for which the distance function becomes $|x|_{\mathcal{A}_\varepsilon} = \max\{0, \ |x| - \varepsilon\}$.

In the case when $\mathcal{A}$ is a compact set (closed and bounded) and it can be established for a solution to (1.6) that the distance $|x(t, x_0)|_{\mathcal{A}}$ is bounded on the maximal interval of existence, then the trajectory itself must necessarily be bounded away from infinity on the maximal interval of existence. By a

contradiction argument it follows that the system must be forward complete. In the case when $\mathcal{A}$ is not bounded (noncompact) this is not necessarily true, and other means must be used to established forward completeness. In stability definitions for such sets, *forward completeness* is therefore a prerequisite that must hold for the system.

Definition 1.1 *If the system (1.6) is forward complete, then for this system a closed, forward invariant set $\mathcal{A}$ is:*

- Uniformly Stable *(US) if there exists $\delta(\cdot) \in \mathcal{K}_\infty$ such that for any $\varepsilon > 0$,*
$$|x_0|_{\mathcal{A}} \leq \delta(\varepsilon),\ t \geq 0 \quad \Rightarrow \quad |x(t, x_0)|_{\mathcal{A}} \leq \varepsilon. \tag{1.8}$$
- Uniformly Globally Asymptotically Stable *(UGAS) if it is US and* Uniformly Attractive *(UA), that is, for each $\varepsilon > 0$ and $r > 0$ there exists $T > 0$ such that*
$$|x_0|_{\mathcal{A}} \leq r,\ t \geq T \quad \Rightarrow \quad |x(t, x_0)|_{\mathcal{A}} \leq \varepsilon. \tag{1.9}$$

See Appendix A for the definitions of class $\mathcal{K}$, $\mathcal{K}_\infty$, and $\mathcal{KL}$ functions. The above stability definitions using $\varepsilon - \delta$ bounds, is as shown by Lin et al. (1996) and Khalil (2002) equivalent to using class-$\mathcal{K}$ and -$\mathcal{KL}$ estimates.

Different mathematical tools can be applied to establish stability of a system of the form (1.6). By far the most important in this thesis is Lyapunov's direct method. Additionally, other tools like Barbalat's Lemma (Barbălat; 1959) and Matrosov's Theorem (Matrosov; 1962) will be used. A comprehensive threatment is given in Appendix A.

Set-stability for time-varying systems

Consider the time-varying system

$$\dot{z} = g(z, t) \tag{1.10}$$

where $z(t, t_0, z_0) \in \mathbb{R}^n$ is the solution, evolving from z_0 at time $t = t_0 \geq 0$. Within the framework of set-stability of noncompact sets it is possible to analyze such a time-varying system as if it is time-invariant. Using a letter p to represent the explicit time-variation t in (1.10), having dynamics $\dot{p} = 1$, $p(0) = t_0$ so that $p(t) = t + t_0$, $\forall t \geq 0$, and defining $x := \mathrm{col}(z, p)$, then we can define the equivalent and seemingly time-invariant system

$$\dot{x} = \begin{bmatrix} \dot{z} \\ \dot{p} \end{bmatrix} = \begin{bmatrix} g(z, p) \\ 1 \end{bmatrix} =: f(x), \qquad x_0 = \begin{bmatrix} z_0 \\ t_0 \end{bmatrix}, \tag{1.11}$$

for which $x(t, x_0)$ is the solution, evolving from x_0 at time $t = 0$. According to Lin (1992, Lemma 5.1.1) it follows that $z(t, t_0, z_0)$ is a solution of (1.10) for $t \geq t_0 \geq 0$ if and only if $x(t, x_0) := \mathrm{col}\,(z(t + t_0, t_0, z_0), t + t_0)$ is a solution of (1.11) for $t \geq 0$.

If stability for the original system (1.10) is analyzed with respect to the origin $z = 0$, then for the new system this is analyzed as stability of the noncompact set

$$\mathcal{A} = \{(z, p) \in \mathbb{R}^n \times \mathbb{R}_{\geq 0} : \ z = 0\},$$

for which the distance function is $|(z, p)|_{\mathcal{A}} = |z|$.

This 'trick' will frequently be applied in this thesis for analysis of closed-loop maneuvering systems. The advantage is to avoid analyzing stability of sets that in the state-space vary with time. One can instead apply the rather extensive theory developed for stability of noncompact sets; see e.g. Lin (1992); Lin, Sontag and Wang (1995); Sontag and Wang (1995a); Lin et al. (1996); Teel and Praly (2000); Teel (2002). A disadvantage is, according to Teel and Praly (2000), that it usually imposes stronger than necessary conditions on the time-dependence of the right-hand side of (1.10), e.g. continuity when only measurability is needed.

It should be noted, that in this thesis we will usually not go to the step of introducing the variable p but rather just use t as is with $\dot{t} = 1$ and $t(0) = 0$. One should therefore be careful to distinguish this explicit time variation from the implicit time, e.g. $t \mapsto x(t)$ where x is a state, in equations of this thesis (though they physically are the same).

Remark 1.2 *Since the explicit time-variation often only enters through the designed reference system, e.g.* $t \mapsto x_d(t)$ *or* $t \mapsto \upsilon_s(\theta, t)$*, we could in principle define a new state* p*, running inside the control computer with dynamics* $\dot{p} = 1$*,* $p(0) = t_0$*, in order to implement* t *in these functions. This would indeed make the closed-loop system time-invariant. There is, however, no quantitative difference in this as compared to just using time* t*, for* $t \geq t_0$*, directly.*

Systems with inputs

In some cases we consider systems with input

$$\dot{x} = f(x, u, t) \tag{1.12}$$

where $x(t) \in \mathbb{R}^n$, $\forall t \geq t_0 \geq 0$, is the state, and $u(\cdot)$ is a measurable, locally essentially bounded input function $u : \mathbb{R}_{\geq 0} \to \mathbb{R}^m$. The space of such input

functions is denoted $\mathcal{L}_\infty^m$ with the norm $||u_{[t_0,\infty)}|| := \operatorname{ess\,sup}\{u(t) : \ t \geq t_0\}$. For each initial time and state $x(t_0) = x_0 \in \mathbb{R}^n$ and each $u \in \mathcal{L}_\infty^m$, let $x(t, t_0, x_0, u)$ denote the solution of (1.12) at time t. More general stability concepts for (1.12) are given in terms of *input-to-state stability* (ISS); see Sontag and Wang (1995b); Lin (1992); Edwards, Lin and Wang (2000):

Definition 1.2 *The system (1.12) is* input-to-state stable *if there exists $\beta \in \mathcal{KL}$ and $\gamma \in \mathcal{K}$ such that, for each input $u \in \mathcal{L}_\infty^m$ and each $x_0 \in \mathbb{R}^n$, it holds that*

$$|x(t, t_0, x_0, u)| \leq \beta\left(|x_0|\,,\ t - t_0\right) + \gamma\left(\left|\left|u_{[t_0,\infty)}\right|\right|\right) \tag{1.13}$$

for each $t \geq t_0 \geq 0$.

By causality the same definition holds if we replace $||u_{[t_0,\infty)}||$ with $||u_{[t_0,t]}||$.

ISS is a robust stability concept that guarantees bounded state for all bounded inputs and UGAS of the origin when the input vanishes. ISS also generalizes to set-stability, and a treatment is given in Appendix A.3.

An application of the set-stability and ISS tools is illustrated by the following example.

Example 1.5 ***Claim:*** *The noncompact set*

$$\mathcal{A} = \{(x, t) : \ x = x_d(t)\}$$

is UGAS with respect to the scalar system

$$\dot{x} = -\left(x^3 - x_d(t)^3\right) + \dot{x}_d(t) =: f(x, t)$$

where the desired state $x_d(t)$ is bounded and absolutely continuous, and $|\dot{x}_d(t)| \leq M$, a.a. $t \geq 0$.

Proof: *Forward completeness is established by the auxiliary function $W := \frac{1}{2}x^2$ having a derivative $\dot{W} = -x^4 + x\delta(t) \leq -\varepsilon\,|x|^4$, $\forall\,|x| \geq \sqrt[3]{\frac{\delta_0}{1-\varepsilon}}$ where δ_0 is a bound on $\delta(t) := x_d(t)^3 + \dot{x}_d(t)$ and $\varepsilon \in (0, 1)$. This shows input-to-state stability (ISS) of the system with δ as input (see Appendix A.3), and consequently that $x(t)$ and $f(x(t), t)$ are bounded for all $t \geq 0$.*
For the distance function we have that

$$|(x, t)|_{\mathcal{A}} = \inf_{(y,\tau)\in\mathcal{A}} \left|\begin{bmatrix} x - y \\ t - \tau \end{bmatrix}\right| = \inf_{\tau} \left|\begin{bmatrix} x - x_d(\tau) \\ t - \tau \end{bmatrix}\right| \leq |x - x_d(t)|\,.$$

The absolute continuity of $x_d(t)$ together with boundedness of $\dot{x}_d(t)$ implies that $x_d(t)$ is globally Lipschitz such that $|x_d(t) - x_d(\tau)| \leq M\,|t - \tau|$ holds. Let τ^* be the (optimal) value that satisfies the above infimum. Then

$$\begin{aligned} |x - x_d(t)| &= |x - x_d(\tau^*) + x_d(\tau^*) - x_d(t)| \\ &\leq |x - x_d(\tau^*)| + |x_d(\tau^*) - x_d(t)| \\ &\leq |x - x_d(\tau^*)| + M\,|t - \tau^*| \leq \max\{1, M\} \left| \begin{bmatrix} x - x_d(\tau^*) \\ t - \tau^* \end{bmatrix} \right|_1 \\ &\leq \sqrt{2}\max\{1, M\}\,|(x,t)|_{\mathcal{A}}\,. \end{aligned}$$

Defining $k := \sqrt{2}\max\{1, M\}$ the result is the equivalence relation

$$\frac{1}{k}\,|x - x_d(t)| \leq |(x,t)|_{\mathcal{A}} \leq |x - x_d(t)|\,.$$

Let a smooth Lyapunov function be $V(x,t) := \frac{1}{2}\,(x - x_d(t))^2$. This has the bounding functions, according to (A.19) and (A.20), defined as:

$$\begin{aligned} \alpha_1\left(|(x,t)|_{\mathcal{A}}\right) := \frac{1}{2}\,|(x,t)|^2_{\mathcal{A}} \leq V(x,t) \leq \frac{k^2}{2}\,|(x,t)|^2_{\mathcal{A}} =: \alpha_2\left(|(x,t)|_{\mathcal{A}}\right) \\ V^x(x,t)f(x,t) + V^t(x,t) = -\left(x - x_d(t)\right)\left(x^3 - x_d(t)^3\right) =: -\alpha_3(|(x,t)|_{\mathcal{A}}). \end{aligned}$$

Recall the property $(x - y)(d(x) - d(y)) > 0$, $\forall x \neq y$, of a monotonically strictly increasing function $d(x)$. Using this with $d(x) = x^3$ shows that α_3 is a positive definite function, and $\mathcal{A}$ is therefore UGAS according to Theorem A.10.

1.4.3 Geometric relationships

Vectors and reference frames

A *vector* $\vec{x}$ is a quantity describing a magnitude and a direction. When not related to any reference frame[2], the vector is said to be *coordinate-free*. However, in this thesis a vector will be related to a Euclidean space $\mathbb{R}^n$ (sometimes called a Cartesian space) spanned by a set of orthogonal unit vectors $\{\vec{\epsilon}_1, \vec{\epsilon}_2, \ldots, \vec{\epsilon}_n\}$ so that

$$\vec{x} = x_1\vec{\epsilon}_1 + x_2\vec{\epsilon}_2 + \cdots + x_n\vec{\epsilon}_n \tag{1.14}$$

[2]The names 'coordinate frame' and 'reference frame' means the same thing and will be used interchangeably.

where $x_i = \vec{x} \cdot \vec{\epsilon}_i$, $i \in \{1, 2, \ldots, n\}$, are the *Cartesian coordinates* of $\vec{x}$ in $\mathbb{R}^n$. The vector $\vec{x}$ can then be conveniently described as a *coordinate vector*

$$x = \mathrm{col}\,(x_1, x_2, \ldots, x_n)\,,$$

for which we drop the 'arrow' notation. This gives the orthogonal unit coordinate vectors $\epsilon_1 = \mathrm{col}(1, 0, 0, \ldots, 0)$, $\epsilon_2 = \mathrm{col}(0, 1, 0, \ldots, 0)$, $\ldots$, $\epsilon_n = \mathrm{col}(0, 0, 0, \ldots, 1)$ representing the 'axes' of $\mathbb{R}^n$.

In rigid-body dynamics the 3-dimensional space $\mathbb{R}^3$ is of particular interest. The dynamic equations of motion involve *kinematics,* which is "the study of motion without reference to the forces which cause motion," and *kinetics* which is "the study of the relationships between the motion and the forces that cause or accompany the motion" (Meriam and Kraige; 1993). Several Cartesian *reference frames* are important in this context. The absolute motion of a rigid body must be measured in a fixed coordinate frame $\mathcal{E}$, called an *inertial reference frame*, in $\mathbb{R}^3$ for Newton's laws of motion to apply. An inertial frame is not unique. Any fixed coordinate frame in $\mathbb{R}^3$ (our universe) can be used, and two such equivalent frames are related by a *translation* and *rotation.*

For terrestrial navigation the interesting reference frames are:

ECI: The Earth-Centered Inertial reference frame. This is approximately an inertial frame in which Newton's laws of motion apply. It is a nonrotating frame with origin at the center of mass of the Earth, z-axis along the Earth's spin axis and directed towards north, x-axis directed towards the vernal equinox, and y-axis directed to make out a right-hand triad.

ECEF: The Earth-Centered Earth-Fixed reference frame. This frame rotates with the Earth. Its origin and z-axis coincide with the ECI-frame, while the x-axis intersects the Greenwich meridian ($0\,^\circ$ longitude) and the y-axis is directed to make out a right-hand triad. For slow speed vehicles, navigating close to the Earth's surface, this frame is usually assumed inertial since the Earth's angular rate of rotation ($\omega_e = 7.2921 \cdot 10^{-5}\,\mathrm{rad/\,s}$) is small.

NED: The North-East-Down reference frame. The origin of this frame is located at the surface of the Earth with coordinates determined by two angles (l, μ) denoting the *longitude* and *latitude.* Its x-axis is pointing towards true North, y-axis towards East, and z-axis pointing downwards and normal to the Earth's surface. For local navigation of

vehicles, close to the surface, it is common to assume that this frame is inertial, and that the coordinates of the vehicle is given in the xy-plane (tangential plane) of the NED frame (flat Earth navigation). It will frequently be referred to as the $\mathcal{E}$-frame.

In addition, there are some particularly interesting local frames:

Body: A reference frame fixed to the body of the vehicle. For a marine vessel the origin of this frame is usually chosen in the *principal plane of symmetry* (The Society of Naval Architects and Marine Engineers; 1950) with x-axis – the longitudinal axis – directed from the aft to the bow, y-axis – the transverse axis – directed from port to starboard, and z-axis – the normal axis – directed from top to bottom. It will frequently be referred to as the $\mathcal{B}$-frame.

Path: A reference frame with origin at a point along a path. Its axes are given by the x-axis directed along the *unit tangent vector*, the y-axis directed along the *unit principal normal vector*, and the z-axis directed along the *unit binormal vector* (Lipschutz; 1969). For a continuously parametrized path it is often called the *Serret-Frenet frame*. It will be referred to as the $\mathcal{R}$-frame.

See Fossen (2002); Skjetne and Fossen (2001) for more details on these frames and the transformations between them.

Rotations

It is pertinent in control applications for robotics, vehicles, aerospace, marine systems, and navigation systems to represent a vector $\vec{x}$ with respect to several Cartesian frames. Let $\mathcal{A}$ and $\mathcal{B}$ be two such frames with orthogonal unit vectors $\vec{a}_1$, $\vec{a}_2$, $\vec{a}_3$ and $\vec{b}_1$, $\vec{b}_2$, $\vec{b}_3$, respectively. Let $x_a \in \mathcal{A}$ and $x_b \in \mathcal{B}$ be[3] the corresponding coordinate vectors of $\vec{x}$. It can then be shown (Egeland and Gravdahl; 2002) that these are related as

$$x_a = R_b^a x_b, \quad R_b^a := \left\{ \vec{a}_i \cdot \vec{b}_j \right\} \tag{1.15}$$

where R_b^a is the rotation matrix from $\mathcal{B}$ to $\mathcal{A}$. Since $R_a^b := \left\{ \vec{b}_i \cdot \vec{a}_j \right\}$ we get that $x_b = R_a^b x_a = R_a^b R_b^a x_b$ which implies that

$$R_a^b R_b^a = I \quad \text{and} \quad R_b^a = \left(R_a^b \right)^{-1}. \tag{1.16}$$

[3] The notation $x \in \mathcal{A}$ means in this context that the elements of x are the coordinates of $\vec{x}$ along the axes of $\mathcal{A}$. In other words, x is decomposed in $\mathcal{A}$.

Two other important properties hold for a rotation matrix:

$$R_b^a = \left(R_a^b\right)^\top \tag{1.17}$$

$$\det R_b^a = 1. \tag{1.18}$$

showing that R_{ab} is orthogonal with a unitary determinant. Such matrices belongs to the set

$$\mathcal{SO}(3) := \left\{ R \in \mathbb{R}^{3\times 3} : \; R^\top R = I \text{ and } \det R = 1 \right\}$$

called the *Special Orthogonal group of order 3*. A matrix R is a rotation matrix iff $R \in \mathcal{SO}(3)$.

A rotation about a fixed axis is called a *simple rotation*. Euler's Theorem states that the relative orientation between two reference frames $\mathcal{A}$ and $\mathcal{B}$ can be produced by a simple rotation of $\mathcal{B}$ about some line in $\mathcal{A}$. Any simple rotation can again be produced by three rotations, called the *principal rotations*, about the axes of $\mathcal{A}$. For the nine elements in a rotation matrix, $R \in \mathbb{R}^{3\times 3}$, six constraints due to orthogonality implies that a minimum of three variables are necessary to parametrize it. These are conveniently given by the Euler angles: *roll* ϕ – rotation about the x-axis, *pitch* θ – rotation about the y-axis[4], and *yaw* ψ – rotation about the z-axis. The principal rotations of angles ϕ, θ, and ψ about the axes x, y, and z are then given by the rotation matrices

$$R_{x,\phi} = \begin{bmatrix} 1 & 0 & 0 \\ 0 & \cos\phi & -\sin\phi \\ 0 & \sin\phi & \cos\phi \end{bmatrix} \tag{1.19}$$

$$R_{y,\theta} = \begin{bmatrix} \cos\theta & 0 & \sin\theta \\ 0 & 1 & 0 \\ -\sin\theta & 0 & \cos\theta \end{bmatrix} \tag{1.20}$$

$$R_{z,\psi} = \begin{bmatrix} \cos\psi & -\sin\psi & 0 \\ \sin\psi & \cos\psi & 0 \\ 0 & 0 & 1 \end{bmatrix}. \tag{1.21}$$

Let $\Theta := \mathrm{col}(\phi, \theta, \psi)$ give the orientation of frame $\mathcal{B}$ with respect to frame

[4]Note that since θ is used as the path variable in this thesis, we will frequently use σ as the pitch angle in later chapters.

$\mathcal{A}$. The corresponding rotation matrix from $\mathcal{B}$ to $\mathcal{A}$ becomes

$$\begin{aligned} R(\Theta)_b^a :=& R_{z,\psi} R_{y,\theta} R_{x,\phi} \\ =& \begin{bmatrix} c\theta c\psi & -c\phi s\psi + s\theta c\psi s\phi & s\phi s\psi + c\phi s\theta c\psi \\ c\theta s\psi & c\phi c\psi + s\theta s\phi s\psi & -c\psi s\phi + c\phi s\theta s\psi \\ -s\theta & c\theta s\phi & c\theta c\phi \end{bmatrix} \end{aligned} \tag{1.22}$$

where $c\cdot = \cos(\cdot)$ and $s\cdot = \sin(\cdot)$ and the commonly used zyx-convention have been applied.

The translational part of the motion of a rigid body is now given by the coordinate vector $p_e = \mathrm{col}(x, y, z)$ in the inertial frame $\mathcal{E}$. The rotational part is given by Θ which describes the orientation of the body-fixed frame $\mathcal{B}$ in $\mathcal{E}$. Let $v_b = \mathrm{col}(u, v, w)$ be the velocity vector of the rigid-body, decomposed in $\mathcal{B}$. This gives the kinematic relationship

$$\dot{p}_e = R(\Theta)_b^e v_b \tag{1.23}$$

for a rigid body. Likewise, let $\omega_{eb} = \mathrm{col}(p, q, r)$ be the angular velocity vector of $\mathcal{B}$ in $\mathcal{E}$. This can be related to the Euler rate vector $\dot{\Theta}$ as

$$\dot{\Theta} = T_\Theta(\Theta)\omega_b \tag{1.24}$$

where the transformation matrix $T_\Theta(\cdot)$ is

$$T_\Theta(\Theta) := \begin{bmatrix} 1 & \sin\phi\tan\theta & \cos\phi\tan\theta \\ 0 & \cos\phi & -\sin\phi \\ 0 & \sin\phi/\cos\theta & \cos\phi/\cos\theta \end{bmatrix}. \tag{1.25}$$

It is singular for $\theta = \pm 90\,^\circ$ which can pose a problem in some applications. This is resolved by using for instance *unit quaternions* instead of the Euler angles to parametrize R_{eb} and T_Θ. See Fossen (2002) for more details.

In some applications only the two-dimensional plane is important. In this case the coordinate vector of the origin of $\mathcal{B}$ in $\mathcal{E}$ is $p_e = \mathrm{col}(x, y)$, whereas the orientation of $\mathcal{B}$ in $\mathcal{E}$ is simply given by the yaw angle ψ. Setting $\phi = \theta = 0$ in (1.22) and (1.25) and eliminating the z-dimension gives the rotation matrix from $\mathcal{B}$ to $\mathcal{E}$ in $\mathbb{R}^2$ as

$$R_2(\psi)_b^e := \begin{bmatrix} \cos\psi & -\sin\psi \\ \sin\psi & \cos\psi \end{bmatrix}. \tag{1.26}$$

Letting $v_b = \mathrm{col}(u, v)$ be the body-fixed velocity vector we get $\dot{p}_e = R_2(\psi)_b^e v_b$ and $\dot{\psi} = r$. These two equations are commonly put together by defining

$\eta := \text{col}(p_e, \psi)$, $\nu := \text{col}(v_b, r)$, and $R(\psi) := \text{diag}(R_2(\psi)_b^e, 1)$ to get the kinematic relationship

$$\dot{\eta} = R(\psi)\nu, \tag{1.27}$$

commonly used in 3 degrees-of-freedom control applications for vehicles.

Chapter 2

The Maneuvering Problem

This chapter introduces the concept of a *parametrized path* and how a desired dynamic behavior along the path can be expressed i terms of a *dynamic assignment*. Using these concepts, a new problem statement called the *Maneuvering Problem* is proposed, which involves the primary task of converging to and following the continuously parametrized path, and the secondary task of satisfying the desired dynamic behavior along the path.

Some examples are presented to indicate the applicability of this problem statement for several applications. It is further shown that this problem statement implies the existence of a desired forward invariant manifold to which all solutions of the dynamical system must converge. The main material of this chapter have been published in Skjetne, Fossen and Kokotović (2002) and Skjetne, Fossen and Kokotović (2004).

2.1 Path parametrization

2.1.1 A piecewise linear path

In *maneuvering* the main task is to converge to and follow a desired *parametrized path.* Many parametrizations of a path is possible. It can be continuous, discrete, or even hybrid (a mix of both). Consider for instance the path in Figure 2.1. This is a collection of n straight-line segments $\{l_i\}$ connected at a set of $n+1$ way-points (WP) with locations given by the position vectors $p_i \in \mathbb{R}^2$, $i = 1, \ldots, n+1$ in an Earth-fixed reference (or coordinate) frame $\mathcal{E}$.

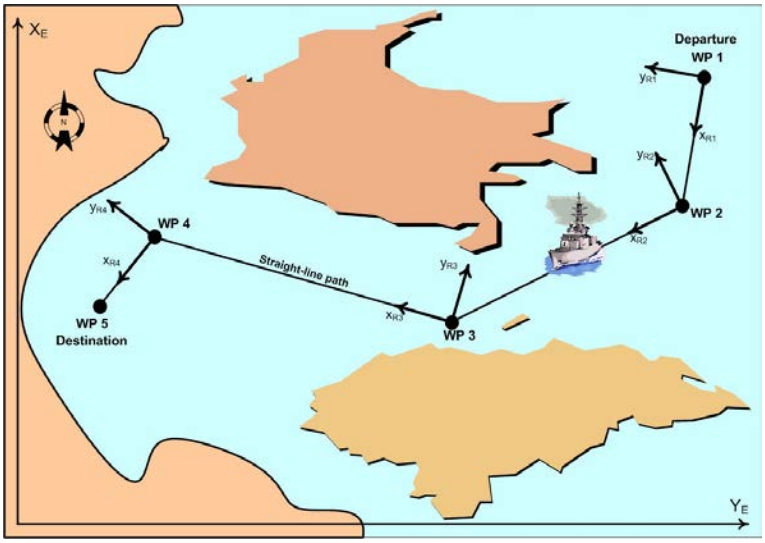

Figure 2.1: A ship maneuvering from way-point to way-point along straight line segments.

Discrete parametrization

A discrete parametrization of this path is found as follows. Let $\mathcal{I} = \{1, 2, \ldots, n\}$ be a set of indices identifying each line-segment l_i in the path. At each line segment l_i, $i \in \mathcal{I}$, we attach a local path reference frame $\mathcal{R}_i$ with origin at way-point p_i and x-axis pointed towards p_{i+1}. Letting $\epsilon_1 := \mathrm{col}(1, 0)$, $\epsilon_2 := \mathrm{col}(0, 1)$, and ψ_i be the angle of rotation of frame $\mathcal{R}_i$ in the Earth frame $\mathcal{E}$, this gives

$$\psi_i = \arctan\left(\frac{\epsilon_2^\top (p_{i+1} - p_i)}{\epsilon_1^\top (p_{i+1} - p_i)}\right).$$

A vector $q_{R_i} \in \mathcal{R}_i$ is mapped to $\mathcal{E}$ by use of the rotation matrix $R_2(\psi_i) : [-\pi, \pi) \to \mathbb{R}^{2\times 2}$, that is,

$$q_E = R_2(\psi_i) q_{R_i} \in \mathcal{E}, \qquad R_2(\psi_i) := \begin{bmatrix} \cos\psi_i & -\sin\psi_i \\ \sin\psi_i & \cos\psi_i \end{bmatrix}.$$

For a position vector $p \in \mathcal{E}$, let $\eta(p, i) := R_2(\psi_i)^\top (p - p_i) \in \mathcal{R}_i$ be the local representation of the point p expressed as a vector in reference frame $\mathcal{R}_i$. We then get that $\epsilon_1^\top \eta(p, i)$ is the projection of p onto the line segment l_i,

and $|\epsilon_2^\top \eta(p,i)|$ is the Euclidean distance from p to l_i (often referred to as the cross-track error). The path is defined by those points for which this distance is zero, that is,

$$\mathcal{P} := \left\{ p \in \mathbb{R}^2 : \ \exists i \in \mathcal{I} \text{ s.t. } \left| \epsilon_2^\top R_2(\psi_i)^\top (p - p_i) \right| = 0 \right\}. \tag{2.1}$$

We notice that the path is discretely parametrized by the index i which identifies all points along line segment l_i.

Continuous parametrization

For a continuous parametrization we define

$$p_d(\theta) := \begin{cases} p_1 + \theta\,(p_2 - p_1)\,; & \theta \in [0,1) \\ p_2 + (\theta - 1)\,(p_3 - p_2)\,; & \theta \in [1,2) \\ \quad\vdots & \\ p_i + (\theta - i + 1)\,(p_{i+1} - p_i)\,; & \theta \in [i-1, i) \\ \quad\vdots & \\ p_{n-1} + (\theta - n + 2)\,(p_n - p_{n-1})\,; & \theta \in [n-1, n). \end{cases} \tag{2.2}$$

The path is then simply given by the set

$$\mathcal{P} := \left\{ p \in \mathbb{R}^2 : \ \exists \theta \in [0, n) \text{ s.t. } p = p_d(\theta) \right\}. \tag{2.3}$$

For this path, each point along the path is uniquely determined by a specific value $\theta \in [0, n)$.

Hybrid parametrization

Lastly, we show a hybrid representation. For this we identify each line segment by an index i and continuously parametrize each line segment by θ, taking values in a fixed interval, for instance, $[0, 1)$. An expression for the line segment i is then $p_d(i, \theta) := p_i + \theta\,(p_{i+1} - p_i)$ so that $p_d(i, 0) = p_i$ and $\lim_{\theta \nearrow 1} p_d(i, \theta) = p_{i+1}$. The path becomes

$$\mathcal{P} := \left\{ p \in \mathbb{R}^2 : \ \exists i \in \mathcal{I} \text{ and } \theta \in [0,1) \text{ s.t. } p = p_d(i, \theta) \right\}, \tag{2.4}$$

and we notice that each point along the path (except p_{n+1}) is uniquely determined by a pair $(i, \theta) \in \mathcal{I} \times [0, 1)$.

2.1.2 A $\mathcal{C}^r$ path generated from way-ponts

One method to generate a $\mathcal{C}^r$ path is to first specify a set of $n+1$ way-points (WPs), and then construct a sufficiently differentiable curve that goes through the way-points by using splines and interpolations techniques. The piecewise linear path used as an example in Section 2.1.1 showed one such curve being $\mathcal{C}^0$. Figure 2.5 illustrates another where the guidance tools developed by Corneliussen (2003) were applied to generate a $\mathcal{C}^3$ path, based on 12 specified way-points, encircling an oil production platform.

To construct the overall desired path $p_d(\theta)$ it is first divided into n subpaths $p_{d,i}(\theta)$, $i = 1, \ldots, n$ between the way-points. Each of these is expressed as a polynomial in θ of a certain order. Then the expressions for the subpaths are concatenated at the way-points to assemble the full path. To ensure that the overall path is sufficiently differentiable at the way-points, the order of the polynomials must be sufficiently high.

For simplicity we consider $\mathbb{R}^2$. Let $\mathcal{I} = \{1, 2, \ldots, n\}$ be a set of indices identifying each subpath. The overall desired curve is denoted $p_d(\theta) = \mathrm{col}(x_d(\theta),\, y_d(\theta))$, $\theta \in [0, n]$, while $p_{d,i}(\theta) = \mathrm{col}(x_{d,i}(\theta),\, y_{d,i}(\theta))$, $i \in \mathcal{I}$, are the subpaths and $p_i = \mathrm{col}(x_i, y_i)$, $i \in \mathcal{I} \cup \{n+1\}$, are the way-points. A common choice is to let θ take an integer value at each way-point, starting with $\theta = 0$ at WP 1 and $\theta = i-1$ at WP i. The differentiability requirement, $p_d(\theta) \in \mathcal{C}^r$, means that at the connection of two subpaths, the following must hold

$$
\begin{aligned}
\lim_{\theta \nearrow i-1} x_{d,i-1}(\theta) &= \lim_{\theta \searrow i-1} x_{d,i}(\theta) & \qquad \lim_{\theta \nearrow i-1} y_{d,i-1}(\theta) &= \lim_{\theta \searrow i-1} y_{d,i}(\theta) \\
\lim_{\theta \nearrow i-1} x^{\theta}_{d,i-1}(\theta) &= \lim_{\theta \searrow i-1} x^{\theta}_{d,i}(\theta) & \qquad \lim_{\theta \nearrow i-1} y^{\theta}_{d,i-1}(\theta) &= \lim_{\theta \searrow i-1} y^{\theta}_{d,i}(\theta) \\
&\vdots & &\vdots \\
\lim_{\theta \nearrow i-1} x^{\theta^r}_{d,i-1}(\theta) &= \lim_{\theta \searrow i-1} x^{\theta^r}_{d,i}(\theta) & \qquad \lim_{\theta \nearrow i-1} y^{\theta^r}_{d,i-1}(\theta) &= \lim_{\theta \searrow i-1} y^{\theta^r}_{d,i}(\theta)
\end{aligned}
$$

for $i \in \mathcal{I} \backslash \{1\}$. We consider polynomials of order k, that is,

$$
\begin{aligned}
x_{d,i}(\theta) &= a_{k,i}\theta^k + \ldots + a_{1,i}\theta + a_{0,i} \\
y_{d,i}(\theta) &= b_{k,i}\theta^k + \ldots + b_{1,i}\theta + b_{0,i}
\end{aligned}
\tag{2.5}
$$

where the coefficients $\{a_{j,i},\, b_{j,i}\}$ must be determined. For each subpath there are $(k+1)\cdot 2$ unknowns so that there are $(k+1)\cdot 2n$ unknown coefficients in total to be determined for the full path. Many methods for calculating these coefficients exist. The most obvious is perhaps to set it up as a large set of $(k+1)\cdot 2n$ linear equations, $A\phi = b$, for the full path and solve these in a single operation as $\phi = A^{-1}b$. However, as the number n of

subpaths increases, this soon encounters numerical problems in the inversion of A. Instead, it is possible to calculate the coefficients for each subpath independently. To ensure the desired continuity at the connection points, we assign numerical values which are common for the neighboring subpaths.

Next, two methods for constructing the path is outlined. There exist many other methods for solving this task. In particular, the reader is encouraged to look into constrained optimization techniques for path generation. This is not within the scope here.

Method 1: Direct continuous parametrization

For a k'th order polynomial $x_{d,i}(\theta)$ we have that $x_{d,i}^{\theta^j}(\theta) = 0$ for $j \geq k+1$. Hence, we can only form equations from the first k derivatives of $x_{d,i}(\theta)$. The following equations can be set up:

$\mathcal{C}^0$: For continuity at the way-points we get for $i \in \mathcal{I}$ the $2 \cdot 2n$ equations:

$$\begin{aligned} x_{d,i}(i-1) &= x_i & y_{d,i}(i-1) &= y_i \\ x_{d,i}(i) &= x_{i+1} & y_{d,i}(i) &= y_{i+1}. \end{aligned} \tag{2.6}$$

$\mathcal{C}^1$: At the first way-point the slope is chosen to point against the second way-point. Likewise, at the last way-point the slope is chosen to point against the second-last way-point. This gives the $2 \cdot 2$ equations:

$$\begin{aligned} x_{d,1}^{\theta}(0) &= x_2 - x_1 & y_{d,1}^{\theta}(0) &= y_2 - y_1 \\ x_{d,n}^{\theta}(n) &= x_{n+1} - x_n & y_{d,n}^{\theta}(n) &= y_{n+1} - y_n. \end{aligned} \tag{2.7}$$

At intermediate way-points the slopes are chosen as a formula based on the neighboring way-points, for instance, the $2 \cdot 2(n-1)$ equations:

$$\begin{aligned} &\left.\begin{aligned} x_{d,i}^{\theta}(i-1) &= \lambda\left(x_{i+1} - x_{i-1}\right) \\ y_{d,i}^{\theta}(i-1) &= \lambda\left(y_{i+1} - y_{i-1}\right) \end{aligned}\right\} && i = 2, \ldots, n \\ &\left.\begin{aligned} x_{d,i}^{\theta}(i) &= \lambda\left(x_{i+2} - x_i\right) \\ y_{d,i}^{\theta}(i) &= \lambda\left(y_{i+2} - y_i\right) \end{aligned}\right\} && i = 1, \ldots, n-1 \end{aligned} \tag{2.8}$$

where $\lambda > 0$ is a design constant. $\lambda = 0.5$ means that the slope at WP i is the average of pointing against WP $i-1$ and WP $i+1$, while $\lambda < 0.5$ allows for a sharper corner and $\lambda > 0.5$ outstretches the corner at WP i.

$\mathcal{C}^j$: Derivatives of order $j \geq 2$ can be set to zero. This gives for $i \in \mathcal{I}$ the $2 \cdot 2n$ equations:

$$\begin{array}{ll} x_{d,i}^{\theta^j}(i-1) = 0 & y_{d,i}^{\theta^j}(i-1) = 0 \\ x_{d,i}^{\theta^j}(i) = 0 & y_{d,i}^{\theta^j}(i) = 0. \end{array} \tag{2.9}$$

If the differentiability requirement of the path is $\mathcal{C}^r$, then the above equations up to $j = r$ gives $2(r+1) \cdot 2n$ equations used to solve for $(k+1) \cdot 2n$ unknowns. As a result, the order k of the polynomials must be

$$k = 2r + 1. \tag{2.10}$$

The path generation problem is now set up as n linear, decoupled sets of equations $A_i \phi_i = b_i$, $i \in \mathcal{I}$, where the unknown vector ϕ_i is

$$\phi_i = \text{col}\left(\{a_{j,i}\}_{j=k,\ldots,0}, \ \{b_{j,i}\}_{j=k,\ldots,0,} \right) \in \mathbb{R}^{2(k+1)}$$

and A_i and b_i are formed correspondingly according to the above equations. Unfortunately, there is a numerical problem in this procedure. The matrix A_i will contain in its elements powers of $i-1$, i, and $i+1$ where $i \in \mathcal{I}$, and the powers range from zero to $r = \frac{1}{2}(k-1)$. This indicates a large variation in the singular values for A_i. It was described by Corneliussen (2003) that for $k = 5$ then A_i becomes ill-conditioned for $i \geq 8$ which means that a maximum of 7 way-points can be allowed.

Method 2: Hybrid parametrization

To alleviate the ill-conditioning problem, an alternative method is to continuously parametrize each subpath within a fixed interval $\varepsilon \in [0, 1)$ and let an index i identify the subpath i. This corresponds to the hybrid parametrization described in Section 2.1.1. The equations used to calculate the coefficients are mainly the same as for Method 1 above:

$\mathcal{C}^0$: Continuity at the way-points gives for $i \in \mathcal{I}$:

$$\begin{array}{ll} x_{d,i}(0) = x_i & y_{d,i}(0) = y_i \\ x_{d,i}(1) = x_{i+1} & y_{d,i}(1) = y_{i+1}. \end{array} \tag{2.11}$$

$\mathcal{C}^1$: The slopes at the first and last way-points are chosen as:

$$\begin{array}{ll} x_{d,1}^{\theta}(0) = x_2 - x_1 & y_{d,1}^{\theta}(0) = y_2 - y_1 \\ x_{d,n}^{\theta}(1) = x_{n+1} - x_n & y_{d,n}^{\theta}(1) = y_{n+1} - y_n. \end{array} \tag{2.12}$$

The slopes at the intermediate way-points are chosen as:

$$\left.\begin{array}{l} x'^{\theta}_{d,i}(0) = \lambda\,(x_{i+1} - x_{i-1}) \\ y'^{\theta}_{d,i}(0) = \lambda\,(y_{i+1} - y_{i-1}) \end{array}\right\} \qquad i = 2, \ldots, n$$
$$\left.\begin{array}{l} x'^{\theta}_{d,i}(1) = \lambda\,(x_{i+2} - x_{i}) \\ y'^{\theta}_{d,i}(1) = \lambda\,(y_{i+2} - y_{i}) \end{array}\right\} \qquad i = 1, \ldots, n-1 \tag{2.13}$$

where $\lambda > 0$ is a design constant.

$\mathcal{C}^j$: Setting derivatives of order $j \geq 2$ to zero gives for $i \in \mathcal{I}$:

$$\begin{array}{ll} x^{\theta^j}_{d,i}(0) = 0 & y^{\theta^j}_{d,i}(0) = 0 \\ x^{\theta^j}_{d,i}(1) = 0 & y^{\theta^j}_{d,i}(1) = 0. \end{array} \tag{2.14}$$

The result is a hyprid parametrization of the path,

$$\hat{p}_d(i, \varepsilon) = \left[\begin{array}{c} x_{d,i}(\varepsilon) \\ y_{d,i}(\varepsilon) \end{array}\right], \tag{2.15}$$

where $i \in \mathcal{I}$ and $\varepsilon \in [0, 1)$. This does not conform with the requirement of a continuous parametrization. However, since

$$\lim_{\varepsilon \nearrow 1} \hat{p}_d^{\varepsilon^j}\,(i-1, \varepsilon) = \lim_{\varepsilon \searrow 0} \hat{p}_d^{\varepsilon^j}\,(i, \varepsilon)$$

holds for $j = 0, \ldots, r$ and $i = 2, \ldots, n-1$, a map $p_d(\theta)$ can be constructed so that $\theta \mapsto p_d(\theta)$ is $\mathcal{C}^r$. For $\theta \in [0, n)$, let $i = \lfloor \theta \rfloor + 1 \in \mathcal{I}$ and $\varepsilon = \theta - \lfloor \theta \rfloor \in [0, 1)$ where $\lfloor \cdot \rfloor$ is the floor operation. Then we have the desired $\mathcal{C}^r$ map

$$\theta \mapsto p_d(\theta) := \hat{p}_d\,(i(\theta), \varepsilon(\theta)) \tag{2.16}$$

which is a continuous parametrization by θ; see Figure 2.2.

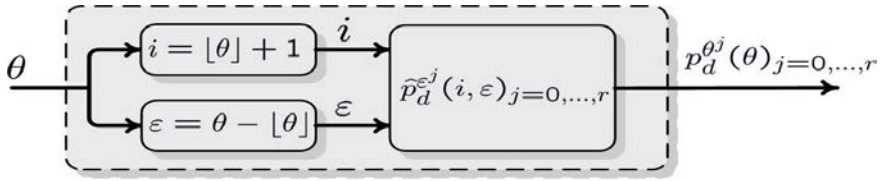

Figure 2.2: Block diagram showing the $\mathcal{C}^r$ map $\theta \mapsto p_d(\theta)$.

Different applications and control design methodologies will require different ways of parametrizing the path. For instance, a discrete parametrization may be most appropriate for the methodology presented by Fossen et al. (2003) and Breivik and Fossen (2004). In the continuation of this thesis, however, the path will be a continuously parametrized curve $y_d(\theta) \in \mathcal{C}^r$ where r is sufficiently large.

2.2 Dynamic assignments

The second task is to satisfy a *desired dynamic behavior* along the path. This can be expressed in terms of a *time assignment*, *speed assignent*, or *acceleration assignment* along the path:

1. A **Time Assignment** means to be at specific points along the path at specific time instants. For a continuous parametrization $y_d(\theta)$, specific values like θ_1, θ_2, etc., must correspond to specific time instants t_1, t_2, etc., perhaps dependent through a design function $\upsilon_t(\cdot)$ so that $\theta_1 = \upsilon_t(t_1)$ and $\theta_2 = \upsilon_t(t_2)$.

2. A **Speed Assignment** is to obtain a desired speed for y along the path. If $y_d(\theta)$ is a continuous parametrization this can be translated into a desired speed for $\dot{\theta}$. This desired speed may depend on the location along the path given by θ (as for instance speed limits along a road), or it may explicitly depend on time. A natural choice is therefore to express the desired speed for $\dot{\theta}$ as a design function $\upsilon_s(\theta, t)$.

3. An **Acceleration Assignment** is to obtain a desired acceleration for y along the path. For a continuous parametrization $y_d(\theta)$ this can be expressed by a design function $\upsilon_a(\dot{\theta}, \theta, t)$ for $\ddot{\theta}$, which may depend on the speed $\dot{\theta}$ along the path in addition to θ and t.

The assignment functions υ_t, υ_s, or υ_a should express the desired dynamic behavior along the path when perfectly tracing it, that is, they should be satisfied in the limit as the output converges to the path. This opens for flexibility in the design since the time evolution of $\theta(t)$, $\dot{\theta}(t)$, or $\ddot{\theta}(t)$ can additionally be shaped by the system state. In the designs presented in later chapters, this flexibility will be exploited to achieve a favorable dynamic response for the closed-loop system. Note that the assignment functions could in principle also depend explicitly on the system state x to give even more flexibility in the design. This is, however, not considered in this treatise.

We also find that a tracking problem corresponds to satisfying a time assignment identically. Indeed, setting $\theta = \upsilon_t(t)$ in $y_d(\theta)$ gives the desired output $\tilde{y}_d(t) := y_d(\upsilon_t(t))$ for a tracking task. In this case the flexibility of only needing to satisfy the assignment in the limit, $\theta(t) \to \upsilon_t(t)$, is lost.

2.3 The Maneuvering Problem Statement

For a system output $y \in \mathbb{R}^m$, the desired path is all points represented by the set

$$\mathcal{P} := \{y \in \mathbb{R}^m : \exists \theta \in \mathbb{R} \text{ s.t. } y = y_d(\theta)\} \tag{2.17}$$

where y_d is continuously parametrized by θ. We will interchangeably call both $y_d(\theta)$ and $\mathcal{P}$ for the desired path. Given the desired path (2.17) and a dynamic assignment, the **Maneuvering Problem** is comprised of the two tasks:

1. **Geometric Task:** For any continuous function $\theta(t)$, force the output y to converge to the desired path $y_d(\theta)$,

$$\lim_{t\to\infty} |y(t) - y_d(\theta(t))| = 0 \tag{2.18}$$

2. **Dynamic Task:** Satisfy one or more of the following assignments:

2.1 **Time Assignment:** Force the path variable θ to converge to a desired time signal $\upsilon_t(t)$,

$$\lim_{t\to\infty} |\theta(t) - \upsilon_t(t)| = 0. \tag{2.19}$$

2.2 **Speed Assignment:** Force the path speed $\dot{\theta}$ to converge to a desired speed $\upsilon_s(\theta, t)$,

$$\lim_{t\to\infty} \left|\dot{\theta}(t) - \upsilon_s(\theta(t), t)\right| = 0. \tag{2.20}$$

2.3 **Acceleration Assignment:** Force the path acceleration $\ddot{\theta}$ to converge to a desired acceleration $\upsilon_a(\dot{\theta}, \theta, t)$,

$$\lim_{t\to\infty} \left|\ddot{\theta}(t) - \upsilon_a\left(\dot{\theta}(t), \theta(t), t\right)\right| = 0. \tag{2.21}$$

The Maneuvering Problem, as defined above, only speaks about the superior goal of convergence to the path and dynamic assignment. To properly define the *Maneuvering Control Objective*, suitable for control design, we will add conditions about feasibility of the geometric and dynamic tasks together with boundedness of the system states.

Example 2.1 *Consider systems that can be transformed into*

$$\dot{z} = g(z, y) \tag{2.22a}$$
$$y^{(r)} = u \tag{2.22b}$$

with uniform relative degree r, where $z \in \mathbb{R}^{n-rm}$ is the state of the zero dynamics, $y \in \mathbb{R}^m$ is the output, and $u \in \mathbb{R}^m$ is the control. In this system, (2.22b) corresponds to m chains of r integrators for which y drives the zero dynamics (2.22a).
Let $y_d(\theta) \in \mathcal{C}^r$ be the desired path corresponding to the geometric task (2.18). Differentiating $y_d(\theta)$ r times with respect to time yields a continuous function $y_d^{(r)} = \Phi(\theta, \dot{\theta}, \ddot{\theta}, \ldots, \theta^{(r)})$. To ensure invariance of the path $y_d(\theta)$ with respect to (2.22), there must then exist an admissible control function $u = u^*$ such that the differential equation

$$\Phi\left(\theta, \dot{\theta}, \ddot{\theta}, \ldots, \theta^{(r)}\right) - u^* = 0 \tag{2.23}$$

has a solution θ^*. If this is true, then the control design task is to develop a control law for u that ensures attractivity and invariance of the path. By the designs presented later in this thesis, this objective is easily achieved for the subsystem (2.22b). However, depending on the stability properties of the zero dynamics (2.22a), one may still encounter the situation where the z state grows unbounded and eventually causes a failure for the complete system. Stable zero dynamics would circumvent this problem, whereas Al-Hiddabi and McClamroch (2002); Dačić and Kokotović (2005); Aguiar, Dačić, Hespanha and Kokotović (2004); Aguiar, Hespanha and Kokotović (2005) provide methods for dealing with unstable zero dynamics.

Example 2.2 *A mechanical system is often parametrized as*

$$M(q)\ddot{q} + C(q, \dot{q})\dot{q} + D(q)\dot{q} + g(q) = B(q)u \tag{2.24}$$

where q, $\dot{q} \in \mathbb{R}^n$ are vectors of generalized coordinates and velocities, $u \in \mathbb{R}^m$ is the control input vector, $M(q)$ is the system inertia matrix, $C(q, \dot{q})$ corresponds to Coriolis forces, $D(q)$ represent dissipative forces, $g(q)$ is the restoring forces, and $B(q)$ is a matrix function with rank equal to the number of

control inputs; see Ortega et al. (1998) for details. Suppose $m < n$ such that the system is underactuated. Then there exists $B^{\perp}(q) \in \mathbb{R}^{(n-m)\times n}$, formed by the basis vectors of the left-nullspace of $B(q)$, such that $B^{\perp}(q)B(q) = 0$. Suppose $q_d(\theta)$ is a desired path for q. Differentiating q_d twice with respect to time and substituting into the plant dynamics, gives

$$\begin{aligned} M(q_d(\theta))\left(q_d^{\theta^2}(\theta)\dot{\theta}^2 + q_d^{\theta}(\theta)\ddot{\theta}\right) + C(q_d(\theta), q_d^{\theta}(\theta))q_d^{\theta}(\theta)\dot{\theta}^2 \\ +D(q_d(\theta))q_d^{\theta}(\theta)\dot{\theta} + g(q_d(\theta)) = B(q_d(\theta))u. \end{aligned} \tag{2.25}$$

Premultiplying (2.25) with $B^{\perp}(q_d(\theta))$ gives then a constraint differential equation of the form

$$\alpha(\theta)\ddot{\theta} + \beta_1(\theta)\dot{\theta}^2 + \beta_2(\theta)\dot{\theta} + \gamma(\theta) = 0. \tag{2.26}$$

It follows from the results of Shiriaev and Canudas-de Wit (2005); Shiriaev, Robertsson, Pacull and Fossen (2005) that if there exists an admissible control function $u = u^*$ that renders the path $q_d(\theta)$ invariant for (2.24), then θ must be a solution to (2.26).

Let the plant under consideration be a nonlinear system

$$\dot{x} = f(x, u) \tag{2.27a}$$
$$y = h(x) \tag{2.27b}$$

where for each $t \geq 0$, $y(t) \in \mathbb{R}^p$ is the output, $x(t) \in \mathbb{R}^n$ is the state, and $u(t) \in \mathbb{R}^m$ is the control. The input u is a measurable, locally essentially bounded function $u : \mathbb{R}_{\geq 0} \to \mathbb{R}^m$. The space of such functions is denoted $\mathcal{L}_\infty^m$ with the norm $||u|| := \operatorname{ess\,sup}\{u(t) : t \geq 0\}$. Let $\mathcal{U} \subset \mathcal{L}_\infty^m$ be the set of all admissible control functions.

Structural constraints in (2.27) or restrictions in the control space may add limitations to the Geometric and Dynamic tasks. Hence, for the maneuvering problem to be solvable, feasibility of the two tasks must be verified.

For the system (2.27), having maximum relative degree r, a *feasibility constraint differential equation* of the form

$$\Phi\left(\theta, \dot{\theta}, \ddot{\theta}, \ldots, \theta^{(r)}, u\right) = 0 \tag{2.28}$$

is derived by differentiating $y = y_d(\theta)$ up to r times and substituting the resulting expressions into (2.27). For each $u \in \mathcal{U}$, let $\Theta(u)$ be the set of all

solutions to (2.28) with u as input. Furthermore, let the set of all admissible u such that $\Theta(u)$ is non-empty, be

$$\mathcal{V} := \{u \in \mathcal{U} : \ \Theta(u) \neq \emptyset\}. \tag{2.29}$$

We then say:

- The Geometric Task of the Maneuvering Problem is feasible for (2.27) if $\mathcal{V}$ is non-empty, i.e., there exists at least one $u^* \in \mathcal{U}$ such that $\Theta(u^*)$ is non-empty.
- The Dynamic Task of the Maneuvering Problem is feasible for (2.27) with respect to a feasible Geometric Task if there exists at least one $u^* \in \mathcal{V}$ such that the corresponding $\theta^* \in \Theta(u^*)$ satisfies the Dynamic Task, that is, either $\theta^*(t) = \upsilon_t(t)$, $\dot{\theta}^*(t) = \upsilon_s(\theta^*(t), t)$, or $\ddot{\theta}^*(t) = \upsilon_a(\dot{\theta}^*(t), \theta^*(t), t)$.

Having defined these feasibility conditions, the **Maneuvering Control Objective** is to construct a control law for (2.27) that solves the Maneuvering Problem with respect to a *feasible Geometric Task* and a *feasible Dynamic Task*, while keeping all system states bounded.

We call a control law solving the Maneuvering Control Objective for a *Maneuvering Controller*. In the special case when the dynamic task is a time assignment which is satisfied identically, that is, $\theta(t) = \upsilon_t(t)$, $\forall t \geq 0$, we call the corresponding maneuvering controller for a *tracking controller*. In this thesis the dynamic task will mostly be specified in terms of a *speed assignment*. However, Section 3.2 shows a modification in the control design where both a speed assignment and time assignment are satisfied in the limit.

2.4 Examples

2.4.1 A typical maneuvering problem

We now return to Example 1.2 and show how the Maneuvering Problem can be used constructively to formally set up the control objective. Suppose the motion of the tip of the cutting tool is represented by

$$M\ddot{x} + D(\dot{x})\dot{x} + K(x)x = u \tag{2.30}$$

where $x \in \mathbb{R}^2$ is the position in the plane, the force $u \in \mathbb{R}^2$ is the control, $M = M^\top > 0$ is the system inertia matrix, and $D(\dot{x}) = D_0 + D_1(\dot{x}) > 0$ and

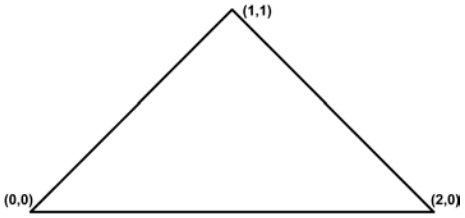

Figure 2.3: The triangular path for the control objective.

$K(x) = K_0 + K_1(x)$ are the respective linear and nonlinear damping and spring matrices. The control objective is for the tip of the cutting tool $y = x$ to trace the triangular path $y_d(\theta)$ in Figure 2.3, continuously parametrized by θ as

$$y_d(\theta) = \begin{cases} [\theta, \quad \theta]^\top; & \theta \in [0,1), \\ [\theta, \quad 2-\theta]^\top; & \theta \in [1,2), \\ [4-\theta, \quad 0]^\top; & \theta \in [2,4). \end{cases} \tag{2.31}$$

To illustrate that many feasible parametrizations are possible, this is neither the same parametrization as proposed for the straight-line path in (2.2), nor is θ the distance travelled by the cutting tool; while θ progresses from 0 to 1, the distance travelled is 1.41 m, and the total distance around the path is 4.83 m.

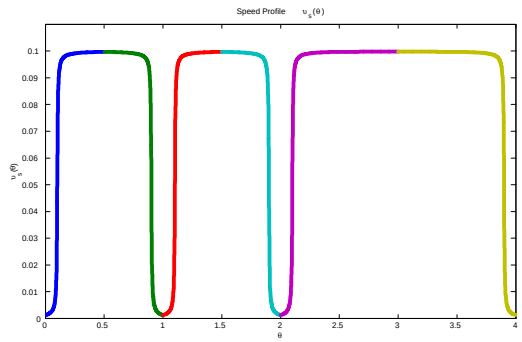

Figure 2.4: The speed assignment $v_s(\theta)$ along the triangular path.

The task is to trace the path as fast as possible under a maximum speed constraint of about $m_s \approx 0.1\,\mathrm{m/s}$, and with a maximum deviation from the

triangular path less than 10^{-3} m. Since the triangular path is not $\mathcal{C}^1$, perfect tracing is not feasible. However, tracing within the maximum deviation constraint is achievable with the strategy for the cutting tool to trace each edge and stop and restart at each corner. The desired speed should be small near the corners to avoid large transients that could exceed the maximum deviation constraint. This motivates a speed assignment $\upsilon_s(\theta)$ that purely depends on the location along the path. Thus, between the corners k and $k+1$, $k = 1, 2, 3$, we assign the following speed profile:

$$\upsilon_s(\theta) = \begin{cases} \frac{m_s}{\pi|y_d^\theta|} \arctan\left(\frac{\theta-\theta_k-a_1}{a_2}\right) + \frac{m_s}{2|y_d^\theta|}; & \theta \in \left[\theta_k, \theta_k + \frac{\theta_{k+1}-\theta_k}{2}\right) \\ \frac{m_s}{\pi|y_d^\theta|} \arctan\left(\frac{\theta_{k+1}-a_1-\theta}{a_2}\right) + \frac{m_s}{2|y_d^\theta|}; & \theta \in \left[\theta_k + \frac{\theta_{k+1}-\theta_k}{2}, \theta_{k+1}\right) \end{cases} \tag{2.32}$$

where $\theta_1 = 0$, $\theta_2 = 1$, $\theta_3 = 2$, and $\theta_4 = 4$, as shown in Figure 2.4 for $\theta \in [0, 4)$. The parameter a_1 sets the width of the low speed regions around the corners, while a_2 smoothens the square wave.

This example is revisited with a controller design in Chapter 4.1.3.

2.4.2 Application to DP

For dynamical positioning (DP) the equations of motion of a ship can be simplified to a 3 degrees-of-freedom (DOF) model. The 3 DOF states are the Cartesian coordinates (x, y) and the heading (ψ) in a local Earth-fixed reference frame $\mathcal{E}$, and the corresponding linear velocities (u, v) and angular rate (r) in the body-fixed reference frame $\mathcal{B}$. In vector form, letting $\eta := \text{col}(x, y, \psi) \in \mathcal{E}$ and $\nu := \text{col}(u, v, r) \in \mathcal{B}$, the resulting dynamics are

$$\begin{aligned} \dot{\eta} &= R(\psi)\nu \\ M\dot{\nu} + D\nu &= \tau + R(\psi)^\top b \end{aligned} \tag{2.33}$$

where $R(\psi) \in \mathbb{R}^{3\times 3}$ is the rotation matrix in (1.27) mapping the vector $\nu \in \mathcal{B}$ to $\dot{\eta} \in \mathcal{E}$, the matrix $M = M^\top > 0$ is the system inertia matrix, $D > 0$ is a constant damping matrix, $\tau \in \mathcal{B}$ is the control input, and $b \in \mathcal{E}$ is a constant (or slowly varying) bias in the system; see Chapter 5 and Appendix B for more details.

As mentioned in Example 1.3, DP station-keeping is a set-point regulation problem, i.e., force the output η of the ship to maintain a constant reference position and heading η_{ref}. However, as illustrated in Example 1.3 we can also set up DP as a maneuvering problem. Since a supply vessel often will have to reposition itself at different locations around a platform, we can construct a curve as a continuous parametrization containing all reference

points and the path between them. By constraining the vessel to the path and commanding online the speed of the vessel along the path, setting it to zero when a reference location is reached and nonzero to move between the locations, the result becomes a safe and functional DP operation.

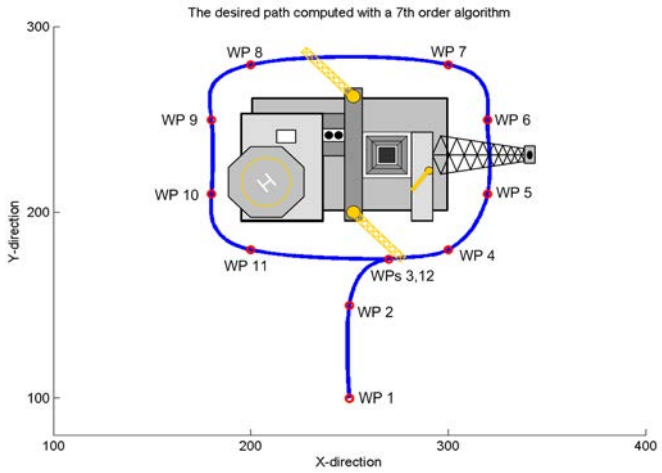

Figure 2.5: A sketch of the Oseberg South platform, seen from above, with a surrounding desired path on which a supply vessel should move. The path is a $\mathcal{C}^3$ curve generated by 12 way-points. See also Figure 1.2.

Path generation: To solve this as a maneuvering problem we let the desired path be

$$\eta_d(\theta) = \mathrm{col}\left(\; x_d(\theta), \quad y_d(\theta), \quad \psi_d(\theta) \; \right)$$

where $p_d(\theta) = \mathrm{col}(x_d(\theta), y_d(\theta))$ is a curve generated by the specification of way-points as described above. One choice for the desired heading $\psi_d(\theta)$ is as a constant reference $\psi_d(\theta) = \psi_{ref}$, or it can be chosen as the angle of the tangent vector along the path,

$$\psi_d(\theta) := \arctan\left(\frac{y_d^\theta(\theta)}{x_d^\theta(\theta)}\right). \tag{2.34}$$

The former choice means that the heading of the vessel can be controlled to a fixed reference, for instance pointing against the resulting environmental force, while the position of the vessel moves along the path. The latter

choice will keep the vessel aligned with the path. Since (2.33) is a vector relative degree two plant (Isidori; 1995), control design will require that the desired path $\eta_d(\theta)$ must be $\mathcal{C}^2$. From (2.34) this means that $p_d(\theta)$ must be $\mathcal{C}^3$ and consequently, by (2.10), the order of the polynomials generating the positional curve must be $k = 7$.

Speed assignment: For the speed assignment $\upsilon_s(\theta, t)$ we let a desired path speed (in m/s) be a commanded input speed $u_d(t)$. Since the identity

$$\begin{aligned} |\dot{p}_d(\theta(t))| &= \sqrt{x_d^\theta(\theta(t))^2\dot{\theta}(t)^2 + y_d^\theta(\theta(t))^2\dot{\theta}(t)^2} \\ &= \sqrt{x_d^\theta(\theta(t))^2 + y_d^\theta(\theta(t))^2}\,|\upsilon_s(\theta(t), t)| = |u_d(t)| \end{aligned} \tag{2.35}$$

must hold along the path, we get the speed assignment

$$\upsilon_s(\theta, t) := \frac{u_d(t)}{\sqrt{x_d^\theta(\theta)^2 + y_d^\theta(\theta)^2}}. \tag{2.36}$$

Setting $u_d(t) = 0$ will stop the vessel on the path, while setting $u_d(t) > 0$ will move the vessel in positive direction along the path and $u_d(t) < 0$ will move it in negative direction.

2.4.3 Path following for a formation of AUVs

An autonomous underwater vehicle (AUV) is a 6 DOF system given by the Cartesian coordinates $p = \text{col}(x, y, z)$ in a local Earth-fixed reference frame $\mathcal{E}$ and orientation given by the Euler angles $\Theta = \text{col}(\phi, \sigma, \psi)$ where ϕ is the roll angle, σ is the pitch angle[1], and ψ is the yaw angle. This gives the state vector $\eta = \text{col}(p, \Theta)$. We let a body-fixed frame $\mathcal{B}$ be attached to the vehicle with axes x_B: the longitudinal axis directed from aft to bow, y_B: the transverse axis directed to starboard, and z_B: the normal axis directed from top to bottom; see Figure (2.6). The body-fixed velocity state vector are then $\nu = \text{col}(u, v, w, p, q, r) \in \mathcal{B}$ where (u, v, w) are the linear velocities in surge, sway, and heave, and (p, q, r) are the angular velocities for roll, pitch, and yaw (Fossen; 2002).

We consider a formation of n AUVs, as motivated in Example 1.4, and let an index $i \in \mathcal{I} := \{1, 2, \cdots, n\}$ identify each individual AUV. Its dynamics are

$$\begin{aligned} \dot{\eta}_i &= J(\Theta_i)\,\nu_i \\ M_i\dot{\nu}_i + C_i(\nu_i)\nu_i + D_i(\nu_i)\nu_i + g_i(\eta_i) &= \tau_i + g_{0i} \end{aligned} \tag{2.37}$$

[1] The normal convention (The Society of Naval Architects and Marine Engineers; 1950) is to use θ for the pitch angle, but σ is chosen here to not confuse it with the path variable.

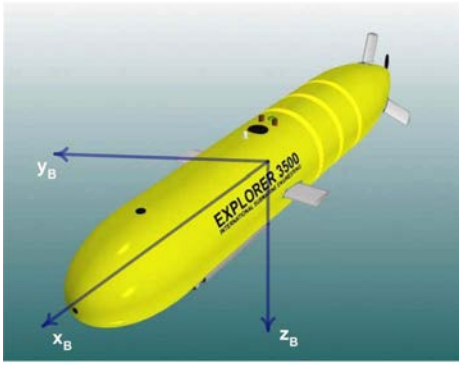

Figure 2.6: The $\mathcal{B}$-frame of the Explorer 3500 AUV. Courtesy: International Submarine Engineering Ltd.

where $J(\Theta_i) = \text{diag}\left(R(\Theta_i)_b^e,\ T_\Theta(\Theta_i)\right)$ is a transformation matrix using (1.22) and (1.25), M_i is the system inertia matrix, C_i accounts for Coriolis and centripetal terms, D_i is a nonlinear damping matrix, g_i is a vector of restoring forces, g_{0i} account for pretrimming and ballast control, and τ_i is the input vector used for control (we assume it is fully actuated). For more details on this model, see Fossen (1994, 2002); Egeland and Gravdahl (2002).

Path generation: To set up the formation, we define a point called the *formation reference point* (FRP) to represent the whole formation as one. Letting $p_d(\theta) \in \mathcal{E}$ be the desired positional curve for the FRP and $\Theta_d(\theta)$ the desired orientation along the curve, the overall desired path for the FRP is $\eta_d(\theta) = \text{col}(p_d(\theta), \Theta_d(\theta))$. We define a new reference frame called the *formation reference frame*, denoted $\mathcal{F}$, with origin in $p_d(\theta)$ and axes x_F: the tangent vector, y_F: the normal vector, and z_F: the binormal vector along the curve $p_d(\theta)$, making out a right-hand system[2]; see Figure 2.7.

Relative to the FRP we assign the desired positions for each AUV by a set of *assignment vectors* $l_i \in \mathcal{F}$. Let $R(\Theta)_f^e$ be the rotation matrix that maps a vector in $\mathcal{F}$ to $\mathcal{E}$; see Section 1.4.3. The paths for the individual AUV members in the formation is then

$$\eta_{d,i}(\theta) = \begin{bmatrix} p_{d,i}(\theta) \\ \Theta_{d,i}(\theta) \end{bmatrix} = \begin{bmatrix} p_d(\theta) + R(\Theta_d(\theta))_f^e\, l_i \\ \Theta_d(\theta) \end{bmatrix}. \tag{2.38}$$

[2]Note that the z_F-axis is chosen to point downwards. This is standard notation according to SNAME (The Society of Naval Architects and Marine Engineers; 1950), having zero depth at the surface and positive depth at the seabed.

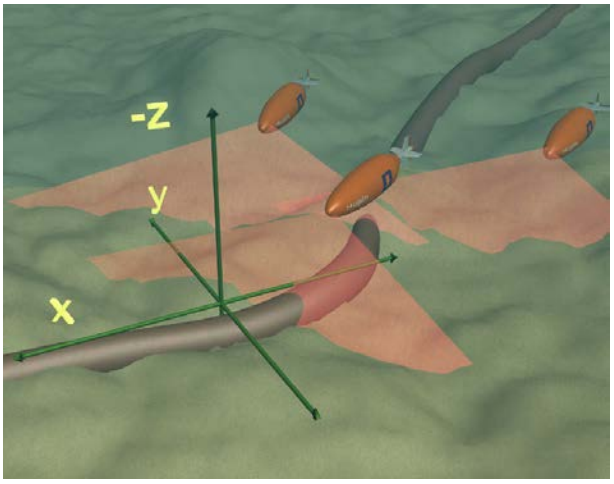

Figure 2.7: Three Hugin AUVs swimming in formation along a pipeline. The coordinate axes indicates the formation reference frame with origin in the FRP. Courtesy: Anders S. Wroldsen.

The curve $p_d(\theta)$ can, for instance, be constructed using the way-point path generation technique discussed in the previous section by extending the methodology to $\mathbb{R}^3$. We choose $\Theta_d(\theta)$ as the orientation of $\mathcal{F}$ in $\mathcal{E}$ along $p_d(\theta)$. This gives

$$\begin{aligned} \phi_d(\theta) &:= \arctan\left(\frac{z_d^\theta(\theta)}{y_d^\theta(\theta)}\right) \\ \sigma_d(\theta) &:= \arctan\left(\frac{-z_d^\theta(\theta)}{x_d^\theta(\theta)}\right) \\ \psi_d(\theta) &:= \arctan\left(\frac{y_d^\theta(\theta)}{x_d^\theta(\theta)}\right) \end{aligned} \tag{2.39}$$

which concludes the path generation.

Speed assignment: The speed assignment can be designed according to a desired path speed $u_d(t)$, as in (2.36), for the FRP. In $\mathbb{R}^3$ this gives

$$\upsilon_s(\theta, t) := \frac{u_d(t)}{\sqrt{x_d^\theta(\theta)^2 + y_d^\theta(\theta)^2 + z_d^\theta(\theta)^2}}. \tag{2.40}$$

Since in this case the AUVs are chosen to be aligned with the path, the speed $u_d(t)$ corresponds to a desired surge speed for the FRP. The desired surge speeds for the AUVs themselves, however, are slightly different according to their assigned positions in the formation. Indeed, using

$|u_d(t)| = \left|p_d^\theta(\theta(t))\right| |\upsilon_s(\theta(t),t)|$ we get that

$$\begin{aligned}
|\dot{p}_{d,i}(\theta(t))| &= \left|\dot{p}_d(\theta(t)) + \dot{R}\left(\Theta_d(\theta(t))\right)_f^e l_i\right| \\
&= \left|p_d^\theta(\theta(t)) + R^\theta\left(\Theta_d(\theta(t))\right)_f^e l_i\right| |\upsilon_s(\theta(t),t)| \\
&= \frac{\left|p_d^\theta(\theta(t)) + R^\theta\left(\Theta_d(\theta(t))\right)_f^e l_i\right|}{\left|p_d^\theta(\theta(t))\right|} |u_d(t)| = |u_{d,i}(t)|
\end{aligned}$$

showing that $u_{d,i}(t)$ is only equal to $u_d(t)$ for straight-line path segments where $R^\theta\left(\Theta_d(\theta)\right)_f^e = 0$. Nevertheless, note that only the common formation speed $u_d(t)$ is commanded to the formation. This will automatically ensure that the AUVs follow their individual paths with individual path speed $u_{d,i}(t)$.

Centralized or decentralized schemes

Notice that the motion of the AUVs in formation along the path $p_d(\theta)$ for the FRP is solely determined by the time evolution of the single path variable $\theta(t)$. In a sense this implies a centralized scheme, at least for the formation guidance system which determines the time evolution of $\theta(t)$. The individual control laws can be decentralized, but they will all depend on the common variable θ.

It is possible to also decentralize the formation guidance system. Having constructed the individual parallel paths (2.38) we can implement them with decentralized θ values, that is, for each AUV we assign an individual path variable θ_i. The formation objective is then solved for $\theta_i = \theta_j$, $\forall i,j \in \mathcal{I}$. The control laws must in this case ensure synchronization of all the path variables to solve the formation control objective.

Another constraint in this case is that the speed assignments between the vehicles must correspond. Recall that the speed assignment (2.40) corresponds to the FRP which is the same point for all vehicles only when they are synchronized. This means that $\upsilon_s(\theta_i,t)$ must be equal in value for all vehicles. A problem is that this depends on the current state of the individual path variables. To circumvent this, we choose a common speed assignment for all vehicles, that is,

$$\upsilon_s(\pi,t) := \frac{u_d(t)}{\sqrt{x_d^\theta(\pi)^2 + y_d^\theta(\pi)^2 + z_d^\theta(\pi)^2}} \tag{2.41}$$

where π is a common path variable. One choice is to let π be chosen as the average of the path variables,

$$\pi = \pi(\theta_1, \cdots, \theta_n) = \frac{1}{n}(\theta_1 + \theta_2 + \ldots + \theta_n).$$

If the formation has a leader vehicle with, say, index 1, another choice is to let $\pi = \pi(\theta_1, \cdots, \theta_n) = \theta_1$.

The formation setups presented here, including designs of control laws, will be discussed in more detail in Chapter 6.

2.5 Existence of a desired manifold

Consider the nonlinear system

$$\begin{aligned} \dot{x} &= f(x, \theta, t) \\ \dot{\theta} &= w(x, \theta, t) \\ y &= h(x), \end{aligned} \tag{2.42}$$

where $\forall t \geq t_0 \geq 0$, $x(t) \in \mathbb{R}^{nm}$, $\theta(t) \in \mathbb{R}$, and $y(t) \in \mathbb{R}^m$, and the functions $f(\cdot,\cdot,\cdot)$, $w(\cdot,\cdot,\cdot)$, and $h(\cdot)$ are smooth. Suppose (2.42) satisfies the maneuvering problem with θ as the path variable. Moreover, suppose $x = \xi(\theta, t)$ is uniquely determined by $h(x) = y_d(\theta)$ and the equations obtained by differentiating $h(x) = y_d(\theta)$ $n-1$ times along the solutions of (2.42) with $\dot{\theta} = \upsilon_s(\theta, t)$. Then, $\xi(\theta, t)$ is the *state path* corresponding to the *output path* $y_d(\theta)$ and speed assignment $\upsilon_s(\theta, t)$. This implies the requirement that $w(\xi(\theta, t), \theta, t) = \upsilon_s(\theta, t)$. Let $\gamma : \mathbb{R}^{nm} \to \mathbb{R}^{nm}$ be such that $z := \gamma(x - \xi(\theta, t))$ is a global change of coordinates, and let p represent t with $\dot{p} = 1$, $p(0) = t_0$; see Section 1.4.2. Then the maneuvering problem with a speed assignment is satisfied for (2.42) if the noncompact 'error' set

$$\mathcal{M} := \{(z, \theta, p) \in \mathbb{R}^{nm} \times \mathbb{R} \times \mathbb{R}_{\geq 0} : \ z = 0\} \tag{2.43}$$

is *uniformly asymptotically stable*. This set corresponds to a desired manifold in the state space $\mathbb{R}^{nm} \times \mathbb{R} \times \mathbb{R}_{\geq 0}$, given by $\{(x, \theta, p) : x - \xi(\theta, p) = 0\}$, which must be attractive and forward invariant for (2.42).

An example is given to illustrate this aspects of the maneuvering problem. In the absence of disturbances in the system, its objective is met by a forward invariant manifold of the closed-loop system.

2.5.1 Example: Manifold interpretation of a maneuvering objective

We investigate the nonlinear system

$$\begin{aligned} \dot{x}_1 &= x_2 + x_1^2 \\ \dot{x}_2 &= u \end{aligned} \tag{2.44}$$

where $u \in \mathcal{U}$ is the control with $\mathcal{U} = \{u \in \mathcal{L}_\infty^1 : \ \|u\| \leq 2\}$. It is required that:

1. the output $y = x_1$ converges to the path $y_d(\theta) = \sin(\theta)$,

2. the path angle θ converges to $t - \phi$, where the constant phase ϕ is left free (this corresponds to $\upsilon_s(\theta, t) = 1$).

The check feasibility, we differentiate $y_d(\theta) = \sin(\theta)$ twice with respect to time and substitute into (2.44). This gives the feasibility constraint differential equation

$$\cos(\theta)\ddot{\theta} - \sin(\theta)\dot{\theta}^2 - 2\sin(\theta)\cos(\theta)\dot{\theta} - u = 0 \tag{2.45}$$

which is on the form of (2.28). It can now be verified that for $u = u^* = -k^2\sin(\theta) - 2k\sin(\theta)\cos(\theta)$ where $k \in \mathbb{R}$ is a constant, then a solution to (2.45) is $\theta^*(t) = kt + \phi$ where ϕ is a constant. The geometric task is then feasible for all k such that $\|u^*\| \leq 2$ (all $|k| \leq 1.09$ satisfies this). It follows that the dynamic task is also feasible by choosing $k = 1$.

A dynamic state feedback controller designed using the backstepping methodology of Chapter 4.1 results in the closed-loop system

$$\begin{aligned} \dot{x}_1 &= x_2 + x_1^2 \\ \dot{x}_2 &= \alpha(x_1, x_2, \omega_s, \theta) \\ \dot{\omega}_s &= \chi(x_1, x_2, \omega_s, \theta) \\ \dot{\theta} &= 1 - \omega_s \end{aligned} \tag{2.46}$$

with two additional states: the path angle θ and the speed assignment error ω_s. The functions α and χ are designed to guarantee that in the state space $\mathbb{R}^4$ the closed-loop system (2.46) possesses a globally attractive, forward invariant manifold which meets the above requirements. To derive the expression of the desired forward invariant manifold we differentiate $y = x_1 = y_d(\theta) = \sin(\theta)$, get $\dot{x}_1 = x_2 + x_1^2 = \cos(\theta)\dot{\theta} = \cos(\theta)(1 - \omega_s)$, and

set the speed assignment error ω_s to zero. Thus, the desired manifold in $\mathbb{R}^4$ is

$$\left\{ (x_1, x_2, \omega_s, \theta) : \begin{array}{c} x_1 = \xi_1(\theta) = \sin(\theta), \\ x_2 = \xi_2(\theta) = \cos(\theta) - \sin(\theta)^2 \\ \omega_s = 0 \end{array} \right\} \tag{2.47}$$

where (ξ_1, ξ_2) defines the state path for (x_1, x_2). This one-dimensional manifold in $\mathbb{R}^4$ is to be made a globally attractive, forward invariant manifold of (2.46). A control law that achieves this is

$$u = -z_1 - z_2 - (2x_1 + 1)\,\dot{x}_1 + \left(y_d^{\theta}(\theta) + y_d^{\theta^2}(\theta) \right) \tag{2.48a}$$

$$\chi = -\omega_s - z_1 y_d^{\theta}(\theta) - z_2 \left[y_d^{\theta}(\theta) + y_d^{\theta^2}(\theta) \right] \tag{2.48b}$$

where $z_1 := x_1 - y_d(\theta)$ and $z_2 := z_1 + x_2 + x_1^2 - y_d^{\theta}(\theta)$. On the designed manifold, the motion of the closed-loop system is that of a harmonic oscillator, $x_1(t)^2 + \dot{x}_1(t)^2 = 1$, as required by $x_1(t) = y_d(\theta(t)) = \sin\theta(t)$ with $\dot{\theta}(t) = 1$. A typical trajectory in the space of (x_1, x_2, θ) is shown in Figure 2.8.

A further design step can be used to assign the phase ϕ, for example to $\phi = 0$. This corresponds to the time assignment $v_t(t) = t$, in addition to the constant speed assignment $v_s = 1$. Introducing $\omega_t = t - \theta$ we can substitute $\dot{\theta} = 1 - \omega_s$ in (2.46) with

$$\dot{\omega}_t = \omega_s, \tag{2.49}$$

and a new update law for $\dot{\omega}_s$ is selected as

$$\begin{aligned} \dot{\omega}_s &= \chi(x_1, x_2, \omega_s, \omega_t, \theta) \\ &= -\omega_s - \omega_t - z_1 y_d^{\theta}(\theta) - z_2 \left[y_d^{\theta}(\theta) + y_d^{\theta^2}(\theta) \right]. \end{aligned} \tag{2.50}$$

An application of Matrosov's Theorem, using $V_1 := \frac{1}{2}(z_1^2 + z_2^2 + \omega_t^2 + \omega_s^2)$ and $V_2 := \omega_t \omega_s$ in Theorem A.20, implies that the equilibrium $(z_1,\, z_2,\, \omega_t,\, \omega_s) = 0$ is UGAS, so that $\phi(t) \to 0$. This means that both the speed assignment $\dot{\theta}(t) \to 1$ and time assignment $\theta(t) \to t$ are satisfied in the limit as $t \to \infty$. Chapter 3.2 will show this extension in a more general design.

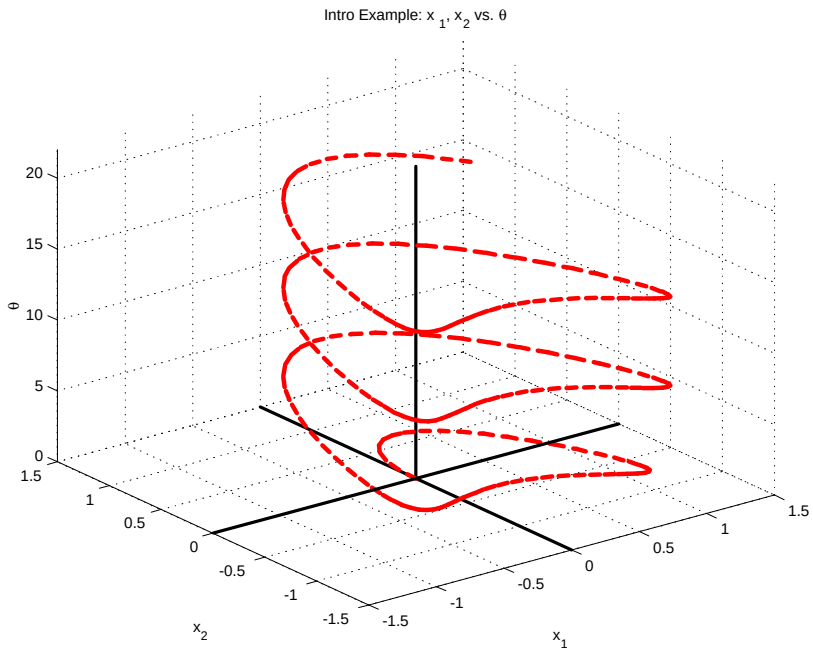

Figure 2.8: The trajectory of (2.46) with $x_1(0) = x_2(0) = \theta(0) = 0$.

Chapter 3

Maneuvering design with gradient optimization

As stated in the last chapter, the maneuvering problem involves two tasks called the geometric task and the dynamic task. While the main concern is to satisfy the geometric task, the dynamic task, further specified as a speed assignment, ensures that the system output follows the path with the desired speed. This chapter gives a design for solving the maneuvering problem for feedback linearizable systems. First the geometric part of the problem is solved. Then an update law is constructed that bridges the geometric part with the speed assignment to complete the design. The main ideas were published in Skjetne, Fossen and Kokotović (2002) and Skjetne, Teel and Kokotović (2002a,b).

Consider the nonlinear affine system

$$\dot{\chi} = f(\chi) + G(\chi)u \tag{3.1a}$$

$$y = h(\chi) \tag{3.1b}$$

where for each $t \geq 0$, $\chi(t) \in \mathbb{R}^{nm}$ is the state vector, $u(t) \in \mathbb{R}^m$ is the control, $y(t) \in \mathbb{R}^m$ is the output, and $f : \mathbb{R}^{nm} \to \mathbb{R}^{nm}$, $G : \mathbb{R}^{nm} \to \mathbb{R}^{nm \times m}$, and $h : \mathbb{R}^{nm} \to \mathbb{R}^m$ are smooth functions. Let the task be to solve the Maneuvering Control Objective for a desired continuously parametrized feasible path

$$\mathcal{P} := \{y \in \mathbb{R}^m : \ \exists \theta \in \mathbb{R} \text{ s.t. } y = y_d(\theta)\} \tag{3.2}$$

and a feasible speed assignment $v_s(\theta, t)$ for $\dot{\theta}$ along the path.

Assumption 3.1 *The following hold:*

1. *For $y_d(\theta) \in \mathcal{C}^n$ there exists $K < \infty$ such that $|y_d^{\theta^i}(\theta)| \leq K$ for all $\theta \in \mathbb{R}$ and $i \in \{0, 1, \ldots, n\}$.*

2. *For $\upsilon_s(\theta, t) \in \mathcal{C}^{n-1}$ there exists $L < \infty$ such that $|\upsilon_s^{\theta^i t^j}(\theta, t)| \leq L$ for all $(\theta, t) \in \mathbb{R} \times \mathbb{R}_{\geq 0}$ and $i, j \in \{0, 1, \ldots, n-1\}$.*

The Assumption 3.1 will be a standing assumption throughout the thesis.

3.1 Maneuvering design for feedback linearizable systems

Suppose the system (3.1) is input-output linearizable and that the vector relative degree adds up to nm (Isidori; 1995; Khalil; 2002). This means that the plant can be transformed into a chain of n integrators

$$y^{(n)} = \Phi(\chi)\left[u - \rho(\chi)\right] \tag{3.3}$$

where $\Phi : \mathbb{R}^{nm} \to \mathbb{R}^{m \times m}$ and $\rho : \mathbb{R}^{nm} \to \mathbb{R}^m$ are well-defined on $\mathbb{R}^{nm}$ and $\Phi(\chi)$ is nonsingular for all $\chi \in \mathbb{R}^{nm}$. This plant can then alternatively be written in the first order state space form as

$$\dot{x} = A_c x + B_c \Phi(\chi)\left[u - \rho(\chi)\right] \tag{3.4a}$$

$$y = C_c x \tag{3.4b}$$

where $x = \mathrm{col}(y, \dot{y}, \ldots, y^{(n-1)})$, and (A_c, B_c, C_c) is in vectorial Brunovsky (1970) canonical form, representing a chain of integrators.

Let the vector function $\xi : \mathbb{R} \times \mathbb{R}_{\geq 0} \to \mathbb{R}^{nm}$ be determined by differentiating $y = y_d(\theta)$ with respect to time $n-1$ times and substituting $\dot{\theta} = \upsilon_s(\theta, t)$ in each step. In other words, we set:

$$\begin{aligned}
\xi_1(\theta, t) &:= y_d(\theta) \\
\xi_2(\theta, t) &:= \xi_1^\theta(\theta, t)\upsilon_s(\theta, t) + \xi_1^t(\theta, t) = y_d^\theta(\theta)\upsilon_s(\theta, t) \\
\xi_3(\theta, t) &:= \xi_2^\theta(\theta, t)\upsilon_s(\theta, t) + \xi_2^t(\theta, t) \\
&\quad = y_d^{\theta^2}(\theta)\upsilon_s(\theta, t)^2 + y_d^\theta(\theta)\upsilon_s^\theta(\theta, t)\upsilon_s(\theta, t) + y_d^\theta(\theta)\upsilon_s^t(\theta, t) \\
&\quad \vdots \\
\xi_n(\theta, t) &:= \xi_{n-1}^\theta(\theta, t)\upsilon_s(\theta, t) + \xi_{n-1}^t(\theta, t)
\end{aligned}$$

and define

$$\xi(\theta, t) := \mathrm{col}\left(\xi_1(\theta, t), \xi_2(\theta, t), \xi_3(\theta, t), \ldots, \xi_n(\theta, t)\right), \tag{3.5}$$

which we call, perhaps with an abuse of notation, the *state path* for x.

Let p represent the 'explicit' time t, with $\dot{p} = 1$, $p(0) = t_0$. A sufficient condition for solving the maneuvering problem of driving $y(t) \to y_d(\theta(t))$ and $\dot{\theta}(t) \to \upsilon_s(\theta(t), p(t))$ is to make the manifold $x - \xi(\theta, p) = 0$ in $\mathbb{R}^{nm} \times \mathbb{R} \times \mathbb{R}_{\geq 0}$ stable and globally attractive. This is verified by differentiating $y \equiv y_d(\theta)$ to get $y_d^\theta(\theta)\dot{\theta} = \dot{y} = x_2 = \xi_2(\theta, p) = y_d^\theta(\theta)\upsilon_s(\theta, p)$ which holds for all (θ, p) and thus shows[1] that $\dot{\theta} = \upsilon_s(\theta, p)$ along the solution $x(t) = \xi(\theta(t), p(t))$. Consequently, rendering the set

$$\mathcal{M}_0 = \{(x, \theta, p) \in \mathbb{R}^{nm} \times \mathbb{R} \times \mathbb{R}_{\geq 0} : \; x - \xi(\theta, p) = 0\} \tag{3.6}$$

UGAS will solve the maneuvering problem.

3.1.1 Control design procedure

In the design we will use the 'explicit' time t directly. We proceed for (3.4a) by choosing the linearizing control

$$u = \rho(\chi) + \Phi(\chi)^{-1} \left[v + \xi_n^\theta(\theta, t)\upsilon_s(\theta, t) + \xi_n^t(\theta, t) \right] \tag{3.7}$$

which transforms (3.4a) into the system

$$\dot{x} = A_c x + B_c \left[v + \xi_n^\theta(\theta, t)\upsilon_s(\theta, t) + \xi_n^t(\theta, t) \right]$$

that is linear in x and v, where v is a new control variable and the last two terms, inside the bracket, are necessary feed-forward terms. To complete the geometric task, we choose the linear control

$$v = -K \left(x - \xi(\theta, t) \right), \tag{3.8}$$

set $A = A_c - B_c K$, and use the fact that $\xi_i(\theta, t) = \xi_{i-1}^\theta(\theta, t)\upsilon_s(\theta, t) + \xi_{i-1}^t(\theta, t)$ for $i = 2, \ldots, n$. The result is the closed-loop system

$$\dot{x} = A \left(x - \xi(\theta, t) \right) + \xi^\theta(\theta, t)\upsilon_s(\theta, t) + \xi^t(\theta, t) \tag{3.9}$$

for which the last two terms set the desired motion along the path.

Since (A_c, B_c) is a controllable pair we choose the gain matrix $K \in \mathbb{R}^{m \times nm}$ so that A is Hurwitz. Let $P = P^\top > 0$ solve the Lyapunov equation

[1] Except for the case $y_d^\theta(\theta) \equiv 0$ when the path $y_d(\theta)$ is reduced to a fixed point.

$PA + A^\top P = -Q$ where $Q = Q^\top > 0$ is selected by design. A Lyapunov function candidate for (3.9) is then the quadratic function

$$V(x, \theta, t) := (x - \xi(\theta, t))^\top P (x - \xi(\theta, t)). \tag{3.10}$$

The time-derivative of V along the solutions of (3.9) and $\dot{\theta}$ becomes

$$\begin{aligned}\dot{V} &= V^x(x, \theta, t)\dot{x} + V^\theta(x, \theta, t)\dot{\theta} + V^t(x, \theta, t) \\ &= 2 (x - \xi(\theta, t))^\top P \left[A (x - \xi(\theta, t)) + \xi^\theta(\theta, t)\upsilon_s(\theta, t) + \xi^t(\theta, t)\right] \\ &\quad + V^\theta(x, \theta, t)\dot{\theta} + V^t(x, \theta, t) \\ &= - (x - \xi(\theta, t))^\top Q (x - \xi(\theta, t)) - V^\theta(x, \theta, t)\omega_s \end{aligned} \tag{3.11}$$

where $\omega_s := \upsilon_s(\theta, t) - \dot{\theta}$ is the speed assignment error, and

$$\begin{aligned} V^x(x, \theta, t)\xi^t(\theta, t) &= -V^t(x, \theta, t) = 2 (x - \xi(\theta, t))^\top P\xi^t(\theta, t), \\ V^x(x, \theta, t)\xi^\theta(\theta, t) &= -V^\theta(x, \theta, t) = 2 (x - \xi(\theta, t))^\top P\xi^\theta(\theta, t) \end{aligned}$$

were used.

It is convenient to introduce the error function $z : \mathbb{R}^{nm} \times \mathbb{R} \times \mathbb{R}_{\geq 0} \to \mathbb{R}^{nm}$, $z = z(x, \theta, t) := x - \xi(\theta, t)$ and apply the global diffeomorphism $(x, \theta, t) \mapsto (z, \theta, t)$. In these new coordinates the closed-loop system becomes

$$\dot{z} = Az + \xi^\theta(\theta, t)\omega_s \tag{3.12a}$$

$$\dot{\theta} = \upsilon_s(\theta, t) - \omega_s, \tag{3.12b}$$

and the set (3.6) is equivalent to the set

$$\mathcal{M} := \{(z, \theta, t) \in \mathbb{R}^{nm} \times \mathbb{R} \times \mathbb{R}_{\geq 0} : \ z = 0\}, \tag{3.13}$$

which has the simplifying distance-to-the-set function $|(z, \theta, t)|_{\mathcal{M}} = |z|$.

By rewriting the Lyapunov function (3.10) as $V(z) = z^\top Pz$, we get the Lyapunov bounds

$$\lambda_{\min}(P) |(z, \theta, t)|^2_{\mathcal{M}} \leq V(z) \leq \lambda_{\max}(P) |(z, \theta, t)|^2_{\mathcal{M}} \tag{3.14a}$$

$$\dot{V} \leq -\lambda_{\min}(Q) |(z, \theta, t)|^2_{\mathcal{M}} + \tau(z, \theta, t)\omega_s \tag{3.14b}$$

where

$$\tau(z, \theta, t) := -V^z(z)z^\theta = -V^\theta(x, \theta, t) = 2z^\top P\xi^\theta(\theta, t). \tag{3.15}$$

Up to this point the control law has been designed based on the certainty equivalence assumption that $\dot{\theta} = \upsilon_s(\theta, t)$. The fact that this equality is

not satisfied identically is captured by the last sign-indefinite term $\tau\omega_s$ in (3.14b). This upper bound on $\dot{V}$ will be used to bridge the geometric task with the dynamic task by rendering the term $\tau(z,\theta,t)\omega_s$ nonpositive. The relationship (3.14b) is thus the principal design inequality for finishing the design, and it will be frequently encountered in the maneuvering designs proposed in this thesis.

3.1.2 Closing the loop by direct speed assignment designs

Recall the dynamic part of the control law (3.12b) for which the design variable is ω_s. Rendering the term $\tau(z,\theta,t)\omega_s$ in (3.14b) nonpositive for all $t \geq t_0 \geq 0$ results in a negative semi-definite $\dot{V}$ and thus solves the Maneuvering Problem.

Theorem 3.2 *The set $\mathcal{M}$ in (3.13) is UGES for the closed-loop system (3.12) for every continuous function $\omega_s = \omega(z,\theta,t)$ that satisfies:*

1. *there exists a continuous positive semi-definite function $\sigma : \mathbb{R}^{nm} \to \mathbb{R}_{\geq 0}$, $\sigma(0) = 0$, such that $|\omega(z,\theta,t)| \leq \sigma(z)$, $\forall\,(z,\theta,t) \in \mathbb{R}^{nm} \times \mathbb{R} \times \mathbb{R}_{\geq 0}$, and*

2. *$\tau(z,\theta,t)\omega(z,\theta,t) \leq 0, \quad \forall\,(z,\theta,t) \in \mathbb{R}^{nm} \times \mathbb{R} \times \mathbb{R}_{\geq 0}$.*

Proof. *Let $\dot{p} = 1$, $p(0) = t_0$ s.t. $p(t) = t + t_0$. The closed-loop system (3.12), with $\omega_s = \omega(z,\theta,p)$, is of the form of the interconnected system (A.40) in Appendix A by setting $x_1 := z$, $x_2 := (\theta, p)$, and $u_1 = u_2 = 0$. Defining, according to (A.40), $f_1 := Az + \xi^{\theta}(\theta,p)\omega(z,\theta,p)$ and $f_2 := \mathrm{col}\,(\upsilon_s(\theta,p) - \omega(z,\theta,p),\ 1)$ then f_2 satisfies Lemma A.21 since $|\omega(z,\theta,p)| \leq \sigma(z)$ is uniformly bounded for all z in the compact set $\mathcal{X}$. Moreover, since (3.14) satisfies (A.44) and (A.45) with $|(z,\theta,p)|_{\mathcal{M}} = |z| = |x_1|_{\mathcal{A}_1}$ then the conclusion of Theorem A.22 gives UGAS of $\mathcal{M}$.* ■

Satisfying Conditions *1* and *2* of Theorem 3.2 for ω_s is accomodated by one of the choices, the *Tracking* or the *Gradient update laws*:

1. Tracking update law: Setting $\omega_s \equiv 0$ satisfies Conditions *1* and *2* and the speed assignment (2.20) identically. The dynamic part of the control law becomes the time-varying reference system

$$\dot{\theta} = \upsilon_s(\theta, t) \tag{3.16}$$

which, through $y_d(\theta)$, sets the desired motion along the path $\mathcal{P}$. This method is thus used to achieve tracking of the desired output $\tilde{y}_d(t) := y_d(\theta(t))$ where (3.16) is integrated to get $\theta(t) = \theta(t_0) + \int_{t_0}^{t} \upsilon_s(\theta(\tau), \tau) d\tau$.

2. Gradient update law: Setting $\omega_s = -\mu\tau(z, \theta, t)$, $\mu \geq 0$, satisfies Conditions *1* and *2* of Theorem 3.2 with $\sigma(z) := 2M\lambda_{\max}(P)\,|z|$ where $M := \sup_{(\theta,t)} \left|\xi^{\theta}(\theta, t)\right|$ exists by Assumption (3.1). We call this a *Gradient update law* because $\tau(z, \theta, t) = -\frac{\partial V}{\partial \theta}(x, \theta, t)$ where $x = z + \xi(\theta, t)$, and the dynamic part of the control law becomes

$$\begin{aligned} \dot{\theta} &= \upsilon_s(\theta, t) + \mu\tau(z, \theta, t) \\ &= \upsilon_s(\theta, t) - \mu V^{\theta}(x, \theta, t). \end{aligned} \tag{3.17}$$

Important properties of this update law are discussed in Section 3.4. Next, we return to the example in Section 2.5.1 and use feedback linearization to solve the maneuvering control objective illustrated there:

Example 3.1 *We reconsider the plant investigated in Section 2.5.1,*

$$\begin{aligned} \dot{x}_1 &= x_2 + x_1^2 \\ \dot{x}_2 &= u, \end{aligned}$$

and the Maneuvering Problem with $y_d(\theta) = \sin\theta$ and $\upsilon_s(\theta, t) = 1$. The plant is of relative degree two for $y = x_1$, so that differentiating y twice gives

$$\ddot{y} = u + 2x_1x_2 + 2x_1^3 =: u - \rho(x)$$

which is of the form of (3.3). The state path for $(y, \dot{y})$ becomes

$$\xi(\theta) = \begin{bmatrix} y_d(\theta) \\ y_d^{\theta}(\theta)\upsilon_s \end{bmatrix} = \begin{bmatrix} \sin\theta \\ \cos\theta \end{bmatrix},$$

and according to the above design we get, with a gradient update law, the control law

$$\begin{aligned} u &= \rho(x) - k_1\,(y - \sin\theta) - k_2\,(\dot{y} - \cos\theta) - \sin\theta, \\ \dot{\theta} &= 1 - \mu_1 V^{\theta}(y, \dot{y}, \theta), \end{aligned}$$

where $k_1, k_2 > 0$,

$$V(y, \dot{y}, \theta) := \begin{bmatrix} y - \sin\theta \\ \dot{y} - \cos\theta \end{bmatrix}^{\top} P \begin{bmatrix} y - \sin\theta \\ \dot{y} - \cos\theta \end{bmatrix}$$

using $PA + A^\top P = -I$, *and*

$$A := \begin{bmatrix} 0 & 1 \\ -k_1 & -k_2 \end{bmatrix}.$$

This will ensure that the set

$$\mathcal{M}_0 = \{(y, \dot{y}, \theta) : \ y = \sin\theta, \ \dot{y} = \cos\theta\},$$

becomes globally attractive and forward invariant for the closed-loop system. This set corresponds to a one-dimensional manifold in $\mathbb{R}^3$, *with motion of a harmonic oscillator, that meets the requirement of the maneuvering objective.*

3.1.3 Closing the loop by filtered speed assignment designs

As an alternative to the direct designs in the last section, where ω_s was assigned to a static function, we can instead apply a filtered design. Let $\omega \in \mathbb{R}^q$, $q \geq 1$, be the state vector in the linear filter

$$\begin{aligned} \dot{\omega} &= A_\omega \omega + v \\ \omega_s &= c_\omega^\top \omega \end{aligned} \tag{3.18}$$

where $A_\omega \in \mathbb{R}^{q\times q}$ is a Hurwitz matrix satisfying the Lyapunov equation $P_\omega A_\omega + A_\omega^\top P_\omega = -Q_\omega$ for $Q_\omega = Q_\omega^\top > 0$, whereas $c_\omega^\top \in \mathbb{R}^{1\times q}$ is an output row vector such that $\left(c_\omega^\top, A_\omega\right)$ is an observable pair, and v is an input to be designed. When V in (3.14) is augmented to

$$W(\omega, z) := V(z) + \omega^\top P_\omega \omega,$$

its derivative becomes

$$\begin{aligned} \dot{W} &= \dot{V} + \dot{\omega}^\top P_\omega \omega + \omega^\top P_\omega \dot{\omega} \\ &= -z^\top Q z + \tau(z, \theta, t)\omega_s - \omega^\top Q_\omega \omega + 2\omega^\top P_\omega v \\ &= -z^\top Q z - \omega^\top Q_\omega \omega + \omega^\top \left[c_\omega \tau(z, \theta, t) + 2P_\omega v\right]. \end{aligned}$$

To make the last term vanish we choose the input function for v as

$$v = -\frac{1}{2} P_\omega^{-1} c_\omega \tau(z, \theta, t), \tag{3.19}$$

which substituted into (3.18) gives the dynamic part of the control law

$$\begin{aligned} \dot{\theta} &= \upsilon_s(\theta, t) - c_\omega^\top \omega \\ \dot{\omega} &= A_\omega \omega - \tfrac{1}{2} P_\omega^{-1} c_\omega \tau(z, \theta, t). \end{aligned} \tag{3.20}$$

This is called a *Filtered-gradient update law* because the negative gradient $\tau = -V^{\theta}(x, \theta, t)$ is filtered (in the Laplace domain) by $\omega_s(s) = -H(s)\tau(s)$ where $H(s) := \frac{1}{2} c_\omega^\top (sI - A_\omega) P_\omega^{-1} c_\omega$ is a stable SISO transfer function. The cut-off frequency of this filter is an important design parameter to mitigate state measurement noise versus bandwidth.

Since the total state space has been extended with $\mathbb{R}^q$, we now consider the set

$$\mathcal{M}' := \{(z, \omega, \theta, p) \in \mathbb{R}^{nm} \times \mathbb{R}^q \times \mathbb{R} \times \mathbb{R}_{\geq 0} : \ z = 0, \omega = 0\} \tag{3.21}$$

for solving the maneuvering problem, where $\dot{p} = 1$, $p(0) = t_0$. Clearly, $z = 0$ solves the Geometric task, while $\omega = 0 \Rightarrow \omega_s = 0$ solves the Dynamic task. We summarize the result in Theorem 3.3. The proof is left as an exercise for the reader.

Theorem 3.3 *The closed, forward invariant set (3.21) is UGES with respect to the closed-loop system (3.12a) and (3.20), and this solves the Maneuvering Problem.*

Note that the filter $H(s)$ is strictly positive real since the state space realization $\left(A_\omega, \frac{1}{2} P_\omega^{-1} c_\omega, c_\omega^\top, 0\right)$ satisfies the Kalman-Yakubovich-Popov lemma[2], and consequently, the filter is strictly passive with storage function $U = \omega^\top P_\omega \omega$.

It is also noticed that the Filtered-gradient update law proposed in Skjetne, Fossen and Kokotović (2004) and Skjetne, Fossen and Kokotović (2005) is the 1st order case of (3.20) by setting $q = 1$, $A_\omega = -\lambda$, $c_\omega = 1$, $P_\omega = \frac{1}{2\lambda\mu}$, and $Q_\omega = \frac{1}{\mu}$ to get the filter $H(s) = \mu \frac{\lambda}{s+\lambda}$.

3.1.4 Resulting closed-loop system

The designed closed-loop system can be divided into four parts, the *Plant*, the *Measurement system*, the *Maneuvering controller*, and the *Guidance system*, according to Section 1.3. As shown in Table 3.1, the controller incorporates the dynamic control law (here without phase assignment), and provides the control signal u to the plant and the state θ to the guidance system. The guidance system generates the state path $\xi(\theta, t)$, the speed assignment $v_s(\theta, t)$, and their partial derivatives. The path definition $y_d(\theta)$ must be specified a priori, while the speed assignment along the path can

Table 3.1: Closed-loop maneuvering system for feedback linearizable systems

Plant :
$\dot{x} = A_c x + B_c \Phi(\chi)\,[u - \rho(\chi)]$
$y = C_c x$
input: $\{u\}$
output: $\{y, x\}$ and/or $\{y, \chi\}$
Control :
$\dot{\theta} = \upsilon_s(\theta) - \omega_s$
$\dot{\omega} = A_\omega \omega - \frac{1}{2} P_\omega^{-1} c_\omega \tau(z, \theta, t)$
$\omega_s = \begin{cases} -\mu\tau(z,\theta,t) & \text{Gradient} \\ c_\omega^\top \omega & \text{Filtered-gradient} \end{cases}$
$u = \rho(\chi) + \Phi(\chi)^{-1}\left[-K\,(x - \xi(\theta,t)) + \xi_n^\theta(\theta,t)\upsilon_s(\theta,t) + \xi_n^t(\theta,t)\right]$
input: $\left\{x, \xi(\theta,t), \xi_n^\theta(\theta,t), \xi_n^t(\theta,t), \upsilon_s(\theta)\right\}$
output: $\{u, \theta\}$
Guidance :
input: $\{\theta, t\}$
output: $\left\{\xi(\theta,t), \xi_n^\theta(\theta,t), \xi_n^t(\theta,t), \upsilon_s(\theta)\right\}$

be modified online (which accounts for the t-dependence in $\upsilon_s(\cdot, t)$).

The maneuvering design is concluded with the choice of any of the direct or filtered speed assignment designs. The different update laws all provide different properties to the closed-loop system. These properties are further explored in Section 3.4 and also by the experimental results in Chapter 5.

3.2 Phase assignment

Suppose that the path $y_d(\theta)$ is constructed such that with the tracking update law $\dot{\theta} = \upsilon_s(\theta, t)$, or in other words,

$$\theta(t) = \theta(t_0) + \int_{t_0}^{t} \upsilon_s(\theta(\tau), \tau) d\tau,$$

then $y_0 = y_d(\theta(t_0))$ is the starting position at time $t = t_0$ and $y_T = y_d(\theta(T))$ is the final position at time $t = T > t_0$. In some guidance applications, this

[2] Choose $\varepsilon > 0$ sufficiently small such that $Q_\omega - \varepsilon P_\omega$ is symmetric positive definite. Perform then a Cholesky factorization to get $Q_\omega - \varepsilon P_\omega = L^\top L$, and set $Q_\omega = L^\top L + \varepsilon P_\omega$ in $P_\omega A_\omega + A_\omega^\top P_\omega = -Q_\omega$, and use this in Lemma 6.3 in Khalil (2002).

time specification along the path, or specifically the arrival time T at the destination y_T, is important. Using the gradient or filtered gradient update laws result in a phase shift of $\theta(t)$ as compared to using the tracking update law. This is verified by

$$\theta(t) = \theta(t_0) + \int_{t_0}^{t} v_s(\theta(\tau), \tau)d\tau - \int_{t_0}^{t} \omega_s(\tau)d\tau,$$

giving the phase $\phi(t) = \int_{t_0}^{t} \omega_s(\tau)d\tau$ for which a limit exists since the convergence of $\omega_s(t) \to 0$ is exponential.

It may be of interest to apply a gradient update law in the design, but at the same time control the phase ϕ to a desired constant phase ϕ_d, perhaps $\phi_d = 0$. This is similar to the objective in Hindman and Hauser (1996), but here we will solve it in a CLF approach. Doing so, we let $\omega_t := \phi - \phi_d$ be the phase error. Then

$$\omega_t(t) = \int_{t_0}^{t} \omega_s(\tau)d\tau - \phi_d = \theta(t_0) + \int_{t_0}^{t} v_s(\theta(\tau), \tau)d\tau - \theta(t) - \phi_d$$

has the derivative

$$\dot{\omega}_t = v_s(\theta, t) - \dot{\theta} = \omega_s. \tag{3.22}$$

The Lyapunov function V is now augmented to

$$W(z, \omega_t) := V(z) + \frac{\mu_0}{2}\omega_t^2 = z^\top P z + \frac{\mu_0}{2}\omega_t^2, \tag{3.23}$$

$\mu_0 > 0$, and using (3.11) the derivative becomes

$$\dot{W} = -z^\top Q z - \left(V^\theta - \mu_0\omega_t\right)\omega_s = -z^\top Q z - V_2^\theta \omega_s \tag{3.24}$$

for which it can be verified that $\frac{\partial W}{\partial \theta} = V^z(z)z^\theta + \mu_0\omega_t\omega_t^\theta = V^\theta - \mu_0\omega_t$ according to (3.15). Hence, both the Gradient or Filtered-Gradient update laws can be constructed as before, to obtain the new feature that $\omega_t(t) \to 0$ as $t \to \infty$. Maneuvering with phase assignment is therefore achieved by the following result:

Theorem 3.4 *For the closed-loop system*

$$\begin{aligned} \dot{z} &= Az + \xi^\theta(\theta, t)\omega_s \\ \dot{\omega}_t &= \omega_s \end{aligned} \tag{3.25}$$

and the Lyapunov function (3.10) the following hold:

1. ***Gradient update law:*** *Setting*

$$\omega_s = \mu_1 \left(V^\theta - \mu_0 \omega_t \right), \quad \mu_1 > 0, \tag{3.26}$$

renders the equilibrium $(z, \omega_t) = 0$ *UGES.*

2. ***Filtered-gradient update law:*** *Setting*

$$\dot{\omega}_s = -\lambda \omega_s + \lambda \mu_1 \left(V^\theta - \mu_0 \omega_t \right), \quad \mu_1 > 0, \tag{3.27}$$

renders the equilibrium $(z, \omega_t, \omega_s) = 0$ *UGAS.*

Proof. *1. Substituting (3.26) and (3.15) into (3.24) gives*

$$\begin{aligned} \dot{W} &= -z^\top Q z - \mu_1 \left(V^\theta - \mu_0 \omega_t \right)^2 \\ &= -z^\top Q z - \mu_1 \left(2 z^\top P \xi^\theta(\theta, t) + \mu_0 \omega_t \right)^2 =: -Y_0(z, \omega_t, \theta, t) \end{aligned}$$

Let $\zeta := \mathrm{col}(z, \omega_t)$. *Claim:* $\exists c > 0$ *such that* $c\zeta^\top \zeta \leq Y_0(\zeta, \theta, t)$, $\forall (\theta, t)$. *Proof:*

$$\begin{aligned} Y_0(z, \omega_t, \theta, t) &= z^\top Q z + \mu_1 \left(2 z^\top P \xi^\theta(\theta, t) + \mu_0 \omega_t \right)^2 \\ &= z^\top Q z + \mu_1 \left[4 z^\top P \xi^\theta(\theta, t) \xi^\theta(\theta, t)^\top P z + 4 \mu_0 \omega_t \xi^\theta(\theta, t)^\top P z + \mu_0^2 \omega_t^2 \right] \\ &= \mu_1 \zeta^\top H(\theta, t) \zeta \end{aligned}$$

where

$$H(\theta, t) = \begin{bmatrix} \frac{1}{\mu_1} Q + 4 P \xi^\theta(\theta, t) \xi^\theta(\theta, t)^\top P & 2 \mu_0 P \xi^\theta(\theta, t) \\ 2 \mu_0 \xi^\theta(\theta, t)^\top P & \mu_0^2 \end{bmatrix}.$$

Since $H(\theta, t)$ *is symmetric positive definite and* $\xi^\theta(\theta, t)$ *is bounded (the smallest eigenvalue would tend to zero if* ξ^θ *would increase to infinity), there exists* $c > 0$, $c \leq \mu_1 \inf_{(\pi, \tau)} \lambda_{\min} \left(H(\pi, \tau) \right)$ *such that* $\mu_1 \zeta^\top H(\theta, t) \zeta \geq c \zeta^\top \zeta$, $\forall (\theta, t)$.
UGES of $(z, \omega_t) = 0$ *follows then as a consequence of the quadratic Lyapunov function (3.23) and its derivative* $\dot{W} = -\mu_1 \zeta^\top H(\theta, t) \zeta \leq -c \zeta^\top \zeta$.

2. For the Lyapunov function $W_1 = z^\top P z + \frac{\mu_0}{2} \omega_t^2 + \frac{1}{2 \lambda \mu_1} \omega_s^2$, *the time-derivative is*

$$\dot{W}_1 = -z^\top Q z - \frac{1}{\mu_1} \omega_s^2 =: Y_1(z, \omega_s, \omega_t) \leq 0$$

which implies UGS of $(z, \omega_t, \omega_s) = 0$. *Define* $W_2(z, \omega_t, \omega_s) := \omega_t \omega_s$. *Differentiating* W_2 *along the trajectories of (3.25) and (3.27) gives* $\dot{W}_2 = Y_2(z, \omega_s, \omega_t, \rho(t))$ *with*

$$Y_2 := \omega_s^2 - \lambda \omega_t \omega_s - \lambda \mu_0 \mu_1 \omega_t^2 - 2\lambda \mu_1 \omega_t z^\top P \rho(t)$$

where (3.15) was used and $\rho(t) := \xi^\theta(\theta(t), t)$ *is bounded by assumption. We get that* $Y_1 = 0 \Rightarrow Y_2 \leq 0$ *for all bounded* (z, ω_t, ω_s) *and further that* $Y_1 = Y_2 = 0 \Leftrightarrow (z, \omega_t, \omega_s) = 0$. *All the assumptions of Matrosov's Theorem as stated in Theorem A.20 are then satisfied, and* $(z, \omega_t, \omega_s) = 0$ *is UGAS.* ■

Note that the filtered-gradient update law chosen here was the 1st order version of the proposed filter in the previous section.

3.3 The projection-type update law

For comparison to the proposed update laws in the previous sections, Hauser and Hindman (1995) constructed a desired state path $\xi(\theta)$ for[3] the full state x and proposed using a numerical projection algorithm from the current state $x(t)$ onto the path. To achieve this they fixed x and considered the minimization problem

$$\min_{\theta \in \mathbb{R}} \left\{ \theta \mapsto V(x, \theta) := (x - \xi(\theta))^\top P (x - \xi(\theta)) \right\} \tag{3.28}$$

where $P = P^\top > 0$ and $\xi(\theta)$ is sufficiently smooth. The cost function V may have multiple extrema with respect to θ (Skjetne, Teel and Kokotović; 2002b). However, suppose sufficient conditions are met so that the function

$$\pi(x) := \arg\min_{\theta \in \mathbb{R}} V(x, \theta) \tag{3.29}$$

exists and is a global minimizer for (3.28). A necessary condition is then that $V^\theta(x, \pi(x)) = 0$ for all feasible x. Hence, by setting

$$\theta(t) := \pi(x(t)), \quad \forall t \geq 0, \tag{3.30}$$

then $V^\theta(x(t), \theta(t))\omega_s(t) = 0$, $\forall t \geq 0$, such that (3.11) becomes negative definite and the maneuvering problem is solved.

[3] The path in (Hauser and Hindman; 1995) was obtained from an assumed available time-parametrized desired trajectory $\tilde{\xi}(t)$ for the state x, and substituting $t \leftrightarrow \theta$ to get $\xi(\theta) := \tilde{\xi}(\theta)$. Their speed assignment was then simply $v_s = 1$.

This is an alternative to the previously proposed update laws. Instead of using ω_s as the design variable to ensure that $V^\theta \omega_s$ in (3.11) is non-negative, this method ensures directly that $V^\theta(x, \theta) = 0$. However, since this method, as described in Hauser and Hindman (1995), relies upon using a numerical projection to solve (3.28), the implementation becomes more complicated (hybrid). In addition, the topological restrictions imposed on the path to ensure that (3.29) is well-defined, is rather strong. For instance, Hindman and Hauser (1996) preclude self-intersecting paths to avoid multiple global minima and further require that $\xi^\theta(\theta)$ is bounded away from zero. An example of a path that fails to satisfy both those restrictions is

$$\xi(\theta) = \begin{bmatrix} \sin(\theta)^3 \\ 3\sin(\theta)^2\cos(\theta) \end{bmatrix}$$

since, for this path, $\xi(0) = \xi(\pm 180\,^\circ) = \xi(\pm 360\,^\circ) = \ldots$ and $\xi^\theta(0) = \xi^\theta(\pm 180\,^\circ) = \xi^\theta(\pm 360\,^\circ) = \ldots = 0$. This path will specifically be used as a design example in Section 3.4.3 to illustrate that these restrictions do not apply when using the dynamic gradient algorithms.

3.4 Gradient optimization

In this section we let the speed assignment, for simplicity, be $v_s(\theta)$, independent of t, so that the state path (3.5) becomes $\xi(\theta)$, also independent of t. However, the implications of the results are also valid for many time-varying closed-loop systems, especially those cases for which the time-dependence enter through bounded functions.

The above proposed control law, (3.7) and (3.8), constitutes a stabilization algorithm that drives the state $x(t)$ to the point $\xi(\theta(t))$, while the gradient update law (3.17) is a smooth dynamic optimization algorithm that selects the point $\xi(\theta)$ that minimizes the weighted distance between x and ξ. Within this control structure, a separation of time scales can be induced between the task of selecting the point on the path closest to the state, and the task of driving the state towards the path. In addition to uniform global convergence to the path, which is achieved without a separation of time scales, the separation of time scales allows us to achieve *near forward invariance* of the path from a large range of initial conditions. The consepts of *near forward invariance* and *near stability* will become clear in the following sections.

The idea is first illustrated on a simple double integrator with the path corresponding to the unit circle, then it is discussed in general for the feed-

back linearizable systems considered in this chapter, and finally an example for a self-intersecting "figure-8" path illustrates the achieved performance.

3.4.1 Motivating example: The double integrator and stabilization of the unit circle

We consider the double integrator

$$\begin{aligned} \dot{x}_1 &= x_2 \\ \dot{x}_2 &= u \end{aligned} \tag{3.31}$$

and the task of stabilizing the path

$$\mathcal{P} := \left\{ x \in \mathbb{R}^2 : x^\top x = 1 \right\} \tag{3.32}$$

without creating any equilibria in $\mathcal{P}$. By converse Lyapunov theory (Teel and Praly; 2000) there does not exist a continuous or discontinuous time-invariant state feedback control that renders the unit circle GAS[4]. The reasoning is this: If such a feedback existed there would exist a smooth Lyapunov function demonstrating GAS of the circle. In particular, this function would be positive definite with respect to the circle and would have a directional derivative, in the direction of the closed-loop vector field, that is negative definite with respect to the circle. The Lyapunov function would obtain its minimum on the circle, and it would therefore have a maximum inside the circle. At the maximum, its gradient would be zero and so the directional derivative in the direction of the closed-loop could not be negative. So there must not be a Lyapunov function, which implies that GAS cannot be achieved by such a control.

An alternative is to try to stabilize the set

$$\mathcal{A} := \left\{ (x, \theta) : x - \begin{bmatrix} \cos\theta \\ -\sin\theta \end{bmatrix} = 0 \right\} \tag{3.33}$$

for the system (3.31) and

$$\dot{\theta} = 1. \tag{3.34}$$

A control rendering the set $\mathcal{A}$ GAS will steer (x, θ) to the set $\mathcal{P} \times \mathbb{R}$ since

$$\begin{bmatrix} \cos\theta \\ -\sin\theta \end{bmatrix}^\top \begin{bmatrix} \cos\theta \\ -\sin\theta \end{bmatrix} = 1$$

[4] In the case of discontinuous feedback, this statement applies when the solution concept used is that due to Filippov; for example, see Filippov (1988).

and[5] thus $\mathcal{A} \subset \mathcal{P} \times \mathbb{R}$. However, choosing to stabilize $\mathcal{A}$ under the constraint (3.34) may introduce large transients in the distance to $\mathcal{P} \times \mathbb{R}$. In an attempt to control these transients, we will consider controlling θ as well. Therefore, we consider the control

$$\begin{aligned} \dot{\theta} &= 1 + \mu\omega\left(x_1, x_2, \theta\right), \qquad \mu > 0 \\ u &= \alpha\left(x_1, x_2, \theta\right) \end{aligned} \tag{3.35}$$

for the system (3.31), and we show that it renders the set $\mathcal{A}$ UGES and achieves good performance for large μ. To design the functions ω and α in (3.35) we select a Hurwitz matrix

$$A := \begin{bmatrix} 0 & 1 \\ -k_1 & -k_2 \end{bmatrix}$$

and let $P = P^\top > 0$ be such that $A^\top P + PA = -Q$ where $Q = Q^\top > 0$. Using

$$V\left(x, \theta\right) := \left(x - \xi(\theta)\right)^\top P \left(x - \xi(\theta)\right) \tag{3.36}$$

$$\xi\left(\theta\right) = \begin{bmatrix} \xi_1(\theta) \\ \xi_2(\theta) \end{bmatrix} := \begin{bmatrix} \cos\theta \\ -\sin\theta \end{bmatrix} \tag{3.37}$$

and $K := [k_1 \; k_2]$, we assign ω and α in (3.35) as

$$\omega\left(x, \theta\right) = -V^\theta\left(x, \theta\right) = 2\left(x - \xi(\theta)\right)^\top P \xi^\theta(\theta) \tag{3.38}$$

$$\alpha\left(x, \theta\right) = -K\left(x - \xi(\theta)\right) + \xi_2^\theta(\theta). \tag{3.39}$$

Differentiating (3.36) along the solutions of the resulting closed-loop equations

$$\begin{aligned} \dot{x} &= A\left(x - \xi(\theta)\right) + \xi^\theta(\theta) \\ \dot{\theta} &= 1 - \mu V^\theta(x, \theta) \end{aligned} \tag{3.40}$$

gives

$$\begin{aligned} \dot{V}(x, \theta) &= -\left(x - \xi(\theta)\right) Q \left(x - \xi(\theta)\right) - \mu V^\theta(x, \theta)^2 \\ &\leq -\lambda_{\min}\left(Q\right) \left|x - \xi(\theta)\right|^2 \leq -cV(x, \theta), \qquad c := \frac{\lambda_{\min}\left(Q\right)}{\lambda_{\max}\left(P\right)} \end{aligned}$$

It follows that $|x(t) - \xi(\theta(t))| \leq ke^{-\frac{c}{2}t} |x(0) - \xi(\theta(0))|$ holds, where $k := \sqrt{\frac{\lambda_{\max}(P)}{\lambda_{\min}(P)}}$, and the set $\mathcal{A}$ is therefore UGES. By definition,

[5] While $\mathcal{P} \times \mathbb{R}$ defines a two-dimensional cylindrical surface in $\mathbb{R}^3$, the set $\mathcal{A}$ defines a one-dimensional spiral on the cylindrical surface in $\mathbb{R}^3$.

$|x|_{\mathcal{P}} = \inf_\theta |x - \xi(\theta)|$. We let $\bar{\theta}(x)$ satisfy $|x|_{\mathcal{P}} = \left|x - \xi(\bar{\theta})\right|$. Then, since $|x(t)|_{\mathcal{P}} \leq |x(t) - \xi(\theta(t))| \leq |x(t)|_{\mathcal{P}} + 2$, we also have

$$|x(t)|_{\mathcal{P}} \leq ke^{-\frac{c}{2}t} \left[|x(0)|_{\mathcal{P}} + 2\right], \qquad \forall t \geq 0 \tag{3.41}$$

which establishes uniform global attractivity of the set $\mathcal{P} \times \mathbb{R}$ for (3.40). This is a prerequisite for the objective we consider in this problem. Stability of $\mathcal{P}$, however, has not been achieved since this set is not forward invariant.

To instead obtain the aforementioned *"near forward invariance"* property, we induce a two time-scale behavior of the closed-loop system (3.40) by increasing μ. Letting $\varepsilon = 1/\mu$ be small, allows us to analyze (3.40) as a singularly perturbed system (Teel, Moreau and Nešić; 2003; Kokotović, Khalil and O'Reilly; 1999; Khalil; 2002). Let the fast time scale be $t_f = t/\varepsilon$ and define $x' := \frac{dx}{dt_f}$. Then the closed-loop can be written as

$$\begin{aligned} x' &= \varepsilon A\left(x - \xi(\theta)\right) + \varepsilon \xi^\theta(\theta) \\ \theta' &= \varepsilon - V^\theta(x, \theta). \end{aligned}$$

The rapid transient of θ is approximately described by the boundary layer system for $\varepsilon = 0$,

$$\theta' = -V^\theta\left(x, \theta\right), \tag{3.42}$$

where x is fixed since $x' = 0$ for $\varepsilon = 0$. Clearly, (3.42) is a continuous gradient algorithm which minimizes V with respect to θ for any fixed x. For a given x, the level curves of $\xi \mapsto (x - \xi)^\top P (x - \xi)$ are shown in Figure 3.1.

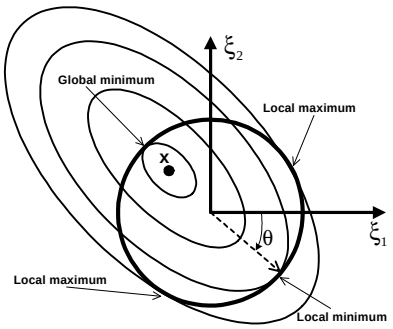

Figure 3.1: Level sets of $V(x, \cdot)$ for a fixed x, that is, for the function $\xi \mapsto (x - \xi)^\top P (x - \xi)$ where the circle, parametrized by θ, is the constraint set for ξ.

The four values of θ satisying $V^{\theta}(x,\theta) = 0$ are given by the locations where the path $\xi(\theta)$, defined in (3.37) and indicated as a solid curve in Figure 3.1, is tangent to a level set of $\xi \mapsto (x-\xi)^{\top} P (x-\xi)$. These four values of θ correspond to the two local maxima and two local minima of $\theta \mapsto V(x,\theta)$. The global minimum is the value of interest, and it is denoted $\theta_V(x)$. The function $\theta_V(\cdot)$ are a locally Lipschitz function for x near the unit circle. The function $\xi(\theta_V(x))$ is substituted into (3.40) to obtain the *reduced system*

$$\dot{x} = A\left(x - \xi(\theta_V(x))\right) + \xi^{\theta}\left(\theta_V(x)\right) \tag{3.43}$$

which approximately describes the true behavior of x in time-scale t. This motion is restricted to the slow manifold $\mathcal{V}_{\varepsilon}$ that is ε-close to the manifold $\mathcal{V}_{\theta}$ defined by

$$V^{\theta}(x,\theta_V(x)) = -2\left(x - \xi(\theta_V(x))\right)^{\top} P \xi^{\theta}(\theta_V(x)) = 0. \tag{3.44}$$

This restriction is the result of the gradient optimization which rapidly positions $\xi(\theta)$ to the most favourable position along the desired circle $x_1^2 + x_2^2 = 1$, to which x is to converge. This convergence is established by differentiating $W(x) := V(x,\theta_V(x))$ with respect to t along the solutions of the *reduced system* (3.43). Employing the identity (3.44), this derivative is

$$\begin{aligned} \dot{W} &= -\left[x - \xi(\theta_V(x))\right]^{\top} Q \left[x - \xi(\theta_V(x))\right] \\ &\leq -\lambda_{\min}(Q)\left|x - \xi(\theta_V(x))\right|^2 \leq -cW(x(t)), \end{aligned}$$

which implies

$$\begin{aligned} |x(t)|_{\mathcal{P}} &= \left|x(t) - \xi(\bar{\theta}(x(t)))\right| \leq \left|x(t) - \xi(\theta_V(x(t)))\right| \\ &\leq \sqrt{\frac{1}{\lambda_{\min}(P)} W(x(t))} \leq \sqrt{\frac{1}{\lambda_{\min}(P)} W(x(0)) e^{-\frac{c}{2}t}} \\ &\leq \sqrt{\frac{1}{\lambda_{\min}(P)} V(x(0),\bar{\theta}(x(0)))} e^{-\frac{c}{2}t} \\ &\leq k\left|x(0) - \xi(\bar{\theta}(x(0)))\right| e^{-\frac{c}{2}t} = k\,|x(0)|_{\mathcal{P}}\, e^{-\frac{c}{2}t} \end{aligned} \tag{3.45}$$

and therefore shows that the set $\mathcal{P}$ is uniformly exponentially stable for the *reduced system* (3.43). The standard approximation theorems of singular perturbation analysis guarantee that the solutions of the designed closed-loop system (3.40) are ε-close, on compact time intervals, to the corresponding trajectories composed of the boundary layer transient of $\theta(t)$ and the subsequent motion $x(t)$ of the reduced system with $\theta(t) = \theta_V(x(t))$.

With proper initialization, $|x(0)|_{\mathcal{P}}$ sufficiently small and $\theta(0)$ in the region of convergence of $\theta_V(x(0))$, it follows from the results of Teel et al. (2003) that for any $\delta > 0$ there exists $\mu^* > 0$ such that $\mu \geq \mu^*$ implies that

$$|x(t)|_{\mathcal{P}} \leq k\,|x(0)|_{\mathcal{P}}\,e^{-\frac{c}{2}t} + \delta, \qquad \forall t \geq 0 \tag{3.46}$$

holds for the true closed-loop system (3.40). The behavior of the solution of the true system (3.40) will therefore be δ-close to the behavior, characterized by the bound (3.45), of the reduced system, and this yields the desired near forward invariance property.

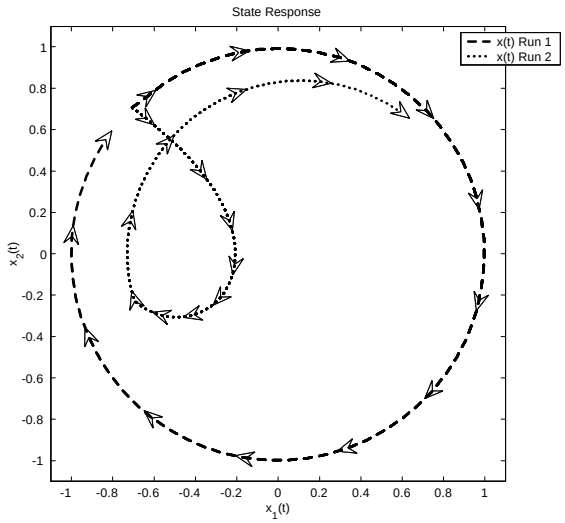

Figure 3.2: State responses projected into the (x_1, x_2)-plane.

Figures 3.2 and 3.3 show the responses of $x(t)$ and $\theta(t)$ in a simulation, using Matlab$^{\text{TM}}$ and Simulink$^{\text{TM}}$, with $k_1 = 2$ and $k_2 = 1$. Initial positions were $x_0 = [-\frac{\sqrt{2}}{2}\ \frac{\sqrt{2}}{2}]^\top$ (on the circle at the angle 225 °) and $\theta_0 = 0\,°$. Figures 3.2 and 3.3a) show the responses for $\mu = 500$.

In *Run 1,* $V(x_0, \cdot)$ only had one unique initial minimum at $\theta_V(x_0) = 225\,°$, to which $\theta(t)$ rapidly converges. Thus, the initial transient in the distance to the circle is small, and $x(t)$ stays close for all time (and eventually converges).

In *Run 2,* on the other hand, we change the P-matrix so that $V(x_0, \cdot)$ has an initial local minimum at $\theta_{loc.min} = 108\,°$. Since $\theta(0)$ is in the basin of attraction of $\theta_{loc.min}$, it rapidly converges to $\theta_{loc.min}$ and causes the bad

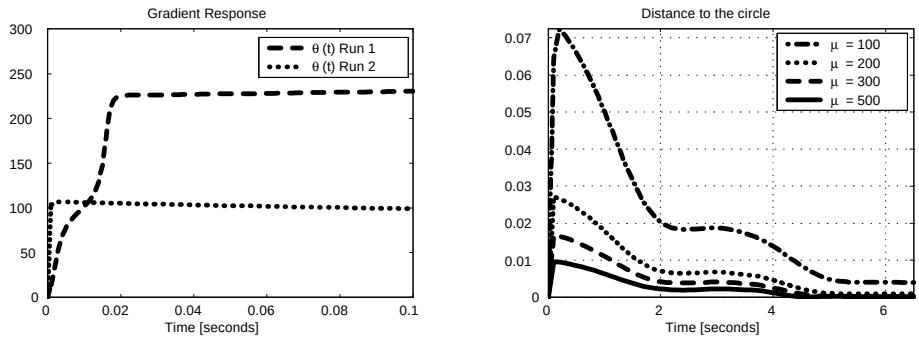

Figure 3.3: a) Time-plots of $\theta(t)$: Rapid transients to the global minimum in Run 1, and a local minimum in Run 2. b) Initial error transients of $|x(t)|_{\mathcal{P}}$ for increasing gains μ in the case of a unique minimum.

transient of $x(t)$. In Figure 3.3 b), the responses correspond to the unique minimum case in Run 1 for different gains μ. It is seen that the excursion of $x(\cdot)$ from the circle decreases as μ increases.

3.4.2 Main result: Near stabilization of sets parametrized by a single variable

In many contexts, stabilization of sets parameterized by a single variable is interesting. Obvious examples are control of robots, vessels, and vehicles where a desired path can be characterized by such a set. In fact, all applications where the states should be forced to a one dimensional manifold or subset in the state space fall into this category.

With the parametrization $\xi(\theta)$ from (3.5), assumed independent of t, define the target set (or path)

$$\mathcal{P} := \{x \in \mathbb{R}^{nm} : \ \exists \theta \in \mathbb{R} \text{ s.t. } x = \xi(\theta)\} \tag{3.47}$$

for the system (3.4). As shown in the motivational example in Section 3.4.1, stabilization of $\mathcal{P}$ may involve some difficulties. While uniform global attractivity can be obtained with relative ease, the forward invariance property may be hard to achieve. Therefore, the set $\mathcal{P}$ cannot, in general, be rendered GAS. The design procedure in Section 3.1, achieves global asymptotic convergence to a subset of $\mathcal{P} \times \mathbb{R}$ but not stability of $\mathcal{P} \times \mathbb{R}$. In what follows we abandon stability in the strict sense and instead construct a control algorithm that ensures *"near stability"*.

"Near forward invariance" and "Near stability"

To achieve near asymptotic stability of a set $\mathcal{A}$ the set has to be attractive, and, additionally, we need the dynamic system to contain a parameter that can be tuned to make the set nearly forward invariant. Consider the system

$$\dot{x} = f(x, \mu), \qquad x \in \mathbb{R}^n, \quad \mu \in \mathbb{R}^p \tag{3.48}$$

where x is the state and μ is a fixed parameter vector. Recall according to Definition A.6 that for a given fixed $\mu \in \mathbb{R}^p$, the set $\mathcal{A}$ is forward invariant for (3.48) if the system is forward complete and

$$\forall x_0 \in \mathcal{A} \quad \Rightarrow \quad |x(t, x_0)|_{\mathcal{A}} = 0, \quad \forall t \geq 0. \tag{3.49}$$

Correspondingly, we say that:

Definition 3.5 *The set $\mathcal{A}$ is* nearly forward invariant *for (3.48) if the system is forward complete and for each $\delta > 0$ there exists a set $\mathcal{G} \subset \mathbb{R}^p$ such that*

$$\forall x_0 \in \mathcal{A}, \ \forall \mu \in \mathcal{G} \quad \Rightarrow \quad |x(t, x_0)|_{\mathcal{A}} \leq \delta, \quad \forall t \geq 0. \tag{3.50}$$

Definition 3.6 *A closed, nearly forward invariant set $\mathcal{A} \subset \mathbb{R}^n$ is* near-US *with respect to (3.48) if the system is forward complete, there exists a class-$\mathcal{K}_\infty$ function φ, a positive constant c, and for each $\delta > 0$ there exists a set $\mathcal{G} \subset \mathbb{R}^p$ such that $\forall \mu \in \mathcal{G}$, the solution satisfies*

$$|x(t, x_0)|_{\mathcal{A}} \leq \varphi\left(|x_0|_{\mathcal{A}}\right) + \delta, \qquad \forall t \geq 0, \quad \forall \, |x_0|_{\mathcal{A}} \leq c. \tag{3.51}$$

If the constant c can be taken arbitrarily large, then the set is near-UGS.

Definition 3.7 *A closed, nearly forward invariant set $\mathcal{A} \subset \mathbb{R}^n$ is* near-UAS *with respect to (3.48) if it is near-US and Uniformly Attractive; that is, for all $|x_0|_{\mathcal{A}} \leq c$ then $|x(t, x_0)|_{\mathcal{A}} \to 0$ as $t \to \infty$. If the constant c can be taken arbitrarily large, then the set is* near-UGAS.

Rendering the target set near-UAS

To make the results in this section applicable to closed-loop systems more general than (3.9) or (3.12) obtained from feedback linearization, we consider the (closed-loop) system

$$\dot{x} = f(x, \theta) + g(x, \theta)\upsilon_s(\theta) \tag{3.52}$$

where, according to the notation of this chapter, $x \in \mathbb{R}^{nm}$ is the plant state, $\theta \in \mathbb{R}$ is the path variable, and $f : \mathbb{R}^{nm} \times \mathbb{R} \to \mathbb{R}^{nm}$ and $g : \mathbb{R}^{nm} \times \mathbb{R} \to \mathbb{R}^{nm}$ are smooth vector functions satisfying $f(\xi(\theta), \theta) = 0$ and $g(\xi(\theta), \theta) = \xi^{\theta}(\theta)$. The (feedback linearized) closed-loop system (3.9) is the case $f(x, \theta) = A(x - \xi(\theta))$ and $g(x, \theta) = \xi^{\theta}(\theta)$.

For (3.52), we further assume there exists a global diffeomorphism $(x, \theta) \leftrightarrow (z, \theta)$, given by $z = z(x, \theta) = \gamma(x - \xi(\theta))$, and that the system is equivalently represented by the error state as

$$\dot{z} = \tilde{f}(z, \theta) + \tilde{g}(z, \theta)\, \omega_s \tag{3.53}$$

where $\omega_s = \upsilon_s(\theta) - \dot{\theta}$ is the speed assignment error, $\tilde{f} : \mathbb{R}^{nm} \times \mathbb{R} \to \mathbb{R}^{nm}$ and $\tilde{g} : \mathbb{R}^{nm} \times \mathbb{R} \to \mathbb{R}^{nm}$ are smooth functions. These are found by differentiating the smooth map $z(x, \theta)$, giving

$$\dot{z} = z^{x}(x, \theta)\left[f(x, \theta) + g(x, \theta)\upsilon_s(\theta)\right] + z^{\theta}(x, \theta)\left[\upsilon_s(\theta) - \omega_s\right],$$

and defining

$$\begin{aligned}
\tilde{f}(z, \theta) &:= z^{x}(x, \theta)\left[f(x, \theta) + g(x, \theta)\upsilon_s(\theta)\right] + z^{\theta}(x, \theta)\upsilon_s(\theta) \\
\tilde{g}(z, \theta) &:= -z^{\theta}(x, \theta)
\end{aligned}$$

where the inverse map $x = \tilde{\gamma}(z, \theta)$ is substituted for x. It is assumed the following hold:

1. There exists a matrix pair $(P, Q) = (P, Q)^{\top} > 0$ such that $z^{\top} P \tilde{f}(z, \theta) + \tilde{f}(z, \theta)^{\top} P z \leq -z^{\top} Q z$ holds for all (z, θ).

2. There exist a continuous nondecreasing function $\sigma_1(z)$ such that $|\tilde{g}(z, \theta)| \leq \sigma_1(|z|)$.

3. There exist class-$\mathcal{K}_{\infty}$ functions γ_1 and γ_2, that are linear for small arguments, such that

$$\gamma_1(|x - \xi(\theta)|) \leq |z(x, \theta)| \leq \gamma_2(|x - \xi(\theta)|). \tag{3.54}$$

For the system (3.53) we can then apply the Lyapunov function $V(x, \theta) = z(x, \theta)^{\top} P z(x, \theta)$ to get the time-derivative

$$\begin{aligned}
\dot{V} &= V^{x}(x, \theta)\left[f(x, \theta) + g(x, \theta)\upsilon_s(\theta)\right] + V^{\theta}(x, \theta)\left[\upsilon_s(\theta) - \omega_s\right] \\
&= 2z(x, \theta)^{\top} P z^{x}(x, \theta)\left[f(x, \theta) + g(x, \theta)\upsilon_s(\theta)\right] \\
&\quad + 2z(x, \theta)^{\top} P z^{\theta}(x, \theta)\upsilon_s(\theta) - V^{\theta}(x, \theta)\omega_s \\
&= 2z(x, \theta)^{\top} P \tilde{f}(z(x, \theta), \theta) - V^{\theta}(x, \theta)\omega_s \\
&= -z(x, \theta)^{\top} Q z(x, \theta) - V^{\theta}(x, \theta)\omega_s
\end{aligned} \tag{3.55}$$

where $V^\theta(x,\theta) := -2z(x,\theta)^\top P\tilde{g}\left(z(x,\theta),\theta\right)$. Choosing the update law $\omega_s = \mu V^\theta(x,\theta)$, $\mu \geq 0$, satisfies Theorem 3.2 (notice that the first condition in the theorem is satisfied by using the assumption point 2 above), and this yields

$$\dot{\theta} = \upsilon_s(\theta) - \mu V^\theta(x,\theta) \tag{3.56}$$

and

$$\dot{V} \leq -z(x,\theta)^\top Q z(x,\theta) \leq -cV(x,\theta), \qquad c := \frac{\lambda_{\min}(Q)}{\lambda_{\max}(P)}. \tag{3.57}$$

This shows that the set $\mathcal{A} \subset \mathcal{P} \times \mathbb{R}$, $\mathcal{A} = \{(z,\theta) : \ z = 0\}$ is UGAS.

The above treatment summarizes the results of the design earlier in this chapter, using a direct gradient update law. Clearly, (3.53) captures (3.12a) by using $z = x - \xi(\theta)$ and setting $\tilde{g}(z,\theta) = \xi^\theta(\theta)$. However, additionally it will also capture the closed-loop systems obtained from backstepping designs in Chapter 4, in which case the nonlinear mapping $z(x,\theta) = \gamma(x - \xi(\theta))$ is constructed recursively.

Define the distance functions:

$$\begin{aligned}
|x|_{\mathcal{P}} &:= \inf_\theta |x - \xi(\theta)| = \left|x - \xi(\bar{\theta}(x))\right| \\
|x|_{\mathcal{P},V} &:= \inf_\theta \sqrt{V(x,\theta)} = \sqrt{V(x,\theta_V(x))} \\
|x|_{\mathcal{P},z} &:= \inf_\theta |z(x,\theta)| = |z(x,\theta_z(x))|
\end{aligned}$$

where $\bar{\theta}$, θ_V, and θ_z are the corresponding values that satisfy the infimums. Recall from the triangular inequality that $|x - \xi(\theta)| \leq |x|_{\mathcal{P}} + \left|\xi(\bar{\theta}(x)) - \xi(\theta)\right|$ $\leq |x|_{\mathcal{P}} + d$ holds where $d := \sup\{|a-b| : \ a,b \in \mathcal{P}\}$ exists due to finite extension of the path in $\mathbb{R}^{nm}$. If (3.57) hold, then for all $t \geq 0$,

$$V(x(t),\theta(t)) \leq V(x(0),\theta(0))e^{-ct}.$$

Define the class-$\mathcal{KL}$ function β as

$$\beta(s,\ t) := \gamma_1^{-1}\left(k\gamma_2(s)\, e^{-\frac{c}{2}t}\right), \qquad k := \sqrt{\frac{\lambda_{\max}(P)}{\lambda_{\min}(P)}}. \tag{3.58}$$

This gives the following sequence of inequalities

$$\begin{aligned}
|x(t)|_{\mathcal{P}} &\leq |x(t) - \xi(\theta_z(x(t)))| \leq \gamma_1^{-1}\left(|x(t)|_{\mathcal{P},z}\right) \leq \gamma_1^{-1}\left(|z(x(t), \theta_V(x(t)))|\right) \\
&\leq \gamma_1^{-1}\left(\sqrt{\frac{1}{\lambda_{\min}(P)}}\,|x(t)|_{\mathcal{P},V}\right) \leq \gamma_1^{-1}\left(\sqrt{\frac{1}{\lambda_{\min}(P)}V\left(x(t), \theta(t)\right)}\right) \\
&\leq \gamma_1^{-1}\left(\sqrt{\frac{1}{\lambda_{\min}(P)}V(x(0), \theta(0))e^{-\frac{c}{2}t}}\right) \leq \gamma_1^{-1}\left(k\,|z(x(0), \theta(0))|\,e^{-\frac{c}{2}t}\right) \\
&\leq \gamma_1^{-1}\left(k\gamma_2\left(|x(0) - \xi(\theta(0))|\right)e^{-\frac{c}{2}t}\right) \leq \gamma_1^{-1}\left(k\gamma_2\left(|x(0)|_{\mathcal{P}} + d\right)e^{-\frac{c}{2}t}\right) \\
&=: \beta\left(\left[|x(0)|_{\mathcal{P}} + d\right],\, t\right), \qquad \forall t \geq 0
\end{aligned} \tag{3.59}$$

which explicitly states uniform global attractivity of $\mathcal{P} \times \mathbb{R}$.

Some issues regarding the minimization of $V(x, \theta)$ with respect to θ need to be resolved. As shown in the motivational example in Section 3.4.1, $V(x, \cdot)$ may have multiple minima which means that the initial search point $\theta(0)$ must be restricted to a local set. There may also be points x in $\mathbb{R}^{nm}$ where this minimization is not feasible. For instance, in the example with the circular path, if $x = 0$ (and $P = I$), then the entire circle is an extremum. We make the assumption:

Assumption 3.8 *There exists $\rho > 0$ such that every fixed x with $|x|_{\mathcal{P}} \leq \rho$ implies that $V(x, \cdot)$ has a global minimizer, denoted $\theta_V(x)$, which is a LAS equilibrium for*

$$\dot{\theta} = -V^{\theta}(x, \theta) \tag{3.60}$$

and with basin of attraction $\mathcal{H}_\theta(x)$. The function $x \mapsto \theta_V(x)$ is locally Lipschitz on $\{x :\ |x|_{\mathcal{P}} \leq \rho\}$.

Define the set

$$\mathcal{H}(\rho) := \{(x, \theta) :\ |x|_{\mathcal{P}} \leq \rho,\ \theta \in \mathcal{H}_\theta(x)\}. \tag{3.61}$$

Choosing μ sufficiently large in (3.56) induces a separation of time scales between the plant dynamics $x(t)$ and the set parameter $\theta(t)$. Letting $\varepsilon = \frac{1}{\mu}$ be small, allows for (3.52) and (3.56) to be analyzed as a singularly perturbed system (see Kokotović et al. (1999); Khalil (2002); Teel et al. (2003)). Let $t_f = \frac{1}{\varepsilon}t$ and define $x' := \frac{dx}{dt_f}$. In the fast time scale t_f, the rapid transient of θ is approximately described by the boundary layer system at $\varepsilon = 0$,

$$x' = 0, \qquad \theta' = -V^{\theta}(x, \theta).$$

By construction, the set $\{(x,\theta):\ \theta=\theta_V(x)\}$ is asymptotically stable for $(x(0),\theta(0))\in\mathcal{H}(\rho)$. The fast variable θ therefore rapidly converges to a slow manifold $\mathcal{V}_\varepsilon$ located in the ε-neighborhood of the manifold $\mathcal{V}_\theta$ defined by $V^\theta(x,\theta)=0$. With θ constrained to be the solution of the minimization problem, $\theta=\theta_V(x)$, we get the *reduced system*

$$\dot{x}=f\left(x,\theta_V(x)\right)+g\left(x,\theta_V(x)\right)\upsilon_s\left(\theta_V(x)\right) \tag{3.62}$$

for which we consider the energy function $W(x):=V(x,\theta_V(x))=|x|^2_{\mathcal{P},V}$. Using the identities

$$V^x(x,\theta)\left[f\left(x,\theta\right)+g\left(x,\theta\right)\upsilon_s(\theta)\right]+V^\theta(x,\theta)\upsilon_s(\theta)=-z(x,\theta)^\top Qz(x,\theta)$$
$$V^\theta(x,\theta_V(x))=0$$

then for $|x(0)|_{\mathcal{P}}\leq\frac{p_m}{p_M}\rho$, we have

$$\dot{W}(x)=-z(x,\theta_V(x))^\top Qz(x,\theta_V(x))\leq -cW(x) \tag{3.63}$$

and the following relationships hold

$$\begin{aligned}
|x(t)|_{\mathcal{P}} &\leq |x(t)-\xi(\theta_z(x(t)))|\leq\gamma_1^{-1}\left(|x(t)|_{\mathcal{P},z}\right)\leq\gamma_1^{-1}\left(|z\left(x(t),\theta_V(x(t))\right)|\right)\\
&\leq\gamma_1^{-1}\left(\sqrt{\frac{1}{\lambda_{\min}\left(P\right)}}\,|x(t)|_{\mathcal{P},V}\right)\leq\gamma_1^{-1}\left(\sqrt{\frac{1}{\lambda_{\min}\left(P\right)}W\left(x(0)\right)}e^{-\frac{c}{2}t}\right)\\
&\leq\gamma_1^{-1}\left(\sqrt{\frac{1}{\lambda_{\min}\left(P\right)}V\left(x(0),\bar{\theta}(x(0))\right)}e^{-\frac{c}{2}t}\right)\\
&\leq\gamma_1^{-1}\left(k\left|z\left(x(0),\bar{\theta}(x(0))\right)\right|e^{-\frac{c}{2}t}\right)\\
&\leq\gamma_1^{-1}\left(k\gamma_2\left(\left|x(0)-\xi(\bar{\theta}(x(0)))\right|\right)e^{-\frac{c}{2}t}\right) \qquad (3.64)\\
&=\gamma_1^{-1}\left(k\gamma_2\left(|x(0)|_{\mathcal{P}}\right)e^{-\frac{c}{2}t}\right)=:\beta\left(|x(0)|_{\mathcal{P}},\ t\right) \qquad (3.65)
\end{aligned}$$

which implies that $\mathcal{P}$ is asymptotically stable for the *reduced system*. It follows, according to the main results in Teel et al. (2003), that for each $\delta>0$ there exists a μ large enough so that with proper initial conditions $(x(0),\theta(0))$, the behavior, characterized by the distance to $\mathcal{P}$, of the solutions to (3.52) and (3.56) are δ-close to the corresponding behavior of the reduced system (3.62) for which $\theta(t)=\theta_V(x(t))$.

We summarize the result in the following theorem:

Theorem 3.9 *There exist a class-$\mathcal{KL}$ function β and a constant $d > 0$ such that, for all initial conditions $(x_0, \theta_0) \in \mathbb{R}^{nm} \times \mathbb{R}$ and all $\mu \geq 0$, the trajectories of (3.52) and (3.56) satisfy*

$$|x(t, x_0)|_{\mathcal{P}} \leq \beta\left([|x_0|_{\mathcal{P}} + d]\,,\ t\right), \qquad \forall t \geq 0 \tag{3.66}$$

and, under Assumption 3.8, for each $\delta > 0$ and each compact set $\mathcal{K} \subseteq \mathcal{H}\left(\frac{p_m}{p_M}\rho\right)$ there exists $\mu^* > 0$ such that $\mu \geq \mu^*$ and $(x_0, \theta_0) \in \mathcal{K}$ imply

$$|x(t, x_0)|_{\mathcal{P}} \leq \beta\left(|x_0|_{\mathcal{P}}\,,\ t\right) + \delta, \qquad \forall t \geq 0. \tag{3.67}$$

Recall that asymptotic stability of the set $\mathcal{A}$ (and thus attractivity of $\mathcal{P}$) guarantees that the maneuvering objective is solved. However, how well the closed-loop maneuvering system performs, especially in the initial transient and convergence to the path, is unanswered by the control design in Section 3.1. In essence, the concept of near stability of the path $\mathcal{P}$ characterizes *performance* of maneuvering. The bound (3.67) states, in particular, that for $x_0 \in \mathcal{P}$ and θ in a compact subset of $\mathcal{H}_\theta(x_0)$, the excursion of $x(\cdot, x_0)$ from $\mathcal{P}$ can be made arbitrarily small. It further states that if x_0 is close to the path, then the solution $x(t, x_0)$ will stay close to the path and eventually converge to it. It therefore follows from Theorem 3.9 that the set $\mathcal{A}$ is near-UAS with respect to the closed-loop system (3.52) and (3.56).

Remark: The Filtered-gradient algorithm

Skjetne, Fossen and Kokotović (2002, 2004) extended the CLF $V(x, \theta)$ with the term $\frac{\varepsilon}{2\mu}\omega_s^2$ to construct a 1^{st} order $\dot{\omega}_s$-update law. Differentiating the extended CLF, the 2^{nd} order filtered-gradient update law was designed as

$$\dot{\theta} = \upsilon_s(\theta) - \omega_s \tag{3.68}$$

$$\varepsilon\dot{\omega}_s = -\omega_s + \mu V^\theta(x, \theta). \tag{3.69}$$

By setting $\varepsilon = 0$, we can again apply singular perturbation techniques on the closed-loop system where x and θ are the slow states and ω_s are the fast state which rapidly converges to an ε-neighborhood of the manifold $\omega_s - \mu V^\theta(x, \theta) = 0$. Substituting the solution $\omega_s = \mu V^\theta(x, \theta)$ into (3.68) gives the *reduced system*

$$\begin{aligned} \dot{x} &= f(x, \theta) + g(x, \theta)\upsilon_s(\theta) \\ \dot{\theta} &= \upsilon_s(\theta) - \mu V^\theta(x, \theta) \end{aligned} \tag{3.70}$$

which approximately describes the motion of x and θ in the slow time-scale. This *reduced system* is exactly the closed-loop (3.52) and (3.56). Consequently, if ε is chosen small and μ large, then the results of near stability from the previous analysis are recovered 'approximately'.

3.4.3 Example: Self-intersecting path

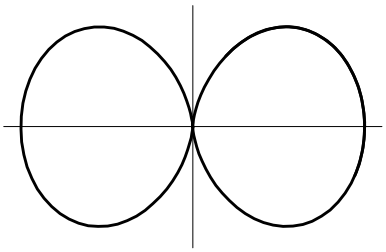

Figure 3.4: Self-intersecting "figure-8" path.

To illustrate how the performance of the closed-loop system changes for varying gains μ, let the path be the self-intersecting "figure-8" in Figure 3.4. (Note that our results, using a gradient-type update law, apply to self-intersecting paths, in contrast to the results in Hindman and Hauser (1996) where such paths were not allowed.) The analytical expression for this "figure-8" is

$$\xi(\theta) = \begin{bmatrix} \xi_1(\theta) \\ \xi_2(\theta) \end{bmatrix} := r \begin{bmatrix} \sin^3(\theta) \\ 3\sin^2(\theta)\cos(\theta)\upsilon_s(\theta) \end{bmatrix} \tag{3.71}$$

where $r > 0$ is a given constant. For the double integrator plant (3.31), the path (3.71) is to be traversed with the assigned speed $\upsilon_s(\theta)$, consistent with $\xi_2(\theta) = \xi_1^\theta(\theta)\upsilon_s(\theta)$. Because of the assigned speed $\upsilon_s(\theta)$, our update law for is

$$\dot{\theta} = \upsilon_s(\theta) - \mu V^\theta(x,\theta), \qquad \mu > 0, \tag{3.72}$$

where $V(x,\theta)$ is as in (3.36). We choose the control law

$$u = -k_1(x_1 - \xi_1(\theta)) - k_2(x_2 - \xi_2(\theta)) + \xi_2^\theta(\theta)\upsilon_s(\theta) \tag{3.73}$$

so that with $x := [x_1\ x_2]^\top$, $k_1, k_2 > 0$, and

$$A = \begin{bmatrix} 0 & 1 \\ -k_1 & -k_2 \end{bmatrix}$$

the resulting closed-loop system is

$$\begin{aligned} \dot{x} &= A\,(x - \xi(\theta)) + \xi^{\theta}(\theta)\upsilon_s(\theta) \\ \dot{\theta} &= \upsilon_s(\theta) - \mu V^{\theta}(x, \theta). \end{aligned} \tag{3.74}$$

A singular perturbation analysis with μ sufficiently large establishes that, after a rapid transient of θ directed by the gradient algorithm, the motion of $x(t)$ asymptotically approaches the desired "figure-8" path.

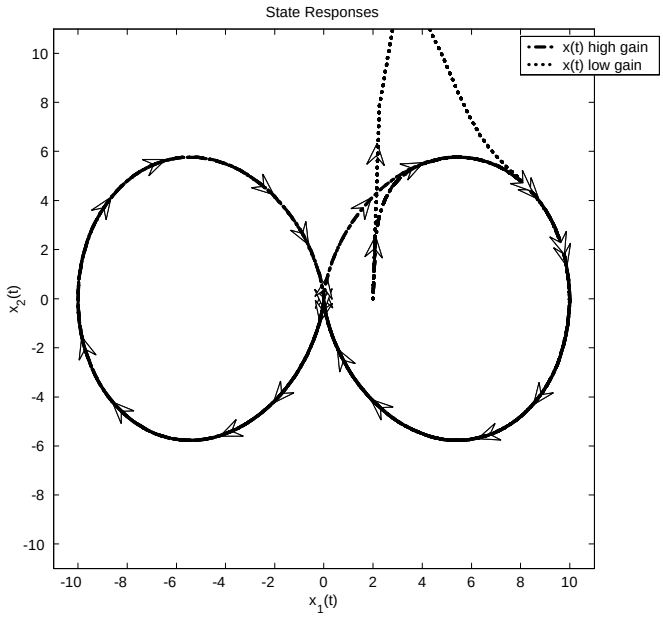

Figure 3.5: Typical state trajectories projected into the (x_1, x_2)-plane for Maneuvering with: 1) high gain gradient optimization, $\mu = 1.0$, and 2) low-gain, $\mu = 0.02$.

Two simulations were performed, with $r = 10$ and speed assigned to $\upsilon_s = 0.5$, controller settings $k_1 = 21$, $k_2 = 11$, and initial conditions $x_0 = [\frac{r}{5},\ 0]^{\top}$ and $\theta_0 = 80\,^{\circ}$. The first simulation employed a high-gain maneuvering controller with gradient optimization. In this case $\mu = 1.0$ is high enough to ensure a rapid transient as shown in Figure 3.6. Typical state trajectories in $\mathbb{R}^3$, projected into the (x_1, x_2)-plane, are shown in Figure 3.5. The corresponding high-gain trajectory has a favourable transient when approaching the desired path.

For the sake of comparison, a low-gain maneuvering controller with $\mu = 0.02$, is superimposed in Figure 3.5 (dotted trajectory). The transient in this

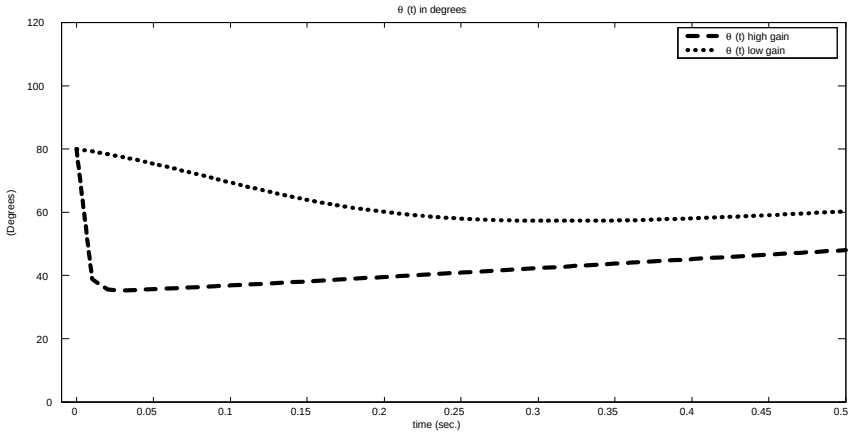

Figure 3.6: Time plots of $\theta(t)$ for the initial response: rapid transient to $\theta_V \approx 34\,^\circ$ in the high-gain case; while both responses follow up with constant speed 0.5.

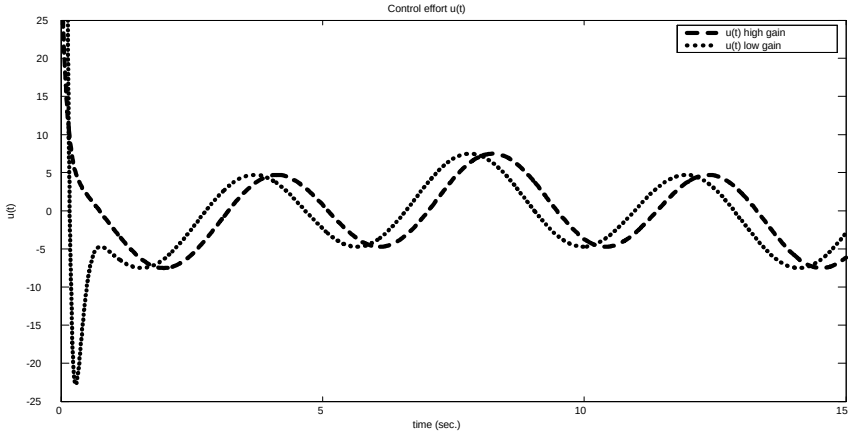

Figure 3.7: Control effort $u(t)$: notice the transient in the low-gain case which is eliminated in the high-gain case.

case exhibit a large overshoot of the path. In fact, in the limit as $\mu \to \infty$, and proper initialization of θ_0, it is impossible for $x(t)$ to start inside the "figure-8" path and go out of it. In the limit as $\mu \to 0$, on the other hand, the controller becomes a pure tracking controller ($\mu = 0$), and in this case we obtain the worst transient performance.

To visualize the two-time scale behavior of θ and the attainement of the assigned speed $\upsilon_s = 0.5$, a comparison of $\theta_{1.0}(t)$ for the $\mu = 1.0$ case with $\theta_{.02}(t)$ in the $\mu = 0.02$ case, is shown in Figure 3.6. After a rapid '*boundary layer*' transient where $\theta_{1.0}(t)$ converged to the minimum $\theta_V(x(0)) \approx 34\,^\circ$, they both settle on a ramp of t-slope 0.5, as required. However, the $\theta_{.02}(t)$ response never converged to the optimal $34\,^\circ$. This difference accounts for the major deterioration in the transient of $x(t)$.

Figure 3.7 shows the control effort in the two cases. Notice how the initial transient is rapidly removed in the high-gain case.

3.5 A reference system interpretation

If we twist our eyes, we can view the speed assignment

$$\dot{\theta} = \upsilon_s(\theta, t), \qquad \theta \in \mathbb{R}^1, \tag{3.75a}$$

$$y_d = y_d(\theta), \qquad y_d \in \mathcal{P} \subset \mathbb{R}^m, \tag{3.75b}$$

as desired dynamics in a reference system design. This reference system, as presented earlier in this chapter, is a one-dimensional system representing a one-dimensional manifold, the path $\mathcal{P} \subset \mathbb{R}^m$, to which the solution $y_d(\theta(t))$ is constrained. By construction, (3.75) solves two relevant objectives for the maneuvering problem,

1. it traces the desired path to be followed, and
2. the speed along the path $|\dot{y}_d| = |y_d^\theta(\theta)||\upsilon_s(\theta, t)|$ satisfies the desired specification.

In the maneuvering control design in Section 3.1, a certainty equivalence principle was used, assuming (3.75a) hold identically, and thus cancelling $\dot{\theta}$ with $\upsilon_s(\theta, t)$ at every occurence. Since the maneuvering problem statement in Chapter 2 allowed for this relationship to only be satisfied in the limit as $t \to \infty$, this introduced the error $\omega_s = \upsilon_s(\theta, t) - \dot{\theta}$. In the end, this error function was used constructively, either to just obtain the reference system

(3.75) by the *tracking update law*, or to design a *gradient* or *filtered-gradient update law*.

Instead of defining θ as a scalar path variable, consider it as the state in a desired reference system of dimension $q \geq 1$. To distinguish it from (3.75), let η be this desired state with desired dynamics

$$\dot{\eta} = f_d(\eta, t), \qquad \eta \in \mathbb{R}^q \tag{3.76a}$$

$$y_d = h_d(\eta), \qquad y_d \in \mathbb{R}^m \tag{3.76b}$$

where f_d and h_d are smooth functions. Clearly, this system captures (3.75) by making the appropriate substitutions. Generalizing the maneuvering problem statement, the control objective is to satisfy the two tasks:

$$1) \qquad \lim_{t\to\infty} |y(t) - y_d(t)| = 0 \tag{3.77}$$

$$2) \qquad \lim_{t\to\infty} |\dot{\eta}(t) - f_d(\eta(t), t)| = 0 \tag{3.78}$$

where y is the output of the system to be controlled.

Consider the feedback linearizable system (3.4). Clearly, the exact same design as the maneuvering design in Section 3.1 can be performed, by first constructing the *"generalized state path"* as

$$\begin{aligned}
\xi_1(\eta, t) &:= h_d(\eta) \\
\xi_2(\eta, t) &:= \xi_1^\eta(\eta, t) f_d(\eta, t) + \xi_1^t(\eta, t) = h_d^\eta(\eta) f_d(\eta, t) \\
&\vdots \\
\xi_n(\eta, t) &:= \xi_{n-1}^\eta(\eta, t) f_d(\eta, t) + \xi_{n-1}^t(\eta, t)
\end{aligned}$$

and defining

$$\xi(\eta, t) := \operatorname{col}(\xi_1(\eta, t),\ \xi_2(\eta, t), \ldots,\ \xi_n(\eta, t)). \tag{3.79}$$

Similarly to (3.7) and (3.8), the design results in the control law

$$u = \rho(\chi) + \Phi(\chi)^{-1}[-K(x - \xi(\eta, t)) + \xi_n^\eta(\eta, t) f_d(\eta, t) + \xi_n^t(\eta, t)] \tag{3.80}$$

and the closed-loop system (using a gradient update law)

$$\dot{x} = A(x - \xi(\eta, t)) + \xi^\eta(\eta, t) f_d(\eta, t) + \xi^t(\eta, t) \tag{3.81a}$$

$$\dot{\eta} = f_d(\eta, t) - \Gamma V^\eta(x, \eta, t)^\top, \qquad \Gamma = \Gamma^\top > 0, \tag{3.81b}$$

where $A = A_c - B_c K$ is Hurwitz. The Lyapunov function for (3.81) is the quadratic function

$$V(x, \eta, t) := (x - \xi(\eta, t))^\top P (x - \xi(\eta, t)), \tag{3.82}$$

$PA + A^\top P = -Q$, resulting in the time derivative

$$\begin{aligned}\dot{V} &= V^x(x,\eta,t)\dot{x} + V^\eta(x,\eta,t)\dot{\eta} + V^t(x,\eta,t) \\ &= -\left(x - \xi(\eta,t)\right)^\top Q\left(x - \xi(\eta,t)\right) - V^\eta(x,\eta,t)\Gamma V^\eta(x,\eta,t)^\top. \end{aligned} \tag{3.83}$$

Assuming that appropriate assumptions hold for (3.76) so that (3.81) is forward complete, then (3.82) and (3.83) ensures that the set

$$\mathcal{M} = \{(z,\eta,t) \in \mathbb{R}^{nm} \times \mathbb{R}^q \times \mathbb{R}_{\geq 0} : \ z = 0\} \tag{3.84}$$

is UGES, where $z := x - \xi(\eta,t)$.

What is interesting here is the implication of allowing η to be of order higher than one. For instance, in Section 3.4 it was shown for μ large that $\theta(t)$ would rapidly converge to a value $\bar{\theta}(x,t)$ that corresponds to a point along the path $\xi(\cdot,t)$ that minimized the error $x(t) - \xi(\theta(t),t)$ according to the Lyapunov cost function $V(x,\theta,t)$. This behavior is also obtained by the solution $\eta(t)$ be choosing Γ large. Suppose by construction of the reference system (3.76), we allow $\xi(\eta,t)$ to span $\mathbb{R}^{nm}$, that is, for each $(x,t) \in \mathbb{R}^{nm} \times \mathbb{R}_{\geq 0}$ there exists $\eta \in \mathbb{R}^q$ such that $\xi(\eta,t) = x$. Then the global minimizer $\bar{\eta}(x,t)$ of $\eta \mapsto V(x,\eta,t)$ corresponds to the minimum $V(x,\bar{\eta}(x,t),t) = 0$ at which $\xi(\bar{\eta},t) = x$. In this minimum, the control law (3.80) is reduced to only necessary feedforward terms, and we have that $V^\eta(x,\bar{\eta}(x,t),t) = 0$ so that (3.81b) reduces to the desired dynamics $\dot{\eta} = f_d(\eta,t)$.

Another advantage in this context is to avoid local minima by ensuring by construction of (3.76) and $\xi(\eta,t)$ that $\eta \mapsto V(x,\eta,t)$ is strictly convex.

In a sense, we introduced in the previous design one *level of flexibility* by letting the system output $y(t)$ converge to the output $y_d(t)$ of the reference system that next satisfied its desired objective in the limit. This gave an extra degree of freedom that here was used to achieve a favorable response by applying the gradient optimization algorithm.

In light of this reflection, we can consider increasing the *levels of flexibility* by for instance letting $y(t)$ converge to one reference system output $y_{d1}(t)$ which again converges to another referense system output $y_{d2}(t)$, and so on, until the last reference system solves for instance the maneuvering objective (or any other desired objective). The advantage of this may be that each level of flexibility will introduce an extra degree of freedom that in the design can be used constructively to solve specific problems at hand. For instance, in the papers by Dačić and Kokotović (2005); Aguiar et al. (2004, 2005), the extra degree of freedom was used to deal with non-minimum phase performance limitations.

Chapter 4

Maneuvering designs for uncertain systems

This chapter presents constructive maneuvering control designs for uncertain systems. In the first section, a robust recursive design technique is developed for nonlinear plants in vectorial strict feedback form, perturbed on the right-hand side by bounded time-varying disturbances. In the second section, the adaptive version of the recursive design is presented for systems in vectorial parametric strict feedback form. Finally, the last section presents a maneuvering design based on sliding-mode control for systems with both additive and multiplicative structural uncertainties. All designs are concluded with the selection of an update law according to the tracking, gradient, or filtered gradient update laws. Stability of the noncompact sets corresponding to the maneuvering problem is proven in each case. The presented material were published in Skjetne, Fossen and Kokotović (2004); Skjetne et al. (2005); Skjetne and Teel (2004).

4.1 ISS backstepping design

Consider the nonlinear plant (3.1) and suppose it can be written in strict feedback form of vector relative degree n :

$$\begin{aligned}
\dot{x}_1 &= G_1(x_1)\,x_2 + f_1(x_1) + W_1(x_1)\,\delta_1(t)\\
\dot{x}_2 &= G_2(\bar{x}_2)\,x_3 + f_2(\bar{x}_2) + W_2(\bar{x}_2)\,\delta_2(t)\\
&\vdots\\
\dot{x}_n &= G_n(\bar{x}_n)\,u + f_n(\bar{x}_n) + W_n(\bar{x}_n)\,\delta_n(t)\\
y &= h(x_1)
\end{aligned} \tag{4.1}$$

where $\forall t \geq 0$, $x_i(t) \in \mathbb{R}^m$, $i = 1, \ldots, n$, are the states, $y(t) \in \mathbb{R}^m$ is the output, $u(t) \in \mathbb{R}^m$ is the control, and $\delta_i(\cdot)$ are unknown bounded disturbances. The matrices $G_i(\bar{x}_i)$ and $h^{x_1}(x_1) := \frac{\partial h}{\partial x_1}(x_1)$ are invertible for all $\bar{x}_i$, $h(x_1)$ is a diffeomorphism, and G_i, f_i, and W_i are smooth.

The design task is to design a *maneuvering controller* that solves the *Maneuvering Control Objective* for a continuously parametrized feasible path $y_d(\theta)$ and a feasible speed assignment $v_s(\theta, t)$ where Assumption 3.1 holds.

Due to the disturbances δ_i in (4.1), the goal is to render the closed-loop system input-to-state stable (ISS) with respect to the desired set $\mathcal{M}$ in which the maneuvering objective is solved. Such a set is said to be 0-invariant for a closed-loop system if it is invariant for the disturbance-free, $\delta_i = 0$, closed-loop system; see Definition A.11. Recall Theorem A.14 that states if a forward complete system admits an ISS-Lyapunov function with respect to a closed, 0-invariant set $\mathcal{M}$, then it is ISS with respect to $\mathcal{M}$. This will be the main tool to solve the maneuvering problem for (4.1).

4.1.1 Design procedure

A backstepping design is employed to solve the maneuvering problem for (4.1). The first two steps are given to show how to deal with $\dot{\theta}$. The *i'th* step for $i = 3, \ldots, n$ is given in Table 4.1. The design procedure borrows much from adaptive tracking by Krstić et al. (1995) including the notion of a *tuning function*.

Step 1: The new variables

$$z_1(x_1, \theta) := y - y_d(\theta) = h(x_1) - y_d(\theta) \tag{4.2}$$

$$z_i(\bar{x}_i, \theta, t) := x_i - \alpha_{i-1}(\bar{x}_{i-1}, \theta, t), \quad i = 2, \ldots, n \tag{4.3}$$

$$\omega_s(\dot{\theta}, \theta, t) := v_s(\theta, t) - \dot{\theta} \tag{4.4}$$

are introduced, where α_{i-1} are *virtual controls* to be specified later. Differentiating (4.2) with respect to time results in

$$\begin{aligned}\dot{z}_1 &= \dot{y} - y_d^\theta(\theta)\dot{\theta} \\ &= h^{x_1}G_1 z_2 + h^{x_1}G_1\alpha_1 + h^{x_1}f_1 + h^{x_1}W_1\delta_1 - y_d^\theta\dot{\theta}.\end{aligned}$$

Choose a Hurwitz matrix A_1 so that $P_1 = P_1^\top > 0$ is the solution to $P_1A_1 + A_1^\top P_1 = -Q_1 < 0$, and define the first control Lyapunov function (CLF)

$$V_1(x_1,\theta) := z_1(x_1,\theta)^\top P_1 z_1(x_1,\theta) \tag{4.5}$$

whose time derivative is

$$\begin{aligned}\dot{V}_1 = {} & 2z_1^\top P_1[h^{x_1}G_1\alpha_1 + h^{x_1}f_1 - y_d^\theta\upsilon_s] \\ & + 2z_1^\top P_1 h^{x_1}G_1 z_2 + 2z_1^\top P_1 h^{x_1}W_1\delta_1 + 2z_1^\top P_1 y_d^\theta\omega_s.\end{aligned}$$

Then the first virtual control law is picked as

$$\begin{aligned}\alpha_1 &= \alpha_1(x_1,\theta,t) \\ &= G_1^{-1}\left(h^{x_1}\right)^{-1}\left[A_1z_1 - h^{x_1}f_1 + y_d^\theta\upsilon_s + \alpha_{10}\right]\end{aligned} \tag{4.6}$$

where α_{10} is a nonlinear damping term to be picked. Define the first *tuning function*, $\tau_1 \in \mathbb{R}$, as

$$\tau_1(x_1,\theta) := 2z_1(x_1,\theta)^\top P_1 y_d^\theta(\theta). \tag{4.7}$$

After an application of Young's inequality, the derivative $\dot{V}_1$ becomes

$$\begin{aligned}\dot{V}_1 &= -z_1^\top Q_1 z_1 + 2z_1^\top P_1 h^{x_1}G_1 z_2 + \tau_1\omega_s + 2z_1^\top P_1 h^{x_1}W_1\delta_1 + 2z_1^\top P_1\alpha_{10} \\ &\le -z_1^\top Q_1 z_1 + \tau_1\omega_s + 2z_1^\top P_1 h^{x_1}G_1 z_2 + \frac{1}{\kappa_1}\delta_1^\top\delta_1 \\ &\quad + 2z_1^\top P_1\{\alpha_{10} + \frac{1}{2}\kappa_1 h^{x_1}W_1W_1^\top\left(h^{x_1}\right)^\top P_1 z_1\}.\end{aligned}$$

The nonlinear damping term is now chosen to cancel the last term. This gives

$$\begin{aligned}&\alpha_{10}(x_1,\theta) = \rho_1(x_1)z_1 \\ &\rho_1(x_1) := -\tfrac{1}{2}\kappa_1 h^{x_1}W_1W_1^\top\left(h^{x_1}\right)^\top P_1, \quad \kappa_1 > 0\end{aligned} \tag{4.8}$$

and the result of *Step 1* is

$$\dot{z}_1 = A_1z_1 - \frac{1}{2}\kappa_1 h^{x_1}W_1W_1^\top\left(h^{x_1}\right)^\top P_1 z_1 + h^{x_1}G_1 z_2 + y_d^\theta\omega_s + h^{x_1}W_1\delta_1 \tag{4.9}$$

$$\dot{V}_1 \le -z_1^\top Q_1 z_1 + 2z_1^\top P_1 h^{x_1}G_1 z_2 + \tau_1\omega_s + \Delta_1^\top K_1\Delta_1 \tag{4.10}$$

where $\Delta_1 := \delta_1$ and $K_1 := \frac{1}{\kappa_1}$. If this was the last step, then $z_2 = 0$ and $\omega_s = 0$ would reduce (4.10) to

$$\dot{V}_1 \leq -q_1 |z_1|^2 + k_1 |\Delta_1|^2 < 0, \quad \forall |z_1| > \sqrt{\frac{k_1}{q_1}} |\Delta_1|$$

where $q_1 = \lambda_{\min}(Q_1)$, $k_1 = \frac{1}{\kappa_1}$, which implies ISS from the disturbance δ_1 to the state z_1. To aid next step, let

$$\dot{\alpha}_1 =: \sigma_1(\bar{x}_2, \theta, t) + \alpha_1^{\theta}(x_1, \theta, t)\dot{\theta} + \varpi_{1,1}(x_1, \theta, t)\delta_1(t) \tag{4.11}$$

where σ_1 collects the terms in $\dot{\alpha}_1$ not containing $\dot{\theta}$ and δ_1, and $\varpi_{1,1}$ collects the terms multiplying the disturbance δ_1

$$\sigma_1(\bar{x}_2, \theta, t) := \alpha_1^{x_1}(x_1, \theta, t)\left[G_1(x_1)x_2 + f_1(x_1)\right] + \alpha_1^{t}(x_1, \theta, t) \tag{4.12}$$

$$\varpi_{1,1}(x_1, \theta, t) := \alpha_1^{x_1}(x_1, \theta, t)W_1(x_1). \tag{4.13}$$

Step 2: Consider x_3 as the next control variable. Differentiating (4.3), $i = 2$, with respect to time gives

$$\begin{aligned}\dot{z}_2 &= \dot{x}_2 - \dot{\alpha}_1 \\ &= G_2 z_3 + G_2\alpha_2 + f_2 + W_2\delta_2 - \sigma_1 - \alpha_1^{\theta}\dot{\theta} - \varpi_{1,1}\delta_1\end{aligned}$$

where $z_3 = x_3 - \alpha_2$. Choose A_2 Hurwitz and let $P_2 = P_2^{\top} > 0$ be the solution to $P_2A_2 + A_2^{\top}P_2 = -Q_2 < 0$. Define the *Step 2* CLF

$$V_2(\bar{x}_2, \theta, t) := V_1(x_1, \theta) + z_2(\bar{x}_2, \theta, t)^{\top} P_2 z_2(\bar{x}_2, \theta, t) \tag{4.14}$$

whose time derivative is

$$\begin{aligned}\dot{V}_2 \leq\ & -z_1^{\top}Q_1z_1 + \tau_1\omega_s + 2z_2^{\top}P_2\alpha_1^{\theta}\omega_s + \frac{1}{\kappa_1}\delta_1^{\top}\delta_1 \\ & + 2z_2^{\top}\{G_1^{\top}\left(h^{x_1}\right)^{\top}P_1z_1 + P_2[G_2\alpha_2 + f_2 - \sigma_1 - \alpha_1^{\theta}\upsilon_s]\} \\ & + 2z_2^{\top}P_2[W_2\delta_2 - \varpi_{1,1}\delta_1] + 2z_2^{\top}P_2G_2z_3.\end{aligned}$$

The second *virtual control law* is picked as

$$\begin{aligned}\alpha_2 &= \alpha_2(\bar{x}_2, \theta, t) \\ &= G_2^{-1}\left[A_2z_2 - P_2^{-1}G_1^{\top}\left(h^{x_1}\right)^{\top}P_1z_1 - f_2 + \sigma_1 + \alpha_1^{\theta}\upsilon_s + \alpha_{20}\right]\end{aligned} \tag{4.15}$$

where α_{20} is a nonlinear damping term to be designed. Define the second *tuning function*, $\tau_2 \in \mathbb{R}$, as

$$\tau_2(\bar{x}_2, \theta, t) := \tau_1(x_1, \theta) + 2z_2(\bar{x}_2, \theta, t)^\top P_2 \alpha_1^\theta(x_1, \theta, t). \tag{4.16}$$

Using Young's inequality again, the derivative $\dot{V}_2$ becomes

$$\begin{aligned}\dot{V}_2 \leq & -z_1^\top Q_1 z_1 - z_2^\top Q_2 z_2 + 2z_2^\top P_2 G_2 z_3 + \tau_2 \omega_s \\ & + 2z_2^\top P_2 \left\{ \alpha_{20} + \frac{1}{2}\kappa_2 \left[W_2 W_2^\top + \varpi_{1,1}\varpi_{1,1}^\top \right] P_2 z_2 \right\} \\ & + \frac{1}{\kappa_1}\delta_1^\top \delta_1 + \frac{1}{\kappa_2}\left[\delta_2^\top \delta_2 + \delta_1^\top \delta_1 \right]\end{aligned}$$

and the second nonlinear damping term α_{20} is chosen as

$$\begin{aligned}&\alpha_{20} = \rho_2(\bar{x}_2, \theta, t) z_2 \\ &\rho_2 = -\tfrac{1}{2}\kappa_2 \left[W_2 W_2^\top + \varpi_{1,1}\varpi_{1,1}^\top \right] P_2, \quad \kappa_2 > 0.\end{aligned} \tag{4.17}$$

Then *Step 2* results in

$$\begin{aligned}\dot{z}_2 = & -P_2^{-1} G_1^\top \left(h^{x_1}\right)^\top P_1 z_1 + A_2 z_2 + G_2 z_3 + \alpha_1^\theta \omega_s \\ & - \frac{1}{2}\kappa_2 \left[W_2 W_2^\top + \varpi_{1,1}\varpi_{1,1}^\top \right] P_2 z_2 - \varpi_{1,1}\delta_1 + W_2 \delta_2 \qquad (4.18) \\ \dot{V}_2 \leq & -z_1^\top Q_1 z_1 - z_2^\top Q_2 z_2 + 2z_2^\top P_2 G_2 z_3 + \tau_2 \omega_s + \Delta_2^\top K_2 \Delta_2 \qquad (4.19)\end{aligned}$$

where $\Delta_2 := [\delta_1^\top,\ \delta_2^\top]^\top$ and $K_2 := \mathrm{diag}(\frac{1}{\kappa_1} + \frac{1}{\kappa_2}, \frac{1}{\kappa_2})$. If this was the last step, then $z_3 = 0$ and $\omega_s = 0$ would give

$$\dot{V}_2 \leq -q_2 |\bar{z}_2|^2 + k_2 |\Delta_2|^2 < 0, \quad \forall |\bar{z}_2| > \sqrt{\frac{k_2}{q_2}} |\Delta_2|$$

where $q_2 = \lambda_{\min}(Q_1, Q_2)$, $k_2 = \frac{1}{\kappa_1} + \frac{1}{\kappa_2}$, which indicates ISS from the disturbances δ_1, δ_2 to the states z_1, z_2. Steps *i=3,...,n* are summarized in Table 4.1.

Upon the completion of *Step n,* the choice

$$\begin{aligned}u &= \alpha_n(\bar{x}_n, \theta, t) \qquad (4.20) \\ &= G_n^{-1}\left[A_n z_n - P_n^{-1} G_{n-1}^\top P_{n-1} z_{n-1} - f_n + \sigma_{n-1} + \alpha_{n-1}^\theta \upsilon_s + u_0 \right] \\ u_0 &= -\frac{1}{2}\kappa_n \left[W_n W_n^\top + \sum_{j=1}^{n-1} \varpi_{n-1,j}\varpi_{n-1,j}^\top \right] P_n z_n \qquad (4.21)\end{aligned}$$

Table 4.1: ISS Maneuvering: Step i = 3,...,n.
Substitute $z_{n+1} = 0$ and $\alpha_n = u$ for *Step n.*

$$\dot{z}_i = \dot{x}_i - \dot{\alpha}_{i-1}$$
$$= G_i z_{i+1} + G_i \alpha_i + f_i + W_i \delta_i - \sigma_{i-1} - \alpha_{i-1}^{\theta} \dot{\theta} - \textstyle\sum_{j=1}^{i-1} \varpi_{i-1,j} \delta_j$$
$$V_i := V_{i-1} + z_i^{\top} P_i z_i$$

$$\dot{V}_i \leq - \textstyle\sum_{j=1}^{i-1} z_j^{\top} Q_j z_j + \sum_{j=1}^{i-1} \sum_{k=j}^{i-1} \frac{1}{\kappa_k} \delta_j^{\top} \delta_j$$
$$+2 z_i^{\top} \left\{ G_{i-1}^{\top} P_{i-1} z_{i-1} + P_i \left[G_i \alpha_i + f_i - \sigma_{i-1} - \alpha_{i-1}^{\theta} \upsilon_s \right] \right\}$$
$$+2 z_i^{\top} P_i \left[W_i \delta_i - \textstyle\sum_{j=1}^{i-1} \varpi_{i-1,j} \delta_j \right]$$
$$+2 z_i^{\top} P_i \alpha_{i-1}^{\theta} \omega_s + \tau_{i-1} \omega_s + 2 z_i^{\top} P_i G_i z_{i+1}$$

$$\Downarrow$$

$$\tau_i := \tau_{i-1} + 2 z_i^{\top} P_i \alpha_{i-1}^{\theta} \qquad i\text{'th Tuning Function}$$
$$\alpha_i = \alpha_i(\bar{x}_i, \theta, t)$$
$$= G_i^{-1} \left[A_i z_i - P_i^{-1} G_{i-1}^{\top} P_{i-1} z_{i-1} - f_i + \sigma_{i-1} + \alpha_{i-1}^{\theta} \upsilon_s + \alpha_{i0} \right]$$
$$\alpha_{i0} = \rho_i(\bar{x}_i, \theta, t) z_i$$
$$\rho_i = -\tfrac{1}{2} \kappa_i \left[W_i W_i^{\top} + \textstyle\sum_{j=1}^{i-1} \varpi_{i-1,j} \varpi_{i-1,j}^{\top} \right] P_i$$
$$P_i A_i + A_i^{\top} P_i = -Q_i < 0 \quad \text{and} \quad \kappa_i > 0$$

$$\Downarrow$$

$$\dot{z}_i = -P_i^{-1} G_{i-1}^{\top} P_{i-1} z_{i-1} + A_i z_i + G_i z_{i+1} + \alpha_{i-1}^{\theta} \omega_s$$
$$-\tfrac{1}{2} \kappa_i \left[W_i W_i^{\top} + \textstyle\sum_{j=1}^{i-1} \varpi_{i-1,j} \varpi_{i-1,j}^{\top} \right] P_i z_i - \textstyle\sum_{j=1}^{i-1} \varpi_{i-1,j} \delta_j + W_i \delta_i$$

$$\dot{V}_i \leq - \textstyle\sum_{j=1}^{i} z_j^{\top} Q_j z_j + 2 z_i^{\top} P_i G_i z_{i+1} + \tau_i \omega_s + \Delta_i^{\top} K_i \Delta_i$$
$$\Delta_i := \operatorname{col}(\delta_1, \delta_2, \cdots, \delta_i)$$
$$K_i := \operatorname{diag}\left(\tfrac{1}{\kappa_1} + \tfrac{1}{\kappa_2} + \ldots + \tfrac{1}{\kappa_i}, \ \tfrac{1}{\kappa_2} + \ldots + \tfrac{1}{\kappa_i}, \cdots, \tfrac{1}{\kappa_i} \right)$$

$$\Downarrow$$

$$\dot{\alpha}_i =: \sigma_i + \alpha_i^{\theta} \dot{\theta} + \textstyle\sum_{j=1}^{i} \varpi_{i,j} \delta_j$$
$$\sigma_i := \alpha_i^{x_1} \left[G_1 x_2 + f_1 \right] + \ldots + \alpha_i^{x_i} \left[G_i x_{i+1} + f_i \right] + \alpha_i^{t}$$
$$\varpi_{i,j} := \alpha_i^{x_j} W_j$$

with $\kappa_n > 0$, results in

$$\dot{z}_n = -P_n^{-1} G_{n-1}^\top P_{n-1} z_{n-1} + A_n z_n + \alpha_{n-1}^\theta \omega_s \tag{4.22}$$
$$- \frac{1}{2}\kappa_n \left[W_n W_n^\top + \sum_{j=1}^{n-1} \varpi_{n-1,j} \varpi_{n-1,j}^\top \right] P_n z_n - \sum_{j=1}^{n-1} \varpi_{n-1,j} \delta_j + W_n \delta_n$$

and

$$\dot{V}_n \leq -\sum_{j=1}^{n} z_j^\top Q_j z_j + \tau_n \omega_s + \Delta_n^\top K_n \Delta_n. \tag{4.23}$$

Resulting system: With $x := \bar{x}_n$, $z := \bar{z}_n$, $\Delta(t) := \Delta_n(t) = \mathrm{col}(\delta_1(t), \ldots, \delta_n(t))$, $P := \mathrm{diag}(P_1, P_2, \ldots, P_n)$, and $Q := \mathrm{diag}(Q_1, Q_2, \ldots, Q_n)$ we rewrite the n'th tuning function as

$$\tau_n(x, \theta, t) = 2b(\bar{x}_{n-1}, \theta, t)^\top P z(x, \theta, t), \tag{4.24}$$

and the closed-loop system becomes

$$\dot{z} = A_z(x, \theta, t) z + b(\bar{x}_{n-1}, \theta, t)\omega_s + W(x, \theta, t)\Delta(t) \tag{4.25a}$$
$$\dot{\theta} = \upsilon_s(\theta, t) - \omega_s, \tag{4.25b}$$

where

$$A_z(x, \theta, t) := \begin{bmatrix} A_1 + \rho_1 & h^{x_1} G_1 & 0 & 0 & \cdots & \\ -P_2^{-1} G_1^\top \left(h^{x_1}\right)^\top P_1 & A_2 + \rho_2 & G_2 & 0 & \cdots & \\ 0 & -P_3^{-1} G_2^\top P_2 & A_3 + \rho_3 & G_3 & \cdots & \\ \vdots & \vdots & \vdots & \ddots & \ddots & \cdots \\ 0 & 0 & 0 & 0 & \cdots & \\ 0 & 0 & 0 & 0 & \cdots & \end{bmatrix}$$
$$\begin{bmatrix} \cdots & 0 & 0 & 0 \\ \cdots & 0 & 0 & 0 \\ \cdots & 0 & 0 & 0 \\ \cdots & \ddots & \ddots & \vdots & \vdots \\ \cdots & -P_{n-1}^{-1} G_{n-2}^\top P_{n-2} & A_{n-1} + \rho_{n-1} & G_{n-1} \\ \cdots & 0 & -P_n^{-1} G_{n-1}^\top P_{n-1} & A_n + \rho_n \end{bmatrix},$$

$$b(\bar{x}_{n-1}, \theta, t) := \mathrm{col}\left(\; y_d^\theta(\theta), \quad \alpha_1^\theta(\bar{x}_1, \theta, t), \quad \ldots, \quad \alpha_{n-1}^\theta(\bar{x}_{n-1}, \theta, t) \; \right),$$

and

$$W(x,\theta,t) := \begin{bmatrix} h^{x_1}W_1 & 0 & 0 & \cdots & 0 & 0 \\ -\varpi_{1,1} & W_2 & 0 & \cdots & 0 & 0 \\ -\varpi_{2,1} & -\varpi_{2,2} & W_3 & \ddots & 0 & 0 \\ \vdots & \vdots & \ddots & \ddots & \vdots & \vdots \\ -\varpi_{n-1,1} & -\varpi_{n-1,2} & -\varpi_{n-1,3} & \cdots & -\varpi_{n-1,n-1} & W_n \end{bmatrix}.$$

The backstepping design has transformed the original system (4.1) into the error coordinates z by a diffeomorphism $(x,\theta,t) \longleftrightarrow (z,\theta,t)$ where $z = \Psi(x,\theta,t)$ is given by (4.2) and (4.3) for $i = 2,\ldots,n$. The inverse map $x = \Upsilon(z,\theta,t)$ of this diffeomorphism is given by

$$\Upsilon(z,\theta,t): \begin{cases} x_1 = \psi_1(\bar{z}_1,\theta,t) = h^{-1}(z_1 + y_d(\theta)) \\ x_2 = \psi_2(\bar{z}_2,\theta,t) = z_2 + \alpha_1(\psi_1(\bar{z}_1,\theta,t),\theta,t) \\ \quad\vdots \\ x_n = \psi_n(\bar{z}_n,\theta,t) = z_n + \alpha_{n-1}(\psi_{n-1}(\bar{z}_{n-1},\theta,t),\theta,t) \end{cases} \tag{4.26}$$

which (for each fixed z) is bounded uniformly in (θ,t) due to Assumption 3.1 and the continuity assumptions on h^{-1}, G_i, f_i, and W_i.

The derivative of the *Step n* CLF satisfies the inequality

$$\dot{V}_n \le -z^\top Q z + \tau_n \omega_s + \Delta^\top K_n \Delta \tag{4.27}$$

which is of the form of the principal design inequality (3.14b). While the expressions (4.20) and (4.21) define the static part of the control law, the dynamic part, specifying either $\dot{\theta}$ or $(\dot{\theta}, \dot{\omega}_s)$, is to render the term $\tau_n\omega_s$ in (4.27) nonpositive. When $\tau_n\omega_s \le 0$ is achieved, then (4.27) guarantees that the closed-loop system is ISS where the damping gains κ_i can be adjusted for a desired level of disturbance attenuation. Following Jiang, Teel and Praly (1994), one can assign the gain from the disturbances δ_i to the output error $z_1 = y - y_d(\theta)$ to ensure any desired output maneuvering accuracy.

4.1.2 Closing the loop by speed assignment designs

The set to be rendered 0-invariant for (4.25) becomes

$$\mathcal{M} = \{(z,\theta,t) \in \mathbb{R}^{nm} \times \mathbb{R} \times \mathbb{R}_{\ge 0} :\ z = 0\}, \tag{4.28}$$

and it is verified, for $\Delta \equiv 0$, that any solution of (4.25) staying identically in (4.28) will solve the Maneuvering Problem. Indeed, $z_1 = 0$ will solve the

geometric task. Moreover, for $z \equiv 0$ and $\Delta = 0$ we get from (4.25) that $\dot{z} = b(\bar{x}_{n-1}, \theta, t)\omega_s = 0$ such that $\omega_s = \dot{\theta} - \upsilon_s(\theta, t) = 0$ must hold for all $(z, \theta, t) \in \mathcal{M}$.

For the dynamic part of the control law, the design variable is ω_s :

Theorem 4.1 *The closed-loop system (4.25) is ISS with respect to the set (4.28) for every continuous function $\omega_s = \omega(z, \theta, t)$ that satisfies:*

1. *there exists a continuous positive semi-definite function $\sigma : \mathbb{R}^{nm} \to \mathbb{R}_{\geq 0}$, $\sigma(0) = 0$, such that $|\omega(z, \theta, t)| \leq \sigma(z)$, $\forall\, (z, \theta, t) \in \mathbb{R}^{nm} \times \mathbb{R} \times \mathbb{R}_{\geq 0}$, and*

2. $\tau_n(\Upsilon(z, \theta, t), \theta, t)\omega(z, \theta, t) \leq 0, \quad \forall\, (z, \theta, t) \in \mathbb{R}^{nm} \times \mathbb{R} \times \mathbb{R}_{\geq 0}$.

   In the case when $\Delta = 0$, then the set (4.28) becomes UGES with respect to (4.25) for this choice of ω_s.

Proof. *The closed-loop system (4.25), with $\omega_s = \omega(z, \theta, t)$, is of the form of the interconnected system (A.40) in Appendix A by setting $x_1 := z$, $x_2 := (\theta, t)$, and $u_1 := \Delta$, $u_2 = 0$ in (A.40). Defining accordingly $f_1 := A_z(x, \theta, t)z + b(\bar{x}_{n-1}, \theta, t)\omega(z, \theta, t) + W(x, \theta, t)\Delta$ where $x = \Upsilon(z, \theta, t)$ and $f_2 := \operatorname{col}(\upsilon_s(\theta, t) - \omega(z, \theta, t),\ 1)$ then f_2 satisfies Lemma A.21 since $|\omega(z, \theta, t)| \leq \sigma(z)$ is uniformly bounded for all z in the compact set $\mathcal{X}$. Moreover, since $V_n(z)$ satisfies (A.44) with $\alpha_1(\cdot) := \lambda_{\min}(P)\,(\cdot)^2$, $\alpha_2(\cdot) := \lambda_{\max}(P)\,(\cdot)^2$, and (A.45) with $\alpha_3(\cdot) := \lambda_{\min}(Q)\,(\cdot)^2$, $\alpha_4(\cdot) := \lambda_{\max}(K_n)\,(\cdot)^2$, using $|(z, \theta, t)|_{\mathcal{M}} = |z| = |x_1|_{\mathcal{A}_1}$, then the conclusion of Theorem A.22 gives ISS from Δ to z with respect to $\mathcal{M}$, and UGES in the disturbance-free case.* ■

The *Tracking* or *Gradient* update laws can be applied to accomodate Conditions *1* and *2* of Theorem 4.1.

Gradient update law: Setting $\omega_s = -\mu\tau_n(x, \theta, t)$, $\mu \geq 0$, satisfies the speed assignment (2.20) asymptotically since $\tau_n \to 0$ as $z \to 0$. The Condition *1* bound $|\mu\tau_n(\Upsilon(z, \theta, t), \theta, t)| \leq \sigma(z)$ of Theorem 4.1 can be verified recursively by applying Assumption 3.1 and (4.26). We call this a *Gradient* update law because

$$\tau_n(x, \theta, t) = -V_n^{\theta}(\Psi(x, \theta, t)), \tag{4.29}$$

and the dynamic part of the control law becomes

$$\begin{aligned} \dot{\theta} &= \upsilon_s(\theta, t) + \mu\tau_n(x, \theta, t) \\ &= \upsilon_s(\theta, t) - \mu V_n^{\theta}(\Psi(x, \theta, t)). \end{aligned} \tag{4.30}$$

For $\mu = 0$ it reduces to the tracking update law $\dot{\theta} = \upsilon_s(\theta, t)$.

This update law has the same gradient properties as shown in Section 3.4. Increasing the gain μ will ensure that θ rapidly converges to a minimizer of $\theta \mapsto V_n(\Psi(x, \theta, t))$. However, since there is now a nonlinear mapping from x to $z = \Psi(x, \theta, t)$ there may exist multiple local minima of $\theta \mapsto V_n(\Psi(x, \theta, t))$ for each fixed (x, t). This should be analyzed on a case-by-case basis.

Filtered-gradient update law: As an alternative to the direct design above, we augment the *Step n* CLF to

$$V = V_n + \frac{1}{2\lambda\mu}\omega_s^2, \qquad \lambda, \mu > 0, \tag{4.31}$$

get the time-derivative

$$\begin{aligned}\dot{V} &= \dot{V}_n + \frac{1}{\lambda\mu}\omega_s\dot{\omega}_s \\ &\leq -z^\top Q z + [\tau_n + \frac{1}{\lambda\mu}\dot{\omega}_s]\omega_s + \Delta_n^\top K_n \Delta_n,\end{aligned}$$

and choose the update law for $\dot{\omega}_s$ as

$$\dot{\omega}_s = -\lambda\left(\omega_s + \mu\tau_n\right) \tag{4.32}$$

resulting in

$$\dot{V} \leq -z^\top Q z - \frac{1}{\mu}\omega_s^2 + \Delta_n^\top K_n \Delta_n. \tag{4.33}$$

We note that (4.32) is (4.29) filtered by $-\mu\frac{\lambda}{s+\lambda}$, and the dynamic part of the control law becomes the Filtered-gradient update law

$$\begin{aligned}\dot{\theta} &= \upsilon_s(\theta, t) - \omega_s \\ \dot{\omega}_s &= -\lambda\omega_s - \lambda\mu\tau_n(x, \theta, t).\end{aligned} \tag{4.34}$$

Theorem 4.2 *The closed-loop system resulting from the Filtered-Gradient update law:*

$$\begin{aligned}\dot{z} &= A_z(x, \theta, t)z + b(\bar{x}_{n-1}, \theta, t)\omega_s + W(x, \theta, t)\Delta(t) \\ \dot{\theta} &= \upsilon_s(\theta, t) - \omega_s \\ \dot{\omega}_s &= -2\lambda\mu b(\bar{x}_{n-1}, \theta, t)^\top P z - \lambda\omega_s\end{aligned} \tag{4.35}$$

is ISS with respect to the closed, 0*-invariant set*

$$\mathcal{M}' = \left\{(z, \omega_s, \theta, t) \in \mathbb{R}^{nm} \times \mathbb{R} \times \mathbb{R} \times \mathbb{R}_{\geq 0} : \ z = 0, \ \omega_s = 0\right\}. \tag{4.36}$$

In the disturbance-free case, the set $\mathcal{M}'$ is UGES with respect to (4.35).

Proof. *By setting $x_1 := (z, \omega_s)$ and $x_2 := (\theta, t)$ in (A.40), the proof follows directly from Theorem A.22 by applying the ISS-Lyapunov function (4.31) with its derivative (4.33), and Assumption 3.1 for boundedness of $\upsilon_s(\theta, t)$. The details are left for the reader to verify.* ■

Note that the filter (4.32) can be designed of any order by using the design procedure of Section 3.1.3. Only the 1st order case was considered here for simplicity. It should also be noted that the design can again be extended with phase assignment according to Section 3.2.

Important: By the achieved ISS property, z and ω_s are only guaranteed to enter a small residual set $\mathcal{Z}$ due to the disturbances. This may cause θ in (4.30) or (4.34), and therefore $y_d(\theta)$, to stop, which happens if $\omega_s(t) = \upsilon_s(\theta(t), t)$ for some t. Reducing $\mathcal{Z}$ with larger nonlinear damping gains κ_i will alleviate this problem.

4.1.3 Example: The robotic cutting tool

We return to the example in Section 2.4.1 and design a robust maneuvering system for the cutting tool application. For the plant (2.30), let D_1 and K_1 be unknown state dependent matrices, bounded by

$$\sup_x ||K_1(x)|| < m_K, \quad \sup_{\dot{x}} ||D_1(\dot{x})|| < m_D$$

where m_K, m_D need not be known. Let $x_1 := x$ and $x_2 := \dot{x}$, and define $W(\bar{x}_2) := [W_1(x_1), W_2(x_2)] \in \mathbb{R}^{2\times 8}$ where $W_i(x_i) := -\operatorname{diag}(x_i^\top, x_i^\top) \in \mathbb{R}^{2\times 4}$ and $\Delta(t) := \operatorname{col}(\delta_1(t),\ \delta_2(t)) \in \mathbb{R}^8$ where $\delta_1(t), \delta_2(t) \in \mathbb{R}^4$ contains the two rows of K_1 and D_1 stacked in one column vector. The plant becomes

$$\begin{aligned} \dot{x}_1 &= x_2 \\ M\dot{x}_2 + D_0 x_2 + K_0 x_1 &= u + W(\bar{x}_2)\Delta(t) \end{aligned}$$

which is in the form of (4.1). The design procedure then yields

$$\begin{aligned} z_1 &= x_1 - y_d(\theta) \\ z_2 &= x_2 - \alpha_1(x_1, y_d(\theta), y_d^\theta(\theta), \upsilon_s(\theta)) \\ \alpha_1 &= -K_p z_1 + y_d^\theta(\theta)\upsilon_s(\theta) \\ \sigma_1 &= -K_p x_2 \\ \alpha_1^\theta &= K_p y_d^\theta(\theta) + y_d^{\theta^2}(\theta)\upsilon_s(\theta) + y_d^\theta(\theta)\upsilon_s^\theta(\theta) \end{aligned}$$

where $A_1 = -K_p$, $K_p = K_p^\top > 0$, and $A_2 = -K_d$, $K_d = K_d^\top > 0$. The control law and the maneuvering update law are given by the closed-loop system in Table 4.2. Stability is verified with $V = p_1 z_1^\top z_1 + p_2 z_2^\top M z_2 + \frac{1}{2\mu_1}\omega_s^2$ and its derivative $\dot{V} \leq -z_1^\top Q_1 z_1 - z_2^\top Q_2 z_2 - \frac{\lambda}{\mu_1}\omega_s^2 + \frac{1}{\kappa}\Delta^\top\Delta$.

Table 4.2: Closed-loop maneuvering system for the cutting tool application

Plant :
$\dot{x}_1 = x_2$
$\dot{x}_2 = M^{-1}\left(u - D(\dot{x})x_2 - K(x)x_1\right)$
input: $\{u\}$
output: $\{x_1, x_2\}$
Control :
$\dot{\theta} = \upsilon_s(\theta) - \omega_s$
$\dot{\omega}_s = -\lambda\omega_s - 2\mu_1\left(p_1 z_1^\top y_d^\theta(\theta) + p_2 z_2^\top M\alpha_1^\theta\right)$
$u = -\frac{p_1}{p_2}z_1 - K_d z_2 + K_0 x_1 + D_0\alpha_1 + M\sigma_1$ $+M\alpha_1^\theta\upsilon_s(\theta) - \frac{1}{2}\kappa W(\bar{x}_2)W(\bar{x}_2)^\top p_2 z_2$
input: $\left\{x_1, x_2, y_d(\theta), y_d^\theta(\theta), y_d^{\theta^2}(\theta), \upsilon_s(\theta), \upsilon_s^\theta(\theta)\right\}$
output: $\{u, \theta\}$
Guidance :
input: $\{\theta\}$
output: $\left\{y_d(\theta), y_d^\theta(\theta), y_d^{\theta^2}(\theta), \upsilon_s(\theta), \upsilon_s^\theta(\theta)\right\}$

To satisfy the performance specifications of the example in Section 2.4.1, we constructed the speed assignment (2.32), which has the derivative

$$\upsilon_s^\theta(\theta) = \begin{cases} \frac{m_s}{\pi\left|y_d^\theta\right|}\frac{a_2}{a_2^2+(\theta-\theta_k-a_1)^2}; & \theta \in \left[\theta_k,\ \theta_k + \frac{\theta_{k+1}-\theta_k}{2}\right) \\ \frac{-m_s}{\pi\left|y_d^\theta\right|}\frac{a_2}{a_2^2+(\theta_{k+1}-a_1-\theta)^2}; & \theta \in \left[\theta_k + \frac{\theta_{k+1}-\theta_k}{2},\ \theta_{k+1}\right). \end{cases}$$

Since the assigned speed is very slow at the nodes, there is a danger that the tracing stops if the disturbances are not attenuated enough. It is therefore important to choose κ large enough. In the simulation shown next, $\upsilon_s(\theta) \geq 0.0013$ for all θ and $\kappa = 150$ ensures that the residual set for ω_s is smaller than 0.0013.

In the simulation, we let the matrices K and D, including the 'unknown'

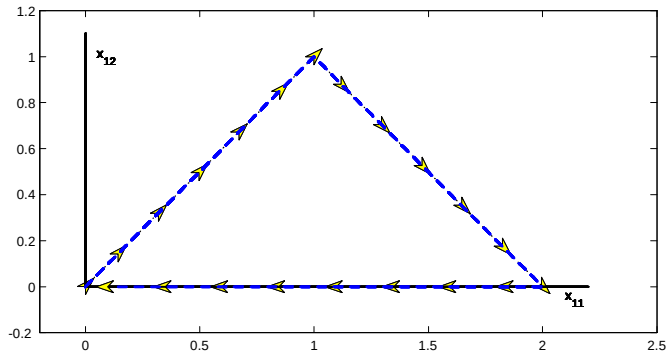

Figure 4.1: Positional motion of the cutting tool in the space of $x \in \mathbb{R}^2$.

trigonometric disturbance terms, be

$$K(x_1) = \begin{bmatrix} 10 + 0.15\sin(7.5x_{11})\cos(7.5x_{12}) & 0 \\ 0 & 10 + 0.15\sin(7.5x_{12})\cos(7.5x_{11}) \end{bmatrix}$$

$$D(x_2) = \begin{bmatrix} 2 & 0.1\sin(x_{21}) \\ 0.1\sin(x_{22}) & 2 \end{bmatrix}$$

and $M = I$. The controller gains were set to $K_p = K_d = 50I$, $p_1 = 5$, $p_2 = 1$, $\kappa = 150$, $\lambda = 40$, $\mu_1 = 1$, and the speed assignment parameters were set to $a_1 = 0.005$, $a_2 = 0.001$, and $m_s = 0.1$.

The position of the tool started from rest at $(0, 0)$ and $(\theta(0), \omega_s(0)) = (0, 0)$. The output, shown in Figure 4.1, accurately traces the path. From Figure 4.2 the output error $|z_1(t)| = |x_1(t) - y_d(\theta(t))|$ is observed to be in the order of 10^{-5} which is well below the specified limit. The speed along the path is seen from Figure 4.3 to be approximately $0.1\,\mathrm{m/s}$ with a small ripple due to the 'disturbances' in $K(x_1(t))$ and $D(x_2(t))$. In Figure 4.4 we also verify that the control effort is far from being excessive, despite the large nonlinear damping gain.

This illustrates the gradient-based maneuvering system's capability to always keep the error signals small. The time spent tracing the path is 51.1 s. If one were able to trace the entire path with speed m_s, then the total time would be 48.3 s so that the time loss is only 5.8%. We conclude that our maneuvering design satisfies the problem specifications well.

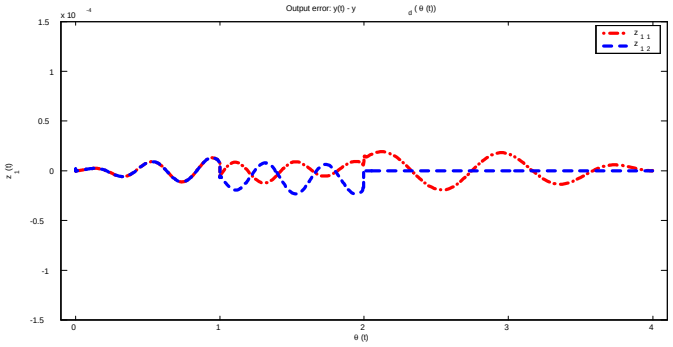

Figure 4.2: Output error $z_1(t) = x(t) - y_d(\theta(t))$.

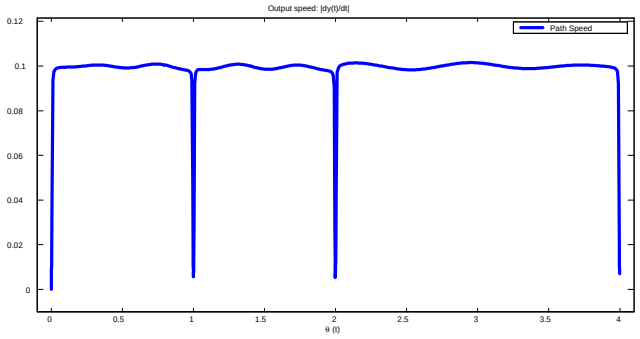

Figure 4.3: Output speed along the path.

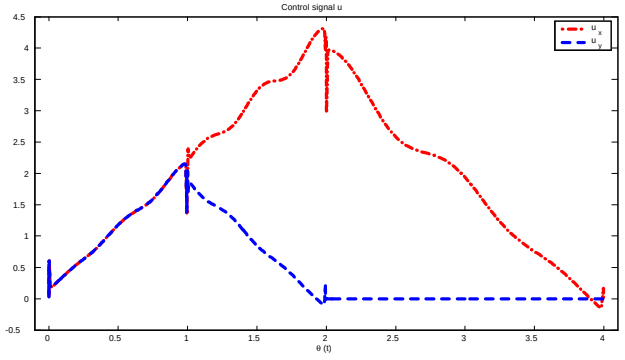

Figure 4.4: Control signal $u(t)$ for the cutting tool.

4.2 Adaptive backstepping design

This section shows how the maneuvering problem is solved by adaptive backstepping for parametrically uncertain nonlinear systems. Consider the plant (3.1) and suppose it can be written in parametric strict feedback form of vector relative degree n :

$$\begin{aligned}
\dot{x}_1 &= G_1(x_1)\, x_2 + f_1(x_1) + \Phi_1(x_1)\,\varphi \\
\dot{x}_2 &= G_2(\bar{x}_2)\, x_3 + f_2(\bar{x}_2) + \Phi_2(\bar{x}_2)\,\varphi \\
&\vdots \\
\dot{x}_n &= G_n(\bar{x}_n)\, u + f_n(\bar{x}_n) + \Phi_n(\bar{x}_n)\,\varphi \\
y &= h(x_1)
\end{aligned} \tag{4.37}$$

where $x_i \in \mathbb{R}^m$, $i = 1, \ldots, n$, are the states, $y \in \mathbb{R}^m$ is the output, $u \in \mathbb{R}^m$ is the control, and $\varphi \in \mathbb{R}^p$ is a vector of constant unknown parameters. The matrices $G_i(\bar{x}_i)$ and $h^{x_1}(x_1) := \frac{\partial h}{\partial x_1}(x_1)$ are invertible for all $\bar{x}_i$, the map $h(x_1)$ is a diffeomorphism, and G_i, f_i, and Φ_i are smooth.

The design task is again to design a *maneuvering controller* that solves the *Maneuvering Control Objective* for a continuously parametrized feasible path $y_d(\theta)$ and a feasible speed assignment $\upsilon_s(\theta, t)$ where the boundedness constraints on the path and speed assignment in Assumption 3.1 are satisfied.

4.2.1 Design procedure

In the recursive procedure that follows, a detailed development of *Step 1* and *2* are shown, while *Step i=3,. . . ,n* is given in Table 4.3. The adaptive procedure of Krstić et al. (1995) is adopted, making the distinction between the notions of a *tuning function* and an *adaptive tuning function*.

Step 1: Define the error variables

$$z_1(x_1, \theta) := y - y_d(\theta) = h(x_1) - y_d(\theta) \tag{4.38}$$

$$z_i(\bar{x}_i, \hat{\varphi}, \theta, t) := x_i - \alpha_{i-1}(\bar{x}_{i-1}, \hat{\varphi}, \theta, t), \quad i = 2, \ldots, n \tag{4.39}$$

$$\omega_s(\dot{\theta}, \theta, t) := \upsilon_s(\theta, t) - \dot{\theta} \tag{4.40}$$

$$\tilde{\varphi} := \varphi - \hat{\varphi}, \tag{4.41}$$

where $\hat{\varphi}$ is the parameter estimate and α_{i-1} are *virtual controls* to be spec-

ified later. Differentiating (4.38) with respect to time yields

$$\begin{aligned}\dot{z}_1 &= \dot{y} - y_d^\theta \dot{\theta} \\ &= h^{x_1} G_1 z_2 + h^{x_1} G_1 \alpha_1 + h^{x_1} f_1 + h_1^{x_1} \Phi_1 \varphi - y_d^\theta \dot{\theta}.\end{aligned}$$

Choose a Hurwitz matrix A_1 so that $P_1 = P_1^\top > 0$ is the solution to $P_1 A_1 + A_1^\top P_1 = -Q_1 < 0$, and let $\Gamma = \Gamma^\top > 0$. Define the first control Lyapunov function (CLF) as

$$V_1(x_1, \hat{\varphi}, \theta) := z_1(x_1, \theta)^\top P_1 z_1(x_1, \theta) + \frac{1}{2} \tilde{\varphi}^\top \Gamma^{-1} \tilde{\varphi} \tag{4.42}$$

whose time derivative is

$$\begin{aligned}\dot{V}_1 &= 2 z_1^\top P_1 [h^{x_1} G_1 \alpha_1 + h^{x_1} f_1 + h_1^{x_1} \Phi_1 \hat{\varphi} - y_d^\theta \upsilon_s] \\ &\quad + 2 z_1^\top P_1 [h^{x_1} G_1 z_2 + h_1^{x_1} \Phi_1 \tilde{\varphi} + y_d^\theta \omega_s] - \tilde{\varphi}^\top \Gamma^{-1} \dot{\hat{\varphi}}\end{aligned}$$

where $\dot{\tilde{\varphi}} = -\dot{\hat{\varphi}}$. The first virtual control law is then picked as

$$\begin{aligned}\alpha_1 &= \alpha_1(x_1, \hat{\varphi}, \theta, t) \\ &= G_1^{-1} \left(h^{x_1}\right)^{-1} [A_1 z_1 - h^{x_1} f_1 - h_1^{x_1} \Phi_1 \hat{\varphi} + y_d^\theta \upsilon_s].\end{aligned} \tag{4.43}$$

Let $\Delta_1(x_1) := h^{x_1}(x_1) \Phi_1(x_1)$, and define the first tuning function, $\tau_1 \in \mathbb{R}$, and the adaptive tuning function, $\rho_1 \in \mathbb{R}^p$, as

$$\tau_1(x_1, \theta) := 2 z_1(x_1, \theta)^\top P_1 y_d^\theta(\theta) \tag{4.44}$$

$$\rho_1(x_1, \theta) := 2 \Delta_1(x_1)^\top P_1 z_1(x_1, \theta). \tag{4.45}$$

The result of *Step 1* becomes

$$\dot{z}_1 = A_1 z_1 + h^{x_1} G_1 z_2 + y_d^\theta \omega_s + \Delta_1 \tilde{\varphi} \tag{4.46}$$

$$\dot{V}_1 = -z_1^\top Q_1 z_1 + 2 z_1^\top P_1 h^{x_1} G_1 z_2 + \tau_1 \omega_s + \tilde{\varphi}^\top [\rho_1 - \Gamma^{-1} \dot{\hat{\varphi}}] \tag{4.47}$$

where the terms containing z_2, ω_s, and $\tilde{\varphi}$ are left for the next step. To aid next step, let

$$\begin{aligned}\dot{\alpha}_1 \;=\; & : \sigma_1(\bar{x}_2, \hat{\varphi}, \theta, t) + \alpha_1^\theta(x_1, \hat{\varphi}, \theta, t) \dot{\theta} \\ & + \chi_{1,1}(x_1, \hat{\varphi}, \theta, t) \tilde{\varphi} + \chi_{1,2}(x_1, \hat{\varphi}, \theta, t) \dot{\hat{\varphi}}\end{aligned} \tag{4.48}$$

where

$$\begin{aligned}\sigma_1(\bar{x}_2, \hat{\varphi}, \theta, t) := {} & \alpha_1^{x_1}(x_1, \hat{\varphi}, \theta, t) [G_1(x_1) x_2 + f_1(x_1) + \Phi_1(x_1) \hat{\varphi}] \\ & + \alpha_1^t(x_1, \hat{\varphi}, \theta, t)\end{aligned} \tag{4.49}$$

$$\chi_{1,1}(x_1, \hat{\varphi}, \theta, t) := \alpha_1^{x_1}(x_1, \hat{\varphi}, \theta, t) \Phi_1(x_1) \tag{4.50}$$

$$\chi_{1,2}(x_1, \hat{\varphi}, \theta, t) := \alpha_1^{\hat{\varphi}}(x_1, \hat{\varphi}, \theta, t). \tag{4.51}$$

Step 2: Consider x_3 as the next control variable. Differentiating (4.39), $i = 2$, with respect to time gives

$$\begin{aligned}\dot{z}_2 &= \dot{x}_2 - \dot{\alpha}_1 \\ &= G_2 z_3 + G_2\alpha_2 + f_2 + \Phi_2\varphi - \sigma_1 - \alpha_1^\theta\dot{\theta} - \chi_{1,1}\tilde{\varphi} - \chi_{1,2}\dot{\tilde{\varphi}}\end{aligned}$$

where $z_3 = x_3 - \alpha_2$. Choose A_2 Hurwitz and let $P_2 = P_2^\top > 0$ be the solution to $P_2A_2 + A_2^\top P_2 = -Q_2 < 0$. Define the *Step 2* CLF

$$V_2(\bar{x}_2, \hat{\varphi}, \theta, t) := V_1(x_1, \hat{\varphi}, \theta) + z_2(\bar{x}_2, \hat{\varphi}, \theta, t)^\top P_2 z_2(\bar{x}_2, \hat{\varphi}, \theta, t) \tag{4.52}$$

whose time derivative is

$$\begin{aligned}\dot{V}_2 = &-z_1^\top Q_1 z_1 + 2z_2^\top P_2 G_2 z_3 + \tau_1\omega_s + 2z_2^\top P_2\alpha_1^\theta\omega_s \\ &+ 2z_2^\top\left\{G_1^\top\left(h^{x_1}\right)^\top P_1 z_1 + P_2\left[G_2\alpha_2 + f_2 + \Phi_2\hat{\varphi} - \sigma_1 - \alpha_1^\theta\upsilon_s - \chi_{1,2}\dot{\hat{\varphi}}\right]\right\} \\ &+ \tilde{\varphi}^\top[\rho_1 - \Gamma^{-1}\dot{\hat{\varphi}}] + 2z_2^\top P_2[\Phi_2 - \chi_{1,1}]\tilde{\varphi}.\end{aligned}$$

The second virtual control law is then picked as

$$\begin{aligned}\alpha_2 &= \alpha_2(\bar{x}_2, \hat{\varphi}, \theta, t) \\ &= G_2^{-1}[A_2 z_2 - P_2^{-1}G_1^\top h^{x_1} P_1 z_1 - f_2 - \Phi_2\hat{\varphi} + \sigma_1 + \alpha_1^\theta\upsilon_s + \chi_{12}\Gamma\rho_2].\end{aligned} \tag{4.53}$$

Let $\Delta_2(\bar{x}_2, \hat{\varphi}, \theta, t) := \Phi_2(\bar{x}_2) - \chi_{1,1}(x_1, \hat{\varphi}, \theta, t)$ and $\varpi_2(\bar{x}_2, \hat{\varphi}, \theta, t)^\top := 2z_2(\bar{x}_2, \hat{\varphi}, \theta, t)^\top P_2\chi_{1,2}(x_1, \hat{\varphi}, \theta, t)$, and define the second tuning function, $\tau_2 \in \mathbb{R}$, and the adaptive tuning function, $\rho_2 \in \mathbb{R}^p$, as

$$\tau_2(\bar{x}_2, \hat{\varphi}, \theta, t) := \tau_1(x_1, \theta) + 2z_2(\bar{x}_2, \hat{\varphi}, \theta, t)^\top P_2\alpha_1^\theta(x_1, \hat{\varphi}, \theta, t) \tag{4.54}$$

$$\rho_2(\bar{x}_2, \hat{\varphi}, \theta, t) := \rho_1(x_1, \theta) + 2\Delta_2(\bar{x}_2, \hat{\varphi}, \theta, t)^\top P_2 z_2(\bar{x}_2, \hat{\varphi}, \theta, t). \tag{4.55}$$

The result of *Step 2* becomes

$$\begin{aligned}\dot{z}_2 = &-P_2^{-1}G_1^\top\left(h^{x_1}\right)^\top P_1 z_1 + A_2 z_2 + G_2 z_3 \\ &+ \alpha_1^\theta\omega_s + \Delta_2\tilde{\varphi} + \chi_{1,2}[\Gamma\rho_2 - \dot{\hat{\varphi}}]\end{aligned} \tag{4.56}$$

$$\begin{aligned}\dot{V}_2 = &-z_1^\top Q_1 z_1 - z_2^\top Q_2 z_2 + 2z_2^\top P_2 G_2 z_3 + \tau_2\omega_s \\ &+ \tilde{\varphi}^\top[\rho_2 - \Gamma^{-1}\dot{\hat{\varphi}}] + \varpi_2^\top[\Gamma\rho_2 - \dot{\hat{\varphi}}]\end{aligned} \tag{4.57}$$

where the terms containing z_3, ω_s, and $\dot{\hat{\varphi}}$ are left for the next step.

Steps $i = 3, \ldots, n$ are summarized in Table 4.3. Notice the introduction of the terms ϖ_i, $i = 2, \ldots, n$ which from adaptive backstepping theory is known to occur for plants of relative degree 3 or higher.

Table 4.3: Adaptive Maneuvering: Step i = 3,...,n.
Substitute $z_{n+1} = 0$ and $\alpha_n = u$ for *Step n.*

$$\dot{z}_i = \dot{x}_i - \dot{\alpha}_{i-1}$$
$$= G_i z_{i+1} + G_i \alpha_i + f_i + \Phi_i \varphi - \sigma_{i-1} - \alpha_{i-1}^{\theta} \dot{\theta} - \chi_{i-1,1} \tilde{\varphi} - \chi_{i-1,2} \dot{\hat{\varphi}}$$
$$V_i := V_{i-1} + z_i^{\top} P_i z_i$$

$$\dot{V}_i = -\sum_{j=1}^{i-1} z_j^{\top} Q_j z_j + 2 z_i^{\top} P_i G_i z_{i+1} + \tau_{i-1} \omega_s$$
$$+2 z_i^{\top} \{ G_{i-1}^{\top} P_{i-1} z_{i-1} + P_i [G_i \alpha_i + f_i + \Phi_i \hat{\varphi} - \sigma_{i-1} - \alpha_{i-1}^{\theta} \upsilon_s - \chi_{i-1,2} \dot{\hat{\varphi}}] \}$$
$$+\tilde{\varphi}^{\top} [\rho_{i-1} - \Gamma^{-1} \dot{\hat{\varphi}}] + \varpi_{i-1}^{\top} [\Gamma \rho_{i-1} - \dot{\hat{\varphi}}]$$
$$+2 z_i^{\top} P_i [\Phi_i - \chi_{i-1,1}] \tilde{\varphi} + 2 z_i^{\top} P_i \alpha_{i-1}^{\theta} \omega_s$$

$$\Downarrow$$

$$\Delta_i := \Phi_i - \chi_{i-1,1}$$
$$\varpi_i^{\top} := \varpi_{i-1}^{\top} + 2 z_i^{\top} P_i \chi_{i-1,2}, \qquad \varpi_1^{\top} = 0$$
$$\tau_i := \tau_{i-1} + 2 z_i^{\top} P_i \alpha_{i-1}^{\theta} \qquad i\text{'th Tuning Function}$$
$$\rho_i := \rho_{i-1} + 2 \Delta_i^{\top} P_i z_i \qquad i\text{'th Adaptive Tuning Function}$$
$$\alpha_i = \alpha_i(\bar{x}_i, \hat{\varphi}, \theta, t)$$
$$= G_i^{-1} [A_i z_i - P_i^{-1} G_{i-1}^{\top} P_{i-1} z_{i-1} - f_i - \Phi_i \hat{\varphi} + \sigma_{i-1}$$
$$+\alpha_{i-1}^{\theta} \upsilon_s + \chi_{i-1,2} \Gamma \rho_i + \Delta_i \Gamma \varpi_{i-1}]$$
$$P_i A_i + A_i^{\top} P_i = -Q_i < 0$$

$$\Downarrow$$

$$\dot{z}_i = -P_i^{-1} G_{i-1}^{\top} P_{i-1} z_{i-1} + A_i z_i + G_i z_{i+1} + \alpha_{i-1}^{\theta} \omega_s$$
$$+\Delta_i \tilde{\varphi} + \chi_{i-1,2} [\Gamma \rho_i - \dot{\hat{\varphi}}]$$
$$\dot{V}_i = -\sum_{j=1}^{i} z_j^{\top} Q_j z_j + 2 z_i^{\top} P_i G_i z_{i+1} + \tau_i \omega_s$$
$$+\tilde{\varphi}^{\top} [\rho_i - \Gamma^{-1} \dot{\hat{\varphi}}] + \varpi_i^{\top} [\Gamma \rho_i - \dot{\hat{\varphi}}]$$

$$\Downarrow$$

$$\dot{\alpha}_i =: \sigma_i + \alpha_i^{\theta} \dot{\theta} + \chi_{i,1} \tilde{\varphi} + \chi_{i,2} \dot{\hat{\varphi}}$$
$$\sigma_i := \sum_{j=1}^{i} \alpha_i^{x_j} [G_j x_{j+1} + f_j + \Phi_j \hat{\varphi}] + \alpha_i^t$$
$$\chi_{i,1} := \sum_{j=1}^{i} \alpha_i^{x_j} \Phi_j$$
$$\chi_{i,2} := \alpha_i^{\hat{\varphi}}$$

Upon the completion of *Step n* the static part of the control law and the adaptive update law are designed as

$$\begin{aligned} u &= \alpha_n(\bar{x}_n, \hat{\varphi}, \theta, t) \qquad (4.58)\\ &= G_n^{-1}[A_n z_n - P_n^{-1} G_{n-1}^\top P_{n-1} z_{n-1} - f_n - \Phi_n \hat{\varphi} \\ &\qquad + \sigma_{n-1} + \alpha_{n-1}^\theta \upsilon_s + \chi_{n-1,2} \Gamma \rho_n + \Delta_n \Gamma \varpi_{n-1}] \\ \dot{\hat{\varphi}} &= \Gamma \rho_n(\bar{x}_n, \hat{\varphi}, \theta, t), \qquad (4.59) \end{aligned}$$

resulting in

$$\dot{z}_n = -P_n^{-1} G_{n-1}^\top P_{n-1} z_{n-1} + A_n z_n + \alpha_{n-1}^\theta \omega_s + \Delta_n \tilde{\varphi} \qquad (4.60)$$

where $\Delta_n(\bar{x}_n, \hat{\varphi}, \theta, t) := \Phi_n(\bar{x}_n) - \chi_{n-1,1}(\bar{x}_{n+1}, \hat{\varphi}, \theta, t)$, and

$$\dot{V}_n = -\sum_{j=1}^{n} z_j^\top Q_j z_j + \tau_n \omega_s. \qquad (4.61)$$

Resulting system: With $x := \bar{x}_n$, $z := \bar{z}_n$, $P := \mathrm{diag}(P_1, P_2, \ldots, P_n)$, and $Q := \mathrm{diag}(Q_1, Q_2, \ldots, Q_n)$ the tuning function $\tau_n(x, \hat{\varphi}, \theta, t)$ and adaptive tuning function $\rho_n(x, \hat{\varphi}, \theta, t)$ are written

$$\tau_n = 2b(\bar{x}_{n-1}, \hat{\varphi}, \theta, t)^\top P z(x, \hat{\varphi}, \theta, t) \qquad (4.62)$$

$$\rho_n = 2\Phi(x)^\top H(\bar{x}_{n-1}, \hat{\varphi}, \theta, t)^\top P z(x, \hat{\varphi}, \theta, t), \qquad (4.63)$$

where

$$b(\bar{x}_{n-1}, \hat{\varphi}, \theta, t) := \mathrm{col}\left(\; y_d^\theta(\theta), \quad \alpha_1^\theta(x_1, \hat{\varphi}, \theta, t), \quad \cdots, \quad \alpha_{n-1}^\theta(\bar{x}_{n-1}, \hat{\varphi}, \theta, t) \; \right),$$

$$H(\bar{x}_{n-1}, \hat{\varphi}, \theta, t) := \begin{bmatrix} h^{x_1} & 0 & 0 & \cdots & 0 \\ -\frac{\partial \alpha_1}{\partial x_1} & I & 0 & \cdots & 0 \\ -\frac{\partial \alpha_2}{\partial x_1} & -\frac{\partial \alpha_2}{\partial x_2} & I & \cdots & 0 \\ \vdots & \vdots & \ddots & \ddots & 0 \\ -\frac{\partial \alpha_{n-1}}{\partial x_1} & -\frac{\partial \alpha_{n-1}}{\partial x_2} & \cdots & -\frac{\partial \alpha_{n-1}}{\partial x_{n-1}} & I \end{bmatrix},$$

and the overall adaptive regressor matrix $\Phi(x) \in \mathbb{R}^{nm \times p}$ is

$$\Phi(x) := \left[\; \Phi_1(x_1)^\top, \quad \Phi_2(\bar{x}_2)^\top, \quad \cdots, \quad \Phi_n(\bar{x}_n)^\top \; \right]^\top$$

with $\kappa_{i,j}(\bar{x}_j, \hat{\varphi}, \theta, t) := -2\chi_{i-1,2}(\bar{x}_{i-1}, \hat{\varphi}, \theta, t) \Gamma \Delta_j(\bar{x}_j, \hat{\varphi}, \theta, t)^\top P_j$,
$i = 2, \ldots, n-1$, $j = i+1, \ldots, n$.

The resulting closed-loop system is at this stage

$$\begin{aligned}\dot{z} &= A_z(x,\hat{\varphi},\theta,t)z + b(\bar{x}_{n-1},\hat{\varphi},\theta,t)\omega_s + H(\bar{x}_{n-1},\hat{\varphi},\theta,t)\Phi(x)\tilde{\varphi}\\ \dot{\tilde{\varphi}} &= -2\Gamma\Phi(x)^\top H(\bar{x}_{n-1},\hat{\varphi},\theta,t)^\top Pz\\ \dot{\theta} &= \upsilon_s(\theta,t) - \omega_s\end{aligned} \tag{4.64}$$

where

$$A_z(x,\hat{\varphi},\theta,t) :=$$

$$\begin{bmatrix} A_1 & h^{x_1}G_1 & 0 & 0 & \cdots & \\ -P_2^{-1}G_1^\top (h^{x_1})^\top P_1 & A_2 & G_2+\kappa_{2,3} & \kappa_{2,4} & \cdots & \\ 0 & -P_3^{-1}G_2^\top P_2 & A_3 & G_3+\kappa_{3,4} & \cdots & \\ \vdots & \vdots & \vdots & \ddots & \ddots & \cdots \\ 0 & 0 & \cdots & 0 & \cdots & \\ 0 & 0 & 0 & 0 & \cdots & \end{bmatrix}$$

$$\begin{bmatrix} \cdots & 0 & 0 & 0 \\ \cdots & \kappa_{2,n-2} & \kappa_{2,n-1} & \kappa_{2,n} \\ \cdots & \kappa_{3,n-2} & \kappa_{3,n-1} & \kappa_{3,n} \\ \cdots & \vdots & \vdots & \vdots \\ \cdots & -P_{n-1}^{-1}G_{n-2}^\top P_{n-2} & A_{n-1} & G_{n-1}+\kappa_{n-1,n} \\ \cdots & 0 & -P_n^{-1}G_{n-1}^\top P_{n-1} & A_n \end{bmatrix}.$$

The adaptive backstepping diffeomorphism $(x,\hat{\varphi},\theta,t) \longleftrightarrow (z,\tilde{\varphi},\theta,t)$ is given by the smooth map $z = \Psi(x,\hat{\varphi},\theta,t)$ defined by (4.38) and (4.39) for $i = 2,\ldots,n$ and $\tilde{\varphi} = \varphi - \hat{\varphi}$. The inverse map $x = \Upsilon(z,\tilde{\varphi},\theta,t)$, constructed as

$$\Upsilon(z,\tilde{\varphi},\theta,t) : \begin{cases} x_1 = \psi_1(\bar{z}_1,\tilde{\varphi},\theta,t) := h^{-1}(z_1 + y_d(\theta)) \\ x_2 = \psi_2(\bar{z}_2,\tilde{\varphi},\theta,t) := z_2 + \alpha_1(\psi_1(\bar{z}_1,\tilde{\varphi},\theta,t),\theta,t) \\ \quad\vdots \\ x_n = \psi_n(\bar{z}_n,\tilde{\varphi},\theta,t) := z_n + \alpha_{n-1}(\psi_{n-1}(\bar{z}_{n-1},\tilde{\varphi},\theta,t),\theta,t), \end{cases} \tag{4.65}$$

is bounded uniformly in (θ,t), that is, for each $c \in [0,\infty)$ there exists $d \in [0,\infty)$ such that $|(z,\tilde{\varphi})| \le c \Rightarrow |\Upsilon(z,\tilde{\varphi},\theta,t)| \le d$, $\forall(\theta,t)$. This can be recursively verified by using Assumption 3.1 and the continuity assumptions on h^{-1}, G_i, f_i, and Φ_i.

The choices (4.58) and (4.59) yields the principal design equation

$$\dot{V}_n = -z^\top Qz + \tau_n\omega_s \tag{4.66}$$

which is of the form of (3.11). Rendering the term $\tau_n\omega_s$ nonpositive will result in a negative semi-definite derivative wich together with the corresponding CLF guarantees that the maneuvering problem is solved, that is, $z(t) \to 0$ as $t \to \infty$, implying that $z_1(t) = y(t) - y_d(\theta(t)) \to 0$ and $\dot{\theta}(t) - \upsilon_s(\theta(t), t) \to 0$.

4.2.2 Closing the loop by speed assignment designs

For the dynamic part of the control law, the design variable is ω_s. Making $\tau_n\omega_s$ nonpositive in (4.66) is accomodated by one of the three choices, the *Tracking*, the *Gradient*, or the *Filtered-gradient* update laws, as in Section 3.1. We summarize for the Gradient and Filtered-gradient cases.

Theorem 4.3 *For the closed-loop system (4.64),*

1. *the* ***Gradient*** *update law*

$$\omega_s = -\mu\tau_n(x, \hat{\varphi}, \theta, t), \qquad \mu \geq 0, \tag{4.67}$$

where $\tau_n = -V_n^\theta(\Psi(x, \hat{\varphi}, \theta, t))$ is given by (4.62), renders the set

$$\mathcal{M} = \{(z, \tilde{\varphi}, \theta, t) : \ z = 0, \ \tilde{\varphi} = 0\} \tag{4.68}$$

UGS, and $\lim_{t\to\infty} |z(t)| = 0$, or

2. *the* ***Filtered-gradient*** *update law*

$$\dot{\omega}_s = -\lambda\left(\omega_s + \mu\tau_n(x, \hat{\varphi}, \theta, t)\right), \qquad \lambda, \mu > 0, \tag{4.69}$$

renders the set

$$\mathcal{M}' = \{(z, \tilde{\varphi}, \omega_s, \theta, t) : \ z = 0, \ \tilde{\varphi} = 0, \ \omega_s = 0\} \tag{4.70}$$

UGS and $\lim_{t\to\infty} |(z(t), \omega_s(t))| = (0, 0)$.

Proof. *The main tool for proving this is Theorem A.18. Clearly, the Gradient (or Filtered-gradient) update law renders the set $\mathcal{M}$ (or $\mathcal{M}'$, respectively), forward invariant for (4.64) (and (4.69), respectively).*
1. Gradient: *For each $K > 0$ s.t. the uniform bound $|(z, \tilde{\varphi}, \theta, t)|_{\mathcal{M}} = |(z, \tilde{\varphi})| \leq K$ holds, it follows from (4.65) that $|x| = |\Upsilon(z, \tilde{\varphi}, \theta, t)|$ is uniformly bounded. This further implies by Assumption 3.1, global invertibility of G_i and h^{x_1}, and smoothness of h, G_i, f_i, and Φ_i that the right-hand side of (4.64) with $\omega_s = -\mu\tau_n$ is uniformly bounded by, say, $L > 0$. For*

the quadratic Lyapunov function $V_n = z^\top Pz + \frac{1}{2}\tilde{\varphi}^\top \Gamma^{-1}\tilde{\varphi}$, *the derivative becomes* $\dot{V}_n \leq -z^\top Qz \leq 0$. *Hence, the conclusion follows from Theorem A.18 in Appendix A.*

2. Filtered-gradient: *For each* $K > 0$ *s.t. the uniform bound* $|(z, \tilde{\varphi}, \omega_s, \theta, t)|_{\mathcal{M}'} = |(z, \tilde{\varphi}, \omega_s)| \leq K$ *holds, it follows for the same reasons as above that the right hand side of (4.64) and (4.69) is uniformly bounded by a constant* $L > 0$. *For the quadratic Lyapunov function* $V = z^\top Pz + \frac{1}{2}\tilde{\varphi}^\top \Gamma^{-1}\tilde{\varphi} + \frac{1}{2\lambda\mu}\omega_s^2$, *the derivative becomes* $\dot{V} = -z^\top Qz - \frac{1}{\mu}\omega_s^2 \leq 0$. *Hence, the conclusion follows from Theorem A.18 in Appendix A.* ■

4.2.3 Passivity

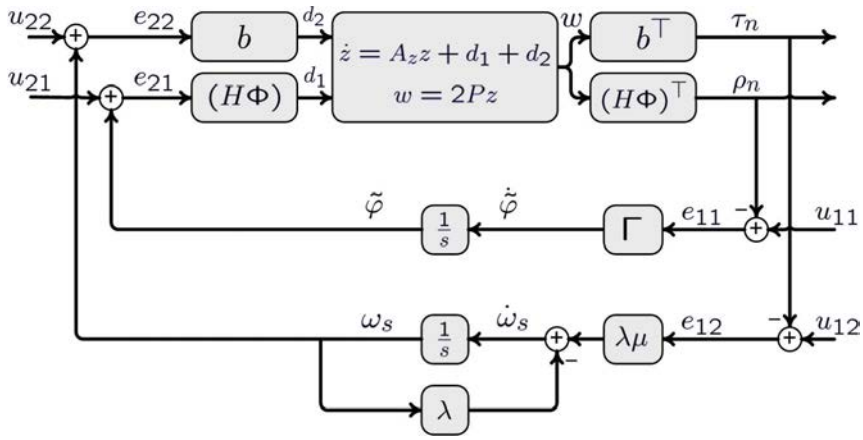

Figure 4.5: Closed-loop adaptive maneuvering system with a Filtered-Gradient update law, disregarding the $\dot{\theta}$-dynamics.

The interconnection structure, in the case of the filtered gradient update law and disregarding the $\dot{\theta}$-dynamics, is shown in Figure 4.5. As seen, the z-subsystem is interconnected with two parallel feedback loops; the adaptive update law and the filtered-gradient update law. These two loops are separated and therefore do not explicitly affect each other.

Another property indicated in Figure 4.5 is the feedback interconnection of passive systems. The system

$$\Sigma_1 : \begin{cases} \dot{z} = A_z z + H\Phi e_{21} + b e_{22} \\ \rho_n = 2\Phi^\top H^\top Pz \\ \tau_n = 2b^\top Pz \end{cases} \tag{4.71}$$

is strictly passive with storage function $U_1 = z^\top P z$, which gives $e_2^\top y_z = \dot{U}_1 + z^\top Q z$ where $e_2 = \mathrm{col}(e_{21}, e_{22})$ is the input, $y_z = \mathrm{col}(\rho_n, \tau_n)$ is the output, and $z^\top Q z$ is the dissipation rate. For the two systems

$$\Sigma_{21} \quad : \quad \{ \ \dot{\tilde{\varphi}} = \Gamma e_{11} \tag{4.72}$$

$$\Sigma_{22} \quad : \quad \{ \ \dot{\omega}_s = -\lambda \omega_s + \lambda \mu e_{12}, \tag{4.73}$$

we have that:

- The system Σ_{21} is lossless with storage function $U_{21} = \frac{1}{2}\tilde{\varphi}^\top \Gamma^{-1} \tilde{\varphi}$. This gives $e_{11}^\top \tilde{\varphi} = \dot{U}_{21}$ where e_{11} is the input and $\tilde{\varphi}$ is the output.
- The system Σ_{22} is strictly passive with storage function $U_{22} = \frac{1}{2\lambda\mu}\omega_s^2$. This gives $e_{12}\omega_s = \dot{U}_{22} + \frac{1}{\mu}\omega_s^2$ where e_{12} is the input, ω_s is the output, and $\frac{1}{\mu}\omega_s^2$ is the dissipation rate.

From beforehand we have seen that the θ dynamics, concealed in this passivity analysis, is well-behaved and that the stability and convergence properties of the $(z, \tilde{\varphi}, \omega_s)$ states are uniform in θ. Hence, standard passivity theorems state that the feedback interconnection $\Sigma_1 + \Sigma_{21}$ is passive with storage function $U_1 + U_{21}$ from input $u_1 = \mathrm{col}(u_{11}, u_{21})$ to output $y_1 = \mathrm{col}(\tilde{\varphi}, \rho_n)$, while $\Sigma_1 + \Sigma_{22}$ is strictly passive with storage function $U_1 + U_{22}$ from input $u_2 = \mathrm{col}(u_{12}, u_{22})$ to output $y_2 = \mathrm{col}(\omega_s, \tau_n)$.

4.3 Sliding-mode design

Motivated by real world applications, and especially automatic navigation of marine craft, there is an interest to explore other robust control design methods to solve the Maneuvering Problem. The focus of this section is therefore on sliding-mode techniques. Such designs are discussed in detail in Utkin (1992); Young, Utkin and Ozguner (1999); Khalil (2002). For marine applications, unknown hydrodynamic effects are a significant source of uncertainty. Sliding-mode control thus quickly became popular for such applications; see for example Yoerger and Slotine (1985); Healey and Lienard (1993); Rodrigues, Tavares and Prado (1996); Zhang, Chen, Sun, Sun and Xu (1998).

The maneuvering designs in this and the previous chapter included the dynamic gradient algorithm. As analyzed in Section 3.4, this gradient algorithm ensures minimization of an instantaneous quadratic cost function in the error states and therefore gives improved performance. In this section

the goal is to recover this behavior for the *nominal* part of the plant. A sliding-mode control law is then proposed to ensure rapid convergence of all states, in finite time, to the subset of the state space where the maneuvering objective is solved for the nominal part of the closed-loop system.

4.3.1 Motivating Example: Stabilizing the Unit Circle with uncertain actuator dynamics

In Section 3.4.1 the problem of stabilizing the unit circle for the double integrator was investigated. We revisit this problem for the same system, but with uncertain actuator dynamics. In particular we consider the plant

$$\dot{x}_1 = x_2 \tag{4.74a}$$
$$\dot{x}_2 = v \tag{4.74b}$$
$$\dot{v} \ = bu + \delta(x, v, t) \tag{4.74c}$$

where $x = \mathrm{col}(x_1, x_2) \in \mathbb{R}^2$ is the positional state, v is the actuator dynamics, $u \in \mathbb{R}$ is the commanded control input, $b \in [b_0, b_1]$, $b_0 > 0$, is an uncertain constant, and $\delta(x, v, t)$ contains uncertain dynamics. We let $\hat{b} \in [b_0, b_1]$ be a nominal value for b and assume that $\delta(x, v, t)$ is bounded uniformly in t by the continuous non-negative function $\rho(x, v)$.

For the nominal states (x_1, x_2) with v as an unconstrained control input, the task in Section 3.4.1 was stabilization of the unit circle

$$\mathcal{P} := \left\{ x : \ x^\top x = 1 \right\} \tag{4.75}$$

without creating any equilibria in $\mathcal{P}$. As argued in Section 3.4.1, there does not exist any continuous or discontinuous time-invariant state feedback control that renders $\mathcal{P}$ GAS. Therefore, dynamic feedback was proposed together with the alternative problem of stabilizing the set $\mathcal{A} \subset \mathcal{P} \times \mathbb{R}$ defined as

$$\mathcal{A} := \left\{ (x, \theta) : \ x = \xi(\theta) = \begin{bmatrix} \xi_1(\theta) \\ \xi_2(\theta) \end{bmatrix} := \begin{bmatrix} \cos\theta \\ -\sin\theta \end{bmatrix} \right\}$$

for (4.74a), (4.74b), and the dynamic control state

$$\dot{\theta} = \omega(x, \theta).$$

To design the functions $\omega(x, \theta)$ and $v = \alpha(x, \theta)$ to render $\mathcal{A}$ UGES, the Hurwitz matrix

$$A = \begin{bmatrix} 0 & 1 \\ -k_1 & -k_2 \end{bmatrix}$$

was selected together with $P = P^\top > 0$ such that $A^\top P + PA = -I$. Using the control Lyapunov function (CLF)

$$V(x,\theta) := (x - \xi(\theta))^\top P (x - \xi(\theta)) \tag{4.76}$$

and $K := [k_1,\ k_2]$, the functions ω and α were assigned as

$$\omega(x,\theta) = 1 - \mu V^\theta(x,\theta) \tag{4.77}$$

$$\alpha(x,\theta) = -K(x - \xi(\theta)) + \xi_2^\theta(\theta) \tag{4.78}$$

where $V^\theta(x,\theta) = -2(x-\xi(\theta))P\xi^\theta(\theta)$. This results in the closed-loop system

$$\begin{aligned} \dot{x} &= A(x - \xi(\theta)) + \xi^\theta(\theta) \\ \dot{\theta} &= 1 - \mu V^\theta(x,\theta) \end{aligned} \tag{4.79}$$

with the following properties:

P1: The set $\mathcal{A}$ is UGES and $\mathcal{P} \times \mathbb{R}$ is uniformly globally attractive.

To verify this, we differentiate (4.76) along the solutions of (4.79) and get

$$\begin{aligned} \dot{V} &= -(x_1 - \xi(\theta))^\top (x_1 - \xi(\theta)) - \mu V^\theta(x,\theta)^2 \\ &\leq -|x - \xi(\theta)|^2 \leq -\frac{1}{p_M} V(x,\theta), \end{aligned} \tag{4.80}$$

which implies that $V(x(t),\theta(t)) \leq V(x(0),\theta(0))e^{-\frac{1}{p_M}t}$. This means that $|x - \xi(\theta)|$ is bounded on the maximal interval of existence, and by boundedness of $\xi^\theta(\theta)$ we have that $V^\theta(x,\theta)$ is bounded. Forward completeness then follows from boundedness of the right-hand side of (4.79). Moreover, because $\xi(\theta)$ is continuously differentiable and $\xi^\theta(\theta)$ is uniformly bounded by unity, $\xi(\theta)$ is absolutely continuous and thus globally Lipschitz with Lipschitz constant $L_\theta = 1$. It can then be shown that

$$|(x,\theta)|_{\mathcal{A}} \leq |x - \xi(\theta)| \leq \sqrt{3}\,|(x,\theta)|_{\mathcal{A}}\,. \tag{4.81}$$

This gives

$$\begin{aligned} |(x(t),\theta(t))|_{\mathcal{A}} \leq |x(t) - \xi(\theta(t))| &\leq \sqrt{\frac{1}{p_m} V(x(t),\theta(t))} \\ &\leq \sqrt{\frac{1}{p_m} V(x(0),\theta(0))}\, e^{-\frac{1}{2p_M}t} \\ &\leq \sqrt{\frac{p_M}{p_m}}\,|x(0) - \xi(\theta(0))|\, e^{-\frac{1}{2p_M}t} \qquad (4.82) \\ &\leq \sqrt{3\frac{p_M}{p_m}}\,|(x(0),\theta(0))|_{\mathcal{A}}\, e^{-\frac{1}{2p_M}t}, \qquad (4.83) \end{aligned}$$

showing that $\mathcal{A}$ is UGES. Furthermore, since $|x|_{\mathcal{P}} \leq |x - \xi(\theta)| \leq |x|_{\mathcal{P}} + 2$ we readily get that

$$|x(t)|_{\mathcal{P}} \leq \sqrt{\frac{p_M}{p_m}} \left[|x(0)|_{\mathcal{P}} + 2\right] e^{-\frac{1}{2p_M}t}, \tag{4.84}$$

showing that $\mathcal{P} \times \mathbb{R}$ is uniformly globally attractive.

P2: Suppose there exists $c > 0$ such that $|x|_{\mathcal{P}} \leq c$ implies $\theta \mapsto V(x, \theta)$ has a global minimizer which is a LAS equilibrium for

$$\dot{\theta} = -V^{\theta}(x, \theta)$$

with basin of attraction $\mathcal{H}_{\theta}(x)$. Let $r \leq c$ and

$$\mathcal{H}(r) := \{(x, \theta) : \ |x|_{\mathcal{P}} \leq r, \ \theta \in \mathcal{H}_{\theta}(x)\}.$$

Then for each $\varepsilon > 0$ and each compact set $\mathcal{K} \subset \mathcal{H}(\frac{p_m}{p_M} c)$ there exists μ^* such that $\mu \geq \mu^*$ and $(x(0), \theta(0)) \in \mathcal{K}$ imply that

$$|x(t)|_{\mathcal{P}} \leq \sqrt{\frac{p_M}{p_m}} |x(0)|_{\mathcal{P}} e^{-\frac{1}{2p_M}t} + \varepsilon \tag{4.85}$$

holds for (4.79) for all $t \geq 0$.

This bound was referred to as *near-stability* in Section 3.4.2 and quantifies the important property that if $x(t)$ starts close to the unit circle $\mathcal{P}$, it stays close for all future time and eventually converges by (4.84).

P3: Let $v = \alpha(x, \theta) + w$ where w is a bounded perturbation. Then the closed-loop system

$$\begin{aligned} \dot{x} &= A\left(x - \xi(\theta)\right) + \xi^{\theta}(\theta) + gw \\ \dot{\theta} &= 1 - \mu V^{\theta}(x, \theta) \end{aligned} \tag{4.86}$$

with $g = [0, 1]^{\top}$ is globally input-to-state stable (ISS) with respect to the closed 0-invariant set $\mathcal{A}$, see Appendix A.3, and the solution $(x(t), \theta(t))$ of (4.86) converges to the set

$$\mathcal{O}\left(||w||\right) := \left\{(x, \theta) : \ |(x, \theta)|_{\mathcal{A}} \leq 6\sqrt{\frac{p_M}{p_m}} \frac{p_M}{1 - \kappa} \, ||w||\right\}.$$

To verify this, we check that (4.76) is an ISS-Lyapunov function for (4.86). Using (4.81), we get

$$p_m \left|(x,\theta)\right|_{\mathcal{A}}^2 \leq V(x,\theta) \leq 3p_M \left|(x,\theta)\right|_{\mathcal{A}}^2 \tag{4.87}$$

and

$$\begin{aligned}\dot{V} &\leq -\left|(x,\theta)\right|_{\mathcal{A}}^2 + 2\sqrt{3}p_M \left|(x,\theta)\right|_{\mathcal{A}} |w| \\ &\leq -\kappa \left|(x,\theta)\right|_{\mathcal{A}}^2, \qquad \forall \left|(x,\theta)\right|_{\mathcal{A}} \geq \frac{2\sqrt{3}p_M}{1-\kappa}|w|\end{aligned} \tag{4.88}$$

where $\kappa \in (0,1)$. Forward completeness is guaranteed by observing that the closed-loop vector field (4.86) is bounded using (4.87) and (4.88) and boundedness of $\xi^\theta(\theta)$ and w. Hence, (4.76) is an ISS-Lyapunov function for (4.86) with respect to $\mathcal{A}$. By the above bounds it also follows that the trajectory $(x(t),\theta(t))$ must converge to the set

$$\left\{(x,\theta):\ V(x,\theta) \leq 3p_M \left(\frac{2\sqrt{3}p_M}{1-\kappa}\,||w||\right)^2\right\}$$

which is contained in $\mathcal{O}(||w||)$.

We are now ready to include the actuator dynamics $\dot{v}$ in the design. The aim is to recover the qualitative properties of the subsystem (x,θ) as listed above. The ISS property guarantees that if the error $v-\alpha(x,\theta)=w$ stays bounded, then the total system will be forward complete. Furthermore, in the set

$$\mathcal{B} := \{(v,x,\theta):\ v=\alpha(x,\theta)\} \tag{4.89}$$

the properties **P1** and **P2** are recovered. Hence, the aim is to render $\mathcal{B}$ forward invariant and to force the trajectories of the total system to (rapidly) converge to $\mathcal{B}$ in finite time while keeping $w=v-\alpha(x,\theta)$ bounded.

To this end we define $s := v-\alpha(x,\theta)$ and the global diffeomorphism $(v,x,\theta)\mapsto(s,x,\theta)$. Differentiating s gives

$$\dot{s} = bu + \delta(x,v,t) + \varphi(v,x,\theta) \tag{4.90}$$

where

$$\varphi(v,x,\theta) := -\alpha^{x_1}(x,\theta)x_2 - \alpha^{x_2}(x,\theta)v - \alpha^\theta(x,\theta)\left(1-\mu V^\theta(x,\theta)\right).$$

We propose the control

$$u = -\frac{L}{\hat{b}}s - \left(\frac{k_s}{\hat{b}} + \sigma(v,x,\theta)\right)\mathrm{sgn}(s) - \frac{1}{\hat{b}}\varphi(v,x,\theta) \tag{4.91}$$

where

$$\begin{aligned}\sigma(v,x,\theta) :=& \frac{\rho(v,x)}{b_0} + \frac{b_1 - b_0}{\hat{b}b_0}\left|\varphi(v,x,\theta)\right| \\ \geq& \left|\frac{\delta(x,v,t)}{b} + \left(\frac{\hat{b}-b}{\hat{b}b}\right)\varphi(v,x,\theta)\right|\end{aligned}$$

and the signum operator $\mathrm{sgn}(\cdot)$ is the traditional *sign* function. Differentiating the Lyapunov-like function

$$U(s) = \frac{1}{2}s^2 \tag{4.92}$$

along the solutions of

$$\begin{aligned}\dot{s} \;=\; & -\left(b/\hat{b}\right)Ls - b\left(k_s/\hat{b} + \sigma(v,x,\theta)\right)\mathrm{sgn}(s) \\ & +\delta(x,v,t) + \left(1 - b/\hat{b}\right)\varphi(v,x,\theta)\end{aligned}$$

gives

$$\dot{U} \leq -\frac{b_0}{\hat{b}}k_s\left|s\right| = -\sqrt{2}\frac{b_0}{\hat{b}}k_s\sqrt{U}. \tag{4.93}$$

This inequality implies that for each initial condition $s_0 = |s(0)|$ the solution[1] satisfies

$$|s(t)| \leq \max\left\{0,\ s_0 - \frac{b_0}{\hat{b}}k_s t\right\}, \qquad \forall t \geq 0. \tag{4.94}$$

This shows that $s(t)$ is bounded, and there exists $t' \in [0, \frac{\hat{b}s_0}{b_0 k_s}]$ such that $s(t') = 0$, and convergence to $\mathcal{B}$ in finite time is achieved. Larger gain k_s implies faster convergence. Equation (4.94) further implies that for all $s(0) \in \mathcal{B} \Rightarrow s(t) \in \mathcal{B}$ for all $t \geq 0$.

The discontinuous switching introduced by the function $\mathrm{sgn}(\cdot)$ in the control law raises some practical issues. Such switching will produce chattering due to limitations in the control devices and the digital implementation. To alleviate these problems, an approximate continuous implementation of the $\mathrm{sgn}(\cdot)$ function by either a continuous saturation function or a smooth hyperbolic function is often used Khalil (2002).

Let the signum function in the control law (4.91) be replaced by the hyperbolic function

[1] In fact, all solutions in the sense of Filippov. This is a solution concept that captures behavior in the presence of small measurement and actuator errors, see Filippov (1988).

$$\psi(s) := (1+\varepsilon_1)\tanh\left(\frac{s}{\varepsilon_2}\right), \tag{4.95}$$

and define $\varepsilon := \varepsilon_2 \operatorname{atanh}(\frac{1}{1+\varepsilon_1})$ where ε_1 and ε_2 are small positive numbers chosen by design. For $|s| \geq \varepsilon$ we have $|\psi(s)| \geq |\mathrm{sgn}(s)|$. This gives $\dot{U} \leq -\frac{b_0}{\hat{b}} k_s |s|$ for all $|s| \geq \varepsilon$ which implies convergence in finite time to the noncompact set

$$\mathcal{B}_\varepsilon := \{(s,x,\theta) : \ |s| \leq \varepsilon\}. \tag{4.96}$$

From Property **P3** and the relationship $v = \alpha(x,\theta) + s$ where s is bounded and converges to $\mathcal{B}_\varepsilon$, we get for each $r > \varepsilon$ that the set

$$\{(s,x,\theta) : \ |s| \leq r, \ (x,\theta) \in \mathcal{O}(r)\}$$

is forward invariant. Define the set

$$\mathcal{A}_\varepsilon := \left\{(s,x,\theta) : \ |(x,\theta)|_{\mathcal{A}} \leq 6\sqrt{\frac{p_M}{p_m}}\frac{p_M}{1-\kappa}\varepsilon\right\}.$$

In the state space of (s,x,θ) it follows since r is arbitrary that the trajectories will converge to the set $\mathcal{A}_\varepsilon \cap \mathcal{B}_\varepsilon$.

A simulation has been performed using Matlab/Simulink$^{\mathrm{TM}}$ for the plant (4.74) with $b = 1.5$ and $\delta(x,v,t) = \frac{\sin(t)}{1+x_2^2+v^2}$. The bounding function was taken as $\rho(x,v) = 1$ while $b_0 = 1$, $b_1 = 3$, and $\hat{b} = 2$. Figures 4.6, 4.7, and 4.8 show the responses for two runs using $k_s = 5$, $L = 1$, $\varepsilon_1 = 0.1$, $\varepsilon_2 = 0.01$, $k_1 = 1.0$, $k_2 = 0.5$, $p_{11} = 26.775$, $p_{12} = 10.750$, $p_{22} = 22.100$, and $\mu = 1.0$. Initial position was $x_0 = 0.9[-\frac{\sqrt{2}}{2} \ \frac{\sqrt{2}}{2}]^\top$ (just inside the circle at the angle $225\,^\circ$). This means that $V(x_0,\cdot)$ had a global minimum at $\theta_V(x_0) = 225\,^\circ$, a local minimum at $\theta\,(x_0) = 73\,^\circ$, and a maximum between them at $\theta\,(x_0) = 97\,^\circ$. The simulation and parameters for the nominal part of the plant are identical to those for the simulation example in Section 3.4.1. The objective is to verify that by forcing the error state $s(t)$, through the system state $v(t)$, to converge fast enough to the set given by $\mathcal{B}_\varepsilon$, then the qualitative behavior seen in the simulation in Section 3.4.1 is recovered. Indeed, Figure 4.6 shows an almost identical response as Figure 3.2, with only a small discrepancy near the starting time. The scenario is this: in *Run 1,* we let $\theta_0 = 90\,^\circ$ which is in the basin of attraction of the local minimum. $\theta(t)$ therefore moves towards this local minimum and causes the bad transient of $x(t)$ as shown. If the initial condition is changed to $\theta_0 = 100\,^\circ$ we instead get the response shown in *Run 2.* Since θ_0 in this case is in the basin of attraction of the global minimum to which $\theta(t)$ rapidly converges, see Figure 4.6, the

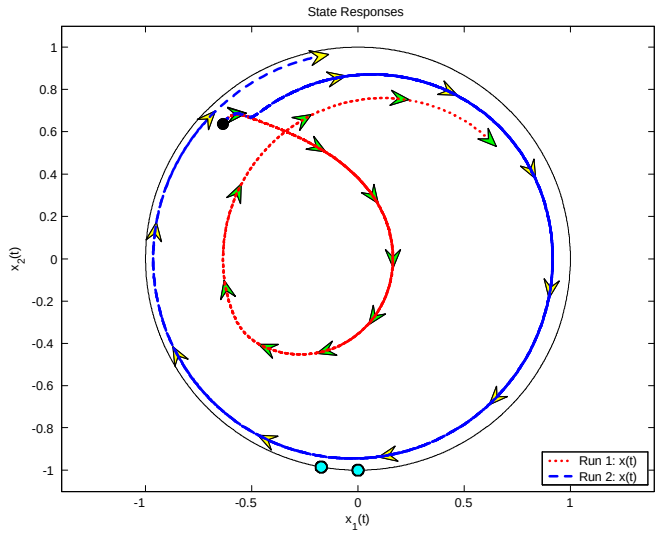

Figure 4.6: State responses projected into the (x_1, x_2) plane for two simulation runs (Run 1: dotted, Run 2: dashed) from two different initial conditions for θ_0. The solid dot indicates x_0 in both runs. The small circles indicate $\xi(\theta_0)$ for $\theta_0 = 90°$ in Run 1 and $\theta_0 = 100°$ in Run 2.

distance to the circle $\mathcal{P}$, after a small transient, is exponentially decreasing and thus indicating near-stability. Figure 4.7 shows the responses of $s(t)$ for the two runs, zoomed in on the boundary layer. Figure 4.8 shows the first 0.5 s of the rapid convergence of $v(t) \to \alpha(x(t), \theta(t))$ for Run 1 only.

4.3.2 Main result

Consider the nonlinear plant

$$\dot{x}_1 = f_1(x_1, x_2, t) \tag{4.97a}$$
$$\dot{x}_2 = f_2(x, t) + G(x)u + \delta(x, u, t) \tag{4.97b}$$

where $x = \mathrm{col}(x_1, x_2) \in \mathbb{R}^{m+n}$ is the state vector, $u \in \mathbb{R}^p$, $p \geq n$, is the control input, f_1, f_2, G, and δ are sufficiently smooth functions where f_1 and f_2 are known, while $G \in \mathbb{R}^{n \times p}$ and δ are uncertain.

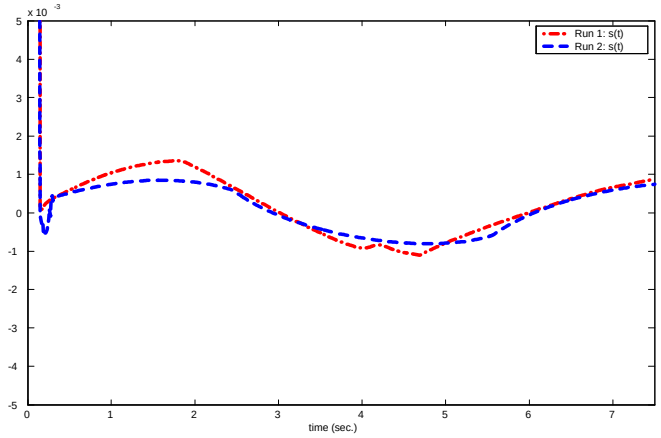

Figure 4.7: Responses for $s(t)$ in the two runs, zoomed in on the boundary layer. The responses were nearly identical for both runs, and they clearly indicate the rapid convergence to $\mathcal{B}_\varepsilon$.

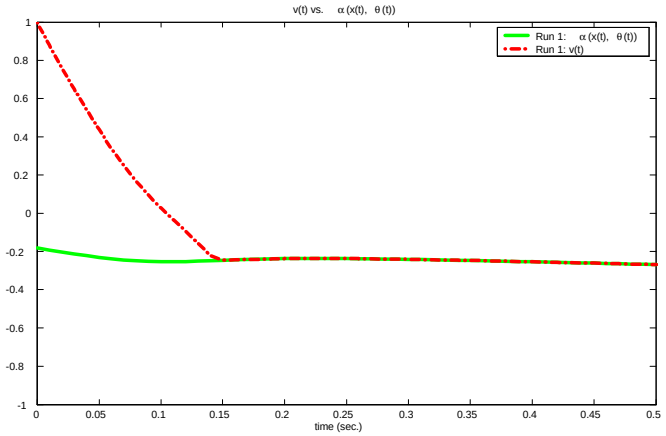

Figure 4.8: Plot showing the convergence of $v(t) \to \alpha(x(t), \theta(t))$ for Run 1 only. The figure has zoomed in on the first 0.5 s.

Design for the nominal part of the plant

Given a desired path $\xi : \mathbb{R} \to \mathbb{R}^m$, continuously parametrized by a variable θ, and a desired speed assignment $v_s(\theta, t)$ along the path, let the control objective be to solve the Maneuvering Problem:

$$\lim_{t\to\infty} |x_1(t) - \xi(\theta(t))| = 0 \tag{4.98a}$$

$$\lim_{t\to\infty} \left|\dot{\theta}(t) - v_s(\theta(t), t)\right| = 0. \tag{4.98b}$$

In addition, we want to assure near-stability of the path

$$\mathcal{P} := \{x_1 \in \mathbb{R}^m : \ \exists\theta \text{ s.t. } x_1 = \xi(\theta)\} \tag{4.99}$$

so that starting close to $\mathcal{P}$ implies staying close (this is a measure of performance in path following).

It is assumed that $\xi(\theta)$ and the partial derivatives $\xi^\theta(\theta)$ and $\xi^{\theta^2}(\theta)$ are uniformly bounded in $\mathbb{R}^m$, and that $v_s(\theta, t)$, $v_s^\theta(\theta, t)$, and $v_s^t(\theta, t)$ are uniformly bounded in (θ, t).

To this end, suppose there exist a global diffeomorphism $(x_1, \theta, t) \mapsto (z(x_1, \theta), \theta, t)$ such that $z(\xi(\theta), \theta) = 0$ and a smooth function $V(x_1, \theta, t)$ satisfying

$$\gamma_1(|z|) \le V(x_1, \theta, t) \le \gamma_2(|z|) \tag{4.100}$$

where $\gamma_1, \gamma_2 \in \mathcal{K}_\infty$. Suppose further there exists a smooth function $\alpha_1(x_1, \theta, t)$ such that for a bounded perturbation w, the system

$$\begin{aligned} \dot{x}_1 &= f_1(x_1, \alpha_1(x_1, \theta, t) + w, t) \\ \dot{\theta} &= v_s(\theta, t) - \mu V^\theta(x_1, \theta, t) \end{aligned} \tag{4.101}$$

is forward complete, and V satisfies

$$\begin{aligned} &V^{x_1}(x_1, \theta, t) f_1(x_1, \alpha_1(x_1, \theta, t) + w, t) \\ &\quad + V^\theta(x_1, \theta, t) v_s(\theta, t) + V^t(x_1, \theta, t) \le -\gamma_3(|z|), \quad \forall\, |z| \ge \gamma_4(|w|) \end{aligned} \tag{4.102}$$

where $\gamma_3 \in \mathcal{K}$ and $\gamma_4 \in \mathcal{K}_\infty$. The bounds (4.100) and (4.102) imply the existence of $\beta \in \mathcal{KL}$ and $\chi \in \mathcal{K}$ such that

$$|z(t)| \le \beta(|z(t_0)|,\ t - t_0) + \chi(\|w\|), \qquad \forall t \ge t_0 \ge 0, \tag{4.103}$$

which shows that the system (4.101) is ISS (see Sontag and Wang (1996) and Lin et al. (1995)) with respect to the closed 0-invariant set

$$\mathcal{A} := \{(x_1, \theta, t) : \ z(x_1, \theta) = 0\}. \tag{4.104}$$

Many designs methods producing the functions α_1 and V can be applied depending on the nature of the plant. The motivational example illustrated one such design, whereas the backstepping designs in the previous sections showed a more general method to satisfy the above conditions. To proceed, we merely assume the existence of z, α_1, and V.

The objective next is to design a control law that will drive $x_2(t)$ rapidly to the manifold in the state space where the function $\alpha_1(x_1, \theta, t)$ solves the Maneuvering Problem for the subsystem (x_1, θ, t).

Structural assumption on $G(x)$: The general case

Assume there exist a known matrix $H(x) \in \mathbb{R}^{p\times n}$, a constant $c > 0$, and a continuous nonnegative function $\rho(x)$ such that

$$G(x)H(x) + H(x)^\top G(x)^\top \geq cI, \qquad \forall x, \tag{4.105}$$

$$|\delta(x, u, t)| \leq \rho(x), \qquad \forall (x, u, t). \tag{4.106}$$

We then have the theorem:

Theorem 4.4 *Suppose the smooth functions $\alpha_1(x_1, \theta, t)$ and $V(x_1, \theta, t)$ solves the Maneuvering Problem (4.98a) and (4.98b) for*

$$\dot{x}_1 = f_1(x_1, \alpha_1(x_1, \theta, t), t) \tag{4.107}$$

according to the conditions in (4.100) and (4.102). Let

$$\begin{aligned}\varphi(x, \theta, t) := {} & f_2(x, t) - \alpha_1^t(x_1, \theta, t) - \alpha_1^{x_1}(x_1, \theta, t) f_1(x_1, x_2, t) \\ & -\alpha_1^\theta(x_1, \theta, t)\left(\upsilon_s(\theta, t) - \mu V^\theta(x_1, \theta, t)\right) \\ \alpha_2(x, \theta, t) := {} & -L(x)s - \sigma(x)H(x)\Psi_1(s)\end{aligned}$$

and

$$\Psi_1(s) := \frac{s}{\max\{|s|, \varepsilon\}} \tag{4.108}$$

where ε is a small positive number chosen by design, $L(x)$ and $H(x)$ both satisfy (4.105) with $c_L > 0$ and $c_H > 0$, respectively, and

$$\begin{aligned}& s := x_2 - \alpha_1(x_1, \theta, t), \\ & \sigma(x) := \tfrac{1}{c_H}\left(k_s + 2\left|\varphi(x, \theta, t)\right| + 2\rho(x)\right), \quad k_s > 0.\end{aligned}$$

Using the control law

$$u = \alpha_2(x, \theta, t) \tag{4.109}$$

$$\dot{\theta} = \upsilon_s(\theta, t) - \mu V^\theta(x_1, \theta, t), \tag{4.110}$$

then, for all initial conditions $(s(t_0), z(t_0), \theta(t_0), t_0) \in \mathbb{R}^{m+n} \times \mathbb{R} \times \mathbb{R}_{\geq 0}$, *the corresponding trajectories* $(s(t), z(t), \theta(t), t)$ *will exist on* $[t_0, \infty)$ *and reach the forward invariant set*

$$\mathcal{B}_\varepsilon := \{(s, z, \theta, t) : \ |s| \leq \varepsilon\}$$

within the time interval $[t_0, t_0 + \frac{2}{k_s}(|s(t_0)| - \varepsilon)]$. *This implies convergence to the forward invariant set* $\mathcal{A}_\varepsilon \cap \mathcal{B}_\varepsilon$ *where*

$$\mathcal{A}_\varepsilon := \left\{(s, z, \theta, t) : \ |z| \leq \gamma_1^{-1}\left(\gamma_2\left(\gamma_4(\varepsilon)\right)\right)\right\}.$$

Proof. *To save space, we leave out the argument lists where convenient. Differentiating* s *with* $u = \alpha_2(x, \theta, t)$ *gives*

$$\dot{s} = -GLs - \sigma GH \frac{s}{\max\{|s|, \varepsilon\}} + \varphi + \delta. \tag{4.111}$$

Define the Lyapunov-like function $U := s^\top s$. *Its derivative along the solutions of (4.111) becomes*

$$\begin{aligned}
\dot{U} &= -s^\top \left[GL + L^\top G^\top\right] s - \tfrac{\sigma}{|s|} s^\top \left[GH + H^\top G^\top\right] s \\
&\qquad +2s^\top (\varphi + \delta), \quad \forall\, |s| \geq \varepsilon \\
&\leq -c_L |s|^2 - c_H \sigma(x) |s| + 2 |s| \left(|\varphi(x, \theta, t)| + \rho(x)\right) \\
&< -k_s |s|, \qquad \forall\, |s| \geq \varepsilon.
\end{aligned}$$

This implies that

$$|s(t)| \leq \max\left\{\varepsilon, \ |s(t_0)| - \frac{k_s}{2}(t - t_0)\right\}, \quad \forall t \geq t_0 \tag{4.112}$$

so that $\mathcal{B}_\varepsilon$ *is forward invariant and there exists* $t' \in [t_0, t_0 + \frac{2}{k_s}(|s(t_0)| - \varepsilon)]$ *for which* $s(t') \leq \varepsilon$ *and convergence in finite time to* $\mathcal{B}_\varepsilon$ *is achieved. Moreover, because* $|s(t)| \leq \max\{\varepsilon, \ |s(t_0)|\}$, $\forall t \geq t_0$, *we get by construction of* $\alpha_1(x_1, \theta, t)$,

$$\dot{x}_1 = f_1\left(x_1, \alpha_1(x_1, \theta, t) + s, t\right), \tag{4.113}$$

and (4.103) that the solution $z(t)$ *is bounded for all* $t \geq t_0$. *It follows by the assumptions and the above Lyapunov arguments that the trajectory* $(s(t), z(t), \theta(t), t)$ *exist on* $[t_0, \infty)$ *so that the closed-loop system is forward complete. Since* $\mathcal{B}_\varepsilon$ *is forward invariant it follows from ISS of (4.101) with respect to* $\mathcal{A}$, *see Lin et al. (1995), that if there exists* $t_1 \geq t_0$ *such that* $(s(t_1), z(t_1), \theta(t_1), t_1) \in \mathcal{A}_\varepsilon \cap \mathcal{B}_\varepsilon$ *then* $(s(t), z(t), \theta(t), t) \in \mathcal{A}_\varepsilon \cap \mathcal{B}_\varepsilon$ *for all* $t \geq t_1$. *Convergence to* $\mathcal{A}_\varepsilon \cap \mathcal{B}_\varepsilon$ *for any initial condition is a consequence of convergence in finite time to* $\mathcal{B}_\varepsilon$ *and subsequent convergence to* $\mathcal{A}_\varepsilon$. ■

Remark 4.1 *If $G(x)$ is known and satisfies*

$$\left| w^\top G(x) G(x)^\top w \right| \geq c_0, \qquad \forall x, |w| = 1 \tag{4.114}$$

for some $c_0 > 0$, then two choices for $H(x)$ are imminent:

$$\textit{1.}\ H(x) = W G(x)^\top \tag{4.115}$$

$$\textit{2.}\ H(x) = W^{-1} G(x)^\top \left(G(x) W^{-1} G(x)^\top \right)^{-1}. \tag{4.116}$$

The matrix $W = W^\top > 0$ is a gain matrix in the first case. In the second case, $W = W^\top > 0$ is a control allocation weight matrix, and $H(x)$ is recognized as the generalized pseudo-inverse.

Remark 4.2 *The function (4.108) is a vector version of the continuous 'saturation-type' approximation to the sign function as described by Khalil (2002). The advantage with this function is that it maintains the direction of s, thus making it possible to apply (4.105). Another alternative is to use the smooth approximation*

$$\Psi_2(s) := \operatorname{col}\left(\psi(s_1), \psi(s_2), \ldots, \psi(s_n)\right) \tag{4.117}$$

where $\psi(s_i)$ is defined in (4.95). However, (4.117) is not directly applicable to the general case since it does not maintain the direction of s. In the special case when $G(x)$ is known, (4.117) can be utilized because $H(x)$ can then be taken as the generalized pseudo-inverse (4.116) so that $G(x)H(x) = I$.

Structural assumption on $G(x)$: A special case

Suppose, instead of (4.105), there exist a known matrix $H(x) \in \mathbb{R}^{p \times n}$ and a constant $c > 0$ such that the uncertain matrix $G(x)$ satisfies:

$$s_1^\top G(x) H(x) s_2 \geq c \left|s_1\right| \left|s_2\right| > 0 \tag{4.118}$$

for all s_1, s_2 whose components have the same sign. A sufficient condition for (4.118) is that $G(x)H(x)$ is diagonal, positive definite. The structural assumption (4.118) is a special case of (4.105). Indeed, take $s_1 = s_2 = s \in \mathbb{R}^n$ so that (4.118) gives

$$\begin{aligned} s^\top G(x) H(x) s &= \frac{1}{2} s^\top \left[G(x)H(x) + H(x)^\top G(x)^\top \right] s \geq c\left|s\right|^2 \\ &\Rightarrow \quad G(x)H(x) + H(x)^\top G(x)^\top \geq 2cI \end{aligned}$$

implying that (4.105) holds.

In the case (4.118) holds we can apply the control law (4.110) and

$$u = -L(x)s - \sigma(x)H(x)\Psi_2(s) \tag{4.119}$$

where $L(x)$ and $H(x)$ both satisfy (4.118) with $c_L > 0$ and $c_H > 0$, respectively,

$$\sigma(x) := \frac{\sqrt{n}}{c_H}\left(k_s + |\varphi(x,\theta,t)| + \rho(x)\right), \quad k_s > 0, \tag{4.120}$$

and $\Psi_2(\cdot)$ is the smooth function (4.117) with

$$\psi(s_i) := (1+\varepsilon_1)\tanh\left(\frac{s_i}{\varepsilon_2}\right) \tag{4.121}$$

where ε_1 and ε_2 are small positive numbers chosen by design. With $\varepsilon = \varepsilon_2\,\mathrm{atanh}(\frac{1}{1+\varepsilon_1})$ we have the following lemma:

Lemma 4.5 *For each $s \in \mathbb{R}^n$ such that $|s| \geq \sqrt{n}\varepsilon$ it holds for (4.117) that $\frac{1}{\sqrt{n}}|s| \leq s^\top \Psi_2(s) \leq |s|\,|\Psi_2(s)|$.*

Proof. *From the equivalence between the 2-norm and the ∞-norm we get $|s| \geq \sqrt{n}\varepsilon \Rightarrow |s|_\infty \geq \varepsilon$. Let s_i correspond to the "largest" element in s such that $|s|_\infty = |s_i|$. Then $s^\top\Psi_2(s) = s_1\psi(s_1) + \ldots + s_i\psi(s_i) + \ldots + s_n\psi(s_n) \geq |s_i| = |s|_\infty \geq \frac{1}{\sqrt{n}}|s|$.* ■

Differentiating $U = \frac{1}{2}s^\top s$ along the solutions of

$$\dot{s} = -G(x)L(x)s - \sigma(x)G(x)H(x)\Psi_2(s) + \varphi + \delta$$

gives

$$\begin{aligned}
\dot{U} &= -s^\top GLs - \sigma s^\top GH\Psi_2(s) + s^\top(\varphi+\delta)\\
&\leq -c_L|s|^2 - c_H\sigma|s|\,|\Psi_2(s)| + |s|\,|\varphi+\delta|\\
&\leq -c_L|s|^2 - |s|\left(\frac{c_H}{\sqrt{n}}\sigma - |\varphi| - \rho\right), \qquad \forall\,|s| \geq \sqrt{n}\varepsilon,\\
&< -k_s|s|, \qquad \forall\,|s| \geq \sqrt{n}\varepsilon,
\end{aligned}$$

where (4.106), (4.118), and Lemma 4.5 were applied. The above bound implies that

$$|s(t)| \leq \max\left\{\sqrt{n}\varepsilon,\ |s(t_0)| - k_s(t-t_0)\right\}, \quad \forall t \geq t_0,$$

and in conclusion we then have that for all initial conditions $(s(t_0), z(t_0), \theta(t_0), t_0) \in \mathbb{R}^{m+n} \times \mathbb{R} \times \mathbb{R}_{\geq 0}$, the corresponding trajectories $(s(t), z(t), \theta(t), t)$ will exist on $[t_0, \infty)$ and converge to the forward invariant set $\mathcal{A}'_\varepsilon \cap \mathcal{B}'_\varepsilon$ where

$$\mathcal{A}'_\varepsilon := \left\{(s, z, \theta, t) : \ |z| \leq \gamma_1^{-1}\left(\gamma_2\left(\gamma_4(\sqrt{n}\varepsilon)\right)\right)\right\},$$
$$\mathcal{B}'_\varepsilon := \left\{(s, z, \theta, t) : \ |s| \leq \sqrt{n}\varepsilon\right\}.$$

It was shown in this section that if the maneuvering problem can be solved for the nominal part of the plant, then using sliding-mode techniques the maneuvering problem can be solved for the overall plant. This was obtained by forcing the states of the closed-loop system to rapidly converge to the manifold of the state space where the maneuvering objective was solved for the nominal states, in spite of modeling uncertainties. Indeed, the closed-loop maneuvering system for the nominal part of the plant contains all ingredients necessary to achieve this result. In particular the ISS property with respect to the desired noncompact set played a major role in the stability analysis.

Chapter 5

Maneuvering designs for ships with experimental results

In this chapter three maneuvering designs for fully actuated ships are treated:

(i) **Adaptive maneuvering** - application of the adaptive backstepping procedure presented in Section 4.2.

(ii) **Sliding-mode maneuvering** - application of the sliding-mode maneuvering theory presented in Section 4.3.

(iii) **Nonlinear PID maneuvering** - based on the work by Lindegaard (2003).

All designs are thoroughly detailed and experimentally tested using the model ship CyberShip II in the Marine Cybernetics Laboratory in Trondheim. The main publications resulting from this work is Skjetne (2003), Skjetne, Smogeli and Fossen (2004a,b), and Skjetne et al. (2005).

5.1 A brief historic flashback

Automatic steering of ships started with the invention of the gyrocompass. Based on the earlier developed gyroscope, Dr. Anschütz-Kaempfe (1872-1931) patented the first north seeking gyrocompass in 1908. This work had attracted considerable attention from engineers around the world, and already the same year Elmer Sperry (1860-1930) introduced the first ballistic gyrocompass which subsequently was patented in 1911; see Fossen (2002);

Bennet (1979); Sperry Marine (2004). Soon thereafter, Sperry designed an automatic pilot, the gyropilot, for automatic steering of ships. This was first commercially available in 1922, and it *"had been christened 'Metal-Mike' by the officers of the ship Moffett, ..., and the performance of 'Metal-Mike' seemed uncanny to many because it apparently had built into the 'intuition' of an experienced helmsman"* (Bennet; 1979).

The 'intuition' of a helmsman included proportional action as well as predictive action and the ability to remove offsets with respect to the heading error. This gave way to the three-term control law, today referred to as a Proportional-Integral-Derivative (PID) control, which was first theoretically analyzed by Nicholas Minorsky (1885-1970); see Minorsky (1922).

The gyropilot, today known as a conventional autopilot, is a single-input single-output (SISO) control system where the heading, measured by the gyrocompass, is regulated to a desired heading by corrective action of the rudder. The new features of the autopilot today is, on the one hand, more advanced control techniques including wave filtering, adaptation to varying conditions, optimal control techniques, H_2 and H_∞ control, etc. On the other hand, it includes new agorithms such as line-of-sight (LOS) algorithms to eliminate cross-track positional errors, course-changing algorithms, weather routing to avoid 'bad' weather regions, collision avoidance, and rendezvous maneuvering capabilities.

In spite of the relatively simple ship model the autopilot controller is based on, it has had great success for many years. However, with the introduction of new measurement systems, in particular the *Global Positioning System* (GPS), and the need to perform more advanced maneuvers with a ship, motivated creative thinking which opened new possibilities and directions of research. Preeminently, this resulted in dynamical positioning (DP) systems which were first designed in the 1960s by three decoupled linear PID controllers and later using LQG techniques (Balchen, Jensen and Sælid; 1976). In recent years, nonlinear techniques have been applied by e.g. Strand (1999) and Lindegaard (2003). A further extension was the weather optimal positioning control (WOPC) system, proposed by Fossen and Strand (2001), which will automatically point the ship against the resultant environmental 'weather' force to minimize fuel consumption in station-keeping.

The dynamic equations of motion for a ship have, in the marine research community, evolved from two main directions called *maneuvering theory* and *seekeeping theory*. In maneuvering theory it is common to assume that the ship is moving in restricted calm water (zero-frequency assumption), for instance, in sheltered waters or in a harbor. Seakeeping analysis, on the other

hand, refers to the motions of a vessel at all frequencies in waves, usually at a fixed speed and heading (including station-keeping at zero speed), in a sinusoidal, irregular, or random seaway; see Bishop and Price (1981); Bailey, Price and P. (1998); Fossen and Smogeli (2004); Fossen (2005). *Maneuvering theory* in this context is maritime language and should be distinguished from the *Maneuvering Problem*, which in this thesis is a control technical problem statement valid for any feasible control application. To make the confusion complete, in this chapter we will use maneuvering theory ship models (not seakeeping models) and present different maneuvering control laws with experimental results for CyberShip II.

5.2 CyberShip II

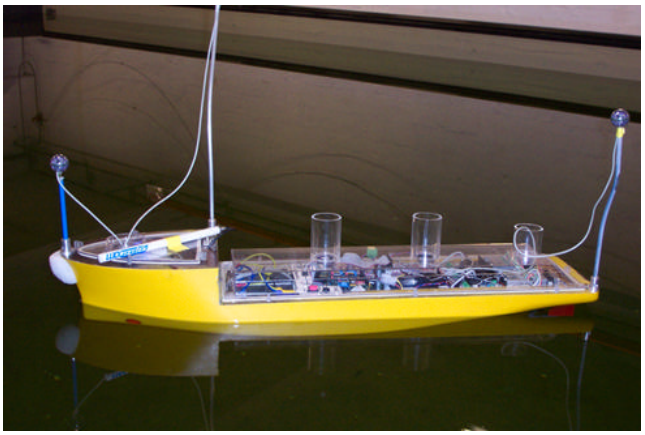

Figure 5.1: A picture of CyberShip II in the Marine Cybernetics Laboratory (MCLab) at NTNU.

The case study of maneuvering the model ship called CyberShip II (CS2) along a desired path is used to illustrate and experimentally test the different maneuvering control designs in this chapter. CS2 is a 1:70 scale replica of a supply ship. Its mass is $m = 23.8\,\text{kg}$, its length is $L_{CS2} = 1.255\,\text{m}$, and its breadth is $B_{CS2} = 0.29\,\text{m}$. It is fully actuated with two main propellers and two rudders aft, and one bow thruster. It is further equipped with a PC104-bus driven by a QNX® real-time operating system which controls the internal hardware achitecture and communicates with onshore computers through a WLAN in the Marine Cybernetics Laboratory (MCLab). To

facilitate real-time feedback control of the ship, Opal RT-Lab® is used for rapid prototyping of a desired control structure programmed in Matlab® and Simulink®. For execution of the experiment, a LabVIEW® interface has been developed for commanding and monitoring the ship.

The MCLab is a Marie Curie EU training site for testing of ships, rigs, underwater vehicles, and propulsion systems in Trondheim, Norway. It is equipped with a towing carriage, a wave maker system, and a measurement system that provides accurate position and attitude measurements.

All maneuvering control designs in this thesis are based on full state feedback. However, since measurements for CyberShip II are only position and attitude, some observer (Skjetne and Shim; 2001) or filter is necessary to estimate velocities and angular rates. Fossen and Strand (1999) developed a passive observer that is valid for slow speed vessels such as CyberShip II. This observer has shown to be easy to tune and robust with respect to disturbances and unmodeled dynamics. Moreover, Loría, Fossen and Panteley (2000) showed for this observer that the separation principle holds. In the experiments for CyberShip II the blanket assumption was thus made that full state measurements were available, while in reality the passive observer was used to provide these.

5.2.1 Ship model

Let $\eta = [x, y, \psi]^\top$ be the 3 DOF position (x, y) and heading (ψ) of the ship in an Earth-fixed inertial frame, and let $\nu = [u, v, r]^\top$ be the corresponding linear velocities (u, v) - called surge and sway - and angular rate (r) - called yaw - in the body-fixed frame. According to Fossen (2002); see also Appendix B, the dynamic model of the ship is

$$\begin{aligned} \dot{\eta} &= R(\psi)\nu \\ M\dot{\nu} &= f - C(\nu)\nu - D(\nu)\nu + R(\psi)^\top b. \end{aligned} \tag{5.1}$$

The vector $b = [b_1, b_2, b_3]^\top$, $\dot{b} = 0$, represents a constant (or slowly-varying) unknown bias due to external environmental forces. $R(\cdot)$ is the 3 DOF rotation matrix with the properties that $R(\psi)^\top R(\psi) = I$, $\|R(\psi)\| = 1$ for all ψ, and $\frac{d}{dt}\{R(\psi)\} = \dot{\psi}R(\psi)S$ where

$$R(\psi) := \begin{bmatrix} \cos\psi & -\sin\psi & 0 \\ \sin\psi & \cos\psi & 0 \\ 0 & 0 & 1 \end{bmatrix}, \quad S := \begin{bmatrix} 0 & -1 & 0 \\ 1 & 0 & 0 \\ 0 & 0 & 0 \end{bmatrix}.$$

The system inertia matrix $M = M^\top > 0$ is

$$M = \begin{bmatrix} m - X_{\dot{u}} & 0 & 0 \\ 0 & m - Y_{\dot{v}} & mx_g - Y_{\dot{r}} \\ 0 & mx_g - N_{\dot{v}} & I_z - N_{\dot{r}} \end{bmatrix}$$

where $Y_{\dot{r}} = N_{\dot{v}}$, the skew-symmetric matrix of Coriolis and centripetal terms is

$$C(\nu) = \begin{bmatrix} 0 & 0 & c_{13}(\nu) \\ 0 & 0 & c_{23}(\nu) \\ -c_{13}(\nu) & -c_{23}(\nu) & 0 \end{bmatrix}$$

where $c_{13}(\nu) = -(m - Y_{\dot{v}})v - (mx_g - Y_{\dot{r}})r$ and $c_{23}(\nu) = (m - X_{\dot{u}})u$, and the nonlinear damping matrix is

$$D(\nu) = \begin{bmatrix} d_{11}(\nu) & 0 & 0 \\ 0 & d_{22}(\nu) & d_{23}(\nu) \\ 0 & d_{32}(\nu) & d_{33}(\nu) \end{bmatrix}$$

where $d_{11}(\nu) = -X_u - X_{|u|u}|u| - X_{uuu}u^2$, $d_{22}(\nu) = -Y_v - Y_{|v|v}|v| - Y_{|r|v}|r|$, $d_{23}(\nu) = -Y_r - Y_{|v|r}|v| - Y_{|r|r}|r|$, $d_{32}(\nu) = -N_v - N_{|v|v}|v| - N_{|r|v}|r|$, and $d_{33}(\nu) = -N_r - N_{|v|r}|v| - N_{|r|r}|r|$. The coefficients $\{X_{(\cdot)}, Y_{(\cdot)}, N_{(\cdot)}\}$ are hydrodynamic parameters according to the notation of The Society of Naval Architects and Marine Engineers (1950); see also Clarke (2003).

The coefficients in M (and therefore $C(\nu)$) are determined quite accurately using semi-empirical methods, hydrodynamic computation programs, or system identification. These have, however, been roughly estimated beforehand by Lindegaard (2003) for CS2 by using system identification procedures. The main difficulty is to find the coefficients in the damping matrix. By towing CS2 at different speeds in different directions and measuring the corresponding drag forces, about half of these parameters have been identified; see Appendix B for details. The numerical values for all identified parameters are shown in Table 5.1. The remaining parameters are in the designs of this chapter dealt with by robust control techniques.

Table 5.1: A priori identified parameters for CS2

m	23.8000	$Y_{\dot{v}}$	-10.0	X_u	-0.7225	$Y_{\|v\|v}$	-36.2823
I_z	1.7600	$Y_{\dot{r}}$	- 0.0	$X_{\|u\|u}$	-1.3274	Y_r	0.1079
x_g	0.0460	$N_{\dot{v}}$	- 0.0	X_{uuu}	-5.8664	N_v	0.1052
$X_{\dot{u}}$	- 2.0	$N_{\dot{r}}$	- 1.0	Y_v	-0.8612	$N_{\|v\|v}$	5.0437

The input $f = [f_u, f_v, f_r]^\top$ of generalized control forces and moments[1] is for CS2 related to the propeller revolutions $n = (n_1, n_2, n_3)$ and rudder angles $\delta = (\delta_1, \delta_2)$ through a nonlinear mapping

$$f = B f_{act}(\nu, n, \delta)$$

where $B \in \mathbb{R}^{3\times 5}$ is an actuator configuration matrix and $f_{act} : \mathbb{R}^3 \times \mathbb{R}^3 \times [-\pi, \pi)^2 \to \mathbb{R}^5$ is a function that for each velocity ν relates the actuator set-points (n, δ) to a vector of forces. Finding optimal actuator set-points (n, δ) for each commanded force f is called control allocation (Johansen, Fuglseth, Tøndel and Fossen; 2003; Johansen, Fossen and Tøndel; 2005; Johansen, Fossen and Berge; 2004). For CS2 this has been developed by Lindegaard and Fossen (2003), and our control input is therefore f for which the saturation limits are approximately $|f_u|, |f_v| \leq 2.0\,\mathrm{N}$, and $|f_r| \leq 1.5\,\mathrm{N\,m}$.

5.2.2 Problem statement

The main task is to converge to and follow the desired path

$$\eta_d(\theta) = \left[\; x_d(\theta), \quad y_d(\theta), \quad \psi_d(\theta) \;\right]^\top \tag{5.2}$$

continuously parametrized by the path variable θ. In all experiments, the desired path will be an ellipsoid with heading along the tangent vector, that is, $x_d(\theta) = 6 + 5\cos(\frac{\pi}{180}\theta)$, $y_d(\theta) = -0.5 + 2.5\sin(\frac{\pi}{180}\theta)$, and $\psi_d(\theta) = \arctan(\frac{y_d^\theta(\theta)}{x_d^\theta(\theta)})$.

The secondary task is to satisfy a desired dynamic behavior along the path, given as a desired surge velocity $u_d(t)$ that must be adjustable online by the operator. This is solved according to the relationship

$$u_d(t) = \sqrt{x_d^\theta(\theta(t))^2 + y_d^\theta(\theta(t))^2}\;\dot{\theta}(t)$$

which gives the speed assignment $\upsilon_s(\theta, t)$ for $\dot{\theta}$ according to

$$\begin{aligned}
\upsilon_s(\theta, t) &= \frac{u_d(t)}{\sqrt{x_d^\theta(\theta)^2 + y_d^\theta(\theta)^2}} \\
\upsilon_s^\theta(\theta, t) &= \frac{-\left[x_d^\theta(\theta) x_d^{\theta^2}(\theta) + y_d^\theta(\theta) y_d^{\theta^2}(\theta)\right]}{\left[x_d^\theta(\theta)^2 + y_d^\theta(\theta)^2\right]^{3/2}} u_d(t) \\
\upsilon_s^t(\theta, t) &= \frac{\dot{u}_d(t)}{\sqrt{x_d^\theta(\theta)^2 + y_d^\theta(\theta)^2}}.
\end{aligned} \tag{5.3}$$

This motivates the following maneuvering problem:

[1] Usually, τ is used to denote the input generalized forces and moments according to the notation of Fossen (1994, 2002). However, not to confuse it with the (maneuvering) tuning function we use f instead.

1. ***Geometric Task:*** For any continuous function $\theta(t)$, force the ship to converge to and follow the desired path:

$$\lim_{t\to\infty} |\eta(t) - \eta_d(\theta(t))| = 0. \tag{5.4}$$

2. ***Dynamic Task:*** Force the path speed $\dot{\theta}$ to converge to the desired speed assignment $\upsilon_s(\theta, t)$:

$$\lim_{t\to\infty} \left|\dot{\theta}(t) - \upsilon_s(\theta(t), t)\right| = 0. \tag{5.5}$$

Additionally, all states must be bounded. Since the ship is fully actuated, both tasks are (trivially) feasible; see Section 2.3. However, a saturation constraint on the propeller forces may place some limitation on the speed assignment.

Assumption 5.1 *To satisfy Assumption 3.1 we impose the following constraints:*

1. *The path functions* $(x_d(\theta),\ y_d(\theta)) \in \mathcal{C}^3$ *and their three first partial derivatives are uniformly bounded with respect to* θ.
2. *The desired surge velocity* $u_d(t) \in \mathcal{C}^1$ *and its derivative* $\dot{u}_d(t)$ *are uniformly bounded in* t.

5.3 Adaptive maneuvering of ships

For CS2 the uncertain (non-identified) constant parameter vector is $\varphi := [Y_{|r|v},\ Y_{|v|r},\ Y_{|r|r},\ N_{|r|v},\ N_r,\ N_{|v|r},\ N_{|r|r},\ b_1,\ b_2,\ b_3]^\top \in \mathbb{R}^{10}$, and the ship dynamic equations (5.1) are rewritten as

$$\begin{aligned} \dot{\eta} &= R(\psi)\nu \\ M\dot{\nu} &= f - C(\nu)\nu + \kappa(\nu) + \Phi(\eta,\nu)\varphi \end{aligned} \tag{5.6}$$

where $\kappa(\nu)$ is the known part of $-D(\nu)\nu$ and

$$\Phi(\eta,\nu) := \begin{bmatrix} 0 & 0 & 0 & 0 & 0 & 0 & 0 & \cos\psi & \sin\psi & 0 \\ |r|\,v & |v|\,r & |r|\,r & 0 & 0 & 0 & 0 & -\sin\psi & \cos\psi & 0 \\ 0 & 0 & 0 & |r|\,v & r & |v|\,r & |r|\,r & 0 & 0 & 1 \end{bmatrix}$$

is the regressor matrix so that $\kappa(\nu) + \Phi(\eta,\nu)\varphi = R(\psi)^\top b - D(\nu)\nu$. Premultiplying by M^{-1}, the model (5.6) is in parametric strict feedback form according to Section 4.2.

The explicit time dependence of $t \mapsto \upsilon_s(\theta, t)$, for all $t \geq t_0$, will make the closed-loop system time-varying. As shown in Section 1.4.2 and Appendix A.2, such a time-varying case can be subsumed into a time-invariant framework by treating time as an additional state with its own dynamics. For clarity, for this purpose we can use the variable p, that is, the extended-state dynamic system will be composed of (5.6) and

$$\dot{p} = 1, \qquad p(0) = t_0. \tag{5.7}$$

Correspondingly, the (internal) time variable for the new extended-state system will be denoted, as usual, by t with initial time $t = 0$. Notice that, in particular, $p(t) = t + t_0$ for all $t \geq 0$ and consequently $\upsilon_s(\cdot, p)$ conforms to (5.5) for each $p \geq t_0$ and each corresponding $t \geq 0$.

This state augmentation guarantees that in the space of $(\eta, \nu, \hat{\varphi}, \theta, p) \in \mathbb{R}^3 \times \mathbb{R}^3 \times \mathbb{R}^{10} \times \mathbb{R} \times \mathbb{R}_{\geq 0}$ the closed-loop system possesses a globally attractive manifold, where $\hat{\varphi}$ is the dynamic estimate of φ. The expression for the desired manifold is obtained by differentiating $\eta = \eta_d(\theta)$ along the solutions of (5.6) with $\dot{\theta} = \upsilon_s(\theta, p)$, which gives

$$\mathcal{E} := \left\{ \eta = \eta_d(\theta),\ \nu = R\left(\psi_d(\theta)\right)^\top \eta_d^\theta(\theta) \upsilon_s(\theta, p) \right\}. \tag{5.8}$$

Clearly, every solution in $\mathcal{E}$ satisfies the Geometric Task (5.4). To see that it also satisfies the Dynamic Task (5.5), we differentiate $\eta_d(\theta) \equiv \eta$ to get $\eta_d^\theta(\theta)\dot{\theta} = \dot{\eta} = R(\psi)\nu = R(\psi_d(\theta))R\left(\psi_d(\theta)\right)^\top \eta_d^\theta(\theta)\upsilon_s(\theta, p) = \eta_d^\theta(\theta)\upsilon_s(\theta, p)$ which holds for all (θ, p) and thus shows[2] that $\dot{\theta} = \upsilon_s(\theta, p)$ in $\mathcal{E}$.

Since the manifold $\mathcal{E}$ is unbounded in the directions of θ and p, the maneuvering problem is recast in the framework of set-stability for closed, noncompact, forward invariant sets. Denoting $\tilde{\varphi} := \varphi - \hat{\varphi}$ the error between the parameter vector φ and its estimate $\hat{\varphi}$, the adaptive backstepping procedure presented in the next section will recursively construct a global diffeomorphism into new error coordinates $z = \mathrm{col}(z_1, z_2) \in \mathbb{R}^6$, $z = \Psi(\eta, \nu, \theta, p)$, such that $z = 0$ if and only if $(\eta, \nu, \hat{\varphi}, \theta, p) \in \mathcal{E}$. By including the constraint $\tilde{\varphi} = 0$, the desired set then becomes the closed, noncompact subset, $\mathcal{M} \subset \mathcal{E}$, given as

$$\mathcal{M} := \{(\eta, \nu, \hat{\varphi}, \theta, p) :\ \Psi(\eta, \nu, \theta, p) = 0,\ \hat{\varphi} - \varphi = 0\}. \tag{5.9}$$

The resulting control law presented in the next section will ensure global attractivity of $\mathcal{E}$, while rendering $\mathcal{M}$ UGS according to Definition A.8. We will use p to represent the explicit time only in the analysis parts of this section, while in the following design section we use t directly.

[2] Except for the case $\eta_d^\theta(\theta) \equiv 0$ when the path $\eta_d(\theta)$ is reduced to a fixed point.

5.3.1 Control design

The design follows the recursive procedure presented in Section 4.2.

Step 1: Define the error variables

$$z_1(\eta,\theta) := R(\psi)^\top (\eta - \eta_d(\theta)) \tag{5.10}$$
$$z_2(\nu,\eta,\theta,t) := \nu - \alpha_1(\eta,\theta,t) \tag{5.11}$$
$$\omega_s(\dot\theta,\theta,t) := \upsilon_s(\theta,t) - \dot\theta \tag{5.12}$$
$$\tilde\varphi := \varphi - \hat\varphi, \tag{5.13}$$

where $\hat\varphi$ is the parameter estimate and α_1 is a *virtual control* to be specified later. Observe that z_1 is decomposed in the body-fixed ship frame. This means that the controller gains will not depend on the ship heading, a common trick in vessel control (Lindegaard and Fossen; 2003) used to aid the tuning process. Differentiating (5.10) with respect to time yields

$$\begin{aligned}\dot z_1 &= \dot R(\psi)^\top (\eta - \eta_d(\theta)) + R(\psi)^\top \left(\dot\eta - \eta_d^\theta(\theta)\dot\theta\right) \\ &= -rSz_1 + z_2 + \alpha_1 - R(\psi)^\top \eta_d^\theta(\theta)\dot\theta \end{aligned} \tag{5.14}$$

where we used $R(\psi)^\top R(\psi) = I$ and $\dot R(\psi) = rR(\psi)S$. Define the first control Lyapunov function (CLF) as

$$V_1(z_1) := \frac{1}{2} z_1^\top z_1 \tag{5.15}$$

whose time derivative becomes

$$\dot V_1 = z_1^\top \left[\alpha_1 - R(\psi)^\top \eta_d^\theta \upsilon_s\right] + z_1^\top z_2 + z_1^\top R(\psi)^\top \eta_d^\theta \omega_s$$

due to skew-symmety of $S = -S^\top$, giving $z_1^\top S z_1 = 0$, $\forall z_1$. With the virtual control law

$$\alpha_1 = \alpha_1(\eta,\theta,t) = -K_p z_1 + R(\psi)^\top \eta_d^\theta(\theta)\upsilon_s(\theta,t), \tag{5.16}$$

where $K_p = K_p^\top > 0$, and the first *tuning function*

$$\tau_1(\eta,\theta) := z_1^\top R(\psi)^\top \eta_d^\theta(\theta), \tag{5.17}$$

the result of *Step 1* becomes

$$\dot z_1 = -K_p z_1 - rSz_1 + z_2 + R(\psi)^\top \eta_d^\theta(\theta)\omega_s \tag{5.18}$$
$$\dot V_1 = -z_1^\top K_p z_1 + z_1^\top z_2 + \tau_1 \omega_s \tag{5.19}$$

leaving the terms containing z_2 and ω_s for the next step. To aid the next step, let

$$\begin{aligned}
\dot{\alpha}_1 &=: \sigma_1 + \alpha_1^\theta \dot{\theta} \\
\sigma_1 &= -K_p\left(\nu - rSz_1\right) - rSR(r)^\top \eta_d^\theta(\theta)\upsilon_s(\theta,t) + R(\psi)^\top \eta_d^\theta(\theta)\upsilon_s^t(\theta,t) \\
\alpha_1^\theta &= K_p R(\psi)^\top \eta_d^\theta(\theta) + R(\psi)^\top[\eta_d^{\theta^2}(\theta)\upsilon_s(\theta,t) + \eta_d^\theta(\theta)\upsilon_s^\theta(\theta,t)].
\end{aligned} \tag{5.20}$$

Step 2: Differentiating (5.11) with respect to time yields

$$\begin{aligned}
M\dot{z}_2 &= M\dot{\nu} - M\dot{\alpha}_1 \\
&= f - C(\nu)\nu + \kappa(\nu) + \Phi(\eta,\nu)\varphi - M\sigma_1 - M\alpha_1^\theta \dot{\theta}
\end{aligned} \tag{5.21}$$

where $M = M^\top > 0$. Let $\Gamma = \Gamma^\top > 0$ and define the second CLF

$$V_2(z_1, z_2, \tilde{\varphi}) := V_1(z_1) + \frac{1}{2} z_2^\top M z_2 + \frac{1}{2}\tilde{\varphi}^\top \Gamma^{-1}\tilde{\varphi} \tag{5.22}$$

whose time derivative is

$$\begin{aligned}
\dot{V}_2 &= \dot{V}_1 + z_2^\top M\dot{z}_2 - \tilde{\varphi}^\top \Gamma^{-1}\dot{\hat{\varphi}} \\
&= -z_1^\top K_p z_1 + \left(\tau_1 + z_2^\top M\alpha_1^\theta\right)\omega_s + \tilde{\varphi}^\top[\Phi^\top z_2 - \Gamma^{-1}\dot{\hat{\varphi}}] \\
&\quad + z_2^\top[z_1 + f - C\nu + \kappa + \Phi\hat{\varphi} - M\sigma_1 - M\alpha_1^\theta \upsilon_s]
\end{aligned}$$

where $\rho_2(\eta,\nu,\theta,t) := \Phi(\eta,\nu)^\top z_2(\nu,\eta,\theta,t)$ is recognized as the *adaptive tuning function* (Krstić et al.; 1995). The static part of the control law and the adaptive update law for $\hat{\varphi}$ are then designed as

$$\begin{aligned}
f &= \alpha_2(\eta,\nu,\hat{\varphi},\theta,t) \\
&= -z_1 - K_d z_2 + C\alpha_1 - \kappa - \Phi\hat{\varphi} + M\sigma_1 + M\alpha_1^\theta \upsilon_s
\end{aligned} \tag{5.23}$$

$$\dot{\hat{\varphi}} = \Gamma\rho_2(\eta,\nu,\theta,t) = \Gamma\Phi(\eta,\nu)^\top z_2 \tag{5.24}$$

where $K_d = K_d^\top > 0$. Defining the second tuning function

$$\begin{aligned}
\tau_2(\eta,\nu,\theta,t) &:= \tau_1(\eta,\theta) + z_2(\eta,\nu,\theta,t)^\top M\alpha_1^\theta(\eta,\theta,t) \\
&= \eta_d^\theta(\theta)^\top R(\psi) z_1(\eta,\theta) + \alpha_1^\theta(\eta,\theta,t)^\top M z_2(\nu,\eta,\theta,t)
\end{aligned} \tag{5.25}$$

and taking into account $z_2^\top C(\nu) z_2 = 0$, $\forall z_2$, we get

$$\dot{V}_2 = -z_1^\top K_p z_1 - z_2^\top K_d z_2 + \tau_2\omega_s. \tag{5.26}$$

The global diffeomorphism

$$(\eta, \nu, \hat{\varphi}, \theta, t) \mapsto (z_1, z_2, \tilde{\varphi}, \theta, t)$$

is now explicitly given by $\tilde{\varphi} = \varphi - \hat{\varphi}$ and $z = \Psi(\eta, \nu, \theta, t)$, where

$$\Psi(\eta, \nu, \theta, t) := \begin{bmatrix} R(\psi)^\top (\eta - \eta_d(\theta)) \\ K_p R(\psi)^\top (\eta - \eta_d(\theta)) + \nu - R(\psi)^\top \eta_d^\theta(\theta) \upsilon_s(\theta, t) \end{bmatrix} \tag{5.27}$$

is bounded in (θ, t) by Assumption 5.1. The resulting closed-loop system becomes

$$\begin{aligned} \dot{z} &= A_z(\nu) z + g(\eta, \theta, t)\omega_s + H\Phi(\eta, \nu)\tilde{\varphi} \\ \dot{\tilde{\varphi}} &= \Gamma \Phi(\eta, \nu)^\top M H^\top z \\ \dot{\theta} &= \upsilon_s(\theta, t) - \omega_s \end{aligned} \tag{5.28}$$

where

$$A_z(\nu) := \begin{bmatrix} -K_p - rS & I \\ -M^{-1} & -M^{-1}(K_d + C(\nu)) \end{bmatrix} \tag{5.29}$$

$$g(\eta, \theta, t) := \begin{bmatrix} R(\psi)^\top \eta_d^\theta(\theta) \\ \alpha_1^\theta(\eta, \theta, t) \end{bmatrix}, \quad H := \begin{bmatrix} 0 \\ M^{-1} \end{bmatrix}. \tag{5.30}$$

Rendering $\tau_2 \omega_s \leq 0$ in (5.26) will finalize the design according to the following theorem:

Theorem 5.2 *For the closed-loop system (5.28), every continuous function $\omega_s = \omega(\eta, \nu, \hat{\varphi}, \theta, t)$, bounded in (θ, t), such that*

$$\begin{aligned} &(i) \qquad \omega_s = 0 \text{ for all } (\eta, \nu, \hat{\varphi}, \theta, t) \in \mathcal{E}, \\ &(ii) \qquad \tau_2(\eta(t), \nu(t), \theta(t), t)\omega_s(t) \leq 0, \quad \forall t \geq t_0 \geq 0, \end{aligned}$$

renders $\mathcal{E}$ in (5.8) globally attractive and $\mathcal{M}$ in (5.9) UGS.

Proof. *Let $\dot{p} = 1$, $p(0) = t_0$ s.t. $p(t) = t + t_0$. For the set (5.9), rewritten as*

$$\mathcal{M} := \{(z, \tilde{\varphi}, \theta, p) \in \mathbb{R}^6 \times \mathbb{R}^{10} \times \mathbb{R} \times \mathbb{R}_{\geq 0} : \ z = 0, \ \tilde{\varphi} = 0\},$$

the distance function is $|(z, \tilde{\varphi}, \theta, p)|_{\mathcal{M}} = |(z, \tilde{\varphi})|$. Since $\mathcal{M} \subset \mathcal{E}$ we have that $\omega_s = 0$ in $\mathcal{M}$, and thus $\mathcal{M}$ is forward invariant for (5.28). Furthermore, (5.22) and (5.26) with $\tau_2 \omega_s \leq 0$ satisfy (A.36), (A.37) with $\alpha_1 := c_1 |(z, \tilde{\varphi})|^2$, $\alpha_2 := c_2 |(z, \tilde{\varphi})|^2$, and $\alpha_3 := c_3 |z|^2$, where $c_1 := \frac{1}{2} \min\{1, \lambda_{\min}(M), \lambda_{\min}(\Gamma^{-1})\}$, $c_2 := \frac{1}{2} \max\{1, \lambda_{\max}(M), \lambda_{\max}(\Gamma^{-1})\}$, and $c_3 := \min\{1, \lambda_{\min}(K_p), \lambda_{\min}(K_d)\}$. Now, for each finite $K > 0$ such that $|(z, \tilde{\varphi}, \theta, p)|_{\mathcal{M}} = |(z, \tilde{\varphi})| \leq K$, it follows by Assumption 5.1 and (5.13),

Table 5.2: Closed-loop in the adaptive ship maneuvering system

Plant :
$\dot{\eta} = R(\psi)\nu$
$M\dot{\nu} = f - C(\nu)\nu + \kappa(\nu) + \Phi(\eta,\nu)\varphi$
input: $\{f\}$ output: $\{\eta,\nu\}$
Control :
$\dot{\omega} = -\lambda\omega - \lambda\mu\left[z_1^\top R(\psi)^\top \eta_d^\theta + z_2^\top M\alpha_1^\theta\right], \quad \mu,\lambda > 0$
$\dot{\theta} = \upsilon_s(\theta) - \omega_s$
$\omega_s = \begin{cases} -\mu\left[z_1^\top R(\psi)^\top \eta_d^\theta + z_2^\top M\alpha_1^\theta\right], & \mu \geq 0, \quad \text{Gradient} \\ \omega, & \text{Filtered-gradient} \end{cases}$
$\dot{\hat{\varphi}} = \Gamma\Phi(\eta,\nu)^\top z_2$
$f = -z_1 - K_d z_2 + C(\nu)\alpha_1 - \kappa - \Phi\hat{\varphi} + M\sigma_1 + M\alpha_1^\theta \upsilon_s$
input: $\left\{\eta,\nu,\eta_d(\theta),\eta_d^\theta(\theta),\eta_d^{\theta^2}(\theta),\upsilon_s(\theta,t),\upsilon_s^\theta(\theta,t),\upsilon_s^t(\theta,t)\right\}$
output: $\{f,\theta\}$
Guidance :
input: $\{\theta,u_d(t),\dot{u}_d(t)\}$
output: $\left\{\eta_d(\theta),\eta_d^\theta(\theta),\eta_d^{\theta^2}(\theta),\upsilon_s(\theta,t),\upsilon_s^\theta(\theta,t),\upsilon_s^t(\theta,t)\right\}$

(5.27) that $(\eta,\nu,\hat{\varphi})$, *and* ω_s *by continuity, are bounded. Hence, there exists, for each* K, *an upper bound* $L > 0$ *on the right-hand side of (5.28). By Theorem A.18 it follows that* $\mathcal{M}$ *is UGS with respect to (5.28), and* $\alpha_3(|(z(t),\tilde{\varphi}(t),\theta(t),p(t))|_{\mathcal{M}}) = c_3|z(t)|^2 \to 0$ *as* $t \to \infty$ *shows that* $\mathcal{E}$ *is globally attractive.* ■

5.3.2 Closed-loop system

To satisfy Theorem 5.2, either the tracking update law $\omega_s = 0$ or the gradient update law $\omega_s = -\mu\tau_2$, $\mu \geq 0$, for which it is verified that $\tau_2 = -V_2^\theta(\Psi(\eta,\nu,\theta,t),\tilde{\varphi})$, can be applied as shown in the previous chapters. Optionally, the filtered-gradient update law can be applied, using $\dot{\omega}_s = -\lambda\omega_s - \lambda\mu\tau_2$ with $\mu,\lambda > 0$. The resulting closed-loop system is summarized in Table 5.2.

5.3.3 Experimental results

In the following we report the results of two experiments performed in the MCLab. In the first we run an adaptive maneuvering system for CS2 ac-

cording to the design in the previous sections. In the second experiment we compare the performance of using the gradient update law implementation versus the tracking update law when the forward thrust f_u is forced to saturate. The path and speed assignments are given by (5.2) and (5.3).

CS2 Experiment 1: Adaptive maneuvering

For this experiment, performed 2003-10-11, the gradient update law was applied. The controller settings were $K_p = \text{diag}(0.2,\, 1.0,\, 0.5)$, $K_d = \text{diag}(3,\, 10,\, 7)$, $\mu = 400$, and $\Gamma = \text{diag}(2, 2, 2, 2, 2, 2, 2, 1, 1, 1)$. The initial condition for the parameter update was $\hat{\varphi}(0) = [0, 0, 0, 0, -0.5, 0, 0, 0, 0, 0]^\top$. The ship was first put to rest in dynamic positioning (zero speed) at $\eta_d(0)$, and then the ship was commanded online to move along the path with different desired surge velocities.

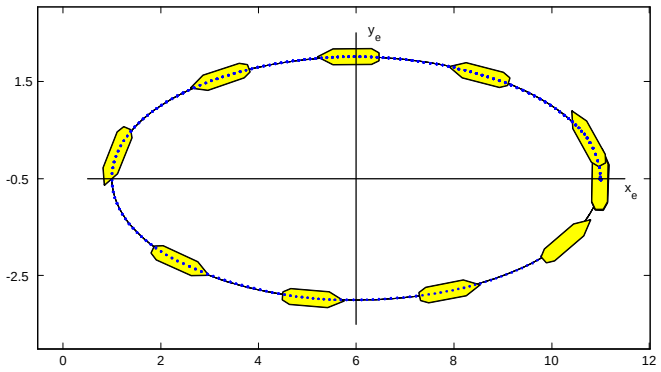

Figure 5.2: Position response of CS2 following the desired ellipsoidal path in MCLab, using an adaptive maneuvering control law with the gradient update law.

Figure 5.2 shows how CS2 accurately traced the path on its first round along the ellipsoid. In the total run it did many rounds, and the upper plot in Figure 5.3 shows the commanded surge velocity $u_d(t)$ and the resulting response $u(t)$. The lower plot shows the corresponding speed assignment $\upsilon_s(\theta(t), t)$ and the resulting response of $\dot{\theta}(t)$. Clearly, $\dot{\theta}(t)$ worked actively to satisfy its twofold objective between the speed assignment and the Lyapunov cost function minimization. The time series of the parameter estimates $\hat{\varphi}(t)$ are shown in Figure 5.4. For the full scale vessel, the commanded velocities

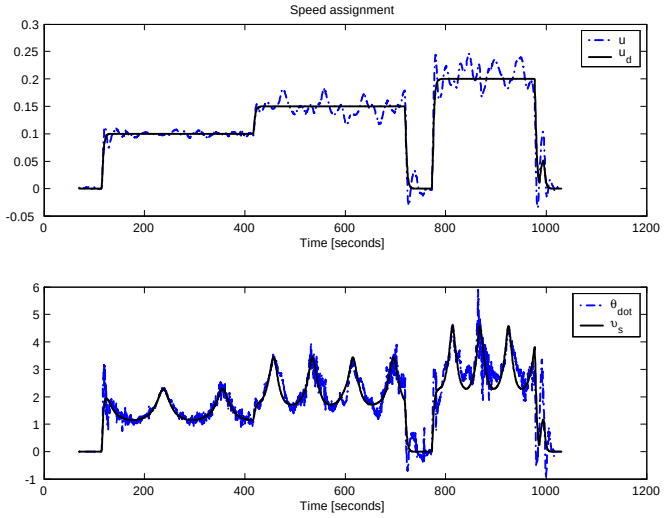

Figure 5.3: Dynamic task: The upper plot shows the online commanded surge $u_d(t)$ and the resulting response of $u(t)$. The lower plot shows the corresponding speed assignment $\upsilon_s(\theta(t), t)$ and the resulting response of $\dot{\theta}(t)$.

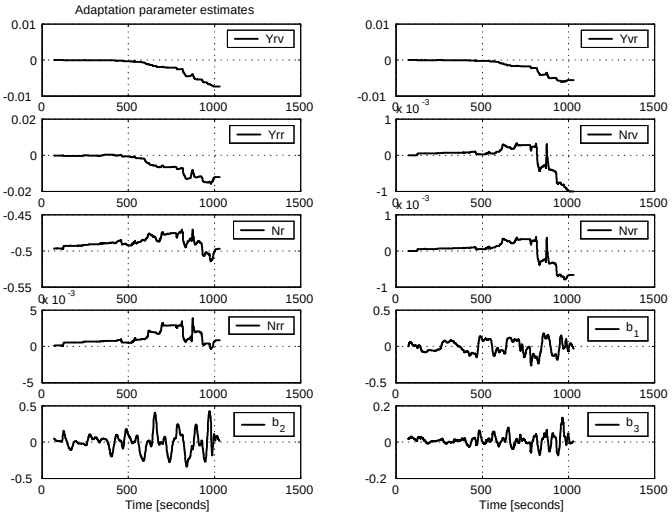

Figure 5.4: The parameter estimates $\hat{\varphi}(t)$ in the first adaptive CS2 maneuvering experiment.

$\{0.10, 0.15, 0.20\}$ m/s corresponds to $\{1.55, 2.32, 3.10\}$ knots. This is within the speed domain of dynamical positioning for which this model ship is built.

Ship Experiment 2: Tracking vs. Gradient in a thrust failure scenario

In this experiment, also performed 2003-10-11, we compared the ship responses using the tracking update law and the gradient update law when the forward thrust f_u cannot deliver enough force for the ship to track the commanded speed. To achieve this we induced the saturation limit $|f_u| \leq 0.1\,\mathrm{N}$ on the ship. The controller gains were the same as in the last experiment; however, for simplicity only the bias b was adapted so that $\Gamma = \mathrm{diag}(0,0,0,0,0,0,0,1,1,1)$ with $\hat{\varphi}(0)$ initialized as before.

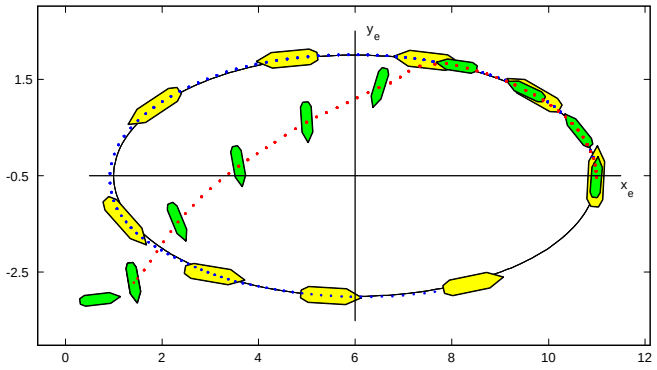

Figure 5.5: Position responses using a tracking update law (small ship) and a gradient update law (large ship) in the second ship experiment with commanded speed $u_d = 0.20\,\mathrm{m/s}$. Both responses are superimposed in the same plot. Since CS2 cannot move with $u_d = 0.20\,\mathrm{m/s}$ under the induced saturation limit, the tracking-based system went unstable. The gradient-based system, on the other hand, safely maneuvered CS2 along the path, but at a slower speed.

In both cases, CS2 was first positioned at $\eta_d(0)$, then commanded for one round with $u_d = 0.10\,\mathrm{m/s}$, and when $\theta \approx 360\,^\circ$ the commanded speed was changed to $u_d = 0.20$ m/s. The ship was tracing the path unproblematically at the speed $u_d = 0.10$ m/s in both the tracking and gradient cases. However, when u_d changed to 0.20 m/s the closed-loop systems started to experience problems, as seen in the position responses for the second round

in Figure 5.5. While not surprisingly the tracking system soon went unstable, it is observed that the gradient-based system kept moving along the path, but with a speed slower than the infeasible $u_d = 0.20$ m/s. The lower plot in Figure 5.6 reveals some of the secret. While the speed assignment $\upsilon_s(\theta(t), t)$ strictly corresponds to the specified speed $u_d(t)$ according to (5.3), the response for $\dot{\theta}(t)$ was modified by the gradient term in the update law (see Section 3.4), trying to minimize the errors z_1 and z_2, and $\dot{\theta}(t)$ therefore tracked a slower value. The result was that $\theta(t)$, and thus $\eta_d(\theta(t))$, moved not faster than the ship was able to follow.

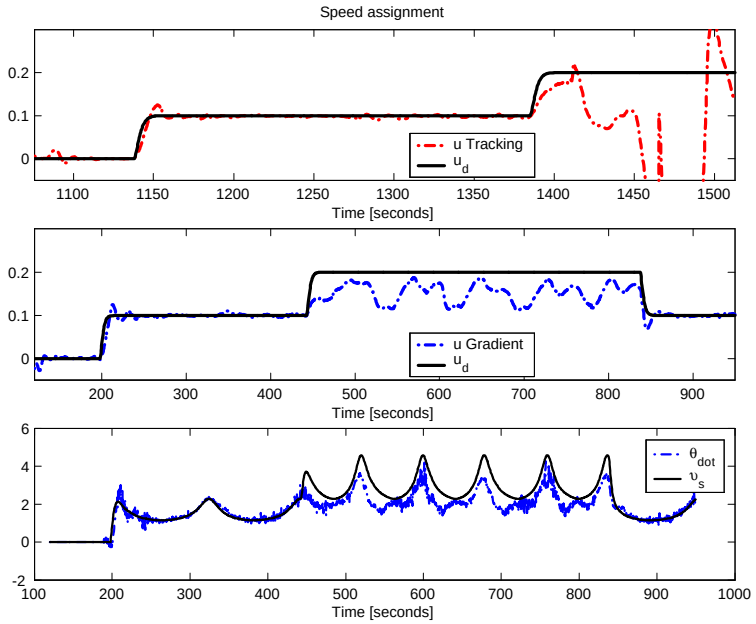

Figure 5.6: Dynamic task: Upper plot shows the commanded surge and resulting speed response for the tracking-based system, while the middle plot shows the same for the gradient-based system. Both systems satisfied the maneuvering objective well when $u_d = 0.10\,\mathrm{m/s}$, but the tracking-based system went unstable when u_d changed to $0.20\,\mathrm{m/s}$. The lower plot shows $\upsilon_s\left(\theta(t), t\right)$ and $\dot{\theta}(t)$ for the gradient-based system only.

This last experiment served to illustrate one of the advantages of using the gradient minimization feature in the gradient or filtered-gradient update laws, as compared to just using the pure tracking update law.

5.4 Sliding-mode control for ship maneuvering

Consider the ship model (5.1). As discussed in the previous section, this model is uncertain with respect to the unidentified hydrodynamic parameters and other unmodeled dynamics. In this section we develop a robust sliding-mode control law to deal with these uncertainties.

The numerical values of the identified parameters of (5.1) are given by Table 5.1. The unidentified parameters are set to zero, that is, $\varphi := [Y_{|r|v},\ Y_{|v|r},\ Y_{|r|r},\ N_{|r|v},\ N_r,\ N_{|v|r},\ N_{|r|r}]^\top = 0$. This results in an uncertainty that together with other unmodeled dynamics are assumed captured by an unknown additive term $\delta(\nu, t)$. The resulting model becomes then

$$\dot{\eta} = R(\psi)\nu \tag{5.31a}$$

$$M\dot{\nu} = f - C(\nu)\nu - D(\nu)\nu + R(\psi)^\top b + \delta(\nu, t), \tag{5.31b}$$

where the terms b and δ are uncertain. We assume there exist known positive reals b_0, k_0, and k_1 such that

$$\begin{array}{ll} (i) & |b| \leq b_0 \\ (ii) & |\delta(\nu, t)| \leq k_0 |\nu| + k_1. \end{array} \tag{5.32}$$

According to Section 4.3.2 we consider (5.31a) as the nominal part of the plant and (5.31b) as the uncertain part.

5.4.1 Control design

Design for the nominal part

To solve the maneuvering control objective (5.4) and (5.5) for the nominal part, we propose the diffeomorphism $(\eta, \theta, t) \mapsto (z, \theta, t)$, where

$$z(\eta, \theta) := R(\psi)^\top (\eta - \eta_d(\theta)) \tag{5.33}$$

is the error variable for the geometric task, and the function

$$V(z(\eta, \theta)) := \frac{1}{2} z(\eta, \theta)^\top z(\eta, \theta) \tag{5.34}$$

satisfying (4.100) with $\gamma_1(\cdot) = \gamma_2(\cdot) = \frac{1}{2}(\cdot)^2$. The nominal control law is then chosen as

$$\dot{\theta} = \upsilon_s(\theta, t) - \mu V^\theta(z(\eta, \theta)), \quad \mu \geq 0, \tag{5.35}$$

$$\alpha_1(\eta, \theta, t) = -K_p z(\eta, \theta) + R(\psi)^\top \eta_d^\theta(\theta) \upsilon_s(\theta, t) \tag{5.36}$$

where $V^\theta = z(\eta,\theta)^\top z^\theta(\eta,\theta) = -z(\eta,\theta)^\top R(\psi)^\top \eta_d^\theta(\theta)$. Optionally, the filtered-gradient update law can be used instead of (5.35). Letting $\nu = \alpha(\eta,\theta,t)+w$ in (5.31a) results in

$$\begin{aligned}\dot{V} &= -z^\top K_p z - \mu V^\theta(z(\eta,\theta))^2 + z^\top w \\ &\leq -\kappa\lambda_{\min}(K_p)\,|z|^2\,, \qquad \forall\,|z| \geq \frac{1}{(1-\kappa)\lambda_{\min}(K_p)}\,|w|\end{aligned} \tag{5.37}$$

where $\kappa \in (0,1)$. It follows that (4.102) is satisfied with $\gamma_3(\cdot) = \kappa\lambda_{\min}(K_p)(\cdot)^2$ and $\gamma_4(\cdot) = \frac{1}{(1-\kappa)\lambda_{\min}(K_p)}(\cdot)$.

Design for the uncertain part

For the uncertain part of the plant (5.31b) we keep the known matrix M on the left-hand side. In this case the matrix $G(x) = I$ as compared to (4.97), and the structural assumptions on $G(x)$ in Section 4.3.2 are trivially satisfied. Define

$$s := \nu - \alpha_1(\eta,\theta,t), \tag{5.38}$$

and calculate

$$\begin{aligned}\dot{\alpha}_1 = {} & rK_pSz - K_p\nu - rSR(\psi)^\top\eta_d^\theta(\theta)\upsilon_s(\theta,t) + R(\psi)^\top\eta_d^\theta(\theta)\upsilon_s^t(\theta,t) \\ & + \left[K_pR(\psi)^\top\eta_d^\theta(\theta) + R(\psi)^\top\left(\eta_d^{\theta^2}(\theta)\upsilon_s(\theta,t) + \eta_d^\theta(\theta)\upsilon_s^\theta(\theta,t)\right)\right]\dot{\theta}\end{aligned} \tag{5.39}$$

where $\dot{\theta}$ is given by (5.35). Differentiating $U(s) = \frac{1}{2}s^\top Ms$ along the solutions of

$$M\dot{s} = f - C(\nu)\nu - D(\nu)\nu + R(\psi)^\top b + \delta(\nu,t) - M\dot{\alpha}_1 \tag{5.40}$$

gives

$$\dot{U} = s^\top\left[f - C(\nu)\nu - D(\nu)\nu - M\dot{\alpha}_1\right] + s^\top\left[R(\psi)^\top b + \delta(\nu,t)\right], \tag{5.41}$$

and the control law is then chosen as

$$f = -Ls - \sigma(\eta,\nu,t)\Psi_2(s) + C(\nu)\nu + D(\nu)\nu + M\dot{\alpha}_1 \tag{5.42}$$

where $L = L^\top > 0$, $\sigma(\eta,\nu,t) \in \mathbb{R}_{\geq 0}$ is yet to be assigned, and

$$\Psi_2(s) := \operatorname{col}\left(\psi(s_1),\psi(s_2),\psi(s_3)\right) \tag{5.43}$$

$$\psi(s_i) := (1+\varepsilon_1)\tanh\left(\frac{s_i}{\varepsilon_2}\right) \tag{5.44}$$

where ε_1 and ε_2 are small positive numbers chosen by design. With $\varepsilon = \varepsilon_2 \operatorname{atanh}(\frac{1}{1+\varepsilon_1})$ it follows from Lemma 4.5 that $\frac{1}{\sqrt{3}}|s| \leq s^\top \Psi_2(s) \leq |s|\,|\Psi_2(s)|$ for all $|s| \geq \sqrt{3}\varepsilon$. Choosing

$$\sigma(\eta, \nu, t) = \sqrt{3}\left[k_s + b_0 + k_0|\nu| + k_1\right] \tag{5.45}$$

gives

$$\begin{aligned}
\dot{U} &= -s^\top L s - \sigma(\eta,\nu,t) s^\top \Psi_2(s) + s^\top \left[R(\psi)^\top b + \delta(\nu,t)\right] \\
&\leq -s^\top L s - \frac{1}{\sqrt{3}}\sigma(\eta,\nu,t)\,|s| + |s|\left[b_0 + k_0|\nu| + k_1\right], \qquad \forall\, |s| \geq \sqrt{3}\varepsilon \\
&< -k_s|s|, \qquad \forall\, |s| \geq \sqrt{3}\varepsilon.
\end{aligned} \tag{5.46}$$

This implies for all $t \geq 0$ that

$$|s(t)| \leq \max\left\{\sqrt{3}\varepsilon, \quad \sqrt{\frac{\lambda_{\max}(M)}{\lambda_{\min}(M)}}\,|s(0)| - \frac{k_s t}{\sqrt{\lambda_{\min}(M)\lambda_{\max}(M)}}\right\}, \tag{5.47}$$

which means that for any initial conditions in the space of $(s, z, \theta, t) \in \mathbb{R}^3 \times \mathbb{R}^3 \times \mathbb{R} \times \mathbb{R}_{\geq 0}$ the corresponding trajectories $(s(t), z(t), \theta(t), t)$ will exist on $[0, \infty)$ and converge in finite time to

$$\mathcal{N}'_\varepsilon = \left\{(s, z, \theta, t) :\ |s| \leq \sqrt{3}\varepsilon\right\} \tag{5.48}$$

and subsequently converge to

$$\mathcal{M}'_\varepsilon = \left\{(s, z, \theta, t) :\ |z| \leq \frac{\sqrt{3}\varepsilon}{(1-\kappa)\lambda_{\min}(K_p)}\right\}. \tag{5.49}$$

5.4.2 Closed-loop system

The closed-loop system consists of the plant (5.31), the gradient update law (5.35), and the static control law (5.42). A summary is given in Table 5.3.

5.4.3 Experimental results

Two experiments performed in the MCLab on 2003-10–06 are reported next. The path and speed assignments are given by (5.2) and (5.3). In both experiments, the controller gains were set to $K_p = \operatorname{diag}\{0.2,\ 0.4,\ 0.5\}$, $L = \operatorname{diag}\{2,\ 3,\ 3.5\}$, $k = k_s + b_0 + k_1 = 0.1$, $k_0 = 4$, $\varepsilon_1 = 0.1$, $\varepsilon_2 = 0.01$, and

Table 5.3: Closed-loop in the sliding-mode ship maneuvering system

Plant :
$\dot{\eta} = R(\psi)\nu$
$M\dot{\nu} = f - C(\nu)\nu - D(\nu)\nu + R(\psi)^\top b + \delta(\nu, t)$
input: $\{f\}$ output: $\{\eta, \nu\}$
Control :
$\dot{\omega} = -\lambda\omega - \lambda\mu z^\top R(\psi)^\top \eta_d^\theta(\theta)$
$\dot{\theta} = \upsilon_s(\theta) - \omega_s$
$\omega_s = \begin{cases} -\mu z^\top R(\psi)^\top \eta_d^\theta(\theta), & \mu \geq 0, \quad \text{Gradient} \\ \omega, & \text{Filtered-gradient} \end{cases}$
$f = -Ls - \sigma(\nu)\Psi_2(s) + C(\nu)\nu + D(\nu)\nu + M\dot{\alpha}_1$
input: $\left\{\eta, \nu, \eta_d(\theta), \eta_d^\theta(\theta), \eta_d^{\theta^2}(\theta), \upsilon_s(\theta, t), \upsilon_s^\theta(\theta, t), \upsilon_s^t(\theta, t)\right\}$
output: $\{f, \theta\}$
Guidance :
input: $\{\theta, u_d(t), \dot{u}_d(t)\}$
output: $\left\{\eta_d(\theta), \eta_d^\theta(\theta), \eta_d^{\theta^2}(\theta), \upsilon_s(\theta, t), \upsilon_s^\theta(\theta, t), \upsilon_s^t(\theta, t)\right\}$

$\mu = 250$. The ship was first put to rest in dynamic positioning (zero speed) at $\eta_d(0)$, and then the ship was commanded online to move along the path with different desired surge velocities.

In the first experiment the tracking update law was used, and the vessel was commanded with velocities $u_d \in \{0.10, 0.15, 0.20\}$ m/ s on calm water. In the second experiment, the gradient update law was used, and the commanded surge velocity was $u_d \in \{0.10, 0.15\}$ m/ s in waves. The wave parameters were: JONSWAP spectrum, significant wave height $h_s = 0.01$ m and peak period $t_s = 1.0$ s. For the full scale vessel this corresponds to a "slight" sea state code with $H_s = 0.70$ m and peak period $T_s = 1.0\sqrt{70} = 8.4$ s (or equivalently, frequency 0.75 rad/ s).

The results for the 'calm water' experiment are discussed with respect to performance in the last section of this chapter. Figures 5.7 and 5.8 show the responses of CyberShip II in the experiment with waves. The direction of the waves came along the x_e-axis in the negative direction. Around the narrowest "corner" of the path the ship therefore experienced both a rapid heading change and waves entering directly from the side. Other experiments with larger wave heights gave the ship increasing problems at these parts of the path; however, in this experiment the ship managed well.

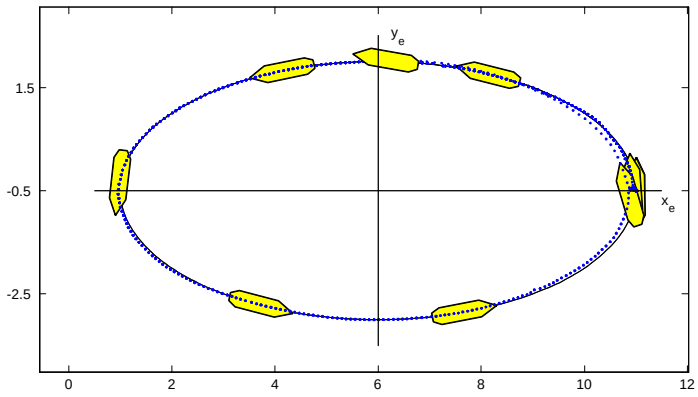

Figure 5.7: CyberShip II moving along the path at various speeds in waves, using the sliding-mode controller with a tracking update law.

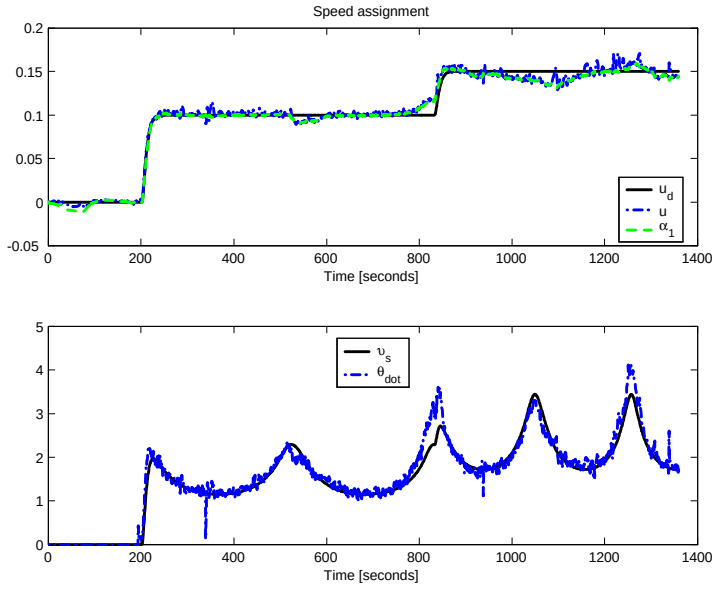

Figure 5.8: The surge speed response of CyberShip II in the sliding-mode experiment with waves and a gradient update law.

Figure 5.9 shows a snapshot at time $t = 353.6\,\mathrm{s}$ of the Lyapunov cost function $V(z(\eta(t),\theta))$ and $V^{\theta}(z(\eta(t),\theta))$ for θ in the interval $[0\,^{\circ}, 360\,^{\circ})$. The discontinuity corresponds to the mapping of the heading error to the interval $[-\pi,\pi)$. Clearly, $\theta \mapsto V(z(\eta,\theta))$ has, as shown by the green curve, a global minimizer at $\theta \approx 90\,^{\circ}$ at which point $\theta \mapsto V^{\theta}(z(\eta,\theta))$ also intersects zero. Additionally, there is a local minimum at approximately $\theta \approx 290\,^{\circ}$ which is on the opposite side of the path. The global minimizer will follow the ship as it traces the path. It therefore requires a rather large perturbation in the system to make $\theta(t)$ jump to the local minimizer and thus cause deteriorated performance.

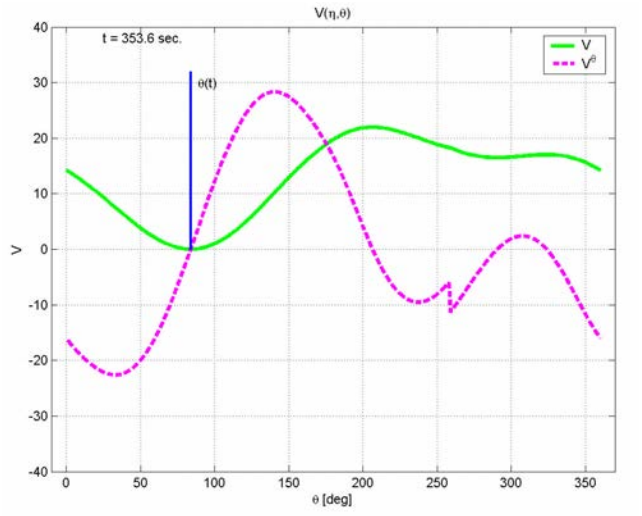

Figure 5.9: A snapshot of $\theta(t)$ showing the minimization of the Lyapunov cost function $V(z(\eta(t),\theta(t)))$ and the gradient $V^{\theta}(z(\eta(t),\theta(t)))$ at $t = 353.6\,\mathrm{s}$ in the sliding-mode experiment.

5.5 Nonlinear PID control for ship maneuvering

In this section we design a nonlinear PID maneuvering controller for a fully actuated surface ship. The tracking controller has originally been developed by Lindegaard and Fossen (n.d.); Lindegaard (2003), and here we propose the maneuvering counterpart. For this purpose we will first develop the path for the full state vector, and then design the control law.

Consider the 3 DOF ship model (5.1), restated here as

$$\begin{aligned} \dot{\eta} &= R(\psi)\nu \\ M\dot{\nu} &= f - C(\nu)\nu - D_L\nu - D_{NL}(\nu)\nu + R(\psi)^\top b \end{aligned} \tag{5.50}$$

where D_L is the linear (constant) part of $D(\nu)$ and $D_{NL}(\nu)$ the remaining nonlinear part. The numerical values of the identified parameters for CyberShip II are given by Table 5.1. The unidentified parameters are set to zero, that is, $\varphi := [Y_{|r|v},\, Y_{|v|r},\, Y_{|r|r},\, N_{|r|v},\, N_r,\, N_{|v|r},\, N_{|r|r}]^\top = 0$. This results in an uncertainty that together with other unmodeled dynamics are assumed captured by the bias b and robustly dealt with by the PID feedback.

The control objective is again to solve the maneuvering problem according to Section 5.2.2. For the desired path $\eta_d(\theta) = \operatorname{col}(x_d(\theta), y_d(\theta), \psi_d(\theta))$, let

$$\begin{aligned} v_d(\theta, t) &:= \eta_d^\theta(\theta)\upsilon_s(\theta, t) \\ a_d(\theta, t) &:= v_d^\theta(\theta, t)\upsilon_s(\theta, t) + v_d^t(\theta, t) \end{aligned}$$

be the earth-fixed desired velocity and acceleration vectors. Then, the maneuvering problem is solved if

$$\begin{aligned} &\dot{\theta}(t) \to \upsilon_s(\theta(t), t) \\ &\eta(t) \to \eta_d(\theta(t)) \\ &\nu(t) \to R(\psi(t))^\top v_d(\theta, t) \\ &\dot{\nu}(t) \to r(t)S^\top R(\psi(t))^\top v_d(\theta(t), t) + R(\psi(t))^\top a_d(\theta(t), t). \end{aligned}$$

Additionally, we define the integral state

$$\sigma(t) := \int_0^t (\eta(\iota) - \eta_d(\theta(\iota)))\, d\iota, \tag{5.51a}$$

$$\dot{\sigma} = \eta - \eta_d(\theta) \tag{5.51b}$$

such that the 'extended plant' state vector becomes (σ, η, ν). Accordingly, the desired state vector containing the path and speed signals represented

in the appropriate coordinate frames, becomes

$$\xi(\psi,\theta,t) := \begin{bmatrix} 0 \\ \eta_d(\theta) \\ R(\psi)^\top v_d(\theta,t) \end{bmatrix} \tag{5.52}$$

where the zero in the top element corresponds to the integral action. With these definitions we embark on the nonlinear PID design.

5.5.1 Control design

The overall control law will consist of the PID feedback term f_{PID}, a reference feedforward term f_{FF}, and a feedback linearizing term f_{FL}. Along the lines of Lindegaard (2003) we propose the static part of the control law as

$$f = f_{PID} + f_{FF} + f_{FL} \tag{5.53}$$

where

$$\begin{aligned} f_{PID} &= -K_I R(\psi)^\top \sigma - K_P R(\psi)^\top (\eta - \eta_d(\theta)) \\ &\quad - K_D \left(\nu - R(\psi)^\top v_d(\theta,t)\right) \end{aligned} \tag{5.54a}$$

$$f_{FF} = D_L R(\psi)^\top v_d(\theta,t) + rMS^\top R(\psi)^\top v_d(\theta,t) + MR(\psi)^\top a_d(\theta,t) \tag{5.54b}$$

$$f_{FL} = C(\nu)\nu + D_{NL}(\nu)\nu. \tag{5.54c}$$

Notice that all the error terms in f_{PID} is decomposed in the body frame, that is, $R(\psi)^\top\sigma$, $R(\psi)^\top(\eta - \eta_d(\theta))$, and $\left(\nu - R(\psi)^\top v_d(\theta,t)\right)$. This essentially means that the PID gains are tuned with respect to errors experienced in the longitudinal, lateral, and rotational directions of the ship. This is more intuitive for tuning since the control technician will himself be onboard the ship and therefore observes these errors in this frame (Lindegaard; 2003). One obstacle for achieving this is that the feedforward term f_{FF} must cancel the r-dependent term, something that would be avoided if all error signals were decomposed in the earth-fixed frame.

It is necessary next to design the dynamic part of the control law to shape the motion of $\theta(t)$. However, postponing this issue for now, the closed-loop

system at this point is

$$\begin{aligned}
\dot{\sigma} &= \eta - \eta_d(\theta) \\
\dot{\eta} &= R(\psi)\left(\nu - R(\psi)^\top v_d(\theta,t)\right) + v_d(\theta,t) \\
\dot{\nu} &= -M^{-1}K_I R(\psi)^\top \sigma - M^{-1}K_P R(\psi)^\top(\eta - \eta_d(\theta)) \\
&\quad -M^{-1}(K_D + D_L)\left(\nu - R(\psi)^\top v_d(\theta,t)\right) \\
&\quad +rS^\top R(\psi)^\top v_d(\theta,t) + R(\psi)^\top a_d(\theta,t) + M^{-1}R(\psi)^\top b.
\end{aligned} \tag{5.55}$$

Define $x := \mathrm{col}(\sigma,\eta,\nu)$, $K_{PID} := \mathrm{row}\,(K_I,K_P,K_D)$, and the state-dependent transformation matrix

$$T(\psi) := \mathrm{diag}\,\{R(\psi),R(\psi),I\}\,. \tag{5.56}$$

The PID feedback control term then takes the simplified form

$$f_{PID} = -K_{PID}T(\psi)^\top(x - \xi(\psi,\theta,t))\,. \tag{5.57}$$

For $b = 0$ the closed-loop can now be written

$$\dot{x} = \mathcal{A}_c(\psi)(x - \xi(\psi,\theta,t)) + \xi^\psi(\psi,\theta,t)r + \xi^\theta(\psi,\theta,t)\upsilon_s(\theta,t) + \xi^t(\psi,\theta,t) \tag{5.58}$$

where

$$\mathcal{A}_c(\psi) = \begin{bmatrix} 0 & I & 0 \\ 0 & 0 & R(\psi) \\ -M^{-1}K_I R(\psi)^\top & -M^{-1}K_P R(\psi)^\top & -M^{-1}(K_D + D_L) \end{bmatrix}. \tag{5.59}$$

It can be verified that $\mathcal{A}_c(\psi) = T(\psi)A_cT(\psi)^\top$ where $A_c = A - BK_{PID}$, and

$$A = \begin{bmatrix} 0 & I & 0 \\ 0 & 0 & I \\ 0 & 0 & -M^{-1}D_L \end{bmatrix}, \quad B = \begin{bmatrix} 0 \\ 0 \\ M^{-1} \end{bmatrix}. \tag{5.60}$$

By controllability of (B,A) there always exists a PID gain matrix K_{PID} such that A_c is Hurwitz. This can be found by pole placement, LQR techniques, or any other applicable linear design synthesis. It can further be shown that for each fixed $t \geq 0$,

$$\mathrm{eig}\,\{\mathcal{A}_c(\psi(t))\} = \mathrm{eig}\,\{A_c\}\,. \tag{5.61}$$

It is well-known that this does not necessarily imply stability; however, it gives a fair indication for it. For A_c Hurwitz, let $P_c = P_c^\top > 0$ satisfy $P_cA_c + A_c^\top P_c = -Q_c$, and define τ as

$$\tau(x,\theta,t) := 2\,(x - \xi(\psi,\theta,t))^\top T(\psi)P_cT(\psi)^\top \xi^\theta(\psi,\theta,t). \tag{5.62}$$

The dynamic part of the control law is then given by (5.51b) and

$$\dot{\theta} = \upsilon_s(\theta, t) - \omega_s \tag{5.63}$$

where ω_s is chosen from one of the alternatives

$$\begin{array}{ll} (i) & \omega_s = 0 \\ (ii) & \omega_s = -\mu\tau(x,\theta,t), \qquad \mu \geq 0 \\ (iii) & \left\{ \begin{array}{ll} \dot{\omega} = -\lambda\left(\omega + \mu\tau(x,\theta,t)\right), & \mu > 0, \lambda > 0 \\ \omega_s = \omega. \end{array} \right. \end{array} \tag{5.64}$$

Stability analysis

The stability analysis follows from the proof by Lindegaard (2003) which is here extended to maneuvering in order to facilitate the gradient update laws. For simplicity, let $b = 0$. Otherwise, it can be shown that if K_I is chosen as $K_I = \text{diag}\{a, a, b\}$ then the equilibrium condition for σ is $\sigma_{eq} = K_I^{-1} b$ and substituting the state σ with $\sigma - K_I^{-1} b$ gives the same, but undisturbed, closed-loop system as (5.55). Define

$$V(x,\theta,t) := \left(x - \xi(\psi,\theta,t)\right)^\top T(\psi) P_c T(\psi)^\top \left(x - \xi(\psi,\theta,t)\right) \tag{5.65}$$

which differentiated gives

$$\begin{aligned} \dot{V} &= V^x(x,\theta,t)\dot{x} + V^\theta(x,\theta,t)\dot{\theta} + V^t(x,\theta,t) \\ &= -\left(x - \xi(\psi,\theta,t)\right)^\top T(\psi) Q_c T(\psi)^\top \left(x - \xi(\psi,\theta,t)\right) \\ &\quad + 2\left(x - \xi(\psi,\theta,t)\right)^\top T(\psi) P_c r S_T^\top T(\psi)^\top \left(x - \xi(\psi,\theta,t)\right) \\ &\quad + 2\left(x - \xi(\psi,\theta,t)\right)^\top T(\psi) P_c T(\psi)^\top \xi^\theta(\psi,\theta,t) \left[\upsilon_s(\theta,t) - \dot{\theta}\right] \\ &\leq -\left(\lambda_{\min}\left(Q_c\right) - 2 r_{\max} \lambda_{\max}\left(P_c\right)\right) \left|x - \xi(\psi,\theta,t)\right|^2 \\ &\quad - V^\theta(x,\theta,t) \left[\upsilon_s(\theta,t) - \dot{\theta}\right] \end{aligned} \tag{5.66}$$

where $|r| \leq r_{\max}$, $\|S_T\| = \|T(\psi)\| = 1$, and $S_T = \text{diag}\{S, S, 0\}$ such that $\dot{T} = r T(\psi) S_T$.

Observe that $\tau(x,\theta,t) = -V^\theta(x,\theta,t)$ such that either of the choices in (5.64) will as shown before render the last term nonpositive. Negativity of the first term relies on the ability to guarantee that

$$\lambda_{\min}\left(-P_c A_c - A_c^\top P_c\right) - 2 r_{\max} \lambda_{\max}\left(P_c\right) > 0 \tag{5.67}$$

for any feasible bound $r_{\max}$ on the yaw rate. Several techniques for this was shown by Lindegaard (2003), using among others LMI tools. We will not go into those details here, but rather just assume that for each $r_{\max}$ there exist a $P_c > 0$ and $c > 0$ such that $\lambda_{\min}\left(-P_c A_c - A_c^\top P_c\right) - 2r_{\max}\lambda_{\max}\left(P_c\right) > c$. The resulting bound for (5.66) becomes

$$\dot{V} \leq -c\left|x - \xi(\psi, \theta, t)\right|^2 \tag{5.68}$$

which proves convergence $x(t) - \xi(\psi(t), \theta(t), t) \to 0$ as $t \to \infty$ and the geometric task is solved in the limit. Since $x = \xi(\psi, \theta, t) \Rightarrow \tau(x, \theta, t) = 0$ the dynamic task is also solved asymptotically.

Let $(x, \theta, t) \mapsto (z, \theta, t)$ be a global diffeomorphism where $z := T(\psi)^\top (x - \xi(\psi, \theta, t))$. For either of the two first choices in (5.64), the tracking update law *(i)*, or the gradient update law *(ii)*, it follows from (5.65) and (5.68) that the closed-loop system is forward complete and the set

$$\mathcal{M} = \{(z, \theta, t) : \ z = 0\} \tag{5.69}$$

is UGES. The same result applies if the filtered-gradient update law *(iii)* in (5.64) is used, in which case the set $\mathcal{M}$ must be extended with ω_s.

5.5.2 Closed-loop system

The closed-loop system is given by Table 5.4.

5.5.3 Experimental results

Two experiments performed in the MCLab on 2003-10–17 are reported next. The path and speed assignments are given by (5.2) and (5.3). The first experiment verifies accurate tracing of the path at various speeds on calm water. The second experiment, on the other hand, shows an example where the gradient algorithm made the ship fail its task when moving in waves. The wave parameters were: JONSWAP spectrum, significant wave height $h_s = 0.01\,\mathrm{m}$ and peak period $t_s = 0.75\,\mathrm{s}$.

In both experiments, the gradient update law was used. The controller gains were calculated from LQR techniques by minimizing the cost function

$$J = \frac{1}{2}\int_0^\infty \left[x^\top Q x + u^\top R u\right] dt \tag{5.70}$$

for the linear system

$$\dot{x} = Ax + Bu \tag{5.71}$$

Table 5.4: Closed-loop in the nonlinear-PID ship maneuvering system

Plant :
$\dot{\eta} = R(\psi)\nu$
$M\dot{\nu} = f - C(\nu)\nu - D_L\nu - D_{NL}(\nu)\nu + R(\psi)^\top b$
input: $\{f\}$ output: $\{\eta, \nu\}$
Control :
$\dot{\omega} = -\lambda\omega - \lambda\mu\tau(x, \theta, t), \quad \mu, \lambda > 0$
$\dot{\theta} = \upsilon_s(\theta) - \omega_s$
$\omega_s = \begin{cases} -\mu\tau(x, \theta, t), & \mu \geq 0, \quad \text{Tracking or Gradient} \\ \omega, & \text{Filtered-gradient} \end{cases}$
$\dot{\sigma} = \eta - \eta_d(\theta)$
$f = -K_{PID}T(\psi)^\top (x - \xi(\psi, \theta, t)) + f_{FF} + f_{FL}$
input: $\left\{\eta, \nu, \eta_d(\theta), \eta_d^\theta(\theta), \eta_d^{\theta^2}(\theta), \upsilon_s(\theta, t), \upsilon_s^\theta(\theta, t), \upsilon_s^t(\theta, t)\right\}$
output: $\{f, \theta\}$
Guidance :
input: $\{\theta, u_d(t), \dot{u}_d(t)\}$
output: $\left\{\eta_d(\theta), \eta_d^\theta(\theta), \eta_d^{\theta^2}(\theta), \upsilon_s(\theta, t), \upsilon_s^\theta(\theta, t), \upsilon_s^t(\theta, t)\right\}$

where A and B are given by (5.60), $Q = \text{diag}\{Q_I, Q_P, Q_D\}$, and $R = I$. This gives the PID gain matrix $K_{PID} = R^{-1}BP = BP$ where $P = P^\top > 0$ is the solution to the algebraic Riccati equation $PA + A^\top P - PBR^{-1}B^\top P + Q = 0$. Given K_{PID} this gives $A_c = A - BK_{PID}$ and the matrix P_c in the gradient update law were simply given by solving $P_cA_c + A_c^\top P_c = 0.01I$. In the experiments, the gradient gain were $\mu = 100$, and the weight matrices were chosen to $Q_I = 0.001I$, $Q_P = \text{diag}\{2000, 3000, 400\}$, and $Q_D = \text{diag}\{1000, 3000, 800\}$.

Figures 5.10 and 5.11 show the responses of the ship in the successful experiment. Very accurate tracing was obtained as confirmed with the cross-track error z_5 in Table 5.5.

In the second experiment, shown in Figure 5.12, the ship experienced significant problems when moving around the narrowest part of the path with waves entering from the right. This is an example where the gradient algorithm made the ship fail its task of accurate path tracing.

A snapshot at time $t = 445.15$ s of the Lyapunov cost function $V(x(t), \theta, t)$ and $V^\theta(x(t), \theta, t)$ for θ in the interval $[0\,^\circ, 360\,^\circ)$ is shown in Figure 5.13. This is the moment when the ship leaves the path for the second time. As

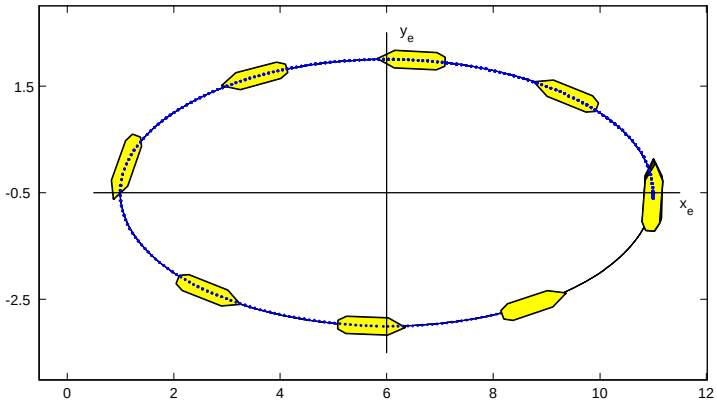

Figure 5.10: CyberShip II moving along the path, using the nonlinear PID controller.

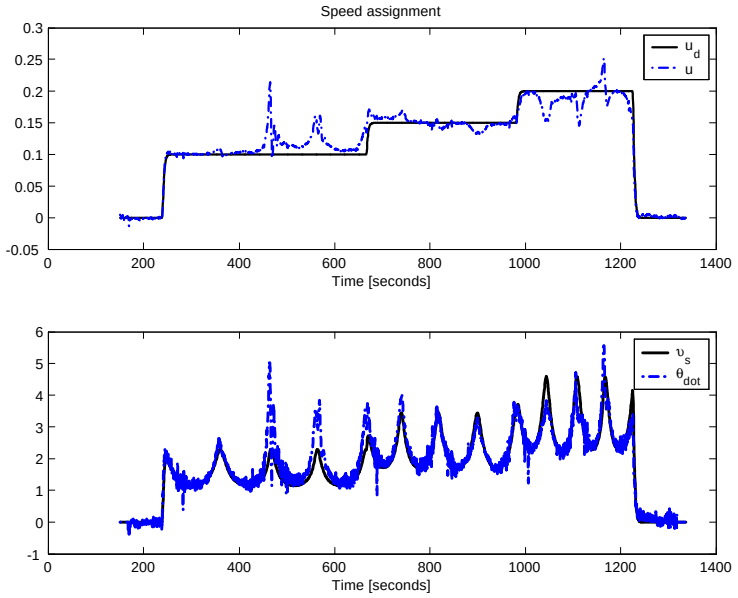

Figure 5.11: The surge speed response of CyberShip II in the nonlinear PID experiment.

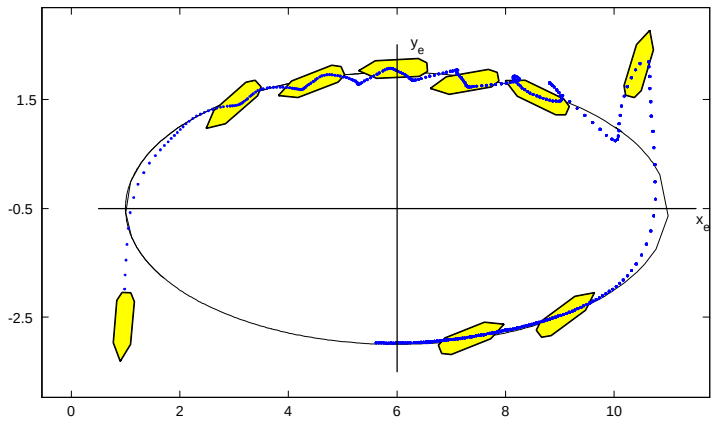

Figure 5.12: CyberShip II moving along the path. Along the narrowest part, perturbations make the desired point $\eta_d(\theta(t))$ jump and cause instability.

seen, a local minimum exist very close to the global minimum to which $\theta(t)$ rapidly converges at this point in time. The following sequence of events was observed in this event of failure:

1. As the ship enters the narrow part, it cannot hold the desired heading due to the waves, with the result that $V(x(t), \theta(t), t)$ increases.

2. The 'previous' global minimum of $\theta \mapsto V(x(t), \theta, t)$ is suddenly converted into a local minimum as a 'new' global minimum arises approximately $50\,^\circ - 100\,^\circ$ further ahead on the path.

3. $\theta(t)$ slowly moves over the intermediate local maximum and then suddenly jumps approximately $50\,^\circ$ towards the new global minimum.

4. The ship experiences large oscillations in its attempt to regain the 'new' desired state $\xi(\psi, \theta, t)$.

For comparison, Figure 5.14 shows the status of $V(x(t), \theta(t), t)$ and $V^\theta(x(t), \theta(t), t)$ for the ship at the same point along the path in the first successful experiment (without waves). As seen, there is only one global minimum for $\theta(t)$ to track in this case; however, the "saddle" shape of $\theta \mapsto V^\theta(x(t), \theta, t)$ suggests a bifurcation of $V(x, \cdot, t)$, splitting the single global minimum into two local minima.

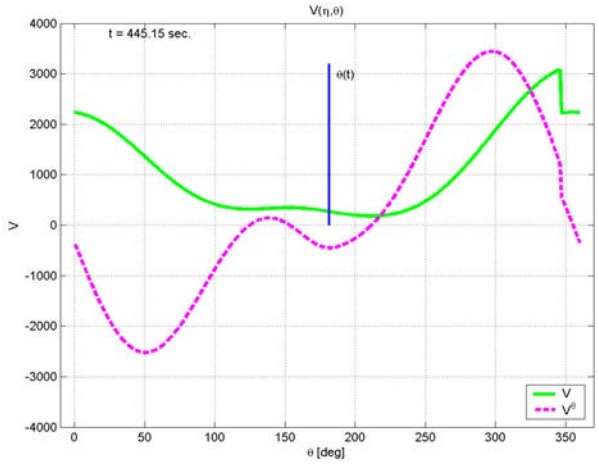

Figure 5.13: A snapshot of $\theta(t)$ showing the minimization of the Lyapunov cost function $V(z(\eta(t), \theta(t)))$ and the gradient $V^{\theta}(z(\eta(t), \theta(t)))$ at $t = 445.15\,\mathrm{s}$ in the experiment with failure. This was just after a second rapid movement occurred for θ. Notice a new global minimum of $V(z(\eta, \cdot))$ has formed, causing a rapid movement of θ of $50\,^{\circ} - 100\,^{\circ}$.

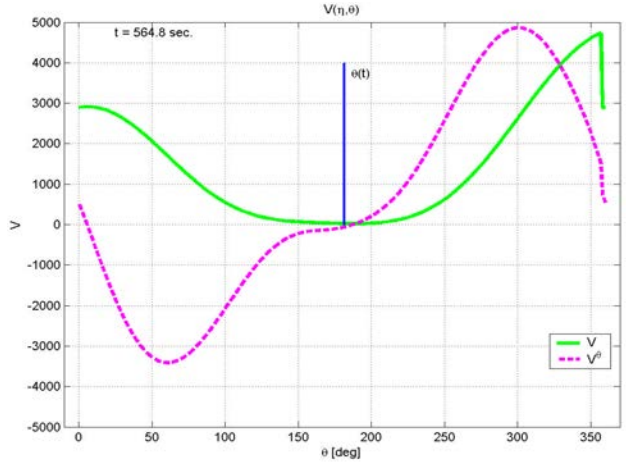

Figure 5.14: A snapshot of $\theta \mapsto V(x(t), \theta, t)$ and $\theta \mapsto V^{\theta}(x(t), \theta, t)$ for the successful nonlinear-PID experiment with a gradient update law. There is in this case one and only one global minimum of $V(x(t), \cdot, t)$ throughout the movement around the "narrowest corner" of the path.

In order to alleviate these dangerous jumps, one should instead consider using the tracking update law. Experiments with the tracking update law gave successful runs with very accurate tracing of the path, both with and without waves, and this is reported in the performance analysis in the next section.

5.6 Brief comparison of control laws

5.6.1 Performance

Table 5.5 shows different standard deviations of important error signals in the three intervals during which the desired speed was $u_d \in \{0.10,\ 0.15,\ 0.20\}$ m/ s. All these experiments were conducted on calm water. The data is collected from the following experiments:

- Adaptive CS2 experiment 1 conducted 2004-10-11, described in Section 5.3.3.
- Sliding-mode experiment conducted 2004-10-06, described as the first experiment in Section 5.4.3, using a tracking update law.
- Nonlinear-PID experiment, conducted 2004-10-17, with gains and setup corresponding to the successful experiment described in Section 5.5.3, but with a tracking update law.

The most important variables for path keeping are z_{12}, z_2, and z_5, respectively, since these correspond to an approximate measure of the cross-track error (provided the ship is pointed along the path). An accuracy of, for instance, 1.1 cm in the highest speed in the nonlinear-PID case corresponds to an accuracy of 0.8 m for the full scale ship having a breadth of 20.3 m and is acceptable.

Investigating the table, it is seen that the best path following accuracy was obtained by the nonlinear-PID controller. In the 0.15 and 0.20 m/s cases this was, in addition, obtained for the lowest amount of control effort. In the 0.10 m/s case, the adaptive controller also behaved very well. However, except for the poor heading response of the sliding-mode controller, the differences were small and mostly acceptable in all cases.

The numbers in the table are not meant for a strict comparison between the three controllers, but rather to give an indication of the achieved performance in the experiments. The controller parameters were mostly tuned by

Table 5.5: Standard deviations for CS2 in the maneuvering experiments.

Adaptive:	$u_d = 0.10\,\mathrm{m/s}$	$u_d = 0.15\,\mathrm{m/s}$	$u_d = 0.20\,\mathrm{m/s}$
z_{11} [m]	0.010	0.038	0.057
z_{12} [m]	0.007	0.017	0.024
z_{13} [deg]	1.564	2.644	3.061
u [m/s]	0.004	0.014	0.020
Mean abs thrust [%]	14.144	20.249	26.727
St.d. abs thrust [%]	6.072	7.766	8.043

Sliding-mode:	$u_d = 0.10\,\mathrm{m/s}$	$u_d = 0.15\,\mathrm{m/s}$	$u_d = 0.20\,\mathrm{m/s}$
z_1 [m]	0.007	0.015	0.017
z_2 [m]	0.010	0.028	0.026
z_3 [deg]	2.929	6.785	6.883
u [m/s]	0.002	0.004	0.006
Mean abs thrust [%]	15.204	23.826	26.230
St.d. abs thrust [%]	6.787	9.179	9.760

Nonlinear PID:	$u_d = 0.10\,\mathrm{m/s}$	$u_d = 0.15\,\mathrm{m/s}$	$u_d = 0.20\,\mathrm{m/s}$
z_4 [m]	0.004	0.008	0.012
z_5 [m]	0.004	0.007	0.011
z_6 [deg]	1.577	2.032	2.979
u [m/s]	0.002	0.003	0.004
Mean abs thrust [%]	16.754	19.865	23.606
St.d. abs thrust [%]	8.140	8.778	9.327

trial-and-error, which means that the bandwidths of the closed-loop systems were probably somewhat different.

For instance, in many experiments it was observed that the sliding-mode controller had a larger mean thrust, and seemed to command thrust more aggressively. The data used here, on the other hand, gave similar thrust expenditure among all three controllers.

5.6.2 Gradient cost functions

Finally, we want to compare the different gradient update laws for the three controllers. The Lyapunov cost functions used in each case were

ADAP: $V_2(\eta,\nu,\theta,\tilde{\varphi},t) := \frac{1}{2}\left(\eta-\eta_d(\theta)\right)^\top\left(\eta-\eta_d(\theta)\right)+\frac{1}{2}\tilde{\varphi}^\top\Gamma^{-1}\tilde{\varphi}$
$+\frac{1}{2}\left(\nu-\alpha_1(\eta,\theta,t)\right)^\top M\left(\nu-\alpha_1(\eta,\theta,t)\right)$

SM: $V(\eta,\theta) := \frac{1}{2}\left(\eta-\eta_d(\theta)\right)^\top\left(\eta-\eta_d(\theta)\right)$

NL-PID: $V(x,\theta,t) := \left(x-\xi(\psi,\theta,t)\right)^\top T(\psi)P_cT(\psi)^\top\left(x-\xi(\psi,\theta,t)\right)$

Of these, the sliding-mode (SM) gradient cost function is the most straightforward, since only the distance to the path $\theta \mapsto |\eta-\eta_d(\theta)|^2$ is minimized directly. For most paths, this cost function will give a "well-defined" global minimum that $\theta(t)$ tracks. Figure 5.9 shows that for the ellipsoidal path, a local minimum is only present on the opposite side of the path.

The adaptive (ADAP) gradient cost function, on the other hand, also includes minimization with respect to the velocity error, that is, $\theta \mapsto |\nu-\alpha_1(\eta,\theta,t)|^2_M$. This introduces more complexity for analyzing the minima structure of $\theta \mapsto V_2(\eta,\nu,\theta,\tilde{\varphi},t)$. An alternative to avoid minimization with respect to the velocity error is to design the gradient update law for $\dot{\theta}$ already in Step 1 in the adaptive backstepping design. The only difference in the design of the control law is that terms with $\dot{\theta}$ would need to be cancelled in Step 2. The resulting cost function will in that case be the same as the SM cost function. Nonetheless, experience indicates no problems with local minima in the adaptive gradient cost function.

The nonlinear-PID (NL-PID) gradient cost function has perhaps the most complext minima structure. This includes minimization with respect to the full error state $\theta \mapsto |x-\xi(\psi,\theta,t)|^2$ where the individual errors σ, $\eta-\eta_d(\theta)$, and $\nu-R(\psi)^\top v_d(\theta,t)$ are mixed through the matrix P_c together with the heading-dependent matrices $T(\psi)$. Not only does this mean that the integral state σ unwantedly affects the minimization, but the cost function itself will be sensitive to heading changes of the ship. In the "failure" experiment described in Section 5.5.3 this resulted in the "out-of-the-blue" creation of two local minima when waves made the ship position and heading slightly deviate.

This problem for the NL-PID control law is illuminated further by Figure 5.15, which shows what happens to the cost function as we vary the heading ψ, only. The left plot shows $\theta \mapsto V(x(t),\theta,t)$ and $\theta \mapsto V^\theta(x(t),\theta,t)$ given the state $x(t)$ at the time instant just prior to the second jump by θ in the experiment. Originally there is, as seen in the left plot, only one global minimum in the system. By changing the ship's heading, however, the middle and right plots show how a saddle point is first formed, and subsequently

a local minimum and a maximum. This bifurcation is given by the roots of $\theta \mapsto V^{\theta}(x(t), \theta, t)$ that for the three different values of ψ changes from a single root to two roots, and finally to the three indicated roots.

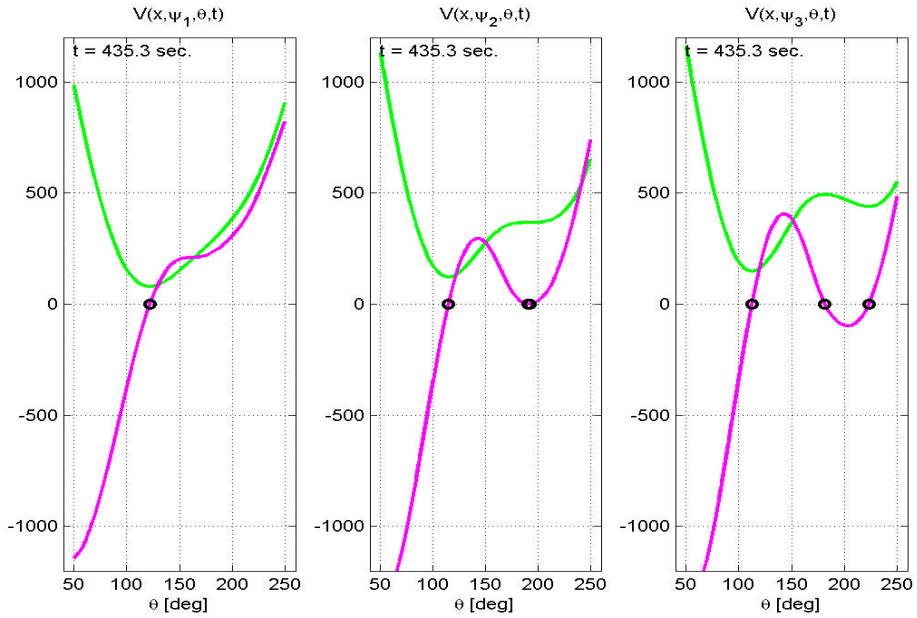

Figure 5.15: Three plots showing the bifurcation in the Lyapunov cost function for the nonlinear-PID experiment with failure. By changing the ship's heading ψ as a parameter (in x) in $\theta \mapsto V(x, \theta, t)$ and keeping the other states constant, a single global minimum is split into two local minima separated by a maximum.

Chapter 6

Formation control

This chapter investigates formation control for the coordination of mechanical systems like vehicles or ships, called throughout this chapter for "vessels". The control objective for each vessel is to converge to and maintain its position in the formation, while the formation as a whole follows a prespecified path with a desired speed. The material has been published in Skjetne, Moi and Fossen (2002); Skjetne, Ihle and Fossen (2003); Ihle, Skjetne and Fossen (2004). All case studies, including the experimental results in the latter publication, consider a rendesvouz operation between ships; see Figure 6.1.

Figure 6.1: Underway replenishment between three naval vessels.

6.1 Introduction

6.1.1 Background

The field of formation control with applications towards mechanical systems, ships, aircraft, satellites, etc., has received a lot of attention. Examples are the works of Kang, Xi and Sparks (2000); Encarnação and Pascoal (2001a); Binetti, Ariyur, Krstić and Bernelli (2003). One of the advantages in formation flight, for instance, is a reduction in power demand obtained when flying in a certain V-formation, as observed for flying goose. Binetti et al. (2003) used extremum seeking to exploit this aerodynamic phenomenon. In another study, Kang et al. (2000) developed a procedure for the design of $r+1$ controllers which ensures that $r+1$ autonomous vehicles follow a path without altering their formation. An orthogonal projection from the state of a chosen leader substitutes the time in the r already existing *tracking* controllers for the follower vehicles. Therefore, the speed and performance of the leader affects all other members in the formation, but not vice versa.

In the first design section of this chapter, published in Skjetne, Moi and Fossen (2002), the control objective is approached using vectorial backstepping to solve the geometric and dynamic tasks in a maneuvering problem. The former guarantees that a virtual *Formation Reference Point* (FRP), representing the formation, tracks the path. The latter ensures accurate speed control along the path. The dynamic gradient update law, taking feedback from the states of all vessels, ensures that all vessels have the same priority (no leader) when moving along the path.

The question of *centralized* or *decentralized* control and communication requirements have been extensively discussed in many publications on formation control; see Stilwell and Bishop (2000) and references therein. Centralized control will in general require a massive multidirectional communication flow of state measurements, internal and external sensory information, and necessary guidance signals. Such requirements are not feasible for numerous applications, for instance, control of a formation of autonomous underwater vehicles which operate in a difficult environment with very restrictive communication options (Schoenwald; 2000, Table 1). In decentralized control, each formation member will have its own controller under the management of a formation guidance system. This can significantly reduce the number of signals being communicated; however, depending on how the formation guidance system is designed, it may still require an undesirable large amount of signal flow.

In the second design section of this chapter, published in Skjetne et al.

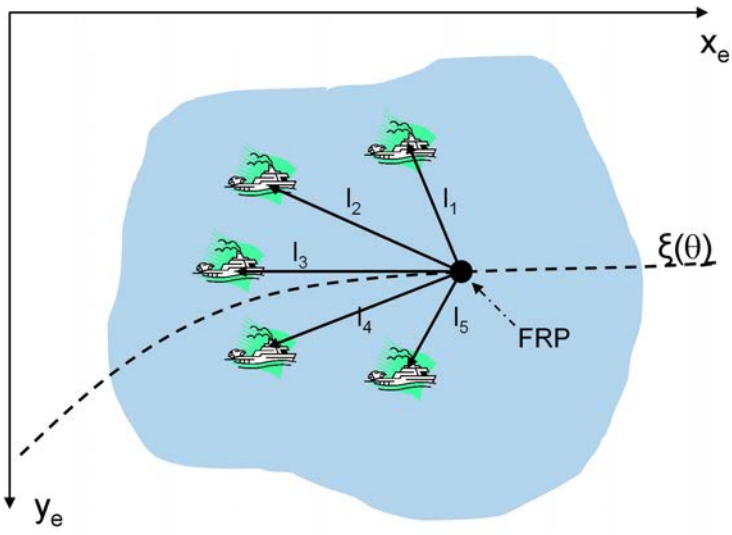

Figure 6.2: Illustration of a formation setup.

(2003) and Ihle et al. (2004), the amount of intervessel communication is reduced by *decentralizing* the dynamic gradient update law with the result that only the individual path variables need to be communicated. The individual dynamic controllers will then be equipped with a synchronization term that ensures that the vessels keep assembled (synchronized) in the desired formation.

Though the examples studied are all 3 DOF ship applications, the theory is general and is, for instance, directly applicable to 6 DOF applications like the AUVs described in Section 2.4.3.

6.1.2 Formation setup

A formation with r vessels is created by a set of formation designation vectors l_i, $i = 1, ..., r$, relative to a Formation Reference Point (FRP), see Figure 6.2. The idea is for the FRP to follow a given parametrized path $\xi(\theta)$ with a desired formation speed along it, while the vessels follow their designated position relative to the FRP.

Let the FRP be the origin of a moving *formation reference frame* $\mathcal{F}$, and denote the earth fixed frame $\mathcal{E}$. The path is in general not a straight line, but a feasible curve in the output space of the vessels. The individual path

for Vessel i is then

$$\xi_i(\theta) = \xi(\theta) + R(\theta)_f^e l_i \tag{6.1}$$

where $R(\theta)_f^e$ is a kinematic rotation matrix from $\mathcal{F}$ to $\mathcal{E}$; see Section 1.4.3.

For ships moving on the ocean surface, the output is the 3 DOF vector $\eta = \text{col}(x, y, \psi)$, where (x, y) is the position and ψ is the heading. The desired path is then given by $\xi(\theta) = \text{col}(x_d(\theta), y_d(\theta), \psi_d(\theta))$. The tangent vector along the path in the (x, y) directions, $T(\theta) = \text{col}(x_d^\theta(\theta), y_d^\theta(\theta))$, is chosen as the x-axis of the moving formation frame $\mathcal{F}$. The angle of the tangent vector in the $\mathcal{E}$ frame then gives the desired heading

$$\psi_d(\theta) = \arctan\left(\frac{T_y(\theta)}{T_x(\theta)}\right) = \arctan\left(\frac{y_d^\theta(\theta)}{x_d^\theta(\theta)}\right) \tag{6.2}$$

where the Matlab atan2 function is used for implementation of arctan to obtain correct quadrant mapping. The rotation matrix $R(\psi_d(\theta))$ for the ships is given by

$$R(\theta)_f^e = R(\psi_d(\theta)) := \begin{bmatrix} \cos\psi_d(\theta) & -\sin\psi_d(\theta) & 0 \\ \sin\psi_d(\theta) & \cos\psi_d(\theta) & 0 \\ 0 & 0 & 1 \end{bmatrix} \tag{6.3}$$

and note that differentiation gives

$$\dot{R}(\psi_d(\theta)) = R^\theta(\psi_d(\theta))\dot{\theta} = R(\psi_d(\theta))S\psi_d^\theta(\theta)\dot{\theta} \tag{6.4}$$

where S is the skew-symmetric matrix

$$S = \begin{bmatrix} 0 & -1 & 0 \\ 1 & 0 & 0 \\ 0 & 0 & 0 \end{bmatrix} \tag{6.5}$$

and

$$\psi_d^\theta(\theta) = \frac{x_d^\theta(\theta)y_d^{\theta^2}(\theta) - x_d^{\theta^2}(\theta)y_d^\theta(\theta)}{x_d^\theta(\theta)^2 + y_d^\theta(\theta)^2}. \tag{6.6}$$

6.1.3 Problem statement

We consider uncertain mechanical systems, called *vessels* hereafter, of vector relative degree two. Their models are given by

$$\begin{aligned} \dot{x}_{1i} &= G_{1i}(x_{1i})x_{2i} + f_{1i}(x_{1i}) + E_{1i}(x_{1i})\delta_{1i}(t) \\ \dot{x}_{2i} &= G_{2i}(x_i)u_i + f_{2i}(x_i) + E_{2i}(x_i)\delta_{2i}(t) \\ y_i &= h_i(x_{1i}) \end{aligned} \tag{6.7}$$

where the subscript i denotes the i'th vessel. $x_{ji} \in \mathbb{R}^m$, $j = 1, 2$, are the states and x_i denotes the vector $x_i := \text{col}(x_{1i}, x_{2i})$. The system outputs are $y_i \in \mathbb{R}^m$, the controls are $u_i \in \mathbb{R}^m$, and δ_{ji} are unknown bounded disturbances. The matrices G_{ji} and $h_i^{x_{1i}} := \frac{\partial h_i}{\partial x_{1i}}$ are invertible for all x_i, the output maps $h_i(x_{1i})$ are diffeomorphisms, and all functions are smooth.

For a cluster of r vessels, each represented by a position output y_i, let the FRP represent the position of the formation as a whole, and let each individual vessel y_i have a designation l_i relative to the FRP. Let $\xi(\theta)$ be the desired path for the FRP and then $\xi_i(\theta) = \xi(\theta) + R(\theta)l_i$ is the corresponding path for the individual vessels. The *Formation manuvering problem* is then to design a set of robust control laws for the individual vessels that ensure boundedness of all states and solve the tasks:

1. **Geometric Task**: For any continuous function $\theta(t)$, force the outputs y_i, $i = 1, \ldots, r$, to converge to their designated paths $\xi_i(\theta)$,

$$\lim_{t\to\infty} |y_i(t) - \xi_i(\theta(t))| = 0 \tag{6.8}$$

2. **Dynamic Task:** Force the path speed $\dot{\theta}$ to converge to a desired speed $\upsilon_s(\theta, t)$,

$$\lim_{t\to\infty} \left|\dot{\theta}(t) - \upsilon_s(\theta(t), t)\right| = 0. \tag{6.9}$$

The geometric task ensures that the individual vessels converge to and stay at their designated positions l_i in the formation. The speed assignment task ensures that the FRP will move along the path $\xi(\theta)$ with a desired velocity $\upsilon_s(\theta, t)$. Both tasks are feasible since the considered vessels are fully actuated.

6.2 Design using a centralized guidance law

In this section a common path variable θ represents the position of the FRP, and thus the desired position of all vehicles. Consequently, this is a direct application of the robust maneuvering design in Section 4.1, and a recursive backstepping design is therefore used to solve the formation maneuvering problem for r vessels with the dynamics given by (6.7).

6.2.1 Control Design

Step 1: Define the error variables

$$z_{1i}(x_{1i},\theta) := y_i - \xi_i(\theta) = h_i(x_{1i}) - \xi(\theta) - R(\psi_d(\theta))l_i \tag{6.10}$$
$$z_{2i}(x_i,\theta,t) := x_{2i} - \alpha_{1i}(x_{1i},\theta,t) \tag{6.11}$$
$$\omega_s(\dot{\theta},\theta,t) := \upsilon_s(\theta,t) - \dot{\theta} \tag{6.12}$$

where α_{1i} are virtual controls to be specified later. Differentiating (6.10) with respect to time results in

$$\dot{z}_{1i} = h_i^{x_{1i}} G_{1i} z_{2,i} + h_i^{x_{1i}} G_{1i}\alpha_{1i} + h_i^{x_{1i}} f_{1i} + h_i^{x_{1i}} E_{1i}\delta_{1i} - \left(\xi^\theta + \psi_d^\theta R(\psi_d) S l_i\right)\dot{\theta}. \tag{6.13}$$

Choose Hurwitz design matrices A_{1i}, so that $P_{1i} = P_{1i}^\top > 0$ are the solutions to $P_{1i}A_{1i} + A_{1i}^\top P_{1i} = -Q_{1i}$ where $Q_{1i} = Q_{1i} > 0$. Define

$$V_1(z_{1i}) := \sum_{i=1}^{r} z_{1i}^\top P_{1i} z_{1i} \tag{6.14}$$

whose time derivative then becomes

$$\dot{V}_1 = \sum_{i=1}^{r} 2z_{1i}^\top P_{1i} h_i^{x_{1i}} G_{1i} z_{2i} + \sum_{i=1}^{r} 2z_{1i}^\top P_{1i}\left(\xi^\theta + \psi_d^\theta R(\psi_d) S l_i\right)\omega_s$$
$$+ \sum_{i=1}^{r} 2z_{1i}^\top P_{1i}\left[h_i^{x_{1i}} G_{1i}\alpha_{1i} + h_i^{x_{1i}} f_{1i} - \left(\xi^\theta + \psi_d^\theta R(\psi_d) S l_i\right)\upsilon_s + h_i^{x_{1i}} E_{1i}\delta_{1i}\right].$$

The first virtual controls $\alpha_{1i}(x_{1i},\theta,t)$ are chosen as

$$\alpha_{1i} = G_{1i}^{-1}\left(h_i^{x_{1i}}\right)^{-1}\left[A_{1i}z_{1i} - h_i^{x_{1i}} f_{1i} + \left(\xi^\theta + \psi_d^\theta R(\psi_d) S l_i\right)\upsilon_s + \alpha_{0i}\right] \tag{6.15}$$

where α_{0i} are damping terms to be picked. Define the first tuning functions, $\tau_{1i}(x_{1i},\theta) \in \mathbb{R}$, as

$$\tau_{1i} := 2z_{1i}^\top P_{1i}\left(\xi^\theta + \psi_d^\theta R(\psi_d) S l_i\right). \tag{6.16}$$

To handle the perturbations we use nonlinear damping and apply Young's inequality

$$\begin{aligned}\dot{V}_1 &= -\sum_{i=1}^{r} z_{1i}^\top Q_{1i} z_{1i} + \sum_{i=1}^{r} \tau_{1i}\omega_s + \sum_{i=1}^{r} 2 z_{1i}^\top P_{1i} h_i^{x_{1i}} G_{1i} z_{2i} \\ &\quad + \sum_{i=1}^{r} 2 z_{1i}^\top P_{1i} h_i^{x_{1i}} E_{1i}\delta_{1i} + \sum_{i=1}^{r} 2 z_{1i}^\top P_{1i}\alpha_{0i} \\ &\leq -\sum_{i=1}^{r} z_{1i}^\top Q_{1i} z_{1i} + \sum_{i=1}^{r} \tau_{1i}\omega_s + \sum_{i=1}^{r} 2 z_{1i}^\top P_{1i} h_i^{x_{1i}} G_{1i} z_{2i} \\ &\quad + \sum_{i=1}^{r} 2 z_{1i}^\top P_{1i} \left[\alpha_{0i} + \frac{1}{2}\kappa_{1i} \left(h_i^{x_{1i}}\right) E_{1i} E_{1i}^\top \left(h_i^{x_{1i}}\right)^\top P_{1i} z_{1i}\right] + \sum_{i=1}^{r} \frac{1}{\kappa_{1i}} \delta_{1i}^\top \delta_{1i}\end{aligned}$$

and the nonlinear damping terms $\alpha_{0i}(x_{1i}, \theta)$ are picked as

$$\begin{aligned}&\alpha_{0i} = \rho_{1i}(x_{1i}) z_{1i}(x_{1i}, \theta) \\ &\rho_{1i} = -\tfrac{1}{2}\kappa_{1i} \left(h_i^{x_{1i}}\right) E_{1i} E_{1i}^\top \left(h_i^{x_{1i}}\right)^\top P_{1i}, \qquad \kappa_{1i} > 0\end{aligned} \tag{6.17}$$

which gives

$$\dot{V}_1 \leq -\sum_{i=1}^{r} z_{1i}^\top Q_{1i} z_{1i} + \sum_{i=1}^{r} \tau_{1i}\omega_s + \sum_{i=1}^{r} 2 z_{1i}^\top P_{1i} h_i^{x_{1i}} G_{1i} z_{2i} + \sum_{i=1}^{r} \frac{1}{\kappa_{1i}} \delta_{1i}^\top \delta_{1i}. \tag{6.18}$$

In aid of the next step, we differentiate α_{1i} to get

$$\dot{\alpha}_{1i} = \sigma_{1i} + \alpha_{1i}^\theta \dot{\theta} + \varpi_{1i}\delta_{1i} \tag{6.19}$$

where

$$\sigma_{1i} := \alpha_{1i}^{x_{1i}} \left[G_{1i} x_{2i} + f_{1i}\right] + \alpha_{1i}^t \tag{6.20}$$

$$\varpi_{1i} := \alpha_{1i}^{x_{1i}} E_{1i}. \tag{6.21}$$

Step 2: Differentiating (6.11) with respect to time gives

$$\dot{z}_{2i} = G_{2i} u_i + f_{2i} + E_{2i}\delta_{2i} - \sigma_{1i} - \alpha_{1i}^\theta \dot{\theta} - \varpi_{1i}\delta_{1i}. \tag{6.22}$$

Choose Hurwitz design matrices A_{2i} so that $P_{2i} = P_{2i}^\top > 0$ are the solutions to $P_{2i}A_{2i} + A_{2i}^\top P_{2i} = -Q_{2i} < 0$, and define

$$V_2(z_{1i}, z_{2i}) := V_1(z_{1i}) + \sum_{i=1}^{r} z_{2i}^\top P_{2i} z_{2i} \tag{6.23}$$

whose time derivative becomes

$$\begin{aligned}\dot{V}_2 \leq & -\sum_{i=1}^{r} z_{1i}^{\top} Q_{1i} z_{1i} + \sum_{i=1}^{r} \tau_{1i}\omega_s + \sum_{i=1}^{r} 2z_{2i}^{\top} P_{2i}\alpha_{1i}^{\theta}\omega_s \\ & + \sum_{i=1}^{r} \frac{1}{\kappa_{1i}}\delta_{1i}^{\top}\delta_{1i} + \sum_{i=1}^{r} 2z_{2i}^{\top} G_{1i}^{\top} \left(h_i^{x_{1i}}\right)^{\top} P_{1i} z_{1i} \\ & + \sum_{i=1}^{r} 2z_{2i}^{\top} P_{2i}\left[G_{2i}u_i + f_{2i} + E_{2i}\delta_{2i} - \sigma_{1i} - \alpha_{1i}^{\theta}\upsilon_s - \varpi_{1i}\delta_{1i}\right]. \end{aligned} \tag{6.24}$$

The control laws are then chosen as

$$\begin{aligned} u_i &= \alpha_{2i}(x_i, \theta, t) \\ &= G_{2i}^{-1}[-P_{2i}^{-1} G_{1i}^{\top} \left(h_i^{x_{1i}}\right)^{\top} P_{1i} z_{1i} + A_{2i} z_{2i} - f_{2i} + \sigma_{1i} + \alpha_{1i}^{\theta}\upsilon_s + u_{0i}] \end{aligned} \tag{6.25}$$

where u_{0i} are nonlinear damping terms to be designed. Define $z_i := \mathrm{col}(z_{1i}, z_{2i})$, $Q_i := \mathrm{diag}\,(Q_{1i},\ Q_{2i})$, and the final tuning functions $\tau_{2i}(x_i, \theta, t) \in \mathbb{R}$ as

$$\tau_{2i} := \tau_{1i} + 2z_{2i}^{\top} P_{2i}\alpha_{1i}^{\theta}. \tag{6.26}$$

Using Young's inequality again, the derivative $\dot{V}_2$ is bounded by

$$\begin{aligned}\dot{V}_2 \leq & -\sum_{i=1}^{r} z_i^{\top} Q_i z_i + \sum_{i=1}^{r} 2z_{2i}^{\top} P_{2i}\left\{u_{0i} + \frac{1}{2}\kappa_{2i}\left[E_{2i}E_{2i}^{\top} + \varpi_{1i}\varpi_{1i}^{\top}\right] P_{2i} z_{2i}\right\} \\ & + \sum_{i=1}^{r} \tau_{2i}\omega_s + \sum_{i=1}^{r} \frac{1}{\kappa_{1i}}\delta_{1i}^{\top}\delta_{1i} + \sum_{i=1}^{r} \frac{1}{\kappa_{2i}}\left[\delta_{2i}^{\top}\delta_{2i} + \delta_{1i}^{\top}\delta_{1i}\right] \end{aligned}$$

and the final nonlinear damping terms $u_{0i}(x_i, \theta, t)$ are assigned as

$$u_{0i} = \rho_{2i}(x_i, \theta, t) z_{2i} \tag{6.27}$$

$$\rho_{2i} = -\frac{1}{2}\kappa_{2i}\left[E_{2i}E_{2i}^{\top} + \varpi_{1i}\varpi_{1i}^{\top}\right] P_{2i}, \qquad \kappa_{2i} > 0. \tag{6.28}$$

Define $\Delta_i := \mathrm{col}\,(\delta_{1i},\ \delta_{2i})$ and $K_i := \mathrm{diag}\left(\frac{1}{\kappa_{1i}} + \frac{1}{\kappa_{2i}},\ \frac{1}{\kappa_{2i}}\right)$. The result is then

$$\dot{V}_2 \leq -\sum_{i=1}^{r} z_i^{\top} Q_i z_i + \omega_s \sum_{i=1}^{r} \tau_{2i} + \sum_{i=1}^{r} \Delta_i^{\top} K_i \Delta_i. \tag{6.29}$$

It follows for $\omega_s = 0$ that each system in the z_i-coordinates is an ISS system from the disturbances Δ_i to z_i.

Next, we must deal with the tuning functions τ_{2i}. Choosing $\omega_s = 0$ to solve the dynamic task is equivalent to a tracking design with $\dot{\theta} = \upsilon_s(\theta, t)$. Another choice is to design an update law for $\dot{\theta}$ or $\dot{\omega}_s$ that uses feedback from the states of the vessels. It can be verified for $x := \mathrm{col}(x_1, \ldots, x_r)$ that

$$\tau(x, \theta, t) := \sum_{i=1}^{r} \tau_{2i}(x_i, \theta, t) = -V_2^{\theta}(x, \theta, t), \tag{6.30}$$

that is, the total tuning function is the *gradient* of V_2 with respect to θ. We therefore consider the *Gradient update law* and the *Filtered-gradient update law* next.

Gradient update law: Letting

$$\omega_s = -\mu \sum_{i=1}^{r} \tau_{2i}(x_i, \theta, t) = \mu V_2^{\theta}(x, \theta, t), \qquad \mu \geq 0, \tag{6.31}$$

renders (6.29), for $\Delta_i = 0$, negative definite, and by choosing the gains K_i large enough we can guarantee any residual bound for $|z_i(t)|$. Defining $z := \mathrm{col}(z_1, \ldots, z_r)$, it follows from Theorem 4.1 that the closed-loop system is ISS with respect to the 0-invariant set

$$\mathcal{M} = \left\{ (z, \theta, t) \in \mathbb{R}^{2mr} \times \mathbb{R} \times \mathbb{R}_{\geq 0} : \ z = 0 \right\}. \tag{6.32}$$

This means that each individual vessel enters its designation within the residual bound for $|z_{1i}(t)|$.

The realization of the update law becomes

$$\dot{\theta} = \upsilon_s(\theta, t) + \mu \sum_{i=1}^{r} \tau_{2i}(x_i, \theta, t) = \upsilon_s(\theta, t) - \mu \frac{\partial V_2}{\partial \theta}(x, \theta, t) \tag{6.33}$$

and since the states $z_i(t)$ are made small, the tuning functions $\tau_{2i}(t)$ are made small. Hence, as $t \to \infty$, $\dot{\theta}(t) \approx \upsilon_s(\theta(t), t)$ which satisfies the speed assignment. It follows by the analysis in Section 3.4 that choosing μ large induces a separation of time scales between the vessel dynamics and $\dot{\theta}$. In the fast time scale, (6.33) becomes a dynamic gradient optimization algorithm that selects the point along the path for the FRP which minimizes $\theta \mapsto V_2(z_{1i}(x_{1i}, \theta), z_{2i}(x_i, \theta, t))$.

Filtered-gradient update law: The update law can alternatively be constructed as

$$\begin{aligned} \dot{\theta} &= \upsilon_s(\theta, t) - \omega_s \\ \dot{\omega}_s &= -\lambda \omega_s - \lambda \mu \sum_{i=1}^{r} \tau_{2i}, \qquad \mu, \lambda > 0 \end{aligned} \tag{6.34}$$

by extending the Lyapunov function to $V = V_2 + \frac{1}{2\lambda\mu}\omega_s^2$, which gives

$$\dot{V} \leq -\sum_{i=1}^{r} z_i^\top Q_i z_i - \frac{1}{\mu}\omega_s^2 + \sum_{i=1}^{r} \Delta_i^\top K_i \Delta_i. \tag{6.35}$$

It follows by Theorem 4.2 that the closed-loop system is ISS with respect to the 0-invariant set

$$\mathcal{M}' = \left\{(z, \omega_s, \theta, t) \in \mathbb{R}^{2mr} \times \mathbb{R} \times \mathbb{R} \times \mathbb{R}_{\geq 0} : \ z = 0, \ \omega_s = 0\right\}. \tag{6.36}$$

It is clear that this solves the Formation Maneuvering Problem for the same reasons as above. It has been demonstrated that (6.34) is just a filtered version of (6.33). It has the same gradient properties as discussed above if λ and μ are chosen large. Experience has shown, however, that the filtered version gives an improved numerical response for $\dot{\theta}(t)$. The caveat is higher order in the controller.

Note that even though each individual static control law $u_i = \alpha_{2i}(x_i, \theta, t)$ only takes feedback from the vessel's own states and the common path variable θ, the dynamics for $\dot{\theta}$ must be run in a computer at a central location, taking feedback from all states of the vessels. The governing equations for this centralized *guidance system* is (6.33) or (6.34) with outputs $\xi_i(\theta) = \xi(\theta) + R(\theta)^e_f l_i$ corresponding to each vessel.

6.2.2 Case Study 1: Rendezvous formation of three ships

For low-speed maneuvering of ships in formation we use, without loss of generality, a linear hydrodynamic model; see Appendix B. The model is written

$$\begin{aligned} \dot{\eta}_i &= R(\psi_i)\nu_i \\ \dot{\nu}_i &= -M_i^{-1} D_i \nu_i + M_i^{-1} f_i + R(\psi_i)^\top w, \end{aligned} \tag{6.37}$$

where the subscript i denotes the i'th ship, $R_i = R(\psi_i)$ is the rotation matrix (6.3) satisfying $\dot{R}_i = \dot{\psi}_i R_i S$ where S is given by (6.5). $M_i = M_i^\top > 0$ is the system inertia matrix including the hydrodynamic added inertia, D_i is the (linear) hydrodynamic damping matrix, $f_i = \mathrm{col}(f_{ui}, f_{vi}, f_{ri})$ is the fully actuated vector of control forces and moments, and w is vector of environmental disturbances decomposed in the $\mathcal{E}$ frame. The numerical values of the M_i and D_i matrices, taken from Fossen and Grøvlen (1998), represent true data of supply ships that operate in the North Sea. Their

nondimensional (Bis-scaled) coefficients are

$$M_i'' = \begin{bmatrix} 1.1274 & 0 & 0 \\ 0 & 1.8902 & -0.0744 \\ 0 & -0.0744 & 0.1278 \end{bmatrix} \tag{6.38a}$$

$$D_i'' = \begin{bmatrix} 0.0358 & 0 & 0 \\ 0 & 0.1183 & -0.0124 \\ 0 & -0.0041 & 0.0308 \end{bmatrix}. \tag{6.38b}$$

The dynamical system (6.37) is in the form of (6.7), where η_i is the output and f_i is the control. Let the desired path for the FRP be

$$\eta_d(\theta) = \begin{bmatrix} x_d(\theta) & y_d(\theta) & \psi_d(\theta) \end{bmatrix}^\top \tag{6.39}$$

where $x_d(\theta)$ and $y_d(\theta)$ are three times differentiable with respect to θ, and $\psi_d(\theta)$ is given by (6.2). The individual paths for each ship are then

$$\eta_{di}(\theta) = \eta_d(\theta) + R(\psi_d(\theta))l_i$$

where $l_i = [l_{xi},\ l_{yi},\ 0]^\top$. Let u_d be the desired surge speed for the FRP along the path. Then $\upsilon_s(\theta, t)$ is given by

$$\upsilon_s(\theta, t) = \frac{u_d(t)}{\sqrt{x_d^\theta(\theta)^2 + y_d^\theta(\theta)^2}}.$$

The design procedure in the previous section gives the following signals:

$$\begin{aligned}
&z_{1i} := \eta_i - \eta_d(\theta) - R(\psi_d(\theta))l_i \\
&z_{2i} := \nu_i - \alpha_{1i} \\
&\alpha_{1i} = R_i^\top \left[A_{1i} z_{1i} + \left(\eta_d^\theta + \psi_d^\theta R(\psi_d) S l_i\right) \upsilon_s\right] \\
&\sigma_{1i} = -r_i S \alpha_{1i} + R_i^\top [A_{1i} R_i \nu_i + \left(\eta_d^\theta + \psi_d^\theta R(\psi_d) S l_i\right) \upsilon_s^t] \\
&\alpha_{1i}^\theta = R_i^\top [-A_{1i} \left(\eta_d^\theta + \psi_d^\theta R(\psi_d) S l_i\right) + \eta_d^{\theta^2} \upsilon_s + \psi_d^\theta(\theta)^2 R(\psi_d) S^2 l_i \upsilon_s \\
&\qquad\qquad + \psi_d^{\theta^2}(\theta) R(\psi_d) S l_i \upsilon_s + \left(\eta_d^\theta + \psi_d^\theta R(\psi_d) S l_i\right) \upsilon_s^\theta] \\
&\\
&\tau_{2i} = 2 z_{1i}^\top P_{1i} \left(\eta_d^\theta + \psi_d^\theta R(\psi_d) S l_i\right) + 2 z_{2i}^\top P_{2i} \alpha_{1i}^\theta \\
&\\
&f_i \ = M_i [-P_{2i}^{-1} R_i^\top P_{1i} z_{1i} + A_{2i} z_{2i} + M_i^{-1} D_i \nu_i + \sigma_{1i} + \alpha_{1i}^\theta \upsilon_s - \tfrac{1}{2} \kappa_{2i} P_{2i} z_{2i}]
\end{aligned}$$

where f_i is the control law for Ship i. The guidance law, using a filtered-gradient update law, is

$$\begin{aligned}
\dot\theta &= \upsilon_s(\theta, t) - \omega_s \\
\dot\omega_s &= -\lambda \omega_s - \mu \sum_{i=1}^{r} \tau_{2i}(\eta_i, \nu_i, \theta, t).
\end{aligned} \tag{6.40}$$

The following two simulations are performed for a formation of 3 ships of length $L = 76\,\mathrm{m}$ and mass $m = 6 \cdot 10^6\,\mathrm{kg}$. In both simulations, the output path is given by (6.39), where $x_d(\theta) = \theta$ and $y_d(\theta) = 500 \sin \frac{2\pi}{4000}\theta$. The desired surge speed of the FRP starts out with the set-point $u_d = 4\,\mathrm{m/s}$. At time $t = 500\,\mathrm{s}$ the formation chief sets the new formation speed to $u_d = 10\,\mathrm{m/s}$.

Simulation 1: Maneuvering with ocean disturbances

The aim of this simulation is to show that with the formation maneuvering design we can robustly perform the path following maneuver for a formation of ships influenced by environmental disturbances. Starting off the path, we want the vessels to converge smoothly to their designated locations in the formation and eventually move along the path with the desired speed.

The formation designation vectors are chosen as $l_1 = [0, 0, 0]^\top$, $l_2 = [0, -150, 0]^\top$ and $l_3 = [0, 150, 0]^\top$. This means that the FRP coincide with Ship 1, and the ships will travel in a transversal line formation as one unit. The environmental disturbances are

$$w = \begin{bmatrix} 2 \\ 0 \\ 0 \end{bmatrix} + \begin{bmatrix} 2 \\ 2 \\ 2 \end{bmatrix} \sin(0.1t)\,, \tag{6.41}$$

acting the same on all the vessels. To attenuate these disturbances, the nonlinear damping gains are set to $\kappa_{2i} = 20$. The other controller parameters are set as: $A_{1i} = -\mathrm{diag}(0.02, 0.02, 0.5)$, $A_{2i} = -\mathrm{diag}(2, 2, 20)$, $P_{1i} = \mathrm{diag}(0.2, 0.2, 1)$, $P_{2i} = \mathrm{diag}(10, 10, 40)$ and $\mu = \lambda = 20$.

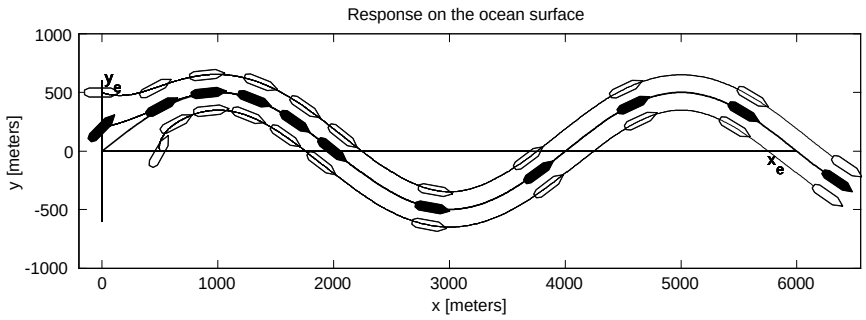

Figure 6.3: Simulation of 3 offshore supply vessels in a line formation following a desired sinusoidal path.

The initial conditions were $\eta_1(0) = \left[0,\ 200,\ \frac{\pi}{4}\right]^\top$, $\eta_2(0) = \left[500,\ 0,\ \frac{\pi}{3}\right]^\top$, $\eta_3(0) = [0,\ 500,\ 0]^\top$, $\nu_1(0) = \nu_2(0) = \nu_3(0) = [1,\ 0,\ 0]^\top$, and $\theta(0) = \omega_s(0) = 0$.

Figure 6.3 shows how the ships in the formation converge smoothly to their designated path and accurately track it. With the substantial environmental disturbances (6.41), the position error was attenuated to less than 1 m in x and y, and less than 1° in heading. In Figure 6.4 the surge speed

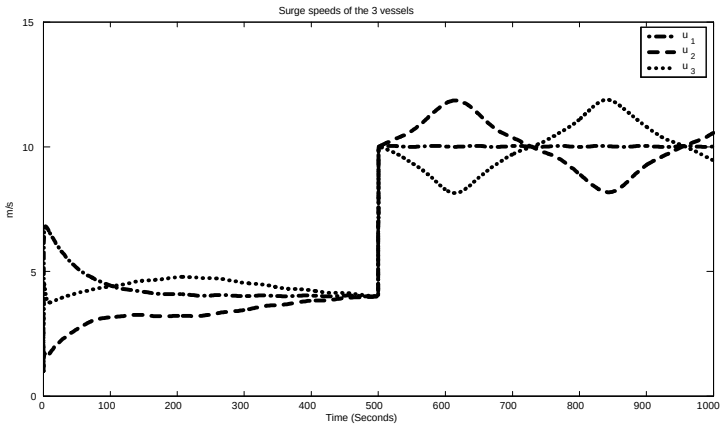

Figure 6.4: Time-plot of the surge speeds, $u_1(t)$, $u_2(t)$, $u_3(t)$, for the three ships.

of the ships are shown. Since the center ship are chosen to coincide with the FRP, this ship is seen to obtain the desired speed u_d as assigned by the formation chief. The two side ships obtain a periodic path speed according to their individual positions, necessary to keep the formation.

Simulation 2: Thrust saturation failure in one ship

It is of interest to see how the formation behave as a whole, if the thrust of one ship saturates. In Kang et al. (2000) the path variable θ is projected from the state of the leader vessel. Hence, only if the leader experiences a problem will the formation as a whole act robustly on it. A failure in one of the other vessels will not influence the others and can therefore easily lead to an accident.

The design procedure proposed in this section, is not based on any leader vessel. The time evolution of $\xi(\theta(t))$ along the path is equally influenced by

the states of all the vessels through the guidance law (6.40). Therefore, if one vessel experiences a problem, all the vessels will act upon it.

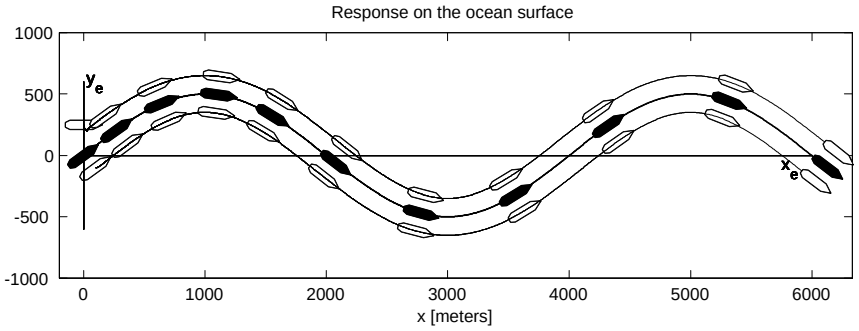

Figure 6.5: Resulting response of the formation when Ship 2 saturates.

We continue the experiment by forcing a saturation constraint on Ship 2, so that it will maximally be able to go with surge speed of 8 *m/s*. The surge speed assignment will be the same as in the previous simulation, that is, 4 *m/s* for $t < 500\,\text{s}$ and 10 *m/s* for $t \geq 500\,\text{s}$, which now is infeasible for Ship 2.

The environment in this simulation is disturbance free, $w = 0$, so that no nonlinear damping is required. The other controller parameters are set to: $A_{1i} = -\operatorname{diag}(0.5, 0.5, 0.5)$, $A_{2i} = -\operatorname{diag}(2, 2, 20)$, $P_{1i} = \operatorname{diag}(0.6,\ 0.6,\ 0.6)$, $P_{2i} = \operatorname{diag}(10, 10, 40)$, and $\mu = \lambda = 20$. The initial conditions were $\eta_1(0) = \left[0,\ 0,\ \frac{\pi}{5}\right]^\top$, $\eta_2(0) = \left[100,\ -100,\ \frac{\pi}{5}\right]^\top$, $\eta_3(0) = [0,\ 250,\ 0]^\top$, $\nu_1(0) = \nu_2(0) = \nu_3(0) = [4,\ 0,\ 0]^\top$, and $\theta(0) = \omega_s(0) = 0$.

Interestingly, Figure 6.5 shows that the formation follows the path as desired in spite of the 'failure' in Ship 2. Figure 6.6 reveals that the speed of the formation is considerable slower than the assigned speed of 10 *m/s*. In fact, the speed of the slowest vessel converges to its maximum speed of 8 *m/s* while the two other vessels follow at what speed necessary to keep the formation assembled. The formation is as fast as its slowest member. The important part is that the vessels keep following the path and therefore do not cause any accidents. This feature is due to the inherent gradient optimization algorithm (see Section 3.4) that tries to minimize the Lyapunov cost function that incorporates the states of all the vessels.

Figure 6.7 shows a time-plot of the assigned speed $v_s(\theta(t), t)$ and the resulting response of $\dot{\theta}(t)$. Clearly, $\dot{\theta}(t)$ is slower than the assigned speed.

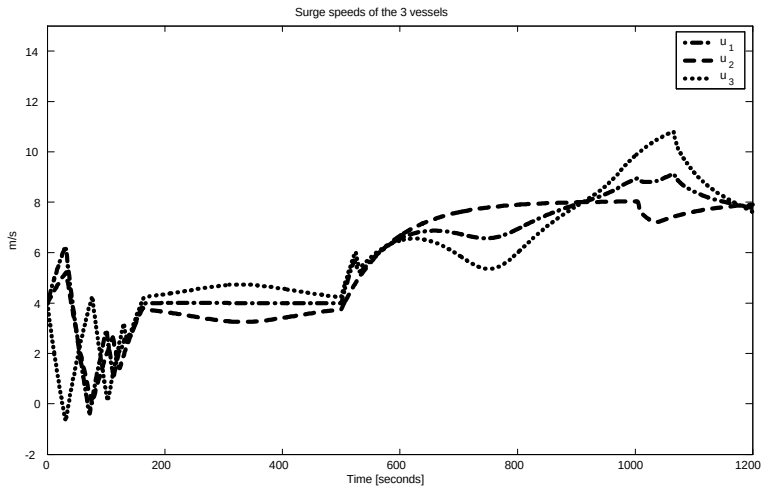

Figure 6.6: Surge speeds of the ships, where Ship 2 maximally makes 8 m/s. Commanded speed for the formation was 10 m/s.

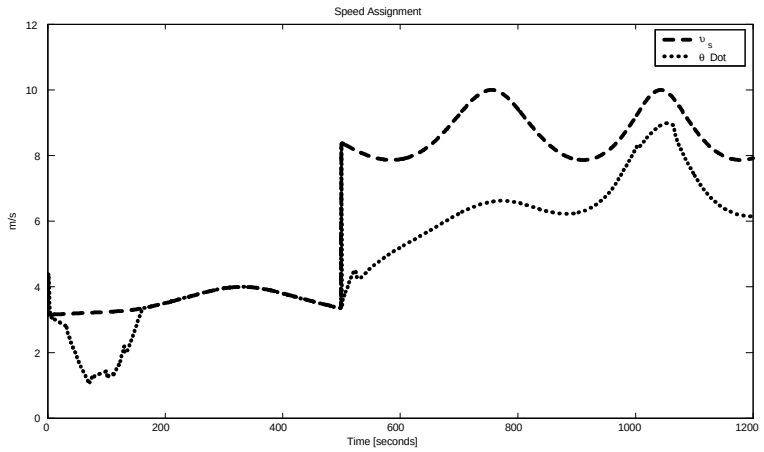

Figure 6.7: Time-plot of the speed assignment $\upsilon_s(\theta(t), t)$ for the FRP and the resulting response of $\dot{\theta}(t)$. Notice that $\dot{\theta}(t)$ is slower than the assigned speed $\upsilon_s(\theta(t), t)$.

6.3 Synchronizing multiple maneuvering systems

In this section, the dynamic gradient update law is decentralized by using individual path variables θ_i for each vessel. The objective is again formation control of r vessels with dynamics given by (6.7). For simplicity we disregard the disturbances and set $\delta_{1i}(t) = \delta_{2i}(t) \equiv 0$.

The path for the FRP and the designated positions for each vessel is set up the same way as shown in Section 6.1.2; however, by using individual path variables the path for each vessel becomes $\xi_i(\theta_i) = \xi(\theta_i) + R(\theta_i)^e_f l_i$, $i = 1, \ldots, r$. It is assumed that the paths $\xi_i(\theta_i) \in \mathcal{C}^2$ and their first and second partial derivatives are bounded in $\mathbb{R}^m$, and when $\theta_1 = \theta_2 = \ldots = \theta_r$ then all vessels are in formation.

We let the speed assignment for $\dot{\theta}_i$ be $\upsilon_i(\theta, t)$ where $\theta := \mathrm{col}(\theta_1, \theta_2, \ldots, \theta_r) \in \mathbb{R}^r$. According to Section 2.4.3, this gives for instance the possibility to use a function $\pi(\theta) = \pi(\theta_1, \ldots, \theta_r) \in \mathbb{R}$ and $\upsilon_i(\theta, t) = \upsilon_s(\pi(\theta), t)$. Nevertheless, the speed assignments $\upsilon_i(\theta, t) \in \mathcal{C}^1$ and their first partial derivatives are assumed bounded in θ and t.

6.3.1 Control Design

The control design follows the backstepping methodology proposed in Section 4.1. In the two steps of backstepping, an individual maneuvering design is performed for each vessel. Accordingly, the state transformation

$$z_{1i} = z_{1i}(x_{1i}, \theta) := y_i - \xi_i(\theta_i) = h_i(x_{1i}) - \xi_i(\theta_i) \tag{6.42}$$

$$z_{2i} = z_{2i}(x_i, \theta, t) := x_{2i} - \alpha_{1i}(x_{1i}, \theta, t) \tag{6.43}$$

$$\omega_i := \upsilon_i(\theta, t) - \dot{\theta}_i \tag{6.44}$$

is defined, using

$$\alpha_{1i} = \alpha_{1i}(x_{1i}, \theta, t) = G_{1i}^{-1}(h_i^{x_{1i}})^{-1}[A_{1i}z_{1i} - h_i^{x_{1i}}f_{1i} + \xi_i^{\theta_i}(\theta_i)\upsilon_i(\theta, t)] \tag{6.45}$$

where A_{1i} are Hurwitz design matrices. Define the vectors $\upsilon(\theta, t) := \mathrm{col}(\upsilon_1(\theta, t), \ldots, \upsilon_r(\theta, t)) \in \mathbb{R}^r$ and $\omega := \mathrm{col}(\omega_1, \ldots, \omega_r) \in \mathbb{R}^r$ such that

$$\dot{\theta} = \upsilon(\theta, t) - \omega, \tag{6.46}$$

and let ϵ_i be the i'th Cartesian coordinate vector such that $\theta_i = \epsilon_i^\top \theta$. Then the Step 1 control Lyapunov functions (CLFs) $V_{1i}(x_{1i}, \theta) := z_{1i}^\top P_{1i} z_{1i}$ have the time derivatives

$$\dot{V}_{1i} = -z_{1i}^\top Q_{1i} z_{1i} + 2z_{1i}^\top P_{1i} h_i^{x_{1i}} G_{1i} z_{2i} + \tau_{1i}\omega \tag{6.47}$$

where $\tau_{1i}(x_{1i},\theta,t) := 2z_{1i}^\top P_{1i}\xi_i^{\theta_i}\epsilon_i^\top \in \mathbb{R}^{1\times r}$ are the Step 1 *tuning functions*.

Skipping some details, Step 2 results in the static part of the control laws

$$\begin{aligned} u_i &= \alpha_{2i}(x_i,\theta,t) \\ &= G_{2i}^{-1}[A_{2i}z_{2i} - P_{2i}^{-1}G_{1i}^\top \left(h_i^{x_{1i}}\right)^\top P_{1i}z_{1i} - f_{2i} \\ &\qquad + \alpha_{1i}^{x_{1i}}\left(G_{1i}x_{2i} + f_{1i}\right) + \alpha_{1i}^t + \alpha_{1i}^\theta \upsilon] \end{aligned} \tag{6.48}$$

and the closed-loops

$$\dot{z}_i = A_i(x_{1i})z_i + B_i(x_{1i},\theta,t)\omega \tag{6.49}$$

$$A_i(x_{1i}) := \begin{bmatrix} A_{1i} & h_i^{x_{1i}}G_{1i} \\ -P_{2i}^{-1}G_{1i}^\top \left(h_i^{x_{1i}}\right)^\top P_{1i} & A_{2i} \end{bmatrix}, \quad B_i(x_{1i},\theta,t) := \begin{bmatrix} \xi_i^{\theta_i}\epsilon_i^\top \\ \alpha_{1i}^\theta \end{bmatrix}$$

where $z_i = \mathrm{col}(z_{1i}, z_{2i})$ and A_{ji} are Hurwitz design matrices satisfying $P_{ji}A_{ji} + A_{ji}^\top P_{ji} = -Q_{ji}$. The corresponding CLFs with time derivatives become

$$V_{2i}(x_i,\theta,t) = V_{1i}(x_{1i},\theta) + z_{2i}^\top P_{2i}z_{2i} = z_i^\top P_i z_i \tag{6.50}$$

$$\dot{V}_{2i} = -z_{1i}^\top Q_{1i}z_{1i} - z_{2i}^\top Q_{2i}z_{2i} + \tau_{2i}\omega = -z_i^\top Q_i z_i + \tau_{2i}\omega \tag{6.51}$$

where $P_i = \mathrm{diag}(P_{1i}, P_{2i})$, $Q_i = \mathrm{diag}(Q_{1i}, Q_{2i})$, and

$$\tau_{2i}(x_i,\theta,t) := \tau_{1i}(x_{1i},\theta,t) + 2z_{2i}^\top P_{2i}\alpha_{1i}^\theta \in \mathbb{R}^{1\times r} \tag{6.52}$$

are the resulting tuning functions. It can be verified that $\tau_{2i}(x_i,\theta,t) = -V_{2i}^\theta(x_i,\theta,t)$.

When designing the update laws, it is now necessary to ensure both synchronization of the θ_i variables as well as satisfying the speed assignments. To make the presentation cleaner, we will collect all states and functions into vector notation by defining $x := \mathrm{col}(x_1,\ldots,x_r) \in \mathbb{R}^{2rm}$, $z := \mathrm{col}(z_1,\ldots,z_r) \in \mathbb{R}^{2rm}$, and the matrices $A := \mathrm{diag}(A_1,\ldots,A_r)$, $B := \mathrm{col}(B_1,\ldots,B_r)$, $P := \mathrm{diag}(P_1,\ldots,P_r)$, and $Q := \mathrm{diag}(Q_1,\ldots,Q_r)$. The overall closed-loop incorporating all vessels is then

$$\dot{z} = A(x)z + B(x,\theta,t)\omega \tag{6.53}$$

$$\dot{\theta} = \upsilon(\theta,t) - \omega \tag{6.54}$$

where the function $\omega = \omega(x,\theta,t)$ is yet to be assigned. Let the composite CLF be $V(x,\theta,t) := V_{21}(x_1,\theta,t) + \cdots + V_{2r}(x_r,\theta,t)$, giving

$$V(x,\theta,t) = z^\top Pz \tag{6.55}$$

$$\dot{V} = -z^\top Qz - V^\theta(x,\theta,t)\omega(x,\theta,t) \tag{6.56}$$

where $V^\theta(x,\theta,t) = V_{21}^\theta(x_1,\theta,t) + \cdots + V_{2r}^\theta(x_r,\theta,t) = z(x,\theta,t)^\top P z^\theta(x,\theta,t)$.

To prepare for synchronization of the θ_i variables, we define the *synchronization constraint function* for θ as

$$\begin{aligned} \Phi_p &: \mathbb{R}^r \to \mathbb{R}^{r-1}, \quad p \geq 1 \\ \Phi_p(\theta) &= \begin{bmatrix} \phi_1(\theta) \\ \phi_2(\theta) \\ \vdots \\ \phi_{r-1}(\theta) \end{bmatrix} = \begin{bmatrix} (\theta_1-\theta_2)^p \\ (\theta_2-\theta_3)^p \\ \vdots \\ (\theta_{r-1}-\theta_r)^p \end{bmatrix} \end{aligned} \tag{6.57}$$

where p is a power on the weight chosen by design, and the Jacobian $\Phi_p^\theta \in \mathbb{R}^{r-1\times r}$ is

$$\Phi_p^\theta(\theta) = \begin{bmatrix} \phi_1^{\theta_1} & \phi_1^{\theta_2} & 0 & & 0 & 0 \\ 0 & \phi_2^{\theta_2} & \phi_2^{\theta_3} & \cdots & 0 & 0 \\ & \vdots & & \ddots & \vdots & \\ 0 & 0 & 0 & \cdots & \phi_{r-1}^{\theta_{r-1}} & \phi_{r-1}^{\theta_r} \end{bmatrix}. \tag{6.58}$$

Note that the nullspace of Φ_p^θ has dimension 1 and is given by

$$\mathcal{N}\left(\Phi_p^\theta(\theta)\right) = \{n \in \mathbb{R}^r : n = k\,\mathrm{col}(1,1,\ldots,1), \qquad k \in \mathbb{R}\backslash\{0\}\}. \tag{6.59}$$

We will need the following lemma:

Lemma 6.1 *Given $\Phi_p : \mathbb{R}^r \to \mathbb{R}^{r-1}$, let $\Psi(\theta) := \Phi_p^\theta(\theta)^\top \Lambda \Phi_p(\theta) \in \mathbb{R}^r$ where $\Lambda = \Lambda^\top > 0$ is a weight matrix. Then $\Psi(\theta) = 0$ iff $\Phi_p(\theta) = 0$. For each pair $0 < \delta_0 < \Delta_0$ there exist $\delta_1, \Delta_1 > 0$ such that*

$$\delta_0 \leq |\Phi_p(\theta)| \leq \Delta_0 \Rightarrow \delta_1 \leq |\Psi(\theta)| \leq \Delta_1. \tag{6.60}$$

Proof. *If $\Phi_p(\theta) = 0$ then clearly $\Psi = 0$. To prove the other direction, note first that $\Phi_p(c\mathbf{1}) = 0$, $\forall c \in \mathbb{R}$, where $\mathbf{1} = \mathrm{col}(1,1,\ldots,1)$. Assume that $\Psi = 0$ but $\Phi_p(\theta) \neq 0$. Hence, $\theta \neq c\mathbf{1}$ for any $c \in \mathbb{R}$. From the structure of $\Phi_p^\theta(\theta)$ we get that $\Phi_p^\theta(\theta)\theta = p\Phi_p(\theta)$. Hence, for $\theta \neq 0$ we get $\frac{1}{p}\theta^\top\Psi = \Phi_p(\theta)^\top\Lambda\Phi_p(\theta) = 0 \;\Rightarrow\; \Phi_p(\theta) = 0$ since $\Lambda = \Lambda^\top > 0$, and this is a contradiction.*

The upper bound on $|\Psi(\theta)|$ is obvious since $|\Phi_p(\theta)| \leq \Delta_0 \Rightarrow \left|\left|\Phi_p^\theta(\theta)\right|\right| < \Delta$ for some Δ. For the lower bound, define $v(\theta) = \mathrm{col}((\theta_1-\theta_r),(\theta_2-\theta_r),\ldots,(\theta_{r-1}-\theta_r),0) \in \mathbb{R}^r$. Then $\Phi_p^\theta(\theta)v(\theta) = p\Phi_p(\theta)$. Note that $|\Phi_p(\theta)| \leq$

$\Delta_0 \Rightarrow |v(\theta)| = |v(\theta)|_2 \leq c_p |v(\theta)|_{2p} \leq c_p \Delta_0^{1/p}$ *where* c_p *relates the* $2p$*-norm to the* 2*-norm. This gives*

$$\begin{aligned} c_p \Delta_0^{1/p} |\Psi(\theta)| &\geq \left| v(\theta)^\top \right| |\Psi(\theta)| \geq \left| v(\theta)^\top \Psi(\theta) \right| \\ &= \left| p \Phi_p(\theta)^\top \Lambda \Phi_p(\theta) \right| \geq p \lambda_m |\Phi_p(\theta)|^2 \\ &\geq p \lambda_m \delta_0^2 \\ |\Psi(\theta)| &\geq \lambda_m \frac{p}{c_p} \frac{\delta_0^2}{\Delta_0^{1/p}} =: \delta_1. \end{aligned} \tag{6.61}$$

■

Synchronizing $\theta_1 = \theta_2 = \ldots = \theta_r$ is now equivalent to the constraint $\Phi_p(\theta) = 0$. The formation maneuvering problem with synchronization is therefore solved by rendering the set

$$\mathcal{M} = \left\{ (z, \theta, t) \in \mathbb{R}^{2rm} \times \mathbb{R}^r \times \mathbb{R}_{\geq 0} : \; z = 0, \; \Phi_p(\theta) = 0 \right\} \tag{6.62}$$

UGAS under the additional requirement that $(z, \theta, t) \in \mathcal{M} \Rightarrow \omega = 0$ to satisfy the speed assignments.

Define the "synchronization CLF"

$$V_s(x, \theta, t) = V(x, \theta, t) + \frac{1}{2} \Phi_p(\theta)^\top \Lambda \Phi_p(\theta) \tag{6.63}$$

where $\Lambda = \Lambda^\top > 0$ is a weight matrix. The derivative of V_s with respect to time becomes

$$\begin{aligned} \dot{V}_s &= \dot{V} + \Phi_p(\theta)^\top \Lambda \Phi_p^\theta(\theta) \, \dot{\theta} \\ &= -z^\top Q z - V^\theta(x, \theta, t) \omega(x, \theta, t) + \Phi_p(\theta)^\top \Lambda \Phi_p^\theta(\theta) \left(v(\theta, t) - \omega \right) \\ &= -z^\top Q z + \Phi_p(\theta)^\top \Lambda \Phi_p^\theta(\theta) \, v(\theta, t) \\ &\quad - \left[V^\theta(x, \theta, t) + \Phi_p(\theta)^\top \Lambda \Phi_p^\theta(\theta) \right] \omega(x, \theta, t), \end{aligned} \tag{6.64}$$

which has two sign indefinite terms. For the term $\Phi_p(\theta)^\top \Lambda \Phi_p^\theta(\theta) \, v(\theta, t)$, notice that $v(\theta(t), t) \in \mathcal{N}\left(\Phi_p^\theta(\theta(t)) \right)$ for all $t \geq 0$ will ensure that this term vanishes. Hence, the logical requirement of equal speed assignment (for the FRP) among all vessels falls directly out of the equation. We will return later with a discussion for how to achieve this.

For the second sign indefinite term in (6.64), notice first that $V^\theta(x,\theta,t) + \Phi_p(\theta)^\top \Lambda \Phi_p^\theta(\theta) = V_s^\theta(x,\theta,t)$. Motivated by the gradient algorithms described in earlier sections, we choose

$$\begin{aligned} \omega(x,\theta,t) &= \Gamma \left[V^\theta(x,\theta,t) + \Phi_p(\theta)^\top \Lambda \Phi_p^\theta(\theta) \right]^\top \\ &= \Gamma V_s^\theta(x,\theta,t)^\top \end{aligned} \tag{6.65}$$

where $\Gamma = \Gamma^\top > 0$ is a gain matrix. The final derivative of V_s along the solutions of the closed-loop system becomes

$$\dot{V}_s = -z^\top Q z - V_s^\theta(x,\theta,t) \Gamma V_s^\theta(x,\theta,t)^\top, \tag{6.66}$$

and this gives the result:

Theorem 6.2 *The overall closed-loop formation maneuvering system*

$$\begin{aligned} \dot{z} &= A(x)z + B(x,\theta,t)\Gamma V_s^\theta(x,\theta,t)^\top \\ \dot{\theta} &= \upsilon(\theta,t) - \Gamma V_s^\theta(x,\theta,t)^\top \end{aligned} \tag{6.67}$$

is forward complete and solves the formation maneuvering problem, that is, the set (6.62) is UGAS.

Proof. *Clearly, the speed assignment is satisfied in $\mathcal{M}$ since $V_s^\theta(x,\theta,t) = V^\theta(x,\theta,t) + \Phi_p(\theta)^\top \Lambda \Phi_p^\theta(\theta) = 0$, $\forall (z,\theta,t) \in \mathcal{M}$. Let $Z := \mathrm{col}(z, \Phi_p(\theta))$. For the Lyapunov function (6.63) we have the bounds $p_1 |Z|^2 \leq V_s \leq p_2 |Z|^2$ and $\dot{V}_s \leq -\lambda_{\min}(Q)|z|^2$ where $p_1 = \min(\lambda_{\min}(P), 0.5\lambda_{\min}(\Lambda))$ and $p_2 = \max(\lambda_{\max}(P), 0.5\lambda_{\max}(\Lambda))$. This implies that for all t in the maximal interval of existence $[0,T)$,*

$$|Z(t)| \leq \sqrt{\frac{p_2}{p_1}} |Z(0)| . \tag{6.68}$$

Consequently, by the smoothness assumption on the plant and boundedness of the path signals, the speed assignment signals, and z, implies that the right-hand side of (6.67) is bounded on the maximal interval of existence (constructing the smooth transformation $x = \Upsilon(z,\theta,t)$ resulting from backstepping will explicitly show this). This rules out finite escape times so that $T = \infty$. It is verified that $|(z,\theta,t)|_{\mathcal{M}} = |Z|$. Hence, (6.68) shows that $\mathcal{M}$ is UGS according to Definition A.8. Let

$$\varphi(z,\theta,t) := z^\top Q z + \left(z^\top P z^\theta + \Psi(\theta)^\top \right) \Gamma \left(z^\top P z^\theta + \Psi(\theta)^\top \right)^\top \tag{6.69}$$

such that $\dot{V}_s = -\varphi(z,\theta,t)$. The claim is that $\varphi(z,\theta,t)$ is positive definite with respect to Z. If this is true, then it follows from Theorem A.10 that

(6.62) is indeed UGAS with respect to (6.67). The following reations, using Lemma 6.1, verify the claim:

$$\begin{array}{ll} (i) & z=0,\ \Phi_p(\theta)=0 \ \Rightarrow\ \varphi(z,\theta,t)=0 \\ (ii) & |z|\geq\delta_0 \ \Rightarrow\ |\varphi(z,\theta,t)|\geq\lambda_{\min}(Q)\delta_0^2 \\ (iii) & z=0,\ |\Phi_p(\theta)|\geq\delta_0 \ \Rightarrow\ |\Psi(\theta)|\geq\delta_1 \ \Rightarrow\ |\varphi(z,\theta,t)|\geq\lambda_{\min}(\Gamma)\delta_1^2. \end{array}$$

■

Remark 6.1 *In Skjetne et al. (2003), Matrosov's Theorem was applied to show UGAS in the previous theorem. This is, however, not necessary since $\dot{V}_s$ is in fact negative definite.*

Constructing the speed assignments

The restriction that $\upsilon(\theta(t),t)$ must for all $t\geq 0$ be in the null-space of $\Phi_p^\theta(\theta(t))$ means that for all $t\geq 0$, then $\upsilon_1(\theta(t),t)=\upsilon_2(\theta(t),t)=\ldots=\upsilon_r(\theta(t),t)$ must hold. Recall that the speed assignment $\upsilon_i(\theta,t)$ sets the desired path speed for the FRP for Vessel i. When the vessels are synchronized, these desired path speeds should obviously be the same. The main problem occurs in the initial state when the vessels are not synchronized since for $\theta_1\neq\theta_2$ then $\upsilon_s(\theta_1,t)$ may not be equal in value to $\upsilon_s(\theta_2,t)$.

One way to circumvent this is to let all speed assignments be the same and only depend on time, that is, $\upsilon_i(\theta,t)=\upsilon_s(t)$ for all $i=1,\ldots,r$. This may, however, be too restrictive. Other choices can also be made depending on the shape of the path and how it is parametrized. An attractive method is to parametrize $\xi(\cdot)$ for the FRP in terms of path length. θ_i will then have unit '*meter*' and a common speed assignment $\upsilon_s(t)$ will directly correspond to a desired tangential velocity in '*m/s*' along the path.

A promising method was proposed in the Example in Section 2.4.3. The suggestion was to use a common speed assignment $\upsilon_i(\theta,t)=\upsilon_s(\pi(\theta),t)$ for all $i=1,\ldots,r$, where $\pi(\theta)$ is any desired function of the path variables. For instance,

$$\pi(\theta)=\frac{1}{r}(\theta_1+\theta_2+\ldots+\theta_r) \tag{6.70}$$

will let $\upsilon_s(\pi,t)$ depend on the average value of the path variables. Another alternative, if the formation has a leader vehicle with, say, index 1, is to let $\pi(\theta)=\theta_1$.

Decentralized controller realizations

In Theorem 6.2 it is established that all θ_i variables will synchronize so that the formation maneuvers along the path as desired. Letting $\Gamma = \text{diag}\{\gamma_1, \ldots, \gamma_r\}$, then from (6.48) and (6.67), the individual controller realizations are

$$\begin{aligned} u_i &= \alpha_2(x_i, \theta, t) \\ \dot{\theta}_i &= \upsilon_i(\theta, t) - \gamma_i \left\{ \epsilon_i^\top V^\theta(x, \theta, t)^\top + \epsilon_i^\top \Phi_p^\theta(\theta)^\top \Lambda \Phi_p(\theta) \right\}. \end{aligned} \tag{6.71}$$

For $\Lambda = \text{diag}\{\lambda_1, \ldots, \lambda_{r-1}\}$ then it follows further that $\epsilon_i^\top \Phi_p^\theta(\theta)^\top \Lambda \Phi_p(\theta) = p\lambda_i (\theta_i - \theta_{i+1})^{2p-1} - p\lambda_{i-1}(\theta_{i-1} - \theta_i)^{2p-1}$ with $\lambda_0 = \lambda_r = \theta_0 = \theta_{r+1} = 0$.

Note that the term $\epsilon_i^\top V^\theta(x, \theta, t)^\top$ may require states x_j of vessels other than Vessel i, and thus resulting in an undesired communication of vessel states. The reason is that υ_i was allowed to depend on the θ_j's of all vessels such that $V^\theta(x, \theta, t) = V_{21}^\theta(x_1, \theta, t) + \cdots + V_{2r}^\theta(x_r, \theta, t)$. If we instead restrict υ_i to only depend on θ_i, that is, $\upsilon_i = \upsilon_i(\theta_i, t)$, then we get $V^\theta(x, \theta, t) = \text{row}(V_{21}^{\theta_1}(x_1, \theta_1, t), \ldots, V_{2r}^{\theta_r}(x_r, \theta_r, t))$, and the modified realizations become

$$\dot{\theta}_i = \upsilon_i(\theta_i, t) - \gamma_i \left\{ V_{2i}^{\theta_i}(x_i, \theta_i, t) + \epsilon_i^\top \Phi_p^\theta(\theta)^\top \Lambda \Phi_p(\theta) \right\}. \tag{6.72}$$

This dynamic equation is seen to be a decentralized guidance law, depending only on the vessel's own states together with all path variables. The communication requirement in this latter case is to only transmit the r path variables between the vessels.

It is observed from (6.72) that $\Lambda = 0$ makes the gradient update law for $\dot{\theta}_i$ identical to the gradient update law for maneuvering of a single ship according to Chapter 5. On the other hand, in the limit as $||\Lambda|| \to \infty$, the θ_i's will be identically synchronized and yield the exact same responses as obtained for the common θ formation control procedure in Section 6.2.

6.3.2 Case study 2: Underway Replenishment Between Three Ships

As an illustration to the synchronization procedure, we consider again a rendezvous maneuvering operation between three offshore supply vessels. The equations of motion in surge, sway, and yaw for each ship is given by (6.37), but for simplicity we assume $w(t) \equiv 0$. In this illustration, two ships are of length $L = 76\,\text{m}$ and mass $m = 6 \cdot 10^6\,\text{kg}$, and one ship is larger, $L = 100\,\text{m}$ and $m = 7 \cdot 10^6\,\text{kg}$. Their nondimensional (Bis-scaled) coefficients are given by (6.38).

Figure 6.8: Italian supply ship "Vesuvio" refueling two ships at sea. Courtesy: Hepburn Engineering Inc.

Given a path $\xi_i(\theta_i)$ and a speed assignment $\upsilon_i(\theta_i, t)$ for each vessel, the maneuvering design yields the following signals

$$
\begin{array}{l}
z_{1i} := \eta_i - \xi_i(\theta_i) \\
z_{2i} := \nu_i - \alpha_{1i} \\
\alpha_{1i} = R(\psi_i)^\top [A_{1i} z_{1i} + \xi_i^{\theta_i}(\theta_i) \upsilon_i(\theta_i, t)], \qquad \dot{\alpha}_{1i} = \sigma_{1i} + \alpha_{1i}^{\theta_i} \dot{\theta}_i \\
\sigma_{1i} = \dot{R}^\top R \alpha_{1i} + R^\top [A_{1i} R \nu_i + \xi_i^{\theta_i} \upsilon_i^t] \\
\alpha_{1i}^{\theta_i} = R^\top [-A_{1i} \xi_i^{\theta_i} + \xi_i^{\theta_i^2} \upsilon_i + \xi_i^{\theta_i} \upsilon_i^{\theta_i}] \\
V_i^{\theta_i} = -2 z_{1i}^\top P_{1i} \xi_i^{\theta_i} - 2 z_{2i}^\top P_{2i} \alpha_{1i}^{\theta_i} \\
\\
f_i = M_i [-P_{2i}^{-1} R(\psi_i)^\top P_{1i} z_{1i} + A_{2i} z_{2i} + M_i^{-1} D_i \nu_i + \sigma_{1i} + \alpha_{1i}^{\theta_i} \upsilon_s]
\end{array}
$$

where f_i is the control law. The synchronization constraint function is given by

$$
\Phi_p(\theta) = \begin{bmatrix} \phi_1(\theta) \\ \phi_2(\theta) \end{bmatrix} = \begin{bmatrix} (\theta_1 - \theta_2)^p \\ (\theta_2 - \theta_3)^p \end{bmatrix} \tag{6.73}
$$

which has the Jacobian

$$
\Phi_p^\theta(\theta) = p \begin{bmatrix} (\theta_1 - \theta_2)^{p-1} & -(\theta_1 - \theta_2)^{p-1} & 0 \\ 0 & (\theta_2 - \theta_3)^{p-1} & -(\theta_2 - \theta_3)^{p-1} \end{bmatrix}.
$$

To ensure that $\upsilon(\theta, t) \in \mathcal{N}\left(\Phi_p^\theta(\theta(t))\right)$ for all $t \geq 0$ we let $\upsilon_1 = \upsilon_2 = \upsilon_3 = \upsilon_s = \textit{constant}$. The path will be parametrized in terms of path length so that the speed assignment for the FRP will correspond to a desired path speed in 'm/s' along the path. The guidance law for Vessel i becomes

$$
\dot{\theta}_i = \upsilon_s - \gamma_i [V_i^{\theta_i} + p\lambda_i (\theta_i - \theta_{i+1})^{2p-1} - p\lambda_{i-1} (\theta_{i-1} - \theta_i)^{2p-1}] \tag{6.74}
$$

where $\lambda_0 = \lambda_3 = \theta_0 = \theta_4 = 0$.

Simulation

The aim of the simulation is to verify the synchronization property of the maneuvering controllers. The path for the FRP is a circle

$$\xi(\theta_i) = \begin{bmatrix} x_d(\theta_i) \\ y_d(\theta_i) \\ \psi_d(\theta_i) \end{bmatrix} = \begin{bmatrix} r\cos(\left(\frac{\theta_i}{r}\right) \\ r\sin\left(\frac{\theta_i}{r}\right) \\ \arctan\left(\frac{y_d^{\theta_i}(\theta_i)}{x_d^{\theta_i}(\theta_i)}\right) \end{bmatrix}$$

where $r = 1200\,\mathrm{m}$. The designation vectors are $l_1 = [0, -150, 0]^\top$, $l_2 = [0, 0, 0]^\top$, and $l_3 = [0, 150, 0]^\top$, which means that the FRP coincide with Ship 2. The speed assignments will be a desired surge speed which starts out with $v_s = 6\,\mathrm{m\,s^{-1}}$. At time $t = 500\,\mathrm{s}$ the formation chief sets the new formation speed to $v_s = 10\,\mathrm{m\,s^{-1}}$. The other controller parameters are set as: $A_{11} = A_{13} = -\operatorname{diag}(0.2, 0.2, 0.2)$, $A_{12} = -\operatorname{diag}(0.1, 0.1, 0.1)$, $A_{21} = A_{23} = -\operatorname{diag}(0.4, 0.4, 0.4)$, $A_{22} = -\operatorname{diag}(0.2, 0.2, 0.2)$, $P_{1i} = \operatorname{diag}(0.2, 0.2, 1)$, $P_{2i} = \operatorname{diag}(10, 10, 40)$, $\gamma_i = 5$, $\Lambda = 0.008I$, and $p = 1$.

Initial conditions were $\eta_1(0) = [1350, 0, \frac{\pi}{2}]^\top$, $\eta_2(0) = [1109, -459, \frac{\pi}{2}]^\top$, $\eta_3(0) = [742, -742, \frac{\pi}{2}]^\top$, $\nu_1(0) = \nu_2(0) = \nu_3(0) = [0, 0, 0]^\top$, and $\theta(0) = 0$.

Figure 6.9 shows the output response of the vessels. Within one revolution along the path, the vessels are synchronized. This is also verified in Figure 6.10 where $|\Phi_1(\theta(t))|$ is plotted. Clearly, after an initial transient, the synchronization constraint function converges to zero. The surge velocities are seen in Figure 6.11 to comply with the speed assignment for the FRP and the individual designations of the vessels. It should be remarked that no saturation limits have been implemented so that the response times are somewhat unrealistic.

It should further be remarked that the scenario of thrust failure described in the case study for the previous design also works for the synchronization-based controller. However, the error that arise in the speed assignment in this case, will propagate to a steady-state error in the synchronization term $\Phi_1(\theta)$. Larger Λ will reduce this error. Alternatively, one can introduce integral feedback (Skjetne and Fossen; 2004) from $\dot{s} = \Phi_p(\theta)$ in the update law for $\dot{\theta}$. Though the theoretical aspects of this is not analyzed, simulation has shown that it may completely eliminate the synchronization error if tuned properly.

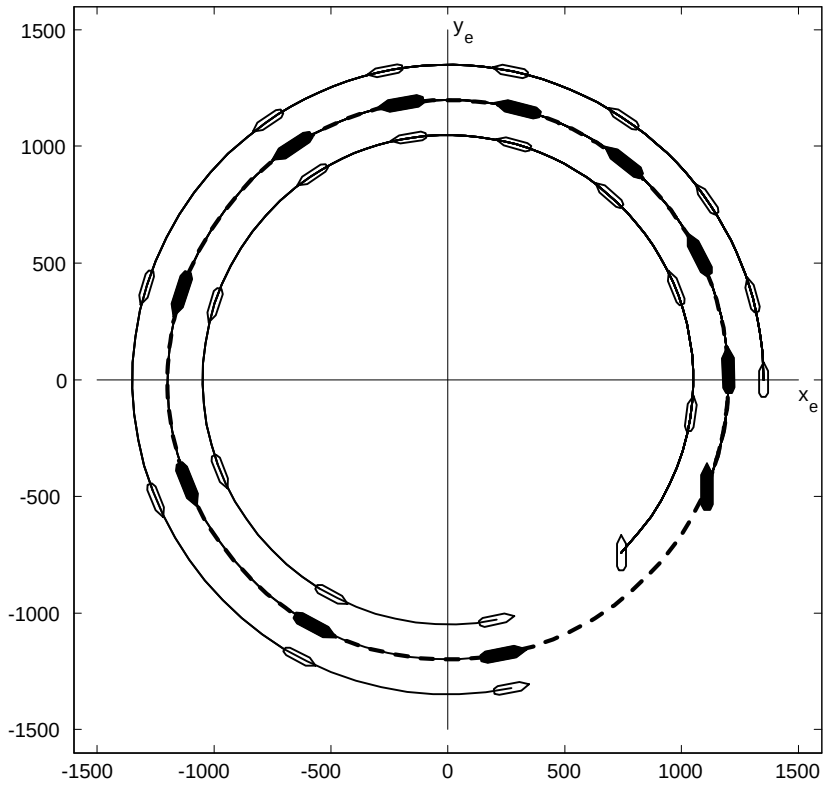

Figure 6.9: Simulation of 3 offshore supply vessels in a rendezvous formation.

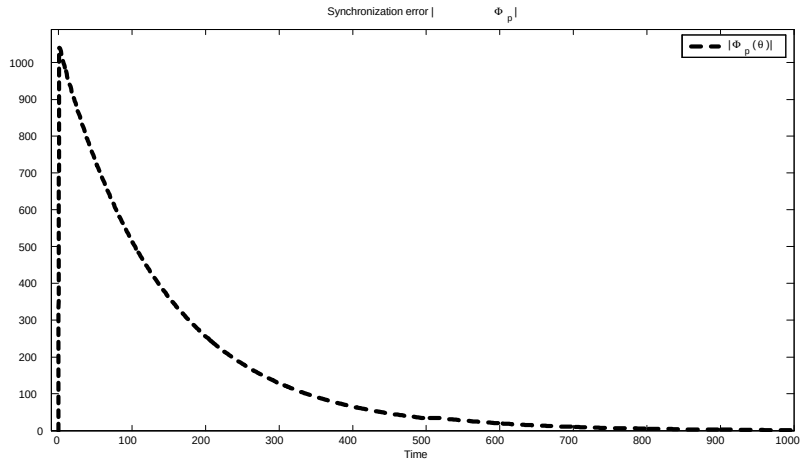

Figure 6.10: Time response of $|\Phi_1(\theta(t))|$ which shows that synchronization is successful.

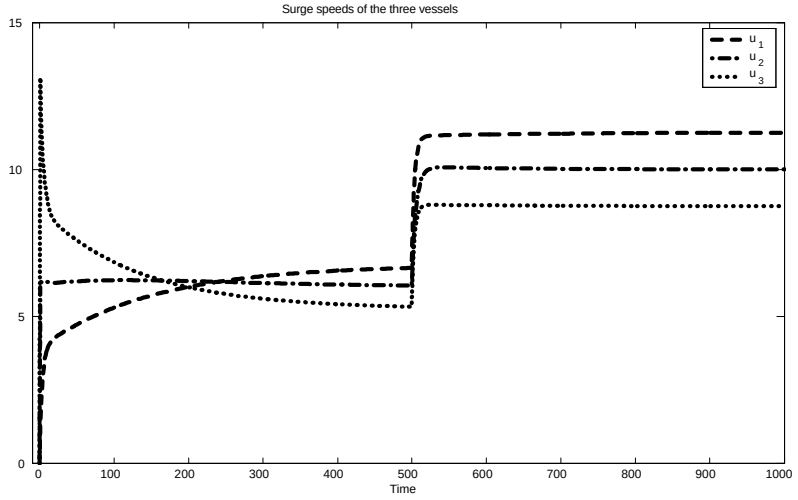

Figure 6.11: Time responses of the surge speeds, $u_1(t)$, $u_2(t)$, $u_3(t)$.

Conclusion

In this thesis we have developed theory around a new problem statement defined by *The Maneuvering Problem* and *The Maneuvering Control Objective* in Chapter 2. The theoretical contributions include constructive control designs, analysis, and applications with experimental results.

The Maneuvering Problem was defined as solving a *Geometric task* and a *Dynamic task*. The geometric task was to converge to, and stay on, a desired path parametrized by θ, whereas the dynamic task was to satisfy a desired dynamic behavior along the path, usually specified as a speed assignment for $\dot{\theta}$. To check feasibility of these tasks for a specific system, a *feasibility constraint differential equation* in θ should be derived. The geometric task was feasible if this differential equation has a solution θ^* for an admissible control input, and the dynamic task was feasible if θ^* additionally satisfied the dynamic assignment.

It was further shown that the maneuvering problem implied the existence of a globally attractive, forward invariant manifold in the state space to which the solutions must converge. In, for instance, the cutting tool design example in Section 2.4, the flexibility of picking a suitable path parametrization and constructing the speed assignment were shown to be powerful tools to satisfy the design specifications.

In Chapter 3, a design procedure using feedback linearization was presented that solved the maneuvering control objective and made the closed-loop system UGES with respect to the noncompact set representing the desired manifold. This was achieved by constructing a static control law that was tied together with a dynamic update law in order to render the time derivative of the control Lyapunov function (CLF) negative definite in the distance to the set.

It was further shown in Chapter 3 that the dynamic update laws, called the *Gradient* or *Filtered-gradient* update laws, included an inherent gradient optimization algorithm. The resulting dynamic controller consisted therefore of a stabilization algorithm that drives the state $x(t)$ to the point

$\xi(\theta(t))$ on the path, and a dynamic optimization algorithm that selects the point $\xi(\theta)$ on the path that minimizes the weighted distance between x and ξ. The fast optimization algorithm was analyzed by singular perturbation techniques, and it was shown that increasing the gain μ induces a two-time scale behavior of the closed-loop plant. In the fast time-scale $\theta(t)$ rapidly converges to the minimizer, and in the slow time-scale, $x(t)$ is driven towards the path. These properties was further used, in an example, to claim *near forward invariance* and *near stability* of the unit circle for a double integrator plant.

With the most important aspects and subtleties explained using feedback linearizable systems in Chapter 3, we embarked on designs for uncertain systems in Chapter 4. ISS and adaptive backstepping maneuvering designs were both conducted. As compared to traditional backstepping designs for *tracking*, it was shown that the maneuvering design recursively constructed a maneuvering tuning function that was finally dealt with in the end by the choice of an update law. This tuning function was indeed shown to be the gradient of the corresponding CLF with respect to θ, and the update laws were therefore again of the gradient or filtered-gradient types with the same performance properties as analyzed in Chapter 3. In the sliding-mode design, a maneuvering control law was first designed for the nominal part of the plant, and then traditional sliding-mode techniques were used to deal with the uncertain part and develop the overall control law.

The maneuvering designs were experimentally tested for a real model ship in a marine control laboratory. This work was presented in Chapter 5 (and Appendix B). The ability to online adjust the forward speed of the ship along the path was easily achieved by constructing the speed assignment properly. To highlight the performance property of the gradient update law, a comparison between a tracking-based controller and a gradient-based controller was done for the adaptive backstepping design. Significant results were in this case obtained in the event of a saturation failure in the ship.

In Chapter 5, a maneuvering design based on a nonlinear PID technique was also developed and tested. However, using the gradient update law in the experiments for the nonlinear PID resulted sometimes in failure. The reason was traced to the minima structure of the Lyapunov cost function, and it was shown that perturbations in the path following performance could create local and global minima close to each other with the result that $\theta(t)$, through the gradient optimization algorithm, could jump between them and consequently cause large transients in the system.

Finally, Chapter 6 proposed two maneuvering designs solving a forma-

tion control problem. This was achieved by designating each vessel of the formation a position relative to a *Formation Reference Point* (FRP). Setting this up as a maneuvering problem for the FRP would then solve the formation objective.

Two formation control designs were proposed. The first developed decentralized control laws and a centralized dynamic guidance law, which incorporated the gradient update law, to solve the problem. In this case, the point along the path $\xi(\theta(t))$ for the FRP was selected based on the state of all vessels. This means that a function of the weighted distance of all vessels to their designated positions were minimized with respect to a common θ. A simulation showed that if one vessel failed to satisfy the commanded speed for the formation, this would then affect the progression of all vessels along the path due to the gradient minimization. In the second design, the guidance law was further decentralized in order to reduce communication demands. This was achieved by using individual path variables θ_i and synchronizing these using an additional synchronization term in the individual update laws. When implemented, this would require for Vessel i, in minimum, only the knowledge of θ_{i-1} and θ_{i+1} (i.e. its neighbors) in order to achieve synchronization.

From a practical point of view, the maneuvering problem may have some impact due to the simplicity of systematically approaching control problems as two separate tasks that are combined in the control law. This methodology differs in this respect from trajectory tracking where both tasks are combined priorly in the design of the desired trajectory and, as a consequence, looses flexibility. With the two-task approach of the maneuvering problem, one can individually design the desired path and the desired dynamic assignment along the path, and it is therefore a convenient solution to many practical problems for vehicle path following, formation control, rendezvous operations, etc. Chapter 2 gave, for instance, an algorithm for generating a feasible path for a ship from the specification of some way-points. By adding some more intelligence into the path-generating algorithm, one can additionally take into account constraints such as sea depth, stationary or moving obstacles, and weather forecast. The desired speed along the path is approached as a separate task, and for the ship experiments it was even shown that the speed could be set online by the vessel operator.

Ideally, the maneuvering problem is applicable to any control problem where the output should be constrained to a one-dimensional trajectory in the output space. It also makes some synchronization problems easier to handle, since synchronizing two scalar variables θ_1 and θ_2 inside a (guidance)

computer can be easier than synchronizing two n-DOF output states η_1 and η_2 by direct control action.

Some aspects of maneuvering are yet to be analyzed. For instance, a deeper analysis of the effect of perturbations on the gradient minimization is necessary. In some sense we have claimed that using the gradient update law will robustify the closed-loop system with respect to failures. The 'failure' referred to here is such as the saturation failure in Section 5.3.3, in which case the ship would still manage to follow the path despite the infeasibly assigned speed. However, the nonlinear PID experiment in Section 5.5.3 showed that a small loss of position and heading would cause θ to jump between local minima due to the dynamic gradient optimization, and thus cause large transients. The differences in those two experiments lies with the shape of the Lyapunov cost function and its minima structure. Consequently, conditions for when the gradient algorithm is sufficiently robust with respect to perturbations should be developed.

Another issue is to derive a method where any desired cost function can be used, not only the applied Lyapunov function. In this case it would be easier to guarantee robustness of the gradient algorithm based on the convexity properties of the chosen cost function.

The maneuvering theory presented in this thesis has inspired ideas and creative thinking beyond the reported material of this thesis. It is further the hope of the author that more applications, new control problem setups, new designs, and more analysis, based on the maneuvering concepts presented in this thesis, can and will be addressed by control researchers in the future.

Bibliography

Abkowitz, M. A. (1964). Lectures on ship hydrodynamics - steering and manoeuvrability, *Technical report Hy-5*, Hydro- and Aerodynamics Laboratory, Lyngby, Denmark.

Aguiar, A. P., Cremean, L. and Hespanha, J. P. (2003). Position tracking for a nonlinear underactuated hovercraft: Controller design and experimental results, *Proc. 42nd IEEE Conf. Decision & Control*, IEEE, Maui, Hawaii, USA.

Aguiar, A. P., Dačić, D. B., Hespanha, J. P. and Kokotović, P. V. (2004). Path-following or reference-tracking? An answer based on limits of performance, *Proc. IFAC/EURON Symposium on Intelligent Autonomous Vehicles*, Lisbon, Portugal.

Aguiar, A. P. and Hespanha, J. P. (2003). Position tracking of underactuated vehicles, *Proc. American Control Conf.*, AACC, Denver, Colorado, USA.

Aguiar, A. P., Hespanha, J. P. and Kokotović, P. V. (2005). Path-following for non-minimum phase systems removes performance limitations, *IEEE Trans. Automat. Contr.* **50**(2).

Al-Hiddabi, S. and McClamroch, N. (2002). Tracking and maneuver regulation control for nonlinear nonminimum phase systems: Application to flight control, *IEEE Trans. Contr. Sys. Tech.* **10**(6): 780–792.

Anderson, B. D. O., Bitmead, R. R., Johnson, Jr., C. R., Kokotović, P. V., Kosut, R. L., Mareels, I. M. Y., Praly, L. and Riedle, B. D. (1986). *Stability of adaptive systems*, MIT Press Series in Signal Processing, Optimization, and Control, 8, The MIT Press, Cambridge, MA, USA. Passivity and averaging systems.

Anderson, B. D. O. and Moore, J. (1989). *Optimal Control: Linear quadratic methods.*, Prentice-Hall, Inc, London.

Åström, K. J. and Wittenmark, B. (1990). *Computer Controlled Systems: Theory and Design*, 2 edn, Prentice-Hall, Inc, New Jersey.

Athans, M. and Falb, P. (1966). *Optimal Control: An introduction to the theory and its applications.*, McGraw-Hill Book Company, New York.

Bailey, P. A., Price, W. G. and P., T. (1998). A unified mathematical model describing the maneuvering of a ship travelling in a seaway, *Trans. RINA* **140**: 131–149.

Balchen, J. G., Jensen, N. A. and Sælid, S. (1976). Dynamic positioning using kalman filtering and optimal control theory, *IFAC/IFIP Symp. On Automation in Offshore Oil Field Operation*, Bergen, Norway, pp. 183–186.

Barbălat, I. (1959). Systèmes d'Équations Différentielles d'Oscillations Non Liné aires, *Revue de Mathématiques Pures et Appliquées* **4**(2): 267–270.

Behal, A., Dawson, D. M., Dixon, W. E. and Fang, Y. (2002). Tracking and regulations control of an underactuated surface vessel with nonitegrable dynamics, *IEEE Trans. Automat. Contr.* **47**: 495–500.

Bennet, S. (1979). *A History of Control Engineering 1800-1930*, Peter Peregrinus Ltd.

Binetti, P., Ariyur, K. B., Krstić, M. and Bernelli, F. (2003). Formation flight optimization using extremum seeking feedback, *J. Guidance, Control, and Dynamics* **26**(1): 132–142.

Bishop, R. E. D. and Price, W. G. (1981). On the use of equilibrium axes and body axes in the dynamics of a rigid ship, *J. Mechanical Eng. Science* **23**(5): 243–256.

Blanke, M. (1981). *Ship Propulsion Losses Related to Automated Steering and Prime Mover Control*, PhD thesis, Technical Univ. of Denmark, Lyngby, Denmark.

Blanke, M. and Christensen, A. (1993). Rudder-roll damping autopilot robustness due to sway-yaw-roll couplings, *Proc. Int. Ship Control Systems Symp.*, Vol. A, Ottawa, Canada, pp. 93–119.

Breivik, M. and Fossen, T. I. (2004). Path following of straight lines and circles for marine surface vessels, *Proc. IFAC Conf. Contr. Appl. Marine Systems*, IFAC, Ancona, Italy.

Brunovsky, P. (1970). A classification of linear controllable systems, *Kybernetika* **6**(3): 173–188.

Chance, T. C., Kleiner, A. A. and Northcutt, J. G. (2000). The HUGIN 3000 AUV, *Sea Technology* **41**(12): 10–14.

Clarke, D. (2003). The foundations of steering and manoeuvring, *Proc. IFAC Conf. Manoeuvering and Contr. Marine Crafts*, IFAC, Girona, Spain.

Corneliussen, J. (2003). *Implementation of a guidance system for CyberShip II*, MSc thesis, Norwegian Univ. Science & Technology, Dept. Eng. Cybernetics, Trondheim, Norway.

Dačić, D. B. and Kokotović, P. V. (2005). Path-following for linear systems with unstable zero dynamics, *Automatica* . Submitted.

Davidson, K. S. M. and Schiff, L. I. (1946). Turning and course keeping qualities, *Trans. Soc. of Nav. Architects Marine Eng.* **54**: 152–200.

Díaz del Río, F., Jiménez, G., Sevillano, J., Vicente, S. and Civit Balcells, A. (1999). A generalization of path following for mobile robots, *Proc. 1999 IEEE Int. Conf. Robotics & Automation*, IEEE, Detroit, Michigan, USA, pp. 7–12.

Do, K. D., Jiang, Z. P. and Pan, J. (2002a). Robust adaptive path following of underactuated ships, *Proc. 41st IEEE Conf. Decision & Control*, IEEE, Las Vegas, Nevada, USA, pp. 3243–3248.

Do, K. D., Jiang, Z. P. and Pan, J. (2002b). Robust global output feedback stabilization of underactuated ships on a linear course, *Proc. 41st IEEE Conf. Decision & Control*, IEEE, Las Vegas, Nevada, USA, pp. 1687–1692.

Do, K. D., Jiang, Z. P., Pan, J. and Nijmeijer, H. (2004). A global output-feedback controller for stabilization and tracking of underactuated ODIN: A spherical underwater vehicle, *Automatica* **40**: 117–124.

Edwards, H. A., Lin, Y. and Wang, Y. (2000). On input-to-state stability for time-varying nonlinear systems, *Proc. 39th IEEE Conf. Decision & Control*, IEEE, Sydney, Australia, pp. 3501–3506.

Egeland, O. and Gravdahl, J. T. (2002). *Modeling and Simulation for Automatic Control*, Marine Cybernetics, Trondheim, Norway.

Encarnação, P. M. M. (2002). *Nonlinear Path Following Control Systems for Ocean Vehicles*, PhD thesis, Instituto Superior Técnico, Technical Univ. of Lisbon, Lisbon, Portugal.

Encarnação, P. and Pascoal, A. (2001a). Combined trajectory tracking and path following: An application to the coordinated control of autonomous marine craft, *Proc. 40th IEEE Conf. Decision & Control*, IEEE, Orlando, Florida, USA, pp. 964–969.

Encarnação, P. and Pascoal, A. (2001b). Combined trajectory tracking and path following for marine craft., *Proc. Mediterranean Conf. Contr. and Automation*, Dubrovnik, Croatia.

Encarnação, P. and Pascoal, A. (2001c). Combined trajectory tracking and path following for underwater vehicles., *Proc. IFAC Conf. Contr. Appl. Marine Systems*, Int. Federation of Automatic Control, Glasgow, Scotland, U.K.

Encarnação, P., Pascoal, A. and Arcak, M. (2000). Path following for autonomous marine craft, *Proc. IFAC Conf. Manoeuvering and Contr. Marine Crafts*, Int. Federation of Automatic Control, Aalborg, Denmark, pp. 117–122.

Faltinsen, O. M. (1990). *Sea Loads on Ships and Offshore Structures*, Cambridge University Press.

Fedyaevsky, K. K. and Sobolev, G. V. (1963). *Control and Stability in Ship Design*, State Union Shipbuilding Publishing House, Leningrad.

Fierro, R. and Lewis, F. L. (1995). Control of a nonholonomic mobile robot: backstepping kinematics into dynamics, *Proc. 34th IEEE Conf. Decision & Control*, Vol. 4, IEEE, Arlington, TX, USA, pp. 3805–3810.

Filippov, A. (1988). *Differential Equations with Discontinuous Right-hand sides*, Kluwer Academic Publishers.

Fjellstad, O. E. and Fossen, T. I. (1994). Singularity-free tracking of unmanned underwater vehicles in 6 DOF, *Proc. 33rd IEEE Conf. Decision & Control*, IEEE, Lake Buena Vista, FL, USA, pp. 1128–1133.

Fossen, T. (1994). *Guidance and Control of Ocean Vehicles*, John Wiley & Sons Ltd, England.

Fossen, T. I. (2002). *Marine Control Systems: Guidance, Navigation, and Control of Ships, Rigs and Underwater Vehicles*, Marine Cybernetics, Trondheim, Norway.

Fossen, T. I. (2005). A nonlinear unified state-space model for ship maneuvering and control in a seaway, *J. Bifurcation and Chaos* . To appear.

Fossen, T. I., Breivik, M. and Skjetne, R. (2003). Line-of-sight path following of underactuated marine craft, *Proc. IFAC Conf. Manoeuvering and Contr. Marine Crafts*, IFAC, Girona, Spain, pp. 244–249.

Fossen, T. I. and Grøvlen, Å. (1998). Nonlinear output feedback control of dynamically positioned ships using vectorial observer backstepping, *IEEE Trans. Contr. Sys. Tech.* **6**(1): 121–128.

Fossen, T. I., Lindegaard, K. P. and Skjetne, R. (2002). Inertia shaping techniques for marine vessels using acceleration feedback, *Proc. 15th IFAC World Congress Automatic Control*, IFAC, Barcelona, Spain.

Fossen, T. I. and Smogeli, Ø. N. (2004). Nonlinear time-domain strip theory formulation for low-speed maneuvering and station-keeping, *Modeling, Identification and Control* **25**(4): 201–221.

Fossen, T. I. and Strand, J. P. (1999). Passive nonlinear observer design for ships using lyapunov methods: full-scale experiments with a supply vessel, *Automatica* **35**(1): 3–16.

Fossen, T. I. and Strand, J. P. (2001). Nonlinear passive weather optimal positioning control (wopc) system for ships and rigs: experimental results, *Automatica* **37**(5): 701–715.

Gilbert, E. and Kolmanovsky, I. (2002). Nonlinear tracking control in the presence of state and control constraints: a generalized reference governor, *Automatica* **38**: 2063–2073.

Godhavn, J.-M., Fossen, T. I. and Berge, S. P. (1998). Non-linear and adaptive backstepping designs for tracking control of ships, *Int. J. Adaptive Contr. Signal Processing* **12**: 649–670.

Hauser, J. and Hindman, R. (1995). Maneuver regulation from trajectory tracking: Feedback linearizable systems, *Proc. IFAC Symp. Nonlinear Control Systems Design*, IFAC, Lake Tahoe, CA, USA, pp. 595–600.

Hauser, J. and Hindman, R. (1997). Aggressive flight maneuvers, *Proc. 36th IEEE Conf. Decision & Control*, IEEE, San Diego, California, USA, pp. 4186–4191.

Healey, A. J. and Lienard, D. (1993). Multivariable sliding-mode control for autonomous diving and steering of unmanned underwater vehicles, *IEEE J. Oceanic Engineering* **18**(3): 327–339.

Hindman, R. and Hauser, J. (1996). Maneuver modified trajectory tracking, *Int. Symp. Mathematical Theory Networks and Systems*, St. Louis, MO, USA.

Holzhter, T. and Schultze, R. (1996). Operating experience with a high-precision track controller for commercial ships, *Contr. Eng. Practice* **4**(3): 343–350.

Holzhüter, T. (1997). LQG approach for the high-precision track control of ships, *IEE Proc. Contr. Theory Appl.* **144**(2): 121–127.

Ihle, I.-A. F., Skjetne, R. and Fossen, T. I. (2004). Formation control of marine craft with experimental results, *Proc. IEEE Conf. Decision & Control*, IEEE, Paradise Island, Bahamas.

Isidori, A. (1995). *Nonlinear control systems*, Communications and Control Engineering Series, third edn, Springer-Verlag, Berlin.

Jiang, Z. P. and Nijmeijer, H. (1999). A recursive technique for tracking control of nonholonomic systems in chained form, *IEEE Trans. Automat. Contr.* **44**(2): 265–279.

Jiang, Z. P., Teel, A. R. and Praly, L. (1994). Small-gain theorem for ISS systems and applications, *Math. Control Signals Systems* **7**(2): 95–120.

Johansen, T. A., Fossen, T. I. and Berge, S. P. (2004). Constrained nonlinear control allocation with singularity avoidance using sequential quadratic programming, *IEEE Trans. Contr. Sys. Tech.* **12**(1): 211–216.

Johansen, T. A., Fossen, T. I. and Tøndel, P. (2005). Efficient optimal constrained control allocation via multi-parametric programming, *AIAA J. Guidance and Dynamics* .

Johansen, T. A., Fuglseth, T. P., Tøndel, P. and Fossen, T. I. (2003). Optimal constrained control allocation in marine vessels with rudders,

Proc. IFAC Conf. Manoeuvering and Contr. Marine Crafts, IFAC, Girona, Spain.

Johansen, V., Skjetne, R. and Sørensen, A. J. (2003). Maneuvering of towed interconnected marine systems, *Proc. IFAC Conf. Manoeuvering and Contr. Marine Crafts*, IFAC, Girona, Spain, pp. 292–297.

Kang, W., Xi, N. and Sparks, A. (2000). Theory and applications of formation control in a perceptive reference frame, *Proc. 39th IEEE Conf. Decision & Control*, IEEE, Sydney, Australia, pp. 352–357.

Khalil, H. K. (2002). *Nonlinear Systems*, 3 edn, Prentice-Hall, Inc, New Jersey.

Kokotović, P., Khalil, H. K. and O'Reilly, J. (1999). *Singular perturbation methods in control*, Society for Industrial and Applied Mathematics (SIAM), Philadelphia, PA. Analysis and design, Corrected reprint of the 1986 original.

Krasovskii, N. N. (1959). Problems of the theory of stability of motion, *Stanford Univ. Press* . 1963; translation of the Russion edition, Moskow.

Krstić, M., Kanellakopoulos, I. and Kokotović, P. (1995). *Nonlinear and Adaptive Control Design*, John Wiley & Sons Ltd, New York.

Lapierre, L., Soetanto, D. and Pascoal, A. (2003). Nonlinear path following with applications to the control of autonomous underwater vehicles, *Proc. 42nd IEEE Conf. Decision & Control*, IEEE, Maui, Hawaii, USA.

LaSalle, J. P. (1960). Some extensions of liapunov's second method, *IRE Trans. Circuit Theory* **CT-7**(4): 520–527.

LaSalle, J. P. (1968). Stability theory for ordinary differential equations, *J. Diff. Equations* **4**: 57–65.

Lefeber, E., Pettersen, K. Y. and Nijmeijer, H. (2001). Underactuated ship tracking control: theory and experiments, *Int. J. of Control* **74**(14): 1435–1446.

Lefeber, E., Pettersen, K. Y. and Nijmeijer, H. (2003). Tracking control of an underactuated ship, *IEEE Trans. Contr. Sys. Tech.* **11**(1): 52–61.

Lewis, E. V. (ed.) (1988). *Principles of Naval Architecture: Volume II - Resistance, Propulsion, and Vibration*, Vol. 2, 2 edn, Soc. Naval Architects & Marine Engineers.

Lin, Y. (1992). *Lyapunov Function Techniques for Stabilization*, PhD thesis, New Brunswick Rutgers, State Univ. New Jersey, New Brunswick, NJ, USA.

Lin, Y., Sontag, E. D. and Wang, Y. (1995). Input to state stabilizability for parameterized families of systems, *Int. J. Robust Nonlinear Contr.* **5**: 187–205.

Lin, Y., Sontag, E. D. and Wang, Y. (1996). A smooth converse Lyapunov theorem for robust stability, *SIAM J. Contr. and Optim.* **34**(1): 124–160.

Lindegaard, K.-P. (2003). *Acceleration Feedback in Dynamic Positioning*, PhD thesis, Norwegian Univ. Science & Technology, Dept. Eng. Cybernetics, Trondheim, Norway.

Lindegaard, K.-P. and Fossen, T. I. (2003). Fuel efficient rudder and propeller control allocation for marine craft: Experiments with a model ship, *IEEE Trans. Contr. Sys. Tech.* **11**(6).

Lindegaard, K.-P. and Fossen, T. I. (n.d.). Increasing performance of dynamically positioned vessels by acceleration feedback: Experimental results, *Automatica* . Submitted Oct. 6, 2002.

Lipschutz, M. (1969). *Schaum's outline of Theory and Problems of Differential Geometry*, McGraw-Hill Book Company, New York.

Loría, A., Fossen, T. I. and Panteley, E. (2000). A Separation Principle for Dynamic Positioning of Ships: Theoretical and Experimental Results, *IEEE Trans. Contr. Sys. Tech.* **8**(2): 332–343.

Loría, A. and Nijmeijer, H. (1998). Bounded output feedback tracking control of fully actuated Euler-Lagrange systems, *Systems Control Lett.* **33**(3): 151–161.

Loría, A., Panteley, E., Popović, D. and Teel, A. R. (2002). An extension of Matrosov's theorem with application to stabilization of nonholonomic control systems, *Proc. 41st IEEE Conf. Decision & Control*, IEEE, Las Vegas, NV, USA, pp. 1528–1533.

Matrosov, V. M. (1962). On the stability of motion, *J. Appl. Math. Mech.* **26**(5): 1337–1353.

Mazenc, F. and Praly, L. (1994). Global stabilization by output feedback: examples and counterexamples, *Systems Contr. Lett.* **23**(2): 119–125.

Meriam, J. L. and Kraige, L. G. (1993). *Engineering Mechanics: Dynamics*, Vol. 2, 3 edn, John Wiley & Sons Ltd, New York.

Micaelli, A. and Samson, C. (1993). Trajectory tracking for unicycle-type and two-steering-wheels mobile robots., *Research Report 2097*, Inst. National de Recherche en Informatique et en Automatique.

Minorsky, N. (1922). Directional stability of automatically steered bodies, *J. Am. Soc. Naval Eng.* **34**: 284.

MSN Learning and Research (2003). Internet. http://encarta.msn.com.

Newman, J. N. (1999). *Marine Hydrodynamics*, 9 edn, The MIT Press, Cambridge, Massachusetts.

Nijmeijer, H. and Fossen, T. (eds) (1999). *New directions in nonlinear observer design*, Springer-Verlag London Ltd., London. Int. Workshop, Geiranger, Norway, June, 1999.

Nomoto, K., Taguchi, T., Honda, K. and Hirano, S. (1957). On the steering qualities of ships, *Technical report 4*, Int. Shipbuilding Progress.

Norrbin, N. H. (1970). Theory and observation on the use of a mathematical model for ship maneuvering in deep and confined waters, *8th Symp. Naval Hydrodynamics*, Pasadena, California, USA.

Ortega, R., Loría, A., Nicklasson, P. J. and Sira-Ramírez, H. (1998). *Passivity-based Control of Euler-Lagrange Systems*, Springer-Verlag, London.

Paden, B. and Panja, R. (1988). Globally asymptotically stable 'PD+' controller for robot manipulators, *Int. J. of Control* **47**(6): 1697–1712.

Pascoal, A. (2003). Control of autonomous marine vehicles, *Proc. IFAC Conf. Manoeuvering and Contr. Marine Crafts*, IFAC, Girona, Spain. Conference Tutorial.

Perez, T. (2005). *Introduction to Ship Motion Control: Autopilots with Rudder Roll Stabilisation and Rudder-Fin Stabilisers*, Springer-Verlag. Advances in Industrial Control Series.

Pettersen, K. Y. and Lefeber, E. (2001). Way-point tracking control of ships., *Proc. 40th IEEE Conf. Decision & Control*, IEEE, Orlando, Florida, USA, pp. 940–945.

Rodrigues, L., Tavares, P. and Prado, M. (1996). Sliding mode control of an AUV in the diving and steering planes, *Proc. MTS/IEEE OCEANS*, Vol. 2, IEEE, Fort Lauderdale, FL, USA, pp. 576–583.

Rouche, N., Habets, P. and Laloy, M. (1977). *Stability Theory by Liapunov's Direct Method*, Vol. 22, Springer-Verlag, New York, USA. Appl. math. sciences.

Sarkar, N., Yun, X. and Kumar, V. (1993). Dynamic Path Following: A new Control Algorithm for Mobile Robots., *Proc. 32nd IEEE Conf. Decision & Control*, IEEE, San Antonio, Texas, USA, pp. 2670–2675.

Schoenwald, D. A. (2000). Auvs: In space, air, water, and on the ground, *IEEE Contr. Sys. Mag.* **20**(6): 15–18.

Shiriaev, A. S. and Canudas-de Wit, C. (2005). Virtual constraints: a constructive tool for orbital stabilization, *IEEE Trans. Automat. Contr.* . To appear.

Shiriaev, A. S., Robertsson, A., Pacull, P. and Fossen, T. I. (2005). Motion planning and its feedback stabilization for underactuated ships: Virtual constraints approach, *Proc. IFAC World Congress Automatic Control*, IFAC, Prague, Czech Republic. To appear.

Skjetne, R. (2003). Ship maneuvering: The past, the present and the future, *Sea Technology* **44**(3): 33–37.

Skjetne, R. and Fossen, T. (2004). On integral control in backstepping: Analysis of different techniques, *Proc. American Control Conf.*, AACC, Boston, USA.

Skjetne, R. and Fossen, T. I. (2001). Nonlinear maneuvering and control of ships, *Proc. MTS/IEEE OCEANS*, IEEE, Honolulu, Hawaii, pp. 1808–1815.

Skjetne, R., Fossen, T. I. and Kokotović, P. (2002). Output maneuvering for a class of nonlinear systems, *Proc. 15th IFAC World Congress Automatic Control*, Barcelona, Spain.

Skjetne, R., Fossen, T. I. and Kokotović, P. V. (2004). Robust output maneuvering for a class of nonlinear systems, *Automatica* **40**(3): 373–383.

Skjetne, R., Fossen, T. I. and Kokotović, P. V. (2005). Adaptive output maneuvering, with experiments, for a model ship in a marine control laboratory, *Automatica* **41**(2): 289–298.

Skjetne, R., Ihle, I.-A. F. and Fossen, T. I. (2003). Formation control by synchronizing multiple maneuvering systems, *Proc. IFAC Conf. Manoeuvering and Contr. Marine Crafts*, IFAC, Girona, Spain, pp. 280–285.

Skjetne, R., Moi, S. and Fossen, T. I. (2002). Nonlinear formation control of marine craft, *Proc. 41st IEEE Conf. Decision & Control*, IEEE, Las Vegas, Nevada, USA, pp. 1699–1704.

Skjetne, R. and Shim, H. (2001). A systematic nonlinear observer design for a class of Euler-Lagrange systems., *Proc. Mediterranean Conf. Contr. and Automation*, Dubrovnik, Croatia.

Skjetne, R., Smogeli, Ø. and Fossen, T. I. (2004a). Modeling, identification, and adaptive maneuvering of cybership ii: A complete design with experiments, *Proc. IFAC Conf. Contr. Appl. Marine Systems*, IFAC, Ancona, Italy.

Skjetne, R., Smogeli, Ø. N. and Fossen, T. I. (2004b). A nonlinear ship maneuvering model: Identification and adaptive control with experiments for a model ship, *Modeling, Identification and Control* **25**(1): 3–27.

Skjetne, R. and Teel, A. R. (2004). Maneuvering dynamical systems by sliding-mode control, *Proc. American Control Conf.*, AACC, Boston, USA.

Skjetne, R., Teel, A. R. and Kokotović, P. V. (2002a). Nonlinear maneuvering with gradient optimization, *Proc. 41st IEEE Conf. Decision & Control*, IEEE, Las Vegas, USA, pp. 3926–3931.

Skjetne, R., Teel, A. R. and Kokotović, P. V. (2002b). Stabilization of sets parametrized by a single variable: Application to ship maneuvering, *Proc. 15th Int. Symp. Mathematical Theory of Networks and Systems*, Notre Dame, IN, USA.

Song, M., Tarn, T. J. and Xi, N. (2000). Integration of task scheduling, action planning, and control in robotic manufacturing systems, *Proc. IEEE Manuf. Syst*, Vol. 88-7, IEEE, Ford Motor Co., Dearborn, MI, USA, pp. 1097–1107.

Sontag, E. D. and Wang, Y. (1995a). On characterizations of input-to-state stability with respect to compact sets, *Proc. IFAC Symp. Nonlinear Control Systems Design*, IFAC, Tahoe City, CA, USA, pp. 226–231.

Sontag, E. D. and Wang, Y. (1995b). On characterizations of the input-to-state stability property, *Systems Contr. Lett.* **24**(5): 351–359.

Sontag, E. D. and Wang, Y. (1996). New characterizations of input-to-state stability, *IEEE Trans. Automat. Contr.* **41**(9): 1283–1294.

Sontag, E. and Wang, Y. (2000). Lyapunov characterizations of input to output stability, *SIAM J. Contr. and Optim.* **39**(1): 226–249 (electronic).

Sørensen, A. (2005). *Marine Cybernetics: Modelling and Control*, 5 edn, Norwegian Univ. Science & Technology, Dept. Marine Technology, Trondheim, Norway. Lecture notes.

Sørensen, A. J., Sagatun, S. I. and Fossen, T. I. (1996). Design of a dynamic positioning system using model-based control, *Contr. Eng. Practice* **4**(3): 359–368.

Sperry Marine (2004). A short history of sperry marine, Internet. <http://www.litton-marine.com/Company-Information/Corporate-History/Sperry-History>.

Stilwell, D. J. and Bishop, B. E. (2000). Platoons of underwater vehicles, *IEEE Contr. Sys. Mag.* **20**(6): 45–52.

Strand, J. P. (1999). *Nonlinear Position Control Systems Design for Marine Vessels*, PhD thesis, Norwegian Univ. Science & Technology, Dept. Eng. Cybernetics, Trondheim, Norway.

Teel, A. R. (2002). Notes on nonlinear control and analysis, Univ. California, Santa Barbara. Lecture Notes: Courses ECE 236, 237, and 594D.

Teel, A. R., Moreau, L. and Nešić, D. (2003). A unified framework for input-to-state stability in systems with two time scales, *IEEE Trans. Automat. Contr.* **48**(9): 1526 – 1544.

Teel, A. R., Panteley, E. and Loría, A. (2002). Integral characterizations of uniform asymptotic and exponential stability with applications, *Math. Control Signals Systems* **15**: 177–201.

Teel, A. R. and Praly, L. (2000). A smooth lyapunov function from a class-$\mathcal{KL}$ estimate involving two positive semidefinite functions, *ESAIM: Control, Optimisation and Calculus of Variations* **5**: 313–367.

The Society of Naval Architects and Marine Engineers (1950). Nomenclature for treating the motion of a submerged body through a fluid, Technical and Research Bulletin No. 1-5.

Utkin, V. I. (1992). *Sliding modes in control and optimization*, Communications and Control Engineering Series, Springer-Verlag, Berlin. Translated and revised from the 1981 Russian original.

Vestgård, K., Hansen, R., Jalving, B. and Pedersen, O. A. (2001). The HUGIN 3000 survey AUV, *ISOPE-2001*, Stavanger, Norway.

Yoerger, D. R. and Slotine, J.-J. E. (1985). Robust trajectory control of underwater vehicles, *IEEE J. Oceanic Engineering* **10**(4): 462–470.

Yoshizawa, T. (1966). Stability theory by lyapunov's second method, *The Mathematical Society of Japan* .

Young, K., Utkin, V. and Ozguner, U. (1999). A control engineer's guide to sliding mode control, *IEEE Trans. Contr. Sys. Tech.* **7**(3): 328–342.

Zhang, F., Dawson, D. M., de Queiroz, M. S. and Dixon, W. E. (1997). Global adaptive output feedback tracking control of robot manipulators, *Proc. 36th IEEE Conf. Decision & Control*, IEEE, San Diego, California, USA, pp. 3634–3639.

Zhang, R., Chen, Y., Sun, Z., Sun, F. and Xu, H. (1998). Path Control of a Surface Ship in Restricted Waters Using Sliding Mode, *Proc. 37th IEEE Conf. Decision & Control*, Tampa, Florida, USA, pp. 3195–3200.

Zhao, H. and Chen, D. (1993). Exact and stable tip trajectory tracking for multi-link flexible manipulator, *Proc. 32nd IEEE Conf. Decision & Control*, IEEE, San Antonio, TX, USA, pp. 1371–1376.

Appendix A

Stability tools

In this appendix we will give a treatment of important tools for analyzing stability in the designs presented in the main chapters of this thesis. This inludes both stability of equilibria and the more general concept of set-stability. A variety of references are used where the most important are Lin (1992); Lin et al. (1995); Sontag and Wang (1995a); Lin et al. (1996); Teel and Praly (2000); Teel (2002); Khalil (2002).

A.1 Ordinary differential equations

Consider the time-varying ordinary differential equation[1]

$$\dot{x} = f(x,t) \tag{A.1}$$

where for each $t \geq 0$ the vector $x(t) \in \mathbb{R}^n$ is the state.

To ensure existence and uniqueness of solutions, f is assumed to satisfy the following properties (Teel; 2002): For each starting point $(x_0, t_0) \in \mathbb{R}^n \times \mathbb{R}$ and each compact set $\mathcal{X} \times \mathcal{T}$ containing (x_0, t_0) then:

- for all $(x,t) \in \mathcal{X} \times \mathcal{T}$, the function $f(\cdot, t)$ is continuous and $f(x, \cdot)$ is piecewise continuous,
- there exists $L > 0$ such that

$$|f(x,t) - f(y,t)| \leq L\,|x-y|\,, \qquad \forall (x,y,t) \in \mathcal{X} \times \mathcal{X} \times \mathcal{T},$$

[1] Since the vector x in reality is a function of time, the notation $\dot{x}(t) = f(x(t),t)$ would perhaps be more precise than (A.1). However, to indicate that t in (A.1) is an explicit time-variation in the system, the notation without the time argument for the states is chosen.

- f is bounded on $\mathcal{X} \times \mathcal{T}$.

This will ensure that there exists $T > t_0 \geq 0$ such that there is one and only one solution of (A.1) on $[t_0, T]$. Often we simply assume that $f(\cdot, \cdot)$ is smooth which implies all the above conditions.

Let $x(t, t_0, x_0)$ denote the solution of (A.1) at time t with initial time and state $x(t_0) = x_0$ where $0 \leq t_0 < \infty$. If there is no ambiguity from the context, the solution is simply written as $x(t)$ with the initial state x_0 at time t_0. The solution is defined on some maximal interval of existence $(T_{\min}(x_0), T_{\max}(x_0))$ where $T_{\min}(x_0) < t_0 < T_{\max}(x_0)$. The system (A.1) is said to be *forward complete* if $T_{\max}(x_0) = +\infty$ for all x_0, *backward complete* if $T_{\min}(x_0) = -\infty$ for all x_0, and *complete* if it is both forward and backward complete (Lin et al.; 1996).

A solution is an absolutely continuous function satisfying $x(t_0, t_0, x_0) = x_0$ and:

- $x(\cdot, t_0, x_0)$ is differentiable a.e. on $(T_{\min}, T_{\max})$,
- $\frac{d}{dt}x(t, t_0, x_0) = f(x(t, t_0, x_0), t)$ is Lesbegue integrable on $(T_{\min}, T_{\max})$,
- $x(t, t_0, x_0) - x_0 = \int_{t_0}^{t} \frac{d}{dt}x(\tau, t_0, x_0)d\tau = \int_{t_0}^{t} f(x(\tau, t_0, x_0), \tau)d\tau$.

A convenient but crude way to ensure forward completeness is:

Proposition A.1 *(Teel; 2002) Suppose the function $f : \mathbb{R}^n \times \mathbb{R}_{\geq 0} \to \mathbb{R}^n$ satisfies the above conditions for existence and uniqueness of solutions. Suppose also that $f(\cdot, \cdot)$ satisfies a global sector bound, that is, $\exists L \geq 0$ and $c \geq 0$ such that $\forall (x, t)$,*

$$|f(x, t)| \leq L\,|x| + c.$$

Then all solutions are defined for all $t \geq t_0$.

To prove this proposition, a differential version of the Gronwall-Bellman lemma is needed:

Lemma A.2 *Let $y : \mathbb{R} \to \mathbb{R}$ be absolutely continuous and satisfy*

$$\dot{y}(t) \leq a(t)y(t) + b(t), \quad \text{a.e. } t \in [t_0, t_1] \tag{A.2}$$

where $a(t)$, $b(t)$ are continuously differentiable functions that satisfy $\dot{a}(t)b(t) - a(t)\dot{b}(t) = 0$ and $0 < a_0 \leq |a(t)| < \infty$ for some a_0 and $|b(t)| < \infty$, $\forall t \in [t_0, t_1]$. Then,

$$y(t) \leq \left(y(t_0) + \frac{b(t_0)}{a(t_0)}\right) \exp\left(\int_{t_0}^{t} a(s)ds\right) - \frac{b(t)}{a(t)}, \quad \forall t \in [t_0, t_1]. \tag{A.3}$$

If $b \equiv 0$ then the above constraints can be relaxed and $a(t)$ needs only be locally integrable to give

$$y(t) \leq y(t_0) \exp\left(\int_{t_0}^{t} a(s)ds\right), \quad \forall t \in [t_0, t_1]. \tag{A.4}$$

Furthermore, when a, b are constants, the result is

$$y(t) \leq \left(y(t_0) + \frac{b}{a}\right) \exp\left(a(t - t_0)\right) - \frac{b}{a}. \tag{A.5}$$

Proof. *Consider the differentiable function*

$$\eta(t) := \left(y(t) + \frac{b(t)}{a(t)}\right) \exp\left(-\int_{t_0}^{t} a(s)ds\right). \tag{A.6}$$

In view of (A.2) and the constraints, differentiation gives

$$\begin{aligned}
\dot{\eta}(t) = &\left(\dot{y}(t) + \frac{\dot{b}(t)a(t) - b(t)\dot{a}(t)}{a(t)^2}\right) \exp\left(-\int_{t_0}^{t} a(s)ds\right) \\
&- a(t)\left(y(t) + \frac{b(t)}{a(t)}\right) \exp\left(-\int_{t_0}^{t} a(s)ds\right) \\
&= \left(\dot{y}(t) - a(t)y(t) - b(t)\right) \exp\left(-\int_{t_0}^{t} a(s)ds\right) \\
&\leq 0.
\end{aligned} \tag{A.7}$$

This implies that $\eta(t) \leq \eta(t_0)$, $\forall t \in [t_0, t_1]$ so that when substituting the definition for $\eta(\cdot)$ and using that $\exp\left(-\int_{t_0}^{t} a(s)ds\right) > 0$ gives (A.3). When $b \equiv 0$, then the fraction b/a in (A.6) vanishes so that the same result follows by only a locally integrable function $a(\cdot)$. ■

Proof of Proposition A.1: *Consider $y := |x| = \sqrt{x^\top x}$ which is continuously differentiable on $\mathbb{R}^n \backslash \{0\}$. Suppose that a solution $x(t, t_0, x_0)$ of $\dot{x} = f(x, t)$ escapes at the finite time $T > t_0$. Then, for each $M < \infty$ there exists $\tau \in [t_0, T)$ such that $|x(\tau, t_0, x_0)| > M$. Differentiating y with respect to time gives for each compact time interval $[t_1, t_2] \subset [t_0, T)$, with $x(t) \neq 0$ $\forall t \in [t_1, t_2]$,*

$$\dot{y}(t) = \frac{d}{dt}\left|x(t, t_1, x_1)\right| = \frac{x(t, t_1, x_1)^\top f(x(t, t_1, x_1), t)}{|x(t, t_1, x_1)|} \leq Ly(t) + c$$

where $x_1 := x(t_1, t_0, x_0)$. *In view of Lemma A.2 this implies that*

$$|x(t, t_1, x_1)| \leq \left(|x_1| + \frac{c}{L}\right) e^{L(t-t_1)} - \frac{c}{L}, \qquad \forall t \in [t_1, t_2].$$

By picking $M > \left(|x_1| + \frac{c}{L}\right) e^{L(T-t_1)} - \frac{c}{L}$ *this last inequality implies that no* $\tau \in [t_0, T)$ *can be found so that* $|x(\tau, t_0, x_0)| > M$. *By contradiction it follows that* $T = \infty$.

Some convenient classes of functions are next defined. These are instrumental in nonlinear control theory.

Definition A.3 *A function* $\alpha : \mathbb{R}_{\geq 0} \to \mathbb{R}_{\geq 0}$ *with* $\alpha(0) = 0$ *is positive semi-definite if* $\alpha(s) \geq 0$ *for* $s > 0$ *and positive definite if* $\alpha(s) > 0$ *for* $s > 0$. *It belongs to class-*$\mathcal{K}$ *(*$\alpha \in \mathcal{K}$*) if it is continuous,* $\alpha(0) = 0$, *and* $\alpha(s_2) > \alpha(s_1)$, $\forall s_2 > s_1$, *and it belongs to class-*$\mathcal{K}_\infty$ *(*$\alpha \in \mathcal{K}_\infty$*) if in addition* $\lim_{s\to\infty} \alpha(s) = \infty$. *A function* $\beta : \mathbb{R}_{\geq 0} \times \mathbb{R}_{\geq 0} \to \mathbb{R}_{\geq 0}$ *belongs to class-*$\mathcal{KL}$ *(*$\beta \in \mathcal{KL}$*) if for each fixed* $t \geq 0$, $\beta(\cdot, t) \in \mathcal{K}$, *and for each fixed* $s \geq 0$, $\beta(s, \cdot)$ *is nonincreasing and* $\lim_{t\to\infty} \beta(s, t) = 0$.

An equilibrium point $x_e \in \mathbb{R}^n$ of (A.1) at $t = t_0$ is a point such that $f(x_e, t) = 0$, $\forall t \geq t_0$. Such an equilibrium can always be shifted to the origin, giving the following stability definitions:

Definition A.4 *For the system (A.1), the origin* $x = 0$ *is:*

- Uniformly Stable *(US) if there exists* $\delta(\cdot) \in \mathcal{K}_\infty$ *such that for any* $\varepsilon > 0$,
$$|x_0| \leq \delta(\varepsilon), \ t \geq t_0 \geq 0 \ \Rightarrow \ |x(t, t_0, x_0)| \leq \varepsilon. \tag{A.8}$$
- Uniformly Globally Asymptotically Stable *(UGAS) if it is US and* Uniformly Attractive *(UA), that is, for each* $\varepsilon > 0$ *and* $r > 0$ *there exists* $T > t_0 \geq 0$ *such that*
$$|x_0| \leq r, \ t \geq T \ \Rightarrow \ |x(t, t_0, x_0)| \leq \varepsilon. \tag{A.9}$$

The following comparison principle (Lin et al.; 1996, Lemma 4.4) is also useful, especially in proving asymptotic stability by Lyapunov arguments and $\mathcal{KL}$-estimates:

Lemma A.5 *For each continuous positive definite function α there exists a $\mathcal{KL}$-function $\beta_\alpha(s,t)$ with the following property: if $y(\cdot)$ is any (locally) absolutely continuous function defined for each $t \geq t_0 \geq 0$ and with $y(t) \geq 0$, $\forall t \geq t_0$, and $y(\cdot)$ satisfies the differential inequality*

$$\dot{y}(t) \leq -\alpha(y(t)), \qquad a.a.\ t \geq t_0 \tag{A.10}$$

with $y(t_0) = y_0 \geq 0$, then it holds that

$$y(t) \leq \beta_\alpha(y_0,\ t - t_0), \qquad \forall t \geq t_0. \tag{A.11}$$

Proof. *See Lin et al. (1996, Lemma 4.4).* ■

A.2 Set-stability

Often we will consider more general attractors than the compact equilibrium set $\mathcal{A}_e = \{x \in \mathbb{R}^n :\ x = x_e\}$. Such attractors will be closed subsets of the state space. They can be compact or noncompact sets. In order to measure the distance away from the set, the "distance to the set $\mathcal{A}$ function" is defined as

$$|x|_{\mathcal{A}} := d\,(x; \mathcal{A}) = \inf\{d(x,y) :\ y \in \mathcal{A}\} \tag{A.12}$$

where the point-to-point distance function is here simply taken as the Euclidean distance $d(x,y) = |x - y|$. Stability of the set is then determined in terms of bounds on the distance function.

In this framework, as shown by Teel and Praly (2000), we can consider the explicit time dependence of $t \mapsto f(x,t)$ in (A.1) as a state with its own dynamics and analyze stability of an augmented system with respect to a noncompact set in which t is free. For clarity, for this purpose we use the variable p, that is, the extended-state dynamic system becomes

$$\dot{z} = \frac{d}{dt}\begin{bmatrix} x \\ p \end{bmatrix} = \begin{bmatrix} f(x,p) \\ 1 \end{bmatrix} =: g(z) \qquad z_0 = \begin{bmatrix} x_0 \\ t_0 \end{bmatrix}. \tag{A.13}$$

Correspondingly, the time variable for the new extended-state system will be denoted by t with initial time $t = 0$. Notice that, in particular, $p(t) = t + t_0$ for all $t \geq 0$ and consequently $f(\cdot, p(t))$ for $t \geq 0$ is equal to $f(\cdot, t)$ for $t \geq t_0 \geq 0$. According to Lin (1992, Lemma 5.1.1) it follows that $x(t, t_0, x_0)$ is a solution of (A.1) for $t \geq t_0 \geq 0$ if and only if $z(t, z_0) := \mathrm{col}\,(x(t + t_0, t_0, x_0), t + t_0)$ is a solution of (A.13) for $t \geq 0$.

Stability of the origin $x = 0$ for (A.1) is captured by stability of the set of points

$$\mathcal{A}' = \{(x,p) \in \mathbb{R}^n \times \mathbb{R}_{\geq 0} :\ x = 0\} \tag{A.14}$$

for which the distance-to-the-set function becomes $|z|_{\mathcal{A}'} = \inf\{|z-y| : \ y \in \mathcal{A}'\} = |x|$.

With this motivation in mind we can therefore, in general, use set-stability analysis for time-invariant ODEs

$$\dot{x} = f(x) \tag{A.15}$$

where $x(t, x_0) \in \mathbb{R}^n, \ \forall t \geq 0$, is the solution with initial condition $x_0 = x(0)$.

Definition A.6 *A nonempty closed set $\mathcal{A} \subset \mathbb{R}^n$ is a forward invariant set for (A.15) if the system is forward complete and $\forall x_0 \in \mathcal{A}$ the solution $x(t, x_0) \in \mathcal{A}$, $\forall t \geq 0$.*

For noncompact sets there is a possibility that a solution may escape to infinity in finite time within the set. Forward completeness is therefore a requirement in stability analysis of such sets. The tool called *finite escape-time detectability through* $|\cdot|_{\mathcal{A}}$ is helpful:

Definition A.7 *(Teel; 2002) The system (A.15) is finite escape-time detectable through $|\cdot|_{\mathcal{A}}$ if, whenever a solution's maximal interval of existence is bounded, that is, $x(t, x_0)$ is defined only on $[0, T)$ with T finite, then $\lim_{t \nearrow T} |x(t, x_0)|_{\mathcal{A}} = \infty$.*

This is equivalent to what is called the *unboundedness observability property* in Mazenc and Praly (1994) by defining the output $y = h(x) = |x|_{\mathcal{A}}$. Nevertheless, we will continue using finite escape-time detectability to ensure forward completeness of the system.

Stability definitions using $\varepsilon - \delta$ neighborhoods as in Definition A.4 is, as shown by Lin et al. (1996); Khalil (2002), equivalent to using class-$\mathcal{K}$ and class-$\mathcal{KL}$ estimates. For stability of sets we have:

Definition A.8 *If the system (A.15) is forward complete, then for this system a closed, forward invariant set $\mathcal{A} \subset \mathbb{R}^n$ is:*

1. *Uniformly Globally Stable (UGS) if there exists a class-$\mathcal{K}_\infty$ function φ such that, $\forall x_0 \in \mathbb{R}^n$, the solution $x(t, x_0)$ satisfies*

$$|x(t, x_0)|_{\mathcal{A}} \leq \varphi\left(|x_0|_{\mathcal{A}}\right), \qquad \forall t \geq 0. \tag{A.16}$$

2. *Uniformly Globally Asymptotically Stable (UGAS) if there exists a class-$\mathcal{KL}$ function β such that, $\forall x_0 \in \mathbb{R}^n$, the solution $x(t, x_0)$ satisfies*

$$|x(t, x_0)|_{\mathcal{A}} \leq \beta\left(|x_0|_{\mathcal{A}}, \ t\right), \qquad \forall t \geq 0, \tag{A.17}$$

3. *Uniformly Globally Exponentially Stable (UGES) if there exist strictly positive real numbers $k > 0$ and $\lambda > 0$ such that, $\forall x_0 \in \mathbb{R}^n$, the solution $x(t, x_0)$ satisfies*

$$|x(t, x_0)|_{\mathcal{A}} \leq k\, |x_0|_{\mathcal{A}}\, e^{-\lambda t}, \qquad \forall t \geq 0. \tag{A.18}$$

When $\mathcal{A}$ is compact (for instance an equilibrium point), the forward completeness assumptions is redundant since in this case the system is finite escape-time detectable through $|\cdot|_{\mathcal{A}}$, and the above bounds therefore imply that solutions are bounded on the maximal interval of existence.

Definition A.9 *A smooth Lyapunov function for (A.15) with respect to a nonempty, closed, forward invariant set $\mathcal{A} \subset \mathbb{R}^n$ is a function $V : \mathbb{R}^n \to \mathbb{R}_{\geq 0}$ that satisfies:*

1. *there exist two $\mathcal{K}_\infty$-functions α_1 and α_2 such that for any $x \in \mathbb{R}^n$,*

$$\alpha_1(|x|_{\mathcal{A}}) \leq V(x) \leq \alpha_2(|x|_{\mathcal{A}}), \tag{A.19}$$

2. *there exists a continuous and, at least, positive semidefinite function α_3 such that for any $x \in \mathbb{R}^n \backslash \mathcal{A}$,*

$$V^x(x) f(x) \leq -\alpha_3(|x|_{\mathcal{A}}). \tag{A.20}$$

Note that when $\mathcal{A}$ is compact, the existence of α_2 is a mere consequence of continuity of V. We now have:

Theorem A.10 *Assume the system (A.15) is finite escape-time detectable through $|\cdot|_{\mathcal{A}}$. If there exists a smooth Lyapunov function for the system (A.15) with respect to a nonempty, closed, forward invariant set $\mathcal{A} \subset \mathbb{R}^n$, then $\mathcal{A}$ is UGS with respect to (A.15). Furthermore, if α_3 is strengthened to a positive definite function, then $\mathcal{A}$ is UGAS with respect to (A.15), and if $\alpha_i(|x|_{\mathcal{A}}) = c_i\, |x|^r_{\mathcal{A}}$ for $i = 1, 2, 3$, where c_1, c_2, c_3, r are strictly positive reals with $r \geq 1$, then $\mathcal{A}$ is UGES with respect to (A.15).*

Proof. *By integrating (A.20) along the solutions of $x(t, x_0)$ we get*

$$\begin{aligned} V(x(t, x_0)) - V(x_0) &= \int_0^t \frac{d}{dt} \{V(x(\tau, x_0))\}\, d\tau \\ &= \int_0^t V^x(x(\tau, x_0)) f(x(\tau, x_0)) d\tau \\ &\leq -\int_0^t \alpha_3(|x(\tau, x_0)|_{\mathcal{A}}) d\tau \leq 0, \quad t \geq 0 \end{aligned}$$

showing that $V(x(t,x_0)) \leq V(x_0)$, *and consequently that*

$$|x(t,x_0)|_{\mathcal{A}} \leq \alpha_1^{-1}\left(V(x(t,x_0))\right) \leq \alpha_1^{-1}\left(V(x_0)\right) \leq \alpha_1^{-1}\left(\alpha_2\left(|x_0|_{\mathcal{A}}\right)\right) \quad \text{(A.21)}$$

for all t *in the maximal interval of existence* $[0,T)$. *Suppose the system escapes at a finite time* $T > 0$. *From the finite escape-time detectability property, this means that for each* $M < \infty$ *there exists* $t_1 \in [0,T)$ *such that* $|x(t_1,x_0)|_{\mathcal{A}} > M$. *Picking* $M > \alpha_1^{-1}\left(\alpha_2\left(|x_0|_{\mathcal{A}}\right)\right)$ *contradicts that (A.21) must hold* $\forall t \in [0,T)$. *Hence,* $T = \infty$ *and the system is forward complete. By defining* $\varphi(\cdot) := \alpha_1^{-1}\left(\alpha_2(\cdot)\right) \in \mathcal{K}_\infty$, *then (A.21) proves UGS according to (A.16). Suppose next that* $\alpha_3(\cdot)$ *is positive definite. From (A.19) and (A.20) we have*

$$\frac{d}{dt}\left\{V(x(t,x_0))\right\} \leq -\alpha(V(x(t,x_0)))$$

where $\alpha(\cdot) := \alpha_3(\alpha_2^{-1}(\cdot))$ *is positive definite. Let* $\beta_\alpha(\cdot,\cdot)$ *be the class-*$\mathcal{KL}$ *function, corresponding to* α, *from Lemma A.5. This gives*

$$\begin{array}{rcll} V(x(t,x_0)) & \leq & \beta_\alpha(V(x_0),\, t), & \forall t \geq 0 \\ & \Downarrow & & \\ |x(t,x_0)|_{\mathcal{A}} & \leq & \alpha_1^{-1}\left(V(x(t,x_0))\right) \leq \alpha_1^{-1}\left(\beta_\alpha(V(x_0),\, t)\right) & \\ & \leq & \alpha_1^{-1}\left(\beta_\alpha(\alpha_2(|x_0|_{\mathcal{A}}),\, t)\right) =: \beta\left(|x_0|_{\mathcal{A}},\, t\right), & \forall t \geq 0, \end{array}$$

where $\beta \in \mathcal{KL}$ *and UGAS follows from (A.17). In the last case we have that* $\alpha_i(|x|_{\mathcal{A}}) = c_i\,|x|_{\mathcal{A}}^r$ *for* $c_i > 0$ *and* $r \geq 1$, *and this gives*

$$\begin{array}{rcll} |x(t,x_0)|_{\mathcal{A}} & \leq & \sqrt[r]{\dfrac{1}{c_1}V(x(t,x_0))} \leq \sqrt[r]{\dfrac{1}{c_1}V(x_0)}e^{-\frac{c_3}{r}t} & \\ & \leq & \sqrt[r]{\dfrac{c_2}{c_1}}\,|x_0|_{\mathcal{A}}\,e^{-\frac{c_3}{r}t}, & \forall t \geq 0, \end{array}$$

which shows UGES according to (A.18). ■

A.3 Set-stability for systems with inputs

Consider the system

$$\dot{x} = f(x,u) \quad \text{(A.22)}$$

where $x(t) \in \mathbb{R}^n$, $u(t) \in \mathbb{R}^m$, $\forall t \geq 0$, and the map $f : \mathbb{R}^n \times \mathbb{R}^m \to \mathbb{R}^n$ is smooth. The input u is a measurable, locally essentially bounded function $u : \mathbb{R}_{\geq 0} \to \mathbb{R}^m$. The space of such functions is denoted $\mathcal{L}_\infty^m$ with the norm

$||u_{[t_0,\infty)}|| := \operatorname{ess\,sup}\{u(t) : t \geq t_0 \geq 0\}$. We use $||u|| = ||u_{[0,\infty)}||$ and let $||u_{[0,t]}||$ be the signal norm over the truncated interval $[0,t]$. For each initial state $x_0 = x(0) \in \mathbb{R}^n$ and each $u \in \mathcal{L}_\infty^m$, let $x(t, x_0, u)$ denote the solution of (A.22) at time t. If there is no ambiguity from the context, the solution is simply written $x(t)$.

For a nonempty closed set $\mathcal{A} \subset \mathbb{R}^n$ we have:

Definition A.11 *The set $\mathcal{A}$ is called a 0-invariant set for (A.22) if, for the associated "zero-input" system*

$$\dot{x} = f(x, 0) =: f_0(x), \tag{A.23}$$

it holds that for each $x_0 \in \mathcal{A}$ then $x(t, x_0, 0) \in \mathcal{A}$ for all $t \geq 0$.

Definition A.12 *The system (A.22) is input-to-state stable (ISS) with respect to a closed, 0-invariant set $\mathcal{A}$ if there exist $\beta \in \mathcal{KL}$ and $\gamma \in \mathcal{K}$ such that for each $u \in \mathcal{L}_\infty^m$ and all initial states x_0, the solution $x(t, x_0, u)$ is defined for all $t \geq 0$ and satisfies*

$$|x(t, x_0, u)|_{\mathcal{A}} \leq \beta\left(|x_0|_{\mathcal{A}},\ t\right) + \gamma\left(\left|\left|u_{[0,t]}\right|\right|\right) \tag{A.24}$$

for each $t \geq 0$.

Definition A.13 *A smooth ISS-Lyapunov function for the system (A.22) with respect to the closed set $\mathcal{A}$ is a smooth function $V : \mathbb{R}^n \to \mathbb{R}_{\geq 0}$ that satisfies:*

1. *there exist two class-$\mathcal{K}_\infty$ functions α_1 and α_2 such that for any $x \in \mathbb{R}^n$,*

$$\alpha_1\left(|x|_{\mathcal{A}}\right) \leq V(x) \leq \alpha_2\left(|x|_{\mathcal{A}}\right), \tag{A.25}$$

2. *there exist a class-$\mathcal{K}$ function α_3 and a $\mathcal{K}_\infty$-function χ such that for all $x \in \mathbb{R}^n$ and $u \in \mathbb{R}^m$,*

$$|x|_{\mathcal{A}} \geq \chi(|u|) \ \Rightarrow\ V^x(x) f(x, u) \leq -\alpha_3\left(|x|_{\mathcal{A}}\right). \tag{A.26}$$

For compact sets $\mathcal{A}$, an equivalent representation of (A.26) is:

2.' *There exist two class-$\mathcal{K}_\infty$ functions α_3 and α_4 such that for all $x \in \mathbb{R}^n$ and $u \in \mathbb{R}^m$,*

$$V^x(x) f(x, u) \leq -\alpha_3\left(|x|_{\mathcal{A}}\right) + \alpha_4\left(|u|\right). \tag{A.27}$$

Note that (A.27) implies (A.26) for both compact and noncompact sets:

$$\begin{array}{rcl} V^x(x)f(x,u) & \leq & -\alpha_3\left(|x|_{\mathcal{A}}\right)+\alpha_4\left(|u|\right) \\ & \Downarrow & \\ V^x(x)f(x,u) & \leq & -\varepsilon\alpha_3\left(|x|_{\mathcal{A}}\right) \end{array}$$

for all $|x|_{\mathcal{A}} \geq \alpha_3^{-1}\left(\frac{1}{1-\varepsilon}\alpha_4\left(|u|\right)\right) =: \chi(|u|)$ where $\varepsilon \in (0,1)$. The converse is a bit more technical (Sontag and Wang; 1995b, Remark 2.4) and not generically true for noncompact sets (Sontag and Wang; 1995a, Remark 2.9).

These preliminaries now lead to the ISS sufficiency theorem. Some powerful converse results are found in Sontag and Wang (2000).

Theorem A.14 *Assume the closed set $\mathcal{A}$ is 0-invariant for (A.22). If the system (A.22) is finite escape-time detectable through $|\cdot|_{\mathcal{A}}$ and admits a smooth ISS-Lyapunov function with respect to $\mathcal{A}$, then it is ISS with respect to $\mathcal{A}$.*

Proof. *It follows from the bounds (A.25) and (A.26) that*

$$\forall\, |x(t)|_{\mathcal{A}} \geq \chi\left(||u||\right) \Rightarrow \frac{d}{dt}\left\{V(x(t))\right\} \leq -\alpha_3\left(\alpha_2^{-1}\left(V(x(t))\right)\right).$$

By Lemma A.5 this shows that $V(x(t))$ and, consequently, $|x(t)|_{\mathcal{A}}$ are bounded on the maximal interval of existence. By the finite escape-time detectability through $|\cdot|_{\mathcal{A}}$ property it follows that the system is forward complete and the solutions exist for all $t \geq 0$. (The proof from here is the same as given in Sontag and Wang (1995b, Lemma 2.14).) Let α_i, $i = 1,2,3$ and χ be as in Definition A.13, 1. and 2. For an inital state x_0 and input function u, let $x(t) = x(t,x_0,u)$ be the corresponding trajectory of (A.22). Define the set $:= \{x : V(x) \leq \alpha_2\left(\chi(||u||)\right)\}$. *If there exists $t_1 \geq 0$ such that $x(t_1) \in$, then $x(t) \in$ for all $t \geq t_1$. To prove this, assume otherwise. Then there exist some $t \geq t_1$ and some $\varepsilon > 0$ such that $V(x(t)) > \alpha_2\left(\chi(||u||)\right) + \varepsilon$. Let $t_2 = \inf\{t \geq t_1 : V(x(t)) \geq \alpha_2\left(\chi(||u||)\right) + \varepsilon\}$. Then $|x(t_2)|_{\mathcal{A}} \geq \chi\left(||u||\right)$ such that*

$$\dot{V}(x(t_2)) \leq -\alpha_3\left(|x(t_2)|_{\mathcal{A}}\right) \leq -\alpha_3\left(\alpha_2^{-1}\left(V(x(t_2))\right)\right) < 0.$$

Hence, there must exist $t \in (t_1,t_2)$ so that $\alpha_2\left(\chi(||u||)\right) + \varepsilon \leq V(x(t_2)) \leq V(x(t))$ which contradicts minimality of t_2.
To continue, let $t_3 = \inf\{t \geq 0 : x(t) \in$ $\}$ where t_3 may be infinite. For all $t \geq t_3$ we have that $V(x(t)) \leq \alpha_2\left(\chi(||u||)\right)$ so that

$$|x(t)|_{\mathcal{A}} \leq \alpha_1^{-1}\left(V(x(t))\right) \leq \alpha_1^{-1}\left(\alpha_2\left(\chi(||u||)\right)\right) =: \gamma\left(||u||\right). \tag{A.28}$$

Moreover, for $0 \leq t < t_3$ *then* $x(t) \notin$ *so that* $|x(t)|_{\mathcal{A}} \geq \chi(||u||)$ *and*

$$\dot{V}(x(t)) \leq -\alpha_3\left(|x(t)|_{\mathcal{A}}\right) \leq -\alpha_3\left(\alpha_2^{-1}\left(V(x(t))\right)\right) =: -\alpha\left(V(x(t))\right).$$

Let β_α *be the class-*$\mathcal{KL}$ *function from Lemma A.5 such that*

$$V(x(t)) \leq \beta_\alpha\left(V(x_0),\, t\right), \quad \forall t \in [0, t_3).$$

Define $\beta(s,\, t) := \alpha_1^{-1}\left(\beta_\alpha\left(\alpha_2\left(s\right),\, t\right)\right) \in \mathcal{KL}$. *Then for all* $0 \leq t < t_3$ *it follows that*

$$|x(t)|_{\mathcal{A}} \leq \beta\left(|x_0|_{\mathcal{A}},\, t\right). \tag{A.29}$$

Note that neither γ *or* β *depends on the initial state* x_0 *or the input function* u. *Therefore, combining (A.28) and (A.29) gives*

$$|x(t)|_{\mathcal{A}} \leq \beta\left(|x_0|_{\mathcal{A}},\, t\right) + \gamma\left(||u||\right) \tag{A.30}$$

for all $t \geq 0$, *and (A.24) follows by causality.* ■

Corollary A.15 *Suppose the system (A.22) is ISS with respect to a closed,* 0*-invariant set* $\mathcal{A}$. *Then*

$$\lim_{t\to\infty} |u(t)| = 0 \;\Rightarrow\; \lim_{t\to\infty} |x(t)|_{\mathcal{A}} = 0. \tag{A.31}$$

Proof. *For each* $\varepsilon > 0, r > 0$, *and each input function* u *such that* $\lim_{t\to\infty} u(t) = 0$, *we need to show that there exists* $T = T(\varepsilon, r, u) > 0$ *such that*

$$|x_0|_{\mathcal{A}} \leq r,\, t \geq T \;\Rightarrow\; |x(t, x_0, u)|_{\mathcal{A}} \leq \varepsilon. \tag{A.32}$$

Existence and uniqueness of solutions for all forward time implies that for all $0 \leq t_1 \leq t$, *a solution satisfies*

$$x\left(t, x(0), u\right) = x\left(t, x(t_1, x(0), u), u\right) \quad a.e. \tag{A.33}$$

This is verified by integrating (A.22) to get

$$\begin{aligned} x\left(t, x(0), u\right) &= x(0) + \int_0^t f\left(x(s), u(s)\right) ds \\ &= x(0) + \int_0^{t_1} f\left(x(s), u(s)\right) ds + \int_{t_1}^t f\left(x(s), u(s)\right) ds \\ &= x(t_1, x(0), u) + \int_{t_1}^t f\left(x(s), u(s)\right) ds \\ &= x\left(t, x(t_1, x(0), u), u\right) \qquad a.e.\ t \geq t_1 \geq 0. \end{aligned}$$

Moreover, for each initial state x_0 and input function u, ISS guarantees a uniform bound $c = c(x_0, u) > 0$ such that

$$|x(t, x_0, u)|_{\mathcal{A}} \leq \beta\left(|x_0|_{\mathcal{A}},\ t\right) + \gamma\left(||u||\right) \leq c\left(x_0, u\right). \tag{A.34}$$

Pick $t_1 \geq 0$ such that $\gamma\left(\left|\left|u_{[t_1,\infty)}\right|\right|\right) \leq \frac{\varepsilon}{2}$, and $T \geq t_1$ such that $\beta\left(c,\, t - t_1\right) \leq \frac{\varepsilon}{2}$ for all $t \geq T$. This gives

$$\begin{aligned} |x(t, x_0, u)|_{\mathcal{A}} &= |x\left(t, x(t_1, x_0, u), u\right)|_{\mathcal{A}} \\ &\leq \beta\left(|x(t_1)|_{\mathcal{A}},\ t - t_1\right) + \gamma\left(\left|\left|u_{[t_1,\infty)}\right|\right|\right), \quad \forall t \geq t_1 \\ &\leq \beta\left(c\left(x_0, u\right),\, t - t_1\right) + \frac{\varepsilon}{2}, \qquad \forall t \geq t_1 \\ &\leq \varepsilon, \qquad \forall t \geq T \geq t_1 \end{aligned} \tag{A.35}$$

where T depends on ε, u, and x_0. ■

A.4 Convergence analysis

Many systems have stronger properties than only stability. A UGS system may also have internal signals that converge to some value, often to zero. For such convergence analysis the most commonly used result is Barbalat's Lemma (Barbălat; 1959):

Lemma A.16 (Barbălat) *Let $\phi : \mathbb{R}_{\geq 0} \to \mathbb{R}$ be a uniformly continuous function on $[0, \infty)$. Suppose that $\lim_{t\to\infty} \int_0^t \phi(\tau) d\tau$ exists and is finite. Then*

$$\phi(t) \to 0 \text{ as } t \to \infty.$$

Proof. *Khalil (2002, Lemma 8.2).* ■

A corollary is the following:

Corollary A.17 *If a function $\phi : \mathbb{R}_{\geq 0} \to \mathbb{R}$ satisfies $\phi, \dot{\phi} \in \mathcal{L}_\infty$ and $\phi \in \mathcal{L}_p$ for some $p \in [1, \infty)$, then $\phi(t) \to 0$ as $t \to \infty$.*

Blending Lyapunov's direct method and Barbalat's Lemma gives the theorem due to LaSalle (1968) and Yoshizawa (1966). This is stated next in terms of stability of closed, forward invariant sets:

Theorem A.18 (LaSalle-Yoshizawa) *Let a closed set $\mathcal{A} \subset \mathbb{R}^n$ be a forward invariant set for (A.15). Suppose for each $K \in [0, \infty)$ there exists*

$L \in [0,\infty)$ such that $|x|_{\mathcal{A}} \leq K \Rightarrow |f(x)| \leq L$. Then, if there exists a smooth function $V : \mathbb{R}^n \to \mathbb{R}_{\geq 0}$ such that

$$\alpha_1\left(|x|_{\mathcal{A}}\right) \leq V(x) \leq \alpha_2\left(|x|_{\mathcal{A}}\right) \tag{A.36}$$

$$\dot{V} = V^x(x)f(x) \leq -\alpha_3\left(|x|_{\mathcal{A}}\right) \leq 0, \tag{A.37}$$

$\forall x \in \mathbb{R}^n$, where $\alpha_1, \alpha_2 \in \mathcal{K}_\infty$ and α_3 is a continuous positive semidefinite function, then $\mathcal{A}$ is UGS with respect to (A.15) and

$$\lim_{t\to\infty} \alpha_3\left(|x(t,x_0)|_{\mathcal{A}}\right) = 0. \tag{A.38}$$

If α_3 is strengthened to continuous positive definite, then $\mathcal{A}$ is UGAS with respect to (A.15).

Proof. *Integration of (A.37) and using the bounds in (A.36) imply that for each $x_0 \in \mathbb{R}^n$, $\exists K \geq 0$ such that*

$$\begin{aligned} |x(t,x_0)|_{\mathcal{A}} &\leq \alpha_1^{-1}\left(V(x(t,x_0))\right) \leq \alpha_1^{-1}\left(V(x_0)\right) \\ &\leq \alpha_1^{-1}\left(\alpha_2\left(|x_0|_{\mathcal{A}}\right)\right) = \varphi\left(|x_0|_{\mathcal{A}}\right) \leq K, \end{aligned} \tag{A.39}$$

holds for all t in the maximal interval of existence $[0,T)$, where $\varphi(\cdot) := \alpha_1^{-1}\left(\alpha_2\left(\cdot\right)\right) \in \mathcal{K}_\infty$ is independent of T. The bound (A.39) implies by assumption that there exists $L \geq 0$ such that $|f(x(t,x_0))| \leq L$, $\forall t \in [0,T)$. Integration along the solutions of (A.15) then yields

$$|x(t,x_0) - x_0| \leq \int_0^t |f(x(s,x_0))|\, ds \leq \int_0^t L ds \leq Lt,$$

$\forall t \in [0,T)$, thus excluding finite escape time so that $T = \infty$. UGS (and UGAS in the case α_3 is positive definite) follows then directly by Theorem A.10. Since V is nonincreasing and bounded from below by zero, it has a limit V_∞ as $t \to \infty$. Integrating (A.37) gives

$$\begin{aligned} \lim_{t\to\infty} \int_0^t \alpha_3\left(|x(s,x_0)|_{\mathcal{A}}\right) ds &\leq -\lim_{t\to\infty} \int_0^t \dot{V}(x(s,x_0)) ds \\ &= \lim_{t\to\infty} \left\{V(x_0) - V(x(t,x_0))\right\} \\ &= V(x_0) - V_\infty \end{aligned}$$

which shows that the first integral exists and is finite. We next show that $t \mapsto \alpha_3\left(|x(t,x_0)|_{\mathcal{A}}\right)$ is uniformly continuous on $\mathbb{R}_{\geq 0}$. For each $\varepsilon > 0$ we let $\delta := \varepsilon/L$, and for any $t_1, t_2 \in \mathbb{R}_{\geq 0}$ with $|t_2 - t_1| \leq \delta$ we get

$$|x(t_2,x_0) - x(t_1,x_0)| \leq \int_{t_1}^{t_2} |f(x(s,x_0))|\, ds \leq L\,|t_2 - t_1| \leq \varepsilon$$

which shows that the solution $x(t, x_0)$ is uniformly continuous. Next,

$$\begin{aligned} ||x|_{\mathcal{A}} - |y|_{\mathcal{A}}| &= \left| \inf_{v \in \mathcal{A}} |x - v| - \inf_{w \in \mathcal{A}} |y - w| \right| \\ &\leq ||x - s| - |y - s||, \qquad s \in \mathcal{A} \\ &\leq |x - y|, \qquad \forall x, y \in \mathbb{R}^n, \end{aligned}$$

shows that $|\cdot|_{\mathcal{A}}$ is globally Lipschitz with Lipschitz constant equal to unity, and consequently, $|\cdot|_{\mathcal{A}}$ is uniformly continuous. Finally, since α_3 is continuous, it is uniformly continuous on the compact set $\{s \in \mathbb{R}_{\geq 0} : \ s \leq K\}$. Putting this together we conclude that $t \mapsto \alpha_3 (|x(t, x_0)|_{\mathcal{A}})$ is uniformly continuous, and $\lim_{t \to \infty} \alpha_3 (|x(t, x_0)|_{\mathcal{A}}) = 0$ follows from Lemma A.16. ■

Another important tool for convergence analysis is the invariance principle that can be used to prove convergence to an equilibrium in the case when the Lyapunov function only yields a negative semidefinite time derivative. One version is due to Krasovskii (1959), while another is given by LaSalle (1960) (see Rouche, Habets and Laloy (1977, Theorem 1.3, pp. 50-51) and Khalil (2002, Theorem 4.4, p. 128)). Since these theorems either require periodic systems or solutions that live in compact sets, they are usually not applicable to the closed-loop maneuvering systems encountered in this thesis.

A powerful theorem that is applicable for time-varying systems and stability analysis of noncompact sets, is the theorem of Matrosov (1962). A version of this theorem, applicable to closed, forward invariant sets, is stated here as presented by Teel, Panteley and Loría (2002):

Theorem A.19 (Matrosov) *Suppose the system (A.15) is finite escape-time detectable through $|\cdot|_{\mathcal{A}}$, and $f(x)$ is continuous. If there exist:*

- *a locally Lipschitz function $V : \mathbb{R}^n \to \mathbb{R}_{\geq 0}$,*
- *a continuous function $U : \mathbb{R}^n \to \mathbb{R}_{\geq 0}$ that for each pair of strictly positive real numbres $\delta \leq \Delta$, is uniformly continuous on*

$$\mathcal{H}_{\mathcal{A}}(\delta, \Delta) := \{x \in \mathbb{R}^n : \ \delta \leq |x|_{\mathcal{A}} \leq \Delta\}$$

- *class-$\mathcal{K}_\infty$ functions α_1 and α_2,*

such that

1. $\alpha_1(|x|_{\mathcal{A}}) \leq V(x) \leq \alpha_2(|x|_{\mathcal{A}})$ for all $x \in \mathbb{R}^n$,

2. $V^x(x)f(x) \leq -U(x) \leq 0$ for a.a. $x \in \mathbb{R}^n$,

and, for each pair of strictly real numbers $\delta \leq \Delta$,

- a $\mathcal{C}^1$ function $W : \mathbb{R}^n \to \mathbb{R}$,
- strictly positive real numbers ε_1, ε_2, and ψ

such that

3. $\max\{|W(x)|, |f(x)W(x)|\} \leq \psi$ for all $x \in \mathcal{H}_{\mathcal{A}}(\delta, \Delta)$,
4. $x \in \mathcal{H}_{\mathcal{A}}(\delta, \Delta) \cap \{\xi \in \mathbb{R}^n : \ U(\xi) \leq \varepsilon_1\} \Rightarrow |W^x(x)f(x)| \geq \varepsilon_2$,

then, for the system (A.15), the set $\mathcal{A}$ *is UGAS.*

See Teel et al. (2002) for the proof. Another useful extension of Matrosov's Theorem is the version by Loría, Panteley, Popović and Teel (2002) where a family of auxiliary functions V_i, $i \in \{1, \ldots, j\}$, are used, instead of a single function W as above, to provide UGAS of the origin of a time-varying system. Consider the system (A.1) and suppose that the origin $x = 0$ is an equilibrium. Then:

Theorem A.20 *The origin of the system (A.1) is UGAS under the following assumptions:*

1. *The origin of the system (A.1) is UGS.*
2. *There exist integers* $j, m > 0$ *and for each* $\Delta > 0$ *there exist*

   - *a number* $\mu > 0$,
   - *locally Lipschitz continuous functions* $V_i : \mathbb{R}^n \times \mathbb{R} \to \mathbb{R}$, $i \in \{1, \ldots, j\}$,
   - *a (continuous) function* $\phi : \mathbb{R}^n \times \mathbb{R} \to \mathbb{R}^m$, $i \in \{1, \ldots, j\}$,
   - *continuous functions* $Y_i : \mathbb{R}^n \times \mathbb{R}^m \to \mathbb{R}$, $i \in \{1, \ldots, j\}$,

   such that, for a.a. $(x, t) \in \mathcal{B}^n(\Delta) \times \mathbb{R}$,

$$\begin{array}{rcl} \max\{|V_i(x,t)|, |\phi(x,t)|\} & \leq & \mu \\ V_i^x(x,t)f(x,t) + V_i^t(x,t) & \leq & Y_i(x, \phi(x,t)) \end{array}$$

   where $\mathcal{B}^n(r) := \{x \in \mathbb{R}^n : \ |x| \leq r\}$.

3. For each integer $k \in \{1, \ldots, j\}$ we have that

$$\begin{array}{c} \{(z,\psi) \in \mathcal{B}^n(\Delta) \times \mathcal{B}^m(\mu),\ Y_i(z,\psi) = 0,\ \forall i \in \{1,\ldots,k-1\}\} \\ \Downarrow \\ \{Y_k(z,\psi) \leq 0\}\,. \end{array}$$

4. We have that

$$\begin{array}{c} \{(z,\psi) \in \mathcal{B}^n(\Delta) \times \mathcal{B}^m(\mu),\ Y_i(z,\psi) = 0,\ \forall i \in \{1,\ldots,j\}\} \\ \Downarrow \\ \{z = 0\}\,. \end{array}$$

See Loría et al. (2002) for the proof.

A.5 Partial set-stability for interconnected systems

Consider the interconnected system

$$\begin{array}{l} \dot{x}_1 = f_1(x_1, x_2, u_1) \\ \dot{x}_2 = f_2(x_1, x_2, u_2) \end{array} \tag{A.40}$$

where $x_1(t) \in \mathbb{R}^{n_1}$ and $x_2(t) \in \mathbb{R}^{n_2}$ are the states, $u_1(t) \in \mathcal{U}_1 \subset \mathbb{R}^{m_1}$ and $u_2(t) \in \mathcal{U}_2 \subset \mathbb{R}^{m_2}$ are inputs where $\mathcal{U}_1$,$\mathcal{U}_2$ are compact sets, and the vector fields f_1, f_2 are smooth. We investigate stability of the set

$$\mathcal{A} := \{(x_1, x_2) \in \mathbb{R}^{n_1} \times \mathbb{R}^{n_2} : |x_1|_{\mathcal{A}_1} = 0\}\,, \tag{A.41}$$

where $\mathcal{A}_1 \subset \mathbb{R}^{n_1}$ is a compact set (for instance an equilibrim point $x_1 = 0$). In this case, we get that $|x|_{\mathcal{A}} = |x_1|_{\mathcal{A}_1}$ where $x := \mathrm{col}(x_1, x_2)$.

The next lemma will be used to guarantee forward completeness:

Lemma A.21 *If for each compact set $\mathcal{X} \subset \mathbb{R}^{n_1}$ there exist $L > 0$ and $c > 0$ such that:*

$$|f_2(\xi, x_2, \upsilon)| \leq L\,|x_2| + c, \qquad \forall x_2 \in \mathbb{R}^{n_2}, \tag{A.42}$$

uniformly for all $(\xi, \upsilon) \in \mathcal{X} \times \mathcal{U}_2$, that is, f_2 satisfies a sector growth condition in x_2, then the system (A.40) is finite escape-time detectable through $|\cdot|_{\mathcal{A}}$.

Proof. *We need to show that for each $x_{20} = x_2(0)$, each bounded function $x_1(\cdot) \in \mathcal{X}$, and each input function $u_2(\cdot) \in \mathcal{U}_2$, then the solution $x_2(t) =$*

$x_2(t, x_{20}, x_1, u_2)$ exists for all $t \geq 0$. Define $y(x_2) := |x_2| = \sqrt{x_2^\top x_2}$ which is continuously differentiable on $\mathbb{R}^{n_2} \backslash \{0\}$. Time-differentiation gives

$$\frac{d}{dt} y\left(x_2(t)\right) = \frac{1}{|x_2(t)|} x_2(t)^\top f_2(x_1(t), x_2(t), u_2(t)) \leq L y\left(x_2(t)\right) + c \quad \text{(A.43)}$$

which in view of Lemma A.2 (and the proof of Proposition A.1) shows that $y(x_2(t))$ (and therefore $x_2(t)$) is bounded on the maximal interval of existence $[0, T)$. Assume that $x_2(t)$ has a finite escape-time at $T < \infty$. Then, for each $M < \infty$ there exists $\tau \in [0, T)$ such that $|x_2(\tau)| > M$. However, this contradicts boundedness of $x_2(t)$ on $[0, T)$, and the solution $x_2(t)$ must exist for all $t \geq 0$. As a result, the solution of (A.40) can only escape to infinity if $x_1(t)$ grows unbounded, but this must necessarily be detected through $|x|_{\mathcal{A}} = |x_1|_{\mathcal{A}_1}$. ■

This gives the following stability result for (A.41) with respect to (A.40):

Theorem A.22 *Assume that the sector bound (A.42) in Lemma A.21 holds for (A.40). If, in addition, there exist a smooth function $V : \mathbb{R}^{n_1} \times \mathbb{R}^{n_2} \to \mathbb{R}_{\geq 0}$ and $\mathcal{K}_\infty$-functions α_i, $i = 1, \ldots, 4$, such that*

$$\alpha_1\left(|x_1|_{\mathcal{A}_1}\right) \leq V(x_1, x_2) \leq \alpha_2\left(|x_1|_{\mathcal{A}_1}\right) \quad \text{(A.44)}$$

and

$$\begin{aligned} &V^{x_1}(x_1, x_2) f_1\left(x_1, x_2, u_1\right) \\ &\quad + V^{x_2}(x_1, x_2) f_2\left(x_1, x_2, u_2\right) \leq -\alpha_3\left(|x_1|_{\mathcal{A}_1}\right) + \alpha_4\left(|u|\right) \end{aligned} \quad \text{(A.45)}$$

hold, where $u := \mathrm{col}(u_1, u_2) \in \mathcal{U}_1 \times \mathcal{U}_2$, then the system (A.40) is ISS with respect to the closed, 0-invariant set (A.41). In the case when $u_1 = 0$ and $u_2 = 0$ then the closed, forward invariant set (A.41) is UGAS with respect to (A.40), and if $\alpha_i(|x|_{\mathcal{A}_1}) = c_i |x|_{\mathcal{A}_1}^r$ for $i = 1, 2, 3$, where c_1, c_2, c_3, r are strictly positive reals with $r \geq 1$, then (A.41) is UGES with respect to (A.40).

Proof. *Since*

$$\begin{aligned} \tfrac{d}{dt} V(x_1(t), x_2(t)) &\leq -\alpha\left(V(x_1(t), x_2(t))\right) + \alpha_4\left(|u(t)|\right) \\ &\leq -\tfrac{1}{2}\alpha\left(V(x_1(t), x_2(t))\right), \end{aligned}$$

for all $V(x_1(t), x_2(t)) \geq \alpha^{-1}\left(2\alpha_4\left(|u(t)|\right)\right)$ where $\alpha = \alpha_3 \circ \alpha_1^{-1} \in \mathcal{K}_\infty$ and u is bounded, then $V(x_1(t), x_2(t))$, and consequently $|x_1(t)|_{\mathcal{A}_1}$, is bounded on the maximal interval of existence $[0, T)$. Since $\mathcal{A}_1$ is compact this implies that

$x_1(t)$ is bounded on $[0,T)$. By Lemma A.21 this means that the system is finite escape-time detectable through $|\cdot|_{\mathcal{A}}$, and forward completeness follows. The fact that $\mathcal{A}$ is 0-invariant for (A.40) follows from the above Lyapunov bounds with $u(t) \equiv 0$. Recall Definition A.13 and Theorem A.14. Since $|x|_{\mathcal{A}} = |x_1|_{\mathcal{A}_1}$, the function V is a smooth ISS-Lyapunov function for (A.40) with respect to $\mathcal{A}$, and this proves ISS. UGAS in the case when $u_1 = 0$ and $u_2 = 0$ follows from the definition of ISS, and UGES further follows from Theorem A.10. ■

Remark A.1 *By defining the output $y = h(x_1, x_2) := |x_1|_{\mathcal{A}_1}$ for (A.40), then ISS for the set $\mathcal{A}$ is equivalently characterized by the concept called State-Independent Input-to-Output Stability (SIIOS) as defined by Sontag and Wang (2000). Indeed, the smooth function V in (A.44) and (A.45) becomes a SIIOS-Lyapunov function for (A.40), and this can be used to deduce that*

$$|y(t, x_0, u)| = |x_1(t, x_0, u)|_{\mathcal{A}_1} \leq \beta\left(|x_{10}|_{\mathcal{A}_1}, t\right) + \gamma\left(\|u\|\right) \tag{A.46}$$

where $\beta \in \mathcal{KL}$ and $\gamma \in \mathcal{K}$. Since $|x|_{\mathcal{A}} = |x_1|_{\mathcal{A}_1}$ ISS of the system (A.40) with respect to the closed, 0-invariant set (A.41) follows from (A.46). The converse also holds as shown in Sontag and Wang (2000).

Appendix B

Modeling, identification, and control of CyberShip II

This appendix presents a modeling, identification, and control design where the objective is to maneuver a ship along a desired path at different velocities. Material from a variety of references have been used to describe the ship model, its difficulties, limitations, and possible simplifications for the purpose of automatic control design. The numerical values of the parameters in the model is identified in towing tests and adaptive maneuvering experiments for CyberShip II in the Marine Cybernetics Laboratory. The material of this appendix have been partly published in Skjetne, Smogeli and Fossen (2004a) and in its entirety in Skjetne, Smogeli and Fossen (2004b).

Introduction

Model-based control for steering and positioning of ships has become state-of-the-art since LQG and similar state-space techniques were applied in the 1960s. For a rigid-body the dynamic equations of motion are divided into two distinctive parts: *kinematics,* which is the study of motion without reference to the forces that cause motion, and *kinetics,* which relates the action of forces on bodies to their resulting motions (Meriam and Kraige; 1993). The rigid-body and hydrodynamic equations of motion for a ship are in reality given by a set of (complicated) differential equations describing the 6 degrees-of-freedom (6 DOF); surge, sway, and heave for translation, and roll, pitch, and yaw for rotation. The models used to represent the physics

of the real world, however, vary as much as the underlying control objectives vary. Roughly divided these control objectives are either slow speed positioning or high speed steering. The first is called dynamical positioning (DP) and includes station keeping, position mooring, and slow speed reference tracking. For DP the 6 DOF model is reduced to a simpler 3 DOF model that is linear in the kinetic part. Such applications with references are thoroughly described by Fossen (1994); Strand (1999), and Lindegaard (2003). High speed steering, on the other hand, includes automatic course control, high speed position tracking, and path following; see for instance Holzhüter (1997); Lefeber et al. (2003); Fossen et al. (2003). For these applications, Coriolis and centripetal forces together with nonlinear viscous effects become increasingly important and therefore make the kinetic part nonlinear. By port-starboard symmetry, the longitudinal (surge) dynamics are essentially decoupled from the lateral (steering; sway-yaw) dynamics and can therefore be controlled independently by forward propulsion. Moreover, for cruising at a nearly constant surge speed and only considering first order approximations of the viscous damping, a linear parametrically varying approximation of the steering dynamics is applicable. The origin of these types of models are traced back to Davidson and Schiff (1946), while Nomoto, Taguchi, Honda and Hirano (1957) gave an equivalent representation. See Clarke (2003) for a historical background and Fossen (2002); Perez (2005) for a complete reference on these original models and their later derivations.

The contribution of the material in this Appendix is a 3 DOF nonlinear maneuvering model for a ship. This model can be simplified further to either a 3 DOF model for DP, a steering model according to Davidson and Schiff or Nomoto, or it can be used as is for nonlinear control design. Furthermore, system identification procedures for a model ship called CyberShip II (CS2) in a towing tank facility have produced numerical values for nearly all the hydrodynamic coefficients. To find the other values, an adaptive maneuvering control law was implemented for CS2, and free-running maneuvering experiments were performed. The adaptive parameter estimates in these experiments then give approximate values for the other hydrodynamic coefficients.

B.1 The 3 DOF ship maneuvering model

Ship dynamics are described by 6 degrees-of-freedom (6 DOF) differential equations of motion. The modes are (x, y, z), referred to as *surge*, *sway*, and *heave*, describing the position in three-dimensional space, and (ϕ, θ, ψ),

called *roll*, *pitch*, and *yaw*, describing the orientation of the ship. Assuming that the ship is longitudinally and laterally metacentrically stable with small amplitudes $\phi = \theta = \dot{\phi} = \dot{\theta} \approx 0$, one can discard the dynamics of roll and pitch. Likewise, since the ship is floating with $z \approx 0$ in mean, one can discard the heave dynamics. The resulting model for the purpose of maneuvering the ship in the horizontal plane becomes a 3 DOF model. Let an inertial frame be approximated by the Earth-fixed reference frame $\mathcal{E}$ called NED (North-East-Down) and let another coordinate frame $\mathcal{B}$ be attached to the ship as seen in Figure B.1. The states of the vessel can then be taken as $\eta = [x, y, \psi]^\top$ and $\nu = [u, v, r]^\top$ where (x, y) is the Cartesian position, ψ is the heading (yaw) angle, (u, v) are the body-fixed linear velocities (surge and sway), and r is the yaw rate.

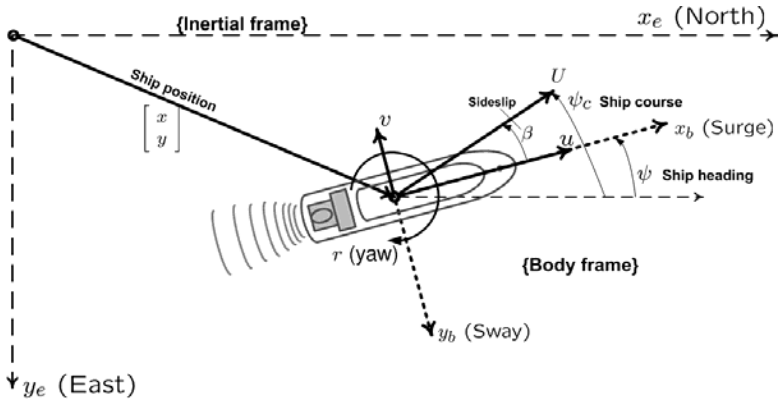

Figure B.1: Figure showing the inertial earth-fixed frame and the body-fixed frame for a ship with the earth-fixed position (x, y), the heading ψ, and the corresponding body-fixed velocities (u, v) and rotation rate r.

B.1.1 Rigid-body dynamics

The Earth-fixed velocity vector is related to the body-fixed velocity vector through the kinematic relationship

$$\dot{\eta} = R(\psi)\nu \tag{B.1}$$

where

$$R(\psi) = \begin{bmatrix} \cos\psi & -\sin\psi & 0 \\ \sin\psi & \cos\psi & 0 \\ 0 & 0 & 1 \end{bmatrix}$$

is the rotation matrix in (1.27). It has the properties that $R(\psi)^\top R(\psi) = I$, $\|R(\psi)\| = 1$ for all ψ, and $\frac{d}{dt}\{R(\psi)\} = \dot{\psi} R(\psi) S$ where

$$S = \begin{bmatrix} 0 & -1 & 0 \\ 1 & 0 & 0 \\ 0 & 0 & 0 \end{bmatrix} = -S^\top$$

is skew-symmetric. By Newton's second law it is shown in Fossen (2002) that the rigid body equations of motion can be written[1]

$$M_{RB}\dot{\nu} + C_{RB}(\nu)\nu = f_{RB} \tag{B.2}$$

where M_{RB} is the rigid-body system inertia matrix, $C_{RB}(\nu)$ is the corresponding matrix of Coriolis and centripetal terms, and $f_{RB} = [X, Y, N]^\top$ is a generalized vector of external forces (X, Y) and moment N. Let the origin 'O' of the body frame be taken as the geometric center point (CP) in the ship structure. Under the assumption that the ship is port-starboard symmetric, the center-of-gravity (CG) will be located a distance x_g along the body x_b-axis. In this case, M_{RB} takes the form

$$M_{RB} = \begin{bmatrix} m & 0 & 0 \\ 0 & m & mx_g \\ 0 & mx_g & I_z \end{bmatrix} \tag{B.3}$$

where m is the mass of the ship and I_z is the moment of inertia about the z_b-axis (i.e., yaw rotation). Several representations for the Coriolis matrix are possible. Based on Theorem 3.2 in Fossen (2002), we choose the skew-symmetric representation

$$C_{RB}(\nu) = \begin{bmatrix} 0 & 0 & -m\,(x_g r + v) \\ 0 & 0 & mu \\ m\,(x_g r + v) & -mu & 0 \end{bmatrix}. \tag{B.4}$$

The force and moment vector f_{RB} is given by the superposition of actuator forces and moments $f = [f_u, f_v, f_r]^\top$, hydrodynamic effects f_H, and exogenous disturbances $w(t)$ due to, for instance, waves and wind forces (Sørensen, Sagatun and Fossen; 1996). The forces and moments in f_{RB} are all expressed with reference to the center point (CP) such that the full set of dynamical equations is given in the body-fixed reference frame.

[1] Usually, τ is used to denote the input generalized forces and moments according to the notation of Fossen (1994, 2002). However, not to confuse it with the (maneuvering) tuning function we use f instead.

B.1.2 Hydrodynamic forces and moments

The vector f_H is the result of several hydrodynamic phenomena, and it involves the *radiation problem* and *diffraction problem*. For an ideal fluid, the components addressed in the radiation problem are *radiation-induced added mass*, *potential damping*, and *restoring forces*. For the 3 DOF states considered here, restoring forces are only important in case of mooring which is not in the scope of this appendix. In addition to potential damping there are also other damping effects such as *linear skin* and *pressure induced viscous damping*, *wave drift damping*, and damping due to *vortex shedding*. The diffraction problem, on the other hand, addresses generalized *Froude-Krylov forces* and generalized *diffraction forces*. These are due to wave excitation and disregarded in this work. For more details, see Faltinsen (1990). See also the works by Bailey et al. (1998), Fossen and Smogeli (2004), and Fossen (2005) where the authors derive a unified frequency dependent model for maneuvering a ship in a seaway.

Due to currents in the ocean fluid, the velocity ν is different than the relative velocity ν_r between the ship hull and the fluid. The hydrodynamic forces and moments depend on this relative velocity. For a nonrotational current with fixed speed V_c and angle β_c in the earth-fixed frame, the current velocity is given by

$$v_c := \begin{bmatrix} V_c \cos\beta_c \\ V_c \sin\beta_c \\ 0 \end{bmatrix}. \tag{B.5}$$

Normally V_c and β_c should be modeled as stochastic processes. However, in the deterministic setting of this paper we simply assume that $\dot{V}_c = \dot{\beta}_c = 0$. In the body-frame this gives the current component $\nu_c := R(\psi)^\top v_c$ and the relative velocity $\nu_r := \nu - \nu_c = [u_r, v_r, r]^\top$. With these definitions it is common (Sørensen; 2005) to model the hydrodynamic effects as

$$f_H = -M_A \dot{\nu}_r - C_A(\nu_r)\nu_r - d(\nu_r) \tag{B.6}$$

where M_A accounts for added mass, $C_A(\nu_r)$ accounts for the corresponding added Coriolis and centripetal terms, and $d(\nu_r)$ sums up the damping effects. By the notation of The Society of Naval Architects and Marine Engineers (1950) the matrix M_A is given by

$$M_A = \begin{bmatrix} -X_{\dot{u}} & 0 & 0 \\ 0 & -Y_{\dot{v}} & -Y_{\dot{r}} \\ 0 & -N_{\dot{v}} & -N_{\dot{r}} \end{bmatrix} \tag{B.7}$$

where the assumption of port-starboard symmetry again is applied. For zero relative velocity, $\nu_r = 0$, zero frequency of motion due to water surface effects (low-frequency assumption), and assuming an ideal fluid, the added mass matrix is constant and $M_A = M_A^\top > 0$. In general, $M_A = M_A(\omega_e)$ where ω_e is the frequency of encounter given by

$$\omega_e = \left| \omega_0 - \frac{\omega_0^2}{g} U \cos\beta \right|. \tag{B.8}$$

Here ω_0 is the dominating wave frequency, g is the acceleration of gravity, $U = \sqrt{u^2 + v^2}$ is the total ship speed, and β is the angle of encounter defined by $\beta = 0\,^\circ$ for following sea.

For control design it is common to assume for the plant model that $M_A = \lim_{\omega_e \to 0} M_A(\omega_e)$ is constant and strictly positive. However, since $M_A = M_A(0)$ is not necessarily symmetric, Theorem 3.2 in Fossen (2002) is not directly applicable to find $C_A(\nu_r)$. To overcome this obstacle, we observe that this theorem is deduced from the kinetic energy $T = \frac{1}{2}\nu^\top M \nu$. A modification for the added mass kinetic energy is

$$T_A = \frac{1}{2}\nu_r^\top M_A \nu_r = \frac{1}{4}\nu_r^\top \left(M_A + M_A^\top \right) \nu_r = \frac{1}{2}\nu_r^\top \bar{M}_A \nu_r$$

where $\bar{M}_A := \frac{1}{2}(M_A + M_A^\top) = \bar{M}_A^\top$. This means that $C_A(\nu_r)$, for a nonsymmetric M_A, is derived from Theorem 3.2 of Fossen (2002) using $\bar{M}_A$ instead of M_A, and this gives

$$C_A(\nu_r) = \begin{bmatrix} 0 & 0 & Y_{\dot{v}} v_r + \frac{1}{2}\left(N_{\dot{v}} + Y_{\dot{r}}\right) r \\ 0 & 0 & -X_{\dot{u}} u_r \\ -Y_{\dot{v}} v_r - \frac{1}{2}\left(N_{\dot{v}} + Y_{\dot{r}}\right) r & X_{\dot{u}} u_r & 0 \end{bmatrix}. \tag{B.9}$$

The most uncertain component in the hydrodynamic model (B.6) is the damping vector $d(\nu_r)$, to which many hydrodynamic phenomena contribute. Let $d(\nu_r) = [X_D(\nu_r), Y_D(\nu_r), N_D(\nu_r)]^\top$. For a constant cruise speed $\nu_r = \nu_0 \approx [u_0, 0, 0]^\top$ one can fit the damping forces and moments at ν_0 to the linear functions

$$\begin{aligned} X_D(\nu_r) &= -X_u(u_r - u_0) - X_v v_r - X_r r \\ Y_D(\nu_r) &= -Y_u(u_r - u_0) - Y_v v_r - Y_r r \\ N_D(\nu_r) &= -N_u(u_r - u_0) - N_v v_r - N_r r \end{aligned} \tag{B.10}$$

where the hydrodynamic coefficients $\{X_{(\cdot)}, Y_{(\cdot)}, N_{(\cdot)}\}$ are called hydrodynamic derivatives because they are the partial derivatives of the forces and

moment with respect to the corresponding velocities, for instance, $Y_r := \frac{\partial Y_D(\nu_r)}{\partial r}$. Seeking in this paper a more globally valid model of the damping effects, we consider a nonlinear representation. Abkowitz (1964) proposed using a truncated Taylor series expansion of $d(\nu_r)$. Since in general $d(\nu_r)$ is dissipative for both positive and negative relative velocities, it must be an odd function, and, hence, only odd terms in the Taylor expansion are required. Using first and third order terms only, and assuming port-starboard symmetry, this gives

$$\begin{aligned} X_D(\nu_r) &= -X_u u_r - X_{uuu} u_r^3 \\ Y_D(\nu_r) &= -Y_v v_r - Y_r r - Y_{vvv} v_r^3 - Y_{vvr} v_r^2 r - Y_{vrr} v_r r^2 - Y_{rrr} r^3 \\ N_D(\nu_r) &= -N_v v_r - N_r r - N_{vvv} v_r^3 - N_{vvr} v_r^2 r - N_{vrr} v_r r^2 - N_{rrr} r^3 \end{aligned} \tag{B.11}$$

which is valid for all feasible velocities. Fedyaevsky and Sobolev (1963) and later Norrbin (1970) and Blanke and Christensen (1993) gave another nonlinear representation

$$\begin{aligned} X_D(\nu_r) &= -X_u u_r - X_{|u|u} \left|u_r\right| u_r \\ Y_D(\nu_r) &= -Y_v v_r - Y_r r - Y_{|v|v} \left|v_r\right| v_r - Y_{|v|r} \left|v_r\right| r - Y_{|r|v} \left|r\right| v_r - Y_{|r|r} \left|r\right| r \\ N_D(\nu_r) &= -N_v v_r - N_r r - N_{|v|v} \left|v_r\right| v_r - N_{|v|r} \left|v_r\right| r - N_{|r|v} \left|r\right| v_r - N_{|r|r} \left|r\right| r \end{aligned} \tag{B.12}$$

called the *second order modulus* model. These functions are not continuously differentiable, and strictly speaking they therefore cannot represent the physical system. However, experiments have shown that they match the damping effects quite accurately and are therefore often used. Based on the experimental data presented in the next section and curve fitting, we choose in this paper the damping model

$$d(\nu_r) = D_L \nu_r + D_{NL}(\nu_r)\nu_r =: D(\nu_r)\nu_r \tag{B.13}$$

where

$$D_L := \begin{bmatrix} -X_u & 0 & 0 \\ 0 & -Y_v & -Y_r \\ 0 & -N_v & -N_r \end{bmatrix}$$

$$D_{NL}(\nu_r) := \begin{bmatrix} -X_{|u|u} \left|u_r\right| - X_{uuu} u_r^2 & 0 & 0 \\ 0 & -Y_{|v|v} \left|v_r\right| - Y_{|r|v} \left|r\right| & -Y_{|v|r} \left|v_r\right| - Y_{|r|r} \left|r\right| \\ 0 & -N_{|v|v} \left|v_r\right| - N_{|r|v} \left|r\right| & -N_{|v|r} \left|v_r\right| - N_{|r|r} \left|r\right| \end{bmatrix}$$

which essentially is the second order modulus model with an extra third order term in surge. The reason for picking this model was that it gave the best fit to the experimental data.

With $f_{RB} = f + f_H + w(t)$ the kinetic equation of motion (B.2) becomes

$$M_{RB}\dot{\nu} + M_A\dot{\nu}_r + C_{RB}(\nu)\nu + C_A(\nu_r)\nu_r + D(\nu_r)\nu_r = f + w(t) \tag{B.14}$$

where

$$\begin{aligned}\nu_r &= \nu - R(\psi)^\top v_c \\ \dot{\nu}_r &= \dot{\nu} - rS^\top R(\psi)^\top v_c.\end{aligned}$$

For the kinetic model (B.14) one must decide upon using either the relative velocity ν_r or the inertial velocity ν as the velocity state. There are different practices in the literature, and the current velocity v_c must in either case be measured or somehow estimated to account for it in (B.14). A simplifying technique was applied by Fossen and Strand (1999) who used ν as the velocity state and assumed that the dynamics related to the current v_c (and other unmodeled dynamics) are captured by a slowly varying bias b in the Earth frame. This gives the simplified model

$$M\dot{\nu} + C(\nu)\nu + D(\nu)\nu = f + R(\psi)^\top b + w(t) \tag{B.15}$$

where $M := M_{RB} + M_A$ and $C(\nu) := C_{RB}(\nu) + C_A(\nu)$. The alternative, applied among others by Holzhüter (1997), is to use ν_r as the state, but in this case the kinematic relationship (B.1) must be rewritten as

$$\dot{\eta} = R(\psi)\nu_r + v_c \tag{B.16}$$

which means that v_c enters both the kinematic and kinetic equations of motion.

For simulator design, a model according to (B.14) or more advanced should be used. For control design, on the other hand, experience shows that (B.1) and (B.15) are adequate provided some type of integral action is used in the controller to compensate for the bias b; see for instance Skjetne and Fossen (2004).

B.1.3 Simplified models

For special applications, simpler models than (B.15) can be used. For instance, for DP a linearization of (B.15) around $\nu = 0$ yields

$$M\dot{\nu} + D_L\nu = f + R(\psi)^\top b + w(t) \tag{B.17}$$

where the Coriolis and nonlinear damping terms were eliminated. Note that the curve-fitted coefficients in D_L for DP will be different from those fitted to the nonlinear (globally valid) model (B.13); see next section.

Another special application is steering a ship at (nearly) constant surge speed. Separating the surge dynamics from the steering dynamics, using (B.10), and assuming port-starboard symmetry and $v_c \equiv 0$, we get a maneuvering model consisting of the surge dynamics

$$(m - X_{\dot{u}})\,\dot{u} - X_u(u - u_0) - (m - Y_{\dot{v}})\,vr - \left(mx_g - \frac{1}{2}N_{\dot{v}} - \frac{1}{2}Y_{\dot{r}}\right) r^2 = f_u \tag{B.18}$$

and the sway-yaw (steering) dynamics

$$\begin{bmatrix} m - Y_{\dot{v}} & mx_g - Y_{\dot{r}} \\ mx_g - N_{\dot{v}} & I_z - N_{\dot{r}} \end{bmatrix} \begin{bmatrix} \dot{v} \\ \dot{r} \end{bmatrix} + \begin{bmatrix} -Y_v & -Y_r + (m - X_{\dot{u}})\,u \\ -N_v + (X_{\dot{u}} - Y_{\dot{v}})\,u & -N_r + \left(mx_g - \frac{1}{2}N_{\dot{v}} - \frac{1}{2}Y_{\dot{r}}\right) u \end{bmatrix} \begin{bmatrix} v \\ r \end{bmatrix} = \begin{bmatrix} f_v \\ f_r \end{bmatrix}. \tag{B.19}$$

For each fixed surge speed $u = u_0$, the steering dynamics become linear. Hence, treating u as a parameter, (B.19) is a linear parametrically varying (LPV) model of the form of Davidson and Schiff (1946). This can be further related to a Nomoto model as described by Clarke (2003). For conventional ships, the inputs are usually linearly related to the rudder angle δ as $f_v = -Y_\delta \delta$ and $f_r = -N_\delta \delta$. As a result, linear design techniques such as gain scheduling or similar can be applied to solve a steering task.

B.1.4 Actuator forces

The actuator forces and moments are generated by a set of thrusters with revolutions per second $n = [n_1, n_2, \ldots, n_{p_1}]^\top \in \mathbb{R}^{p_1}$ and a set of control surfaces (or propeller blade pitch) with angles $\delta = [\delta_1, \delta_2, \ldots, \delta_{p_2}]^\top \in \mathbb{R}^{p_2}$. They are related to the input vector f through the mapping

$$f = B f_{act}\,(\nu_r, n, \delta) \tag{B.20}$$

where $B \in \mathbb{R}^{3\times(p_1+p_2)}$ is an actuator configuration matrix, and $f_{act} : \mathbb{R}^3 \times \mathbb{R}^{p_1} \times [-\pi, \pi)^{p_2} \to \mathbb{R}^{p_1+p_2}$ is a function that for each velocity ν_r relates the actuator set-points (n, δ) to a vector of forces.

As a case we consider CyberShip II which has two main propellers and two rudders aft, and one bow thruster fore; see Figure B.2. The main propellers generate thrust forces $\{T_1, T_2\}$, the bow thruster generates $\{T_3\}$, while the rudders generate lift forces $\{L_1, L_2\}$ and drag forces $\{D_1, D_2\}$.

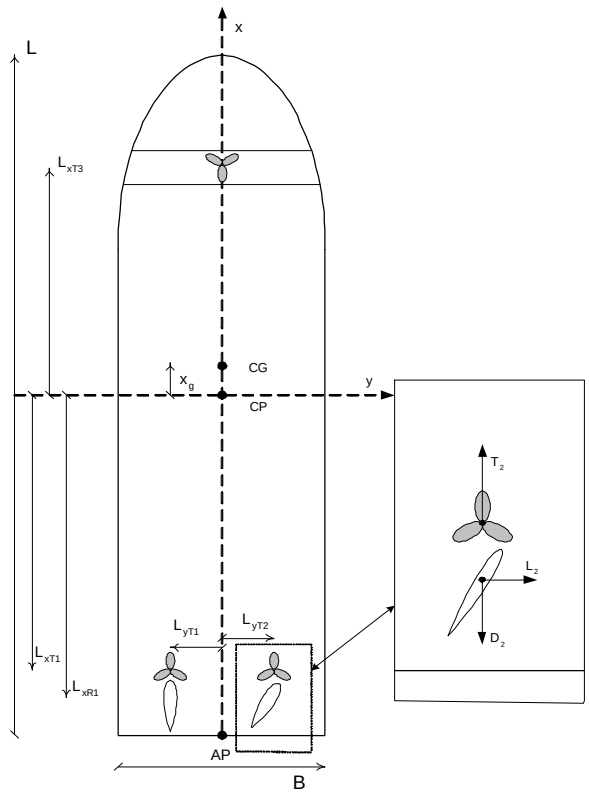

Figure B.2: Actuator configuration of CyberShip II.

Disregarding the drag forces[2], the force vector becomes

$$f_{act}\left(\nu_r, n, \delta\right) = \left[T_1(n_1, u_r), T_2(n_2, u_r), T_3(n_3), L_1(\delta_1, u_{rud,1}), L_2(\delta_2, u_{rud,2})\right]^\top$$

where $u_{rud,i}$, $i = 1, 2$, are given below. Let the force attack points of $\{T_1, T_2, T_3\}$ be located at coordinates $\{(l_{xT_1}, l_{yT_1}), (l_{xT_2}, l_{yT_2}), (l_{xT_3}, l_{yT_3})\}$ in the body-frame, and likewise $\{(l_{xR_1}, l_{yR_1}), (l_{xR_2}, l_{yR_2})\}$ for the rudders. Then the actuator configuration matrix is

$$B = \begin{bmatrix} 1 & 1 & 0 & 0 & 0 \\ 0 & 0 & 1 & 1 & 1 \\ |l_{yT_1}| & -|l_{yT_2}| & |l_{xT_3}| & -|l_{xR_1}| & -|l_{xR_2}| \end{bmatrix}. \tag{B.21}$$

[2] We will show in the next section that the rudder drag forces can be viewed as a perturbation of the hull drag in surge motion and can therefore be eliminated from the actuator model.

The propeller thrust forces $\{T_1, T_2\}$ are according to Blanke (1981) and later Fossen (1994), expressed as

$$T_i = \rho d_i^4 K_T(J_i)\,|n_i|\,n_i \tag{B.22}$$

where ρ is the water density, d_i is the propeller diameter, and K_T is a nondimensional thrust coefficient which depends on the *advance ratio* $J_i = \frac{u_a}{n_i d_i}$ of Thruster i. The ambient flow velocity u_a is given by $u_a = (1-w)u_r$ where $w \in (0,1)$ is the wake fraction number usually assumed constant (generally it is a slowly varying dynamic variable). For a range of J_i, $K_T(J_i)$ is nearly linear and may be expressed according to Blanke (1981) as

$$K_T(J_i) \approx \alpha_0 - \alpha_1 J_i = \alpha_0 - \alpha_1 \frac{u_a}{n_i d_i} \tag{B.23}$$

where $\alpha_0, \alpha_1 > 0$. An approximate formula for the thrust forces is then obtained by substituting (B.23) into (B.22) and grouping all constants, that is

$$T_i = T_{|n|n}\,|n_i|\,n_i - T_{|n|u}\,|n_i|\,u_r, \tag{B.24}$$

where $T_{|n|n} > 0$, $T_{|n|u} > 0$ are the new parameters. However, the experimental results show that the thrust force T_i primarily is dependent on the propeller revolutions n_i and less sensitive to the ambient flow velocity u_a. Additional accuracy is therefore obtained if (B.24) is separated into the equations

$$T_i = \begin{cases} T^+_{|n|n}\,|n_i|\,n_i - T^+_{|n|u}\,|n_i|\,u_r, & n_i \geq \bar{n} \\ T^-_{|n|n}\,|n_i|\,n_i - T^-_{|n|u}\,|n_i|\,u_r, & n_i \leq \underline{n} \\ 0, & \text{otherwise} \end{cases} \tag{B.25}$$

$i = 1, 2$, where $\bar{n} = \max\{0, \frac{T^+_{|n|u}}{T^+_{|n|n}} u_r\}$, $\underline{n} = \min\{0, \frac{T^-_{|n|u}}{T^-_{|n|n}} u_r\}$, and $\{T^+_{|n|n}, T^+_{|n|u}, T^-_{|n|n}, T^-_{|n|u}\}$ are positive coefficients. For each u_r, (B.25) is a monotone function and an inverse function is:

$$n_i = \begin{cases} \frac{T^+_{|n|u}}{2T^+_{|n|n}} u_r + \frac{1}{2T^+_{|n|n}} \sqrt{\left(T^+_{|n|u} u_r\right)^2 + 4T^+_{|n|n} T_i}, & T_i > 0 \\ 0, & T_i = 0 \\ \frac{T^-_{|n|u}}{2T^-_{|n|n}} u_r - \frac{1}{2T^-_{|n|n}} \sqrt{\left(T^-_{|n|u} u_r\right)^2 - 4T^-_{|n|n} T_i}, & T_i < 0. \end{cases} \tag{B.26}$$

The thrust force produced by the bow thruster will also depend on the velocity of the ship. However, because the exact form of this relationship

is not known, we rather choose the speed independent equation used by Lindegaard and Fossen (2003), that is,

$$T_3 = T_{|n_3|n_3} \, |n_3| \, n_3, \qquad T_{|n_3|n_3} > 0. \tag{B.27}$$

This has the inverse function

$$n_3 = \frac{\mathrm{sgn}(T_3)}{T_{|n_3|n_3}} \sqrt{T_{|n_3|n_3} \, |T_3|}. \tag{B.28}$$

Finally we must find the rudder lift forces as a function of rudder angle and the relative velocity of the fluid u_{rud} at the rudder surface. From momentum theory (Lewis; 1988) it can be shown that for a positive velocity $u_r \geq 0$ then at rudder i, $i = 1, 2$,

$$u_{rud,i} = u_r + k_u \left(\sqrt{\frac{8}{\pi \rho d_i^2} T_i + u_r^2} - u_r \right)$$

where T_i is the thrust force from the preceding propeller, d_i is the propeller diameter, and k_u is an induced velocity factor. Normally $k_u \approx 0.5$ when the rudder is close to the propeller. This equation tells that for a positive surge speed and positive propeller thrust, the fluid velocity at the rudder is larger than the surge velocity u_r. However, for $T_i < 0$ the argument inside the root may become negative. In this case we make the blanket assumption that this argument is zero. For negative surge speed we simply assume $u_{rud,i} = u_r$. In summary we then have

$$u_{rud,i} = \begin{cases} u_r + k_u \left(\sqrt{\max\left\{0, \frac{8}{\pi \rho d_i^2} T_i + u_r^2\right\}} - u_r \right), & u_r \geq 0 \\ u_r, & u_r < 0. \end{cases} \tag{B.29}$$

From foil theory (Newman; 1999) the lift and drag forces are modeled as

$$L_i = \frac{\rho}{2} A^e_{rud,i} C_L(\delta_i) \, |u_{rud,i}| \, u_{rud,i} \tag{B.30}$$

$$D_i = -\frac{\rho}{2} A^e_{rud,i} C_D(\delta_i) \, |u_{rud,i}| \, u_{rud,i} \tag{B.31}$$

where $A^e_{rud,i}$ is the effective rudder area, C_L is the nondimensional lift coefficient, and C_D is the nondimensional drag coefficient. These latter coefficients are further modeled as $C_L(\delta_i) = c_1 \delta_i - c_2 \, |\delta_i| \, \delta_i$ and $C_D(\delta_i) = c_3 \, |\delta_i|$

where c_1, c_2, and c_3 are positive constants. Putting this together and grouping all constants, we get the lift and drag force models

$$L_i = \begin{cases} \left(L_\delta^+ \delta_i - L_{|\delta|\delta}^+ |\delta_i| \, \delta_i\right) |u_{rud,i}| \, u_{rud,i}, & u_{rud,i} \geq 0 \\ \left(L_\delta^- \delta_i - L_{|\delta|\delta}^- |\delta_i| \, \delta_i\right) |u_{rud,i}| \, u_{rud,i}, & u_{rud,i} < 0 \end{cases} \tag{B.32}$$

$$D_i = -D_{|\delta|} \, |\delta_i| \, |u_{rud,i}| \, u_{rud,i} \tag{B.33}$$

where $\{L_\delta^+, L_{|\delta|\delta}^+, L_\delta^-, L_{|\delta|\delta}^-, D_{|\delta|}\}$ are positive coefficients. We allow the lift forces to have different coefficients for positive and negative velocities. The drag forces should now be added to the propeller thrust forces, $T_i + D_i$, in the overall actuator model. However, since D_i depends on T_i through $u_{rud,i}$ this expression becomes excessively complicated. To make it less complicated, experimental data suggest that D_i can be viewed as a perturbation of the hull drag force $d_1(\nu_r)$ in surge. Assuming that a robust maneuvering controller is able to deal with this perturbation, we do not consider it hereafter. The inverse function of (B.32) is

$$\delta_i = \begin{cases} \Delta_i^+(L_i, u_{rud,i}), & u_{rud,i} \geq \varepsilon \\ 0, & |u_{rud,i}| < \varepsilon \\ \Delta_i^-(L_i, u_{rud,i}), & u_{rud,i} \leq -\varepsilon \end{cases} \tag{B.34}$$

$$\Delta_i^+(L_i, u_{rud,i}) := \frac{\operatorname{sgn}(L_i)}{2L_{|\delta|\delta}^+} \left(L_\delta^+ - \frac{1}{u_{rud,i}^2} \sqrt{\left(L_\delta^+ u_{rud,i}^2\right)^2 - 4L_{|\delta|\delta}^+ u_{rud,i}^2 \, |L_i|} \right)$$

$$\Delta_i^-(L_i, u_{rud,i}) := \frac{-\operatorname{sgn}(L_i)}{2L_{|\delta|\delta}^-} \left(L_\delta^- - \frac{1}{u_{rud,i}^2} \sqrt{\left(L_\delta^- u_{rud,i}^2\right)^2 - 4L_{|\delta|\delta}^- u_{rud,i}^2 \, |L_i|} \right)$$

where we have introduced an ε-neighborhood around the non-effective point $u_{rud,i} = 0$ to avoid division by zero.

B.2 System identification

The Marine Cybernetics Laboratory (MCLab) is a Marie Curie EU training site for experimental testing of ships, rigs, underwater vehicles, and propulsion systems at the Centre for Ships and Ocean Structures (CESOS) at the Norwegian University of Science and Technology (NTNU). The dimensions of the basin are L x B x D = 40 m x 6.45 m x 1.5 m, and it is equipped

with a towing carriage, a position measurement system, and a wave maker system, while a wind and current system are under construction.

CyberShip II (CS2; see Figure B.3) is a 1:70 scale replica of a supply ship for the North Sea. Its mass is $m = 23.8\,\text{kg}$, its length is $L_{CS2} = 1.255\,\text{m}$, and its breadth is $B_{CS2} = 0.29\,\text{m}$. It is fully actuated with two main propellers and two rudders aft, and one bow thruster; see Figure B.2. It is further equipped with a PC104-bus driven by a QNX® real-time operating system which controls the internal hardware achitecture and communicates with onshore computers through a WLAN. For position and attitude measurements, four cameras onshore in the MCLab observe three infrared emitters on the ship, and a kinematic computer algorithm calculates the 6 degrees-of-freedom (6 DOF) data. The accuracy of these measurements are very high, which means that the corresponding velocities are estimated with high precision to render a full state feedback design possible. To facilitate real-time

Figure B.3: A picture of CyberShip II in the command centre of the Marine Cybernetics Laboratory at NTNU.

feedback control of the ship, Opal RT-Lab® is used for rapid prototyping of a desired control structure programmed in Matlab® and Simulink®. For execution of free-running experiments, a LabVIEW® interface has been developed for commanding and monitoring the ship.

Since there is no current or exogenous disturbances in the model basin, the CS2 ship model is

$$M\dot{\nu} + C(\nu)\nu + D(\nu)\nu = Bf_{act}\left(\nu, n, \delta\right) \tag{B.35}$$

where the parameters in M_{RB}, M_A, D_L, $D_{NL}(\nu)$, B, and $f_{act}(\nu, n, \delta)$ must be identified. We choose the following strategy:

1. The matrices M_{RB}, M_A, and B are found from the main particulars of CS2 (weight, mass distribution, lengths, area, volume, etc.)

2. By towing CS2 at different constant surge and sway velocities, with $f_{act} = 0$, and measuring the average towing forces, one can use least square interpolation to find the damping parameters in D_L and $D_{NL}(\nu)$ that are excited by pure surge and sway motions; see Figure B.4.

3. When the damping parameters for pure surge and sway motions are known, the actuator parameters in $f_{act}(\nu, n, \delta)$ are found by repeating the above towing experiments at different thruster revolutions and rudder angles.

4. The remaining parameters are those damping coefficients excited by the yaw rate. Lacking equipment for turning experiments and moment measurements on the towing carriage, we use *adaptive estimation* in free-running adaptive maneuvering experiments to find those remaining parameters.

The parameters in the rigid-body system inertia matrix M_{RB} and the input matrix B are found from straight-forward measurements of the main particulars of the ship, that is, its dimensions, weight, mass distribution, volume, area, and the actuator setup. The zero frequency added mass coefficients in M_A can be found from semi-empirical formulas or simple engineering "rules-of-thumb." For commercial ships, however, strip theory is usually applied (Faltinsen; 1990). This requires a ship geometry computation program that produces a geometry file which is fed into a hydrodynamic computation program based on strip theory. Nevertheless, for CS2 these parameters have all been roughly estimated beforehand by Lindegaard (2003), and their values are given in Table B.1. The ship model used by Lindegaard (2003) was for DP using a linear damping model according to (B.17). Since we seek a nonlinear representation of the damping effects, the DP values cannot be used. The system identification procedure next will therefore consider the damping and actuator coefficients.

The parameters to be identified in the surge direction are $\{X_u, X_{|u|u}, X_{uuu}\}$ and $\{T^+_{|n|n}, T^+_{|n|u}, T^-_{|n|n}, T^-_{|n|u}\}$. Using the towing carriage, CS2 was pulled both forward and backward at different constant speeds, and for each run the average pull force X_{pull} was measured and recorded; see Figure B.4.

Table B.1: Mass-related parameters with respect to CP for CyberShip II

m	23.800	$Y_{\dot{v}}$	-10.0	(l_{xT_1}, l_{yT_1})	(-0.499,-0.078)
I_z	1.760	$Y_{\dot{r}}$	- 0.0	(l_{xT_2}, l_{yT_2})	(-0.499, 0.078)
x_g	0.046	$N_{\dot{v}}$	- 0.0	(l_{xT_3}, l_{yT_3})	(0.466, 0.000)
$X_{\dot{u}}$	- 2.0	$N_{\dot{r}}$	- 1.0	(l_{xR_1}, l_{yR_1})	(-0.549,-0.078)
				(l_{xR_2}, l_{yR_2})	(-0.549, 0.078)

Since $\dot{u} = v = r = 0$, and letting $n_1 = n_2$ at each run, we have for pure surge motion that

$$0 = \begin{cases} X_{pull} + X_{drag} + 2T^{-}_{|n|n} |n_1| n_1 - 2T^{-}_{|n|u} |n_1| u, & n_1 < 0 \\ X_{pull} + X_{drag} + 2T^{+}_{|n|n} |n_1| n_1 - 2T^{+}_{|n|u} |n_1| u, & n_1 \geq 0 \end{cases} \tag{B.36}$$

where $X_{drag} = X_u u + X_{|u|u} |u| u + X_{uuu} u^3$. Setting this up as a linear set of equations, $Ax = b$, where x contains the unknown parameters, A contains the applied speeds u and propeller rps n_1, and b contains the corresponding measured forces X_{pull}, the unknown coefficients are calculated by a least square fit. For $n_1 = n_2 = 0$ then $X_{drag} = -X_{pull}$. Figure B.5 shows these measured forces and the corresponding interpolation. In addition it shows the linear DP curve $X_{drag} = X_u u$ fitted to those measured points that are within the slow speed region $u \in [-0.15, 0.15]$. Clearly, there is a large discrepancy for higher speeds. Having the nominal drag forces for $n_1 = n_2 = 0$, then the same towing experiments are repeated for different propeller revolutions. These were chosen as $n_1 = n_2 \in \{\pm 200, \pm 500, \pm 1000, \pm 2000\}$, and the thrust forces were estimated from $2T_1 = -X_{pull} - X_{drag}$. The result is shown in Figure B.6 where it is observed that for each revolution set-point, the surge speed has very little effect at positive revolutions, while for negative revolutions the slope is higher. Figure B.7 shows how the rudders affect the drag in surge motion at different speeds. This justifies the argument, previously discussed, of not including the the rudder drag force D_i in the actuator model, but rather viewing it as perturbations of the nominal drag coefficients. A robust control design should compensate for this.

The next step is to identify the parameters $\{Y_v,\ Y_{|v|v},\ N_v,\ N_{|v|v}\}$ which can be found from pure sway motion measurements. In this case we have $\dot{v} = u = r = 0$, and the force equation becomes $Y_{pull} + Y_{drag} = 0$ where $Y_{drag} = Y_v v + Y_{|v|v} |v| v$. Force rings are set up according to Figure B.4 to measure the pull forces at both positive and negative sway speeds. The full set of measurements constitutes a set of linear equations that are solved by

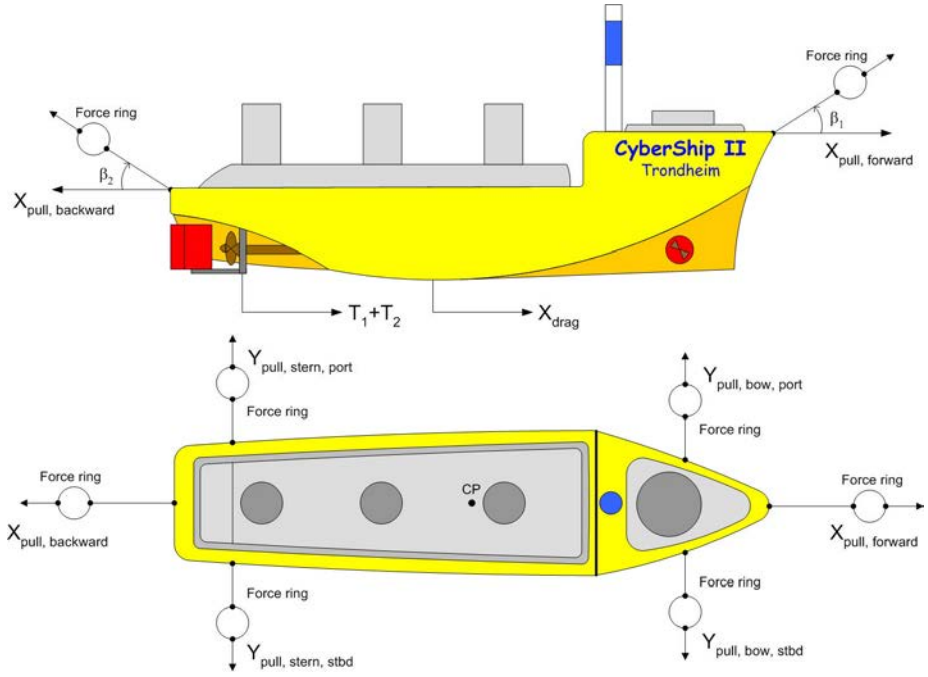

Figure B.4: Two force rings, forward and backward, were applied to measure the drag and propulsion forces when towing CyberShip II longitudinally at different speeds. Four force rings, two port and two starboard, were used to measure the drag force and moment for lateral motion.

least square minimization. These measurements are also used to identify the moment coefficients $\{N_v,\ N_{|v|v}\}$. The moment equation is $N_{pull} + N_{drag} = 0$ where $N_{drag} = N_v v + N_{|v|v}|v|v$. Let the moment arms from CP to the stern and bow measurement points for Y_{pull} be l_{stern} and l_{bow} respectively; see Figure B.4. Then $v > 0 \Rightarrow N_{pull} = Y_{pull,\ bow,\ stbd} \cdot l_{bow} - Y_{pull,\ stern,\ stbd} \cdot l_{stern}$ and $v < 0 \Rightarrow N_{pull} = Y_{pull,\ stern,\ port} \cdot l_{stern} - Y_{pull,\ bow,\ port} \cdot l_{bow}$. The result of this interpolation is shown in Figure B.9.

To identify the rudder lift forces $\{L_\delta^+,\ L_{|\delta|\delta}^+,\ L_\delta^-,\ L_{|\delta|\delta}^-\}$, CS2 is towed forward with $\delta_1 = \delta_2 < 0$ and backward with $\delta_1 = \delta_2 > 0$ for different (equal) rudder angles, and for each run the average force $Y_{pull,\ stern,\ stbd}$ is recorded. The moment equation is $N_{pull} + N_{lift} = 0$ where $N_{lift} = 2\,|l_{xR_1}|\,L_1$ and L_1 is given by (B.32) with $u_{rud} = u$. For these runs, the sideslip angle $\beta = \arctan\frac{v}{u} \approx 0$ such that we can assume that $N_{pull} \approx -Y_{pull,\ stern,\ stbd} \cdot l_{stern}$, that is, not affected by the moment arms from X_{pull}. Separating

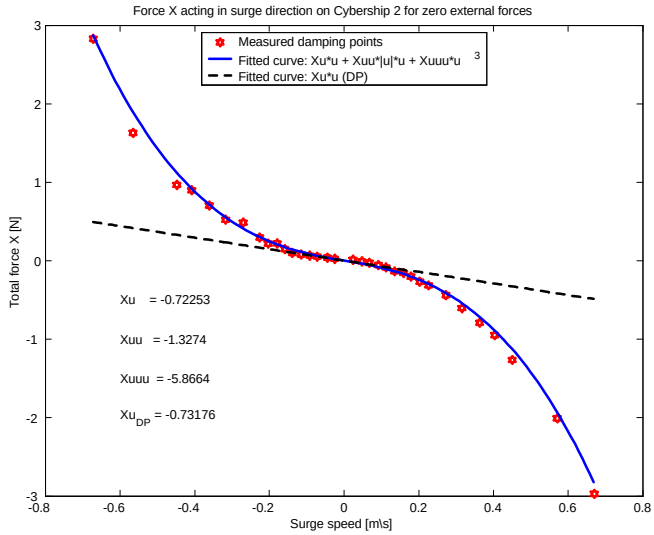

Figure B.5: Measured drag forces of CyberShip II for $n_1 = n_2 = 0$ at different speeds and the corresponding fitted nonlinear curve as well as a linear curve for DP.

positive and negative motion according to (B.32), Figure B.10 shows that the rudders are most effective in forward motion. Finally, we repeat the same experiment for the bow thruster to find the parameter $\{T_{|n_3|n_3}\}$ in (B.27). Unfortunately, the sideslip angle β was rather high in these runs so that hull drag distorted the measurements for higher speeds. Nevertheless, $Y_{pull,\ bow,\ stbd}$ was measured, and since (B.27) is an odd function it is enough to test with negative revolutions for n_3. Figure B.11 shows the measured points and the weighted least square fitted curve.

To sum up, the parameters identified thus far are given in Tables B.1 and B.2.

Since no yaw motion was induced in these towing experiments, the parameters $\{Y_r,\ Y_{|r|v},\ Y_{|v|r},\ Y_{|r|r},\ N_r,\ N_{|r|v},\ N_{|v|r},\ N_{|r|r}\}$ are yet to be identified. We leave these to be estimated in the adaptive maneuvering controller developed and experimentally tested in the next section.

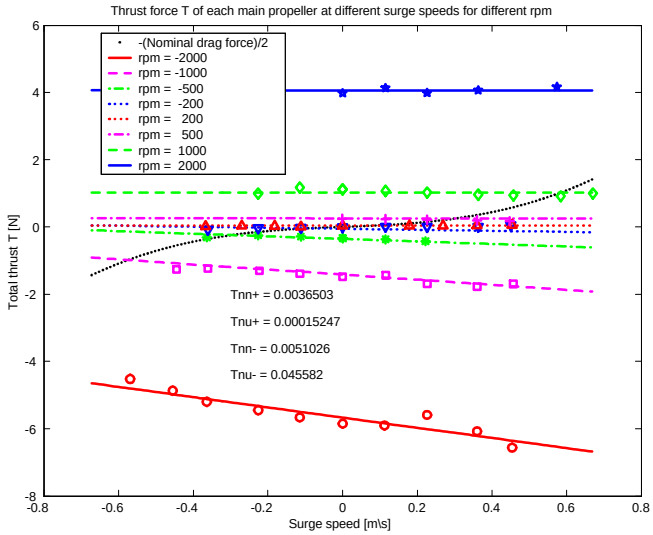

Figure B.6: Measured and interpolated thrust forces $T_1 = T_2$ for different propeller revolutions at different speeds for CyberShip II.

B.3 Adaptive ship maneuvering with experiments

We consider the dynamic ship model (B.1) and (B.35) which for $f = Bf_{act}(\nu, n, \delta)$ can be rewritten in parametric strict feedback form (Krstić et al.; 1995) as

$$\begin{aligned} \dot{\eta} &= R(\psi)\nu \\ M\dot{\nu} &= f - C(\nu)\nu + g(\nu) + \Phi(\nu)\varphi \end{aligned} \tag{B.37}$$

where $g(\nu)$ is the known part of $-D(\nu)\nu$ and

$$\varphi := \left[Y_{|r|v}, Y_r, Y_{|v|r}, Y_{|r|r}, N_{|r|v}, N_r, N_{|v|r}, N_{|r|r}\right]^\top$$

$$\Phi(\nu) := \begin{bmatrix} 0 & 0 & 0 & 0 & 0 & 0 & 0 & 0 \\ |r|\,v & r & |v|\,r & |r|\,r & 0 & 0 & 0 & 0 \\ 0 & 0 & 0 & 0 & |r|\,v & r & |v|\,r & |r|\,r \end{bmatrix}$$

are the vector of unknown parameters and the regressor matrix, respectively, so that $g(\nu)+\Phi(\nu)\varphi = -D(\nu)\nu$. The objective is to design a robust adaptive control law that ensures tracking of $\eta(t)$ to a time-varying reference $\eta_d(t)$ while adapting the parameters φ.

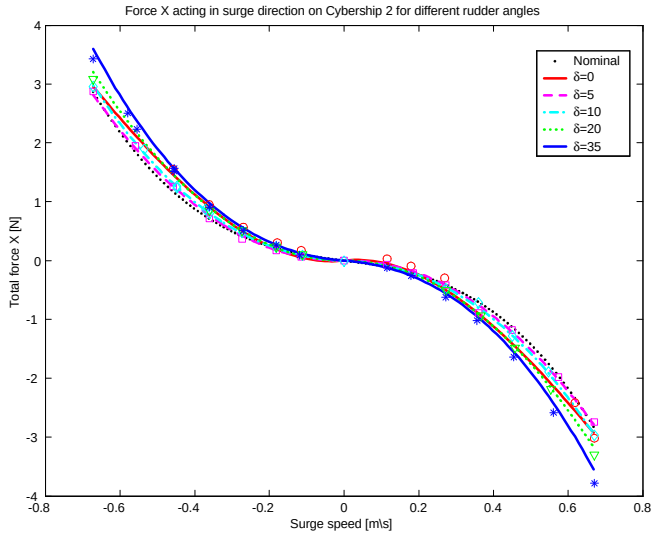

Figure B.7: The measured and curve fitted drag forces for different rudder angles $\delta_1 = \delta_2$ for CyberShip II.

Remark B.1 *Using adaptive tracking to estimate unknown parameters will not in general guarantee convergence to the true values. This is only obtained if the ship model is sufficiently accurate and the inputs to the closed-loop system (references and disturbances) are* persistently exciting *the regressor matrix (Anderson, Bitmead, Johnson, Kokotović, Kosut, Mareels, Praly and Riedle; 1986). Consequently, this step in the parameter identification strategy involves most uncertainty. Nonetheless, the success in the design of a robust tracking control law with subsequent accurate tracking in experiments indicate that* 100% *parameter accuracy of the model is not necessary. Using the obtained (numerical) model with integral action to compensate for the bias b in (B.15) for control design should guarantee success in practical implementations.*

The time-varying reference $\eta_d(t)$ must trace out a *desired path* on the surface as well as satisfying a desired speed specification along the path. Such problems are conveniently solved according to the methodology in Skjetne, Fossen and Kokotović (2004); Skjetne et al. (2005) where the tracking objective is divided into two tasks. Instead of constructing a desired reference $\eta_d(t)$ that contains both the path and speed objectives in one package, one

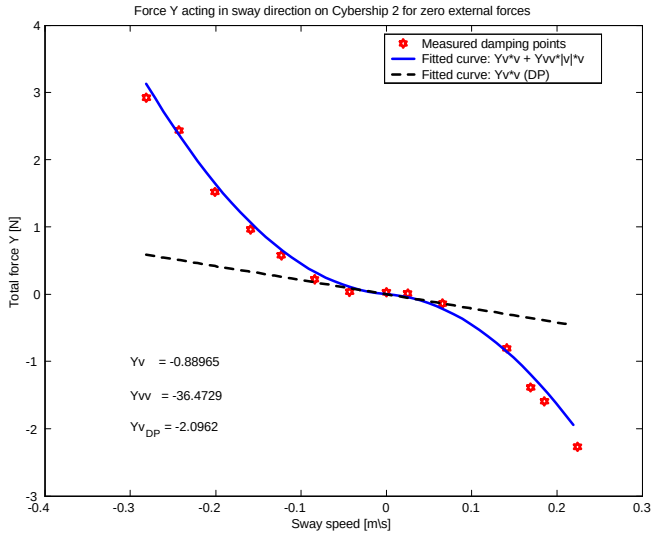

Figure B.8: Measured drag forces in sway motion and the corresponding fitted nonlinear curve as well as a linear curve for DP for CyberShip II.

can keep these objectives separate by solving the *maneuvering problem*.

Using θ as a scalar parametrization variable, we want the desired path to be an ellipsoid with heading along the tangent vector, that is,

$$\eta_d(\theta) = \left[\; x_d(\theta), \quad y_d(\theta), \quad \arctan(\frac{y_d^\theta}{x_d^\theta}) \; \right]^\top \tag{B.38}$$

where $x_d(\theta) = 5 + 4.5\cos(\frac{\pi}{180}\theta)$ and $y_d(\theta) = -0.75 - 2.25\sin(\frac{\pi}{180}\theta)$. For the speed specification, we want the surge speed $u(t)$ to track a desired surge speed $u_d(t)$ which is adjustable online by an operator. This latter objective can be translated into a *speed assignment* for $\dot{\theta}(t)$ by noting the relationship

$$u_d(t) = \sqrt{x_d^\theta(\theta(t))^2 + y_d^\theta(\theta(t))^2}\dot{\theta}(t).$$

The corresponding speed assignment for $\dot{\theta}$ becomes

$$v_s(\theta, t) := \frac{u_d(t)}{\sqrt{x_d^\theta(\theta)^2 + y_d^\theta(\theta)^2}} \tag{B.39}$$

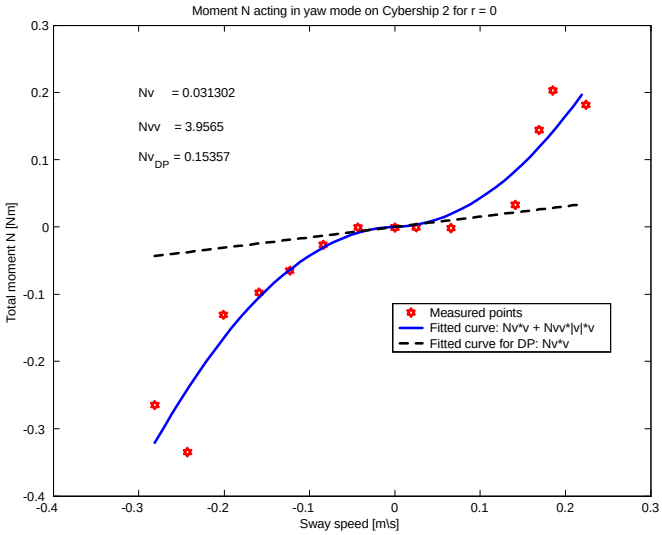

Figure B.9: Measured drag moments in sway motion and the corresponding fitted nonlinear curve as well as a linear curve for DP for CyberShip II.

which has the partial derivatives

$$\begin{aligned} \upsilon_s^{\theta}(\theta,t) &= \frac{-\left[x_d^{\theta}(\theta)x_d^{\theta^2}(\theta)+y_d^{\theta}(\theta)y_d^{\theta^2}(\theta)\right]}{\left[x_d^{\theta}(\theta)^2+y_d^{\theta}(\theta)^2\right]^{3/2}}u_d(t) \\ \upsilon_s^{t}(\theta,t) &= \frac{\dot{u}_d(t)}{\sqrt{x_d^{\theta}(\theta)^2+y_d^{\theta}(\theta)^2}} \end{aligned} \tag{B.40}$$

where $u_d(t)$ and $\dot{u}_d(t)$ are provided online by the operator, for example, by filtering a constant reference u_{REF} through a reference filter.

The control objective is then, according to Skjetne, Fossen and Kokotović (2004); Skjetne et al. (2005), formally stated as a *maneuvering problem*:

1. ***Geometric Task:*** Force the ship position and heading η to converge to and follow the desired path $\eta_d(\theta)$,

$$\lim_{t\to\infty} |\eta(t) - \eta_d(\theta(t))| = 0. \tag{B.41}$$

2. ***Dynamic Task:*** Force the path speed $\dot{\theta}$ to converge to the desired speed assignment $\upsilon_s(\theta,t)$,

$$\lim_{t\to\infty} \left|\dot{\theta}(t) - \upsilon_s(\theta(t),t)\right| = 0. \tag{B.42}$$

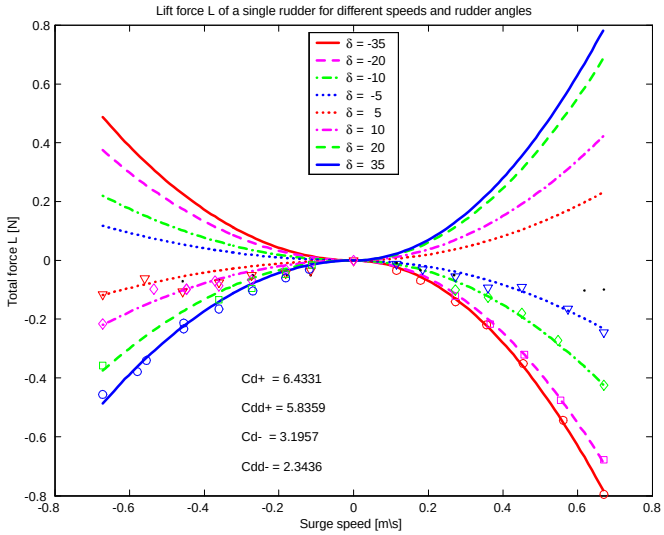

Figure B.10: Curve interpolation to the measured lift forces for the rudders. Notice that CyberShip II generate more lift force in forward motion than backward motion.

Note that the dynamic task can be solved identically by letting $\dot{\theta} = \upsilon_s(\theta, t)$ be a dynamic state in the control law, called a *tracking update law*, which is decoupled from the rest of the dynamics of the ship. Other update laws are also possible based on the results in Skjetne et al. (2005).

The maneuvering control design is based on adaptive backstepping (Krstić et al.; 1995). A complete adaptive design procedure with stability analysis for solving the maneuvering problem is reported in Skjetne et al. (2005) where CS2 is used in a case study. This gives the internal control signals

$$
\begin{aligned}
z_1 &:= R(\psi)^\top \left(\eta - \eta_d\left(\theta\right)\right) \\
z_2 &:= \nu - \alpha_1\left(\eta, \theta, t\right) \\
\alpha_1 &= -K_p z_1 + R(\psi)^\top \eta_d^\theta(\theta)\upsilon_s(\theta, t) \\
\sigma_1 &= -K_p\left(\dot{R}(r)^\top R(\psi) z_1 + \nu\right) + \dot{R}(r)^\top \eta_d^\theta(\theta)\upsilon_s(\theta, t) + R(\psi)^\top \eta_d^\theta(\theta)\upsilon_s^t(\theta, t) \\
\alpha_1^\theta &= -K_p R(\psi)^\top \eta_d^\theta(\theta) + R(\psi)^\top [\eta_d^{\theta^2}(\theta)\upsilon_s(\theta, t) + \eta_d^\theta(\theta)\upsilon_s^\theta(\theta, t)]
\end{aligned}
$$

where the error vector z_1 is rotated to the body-frame for convenience. This means that the controller gains are not dependent on the ship heading (which

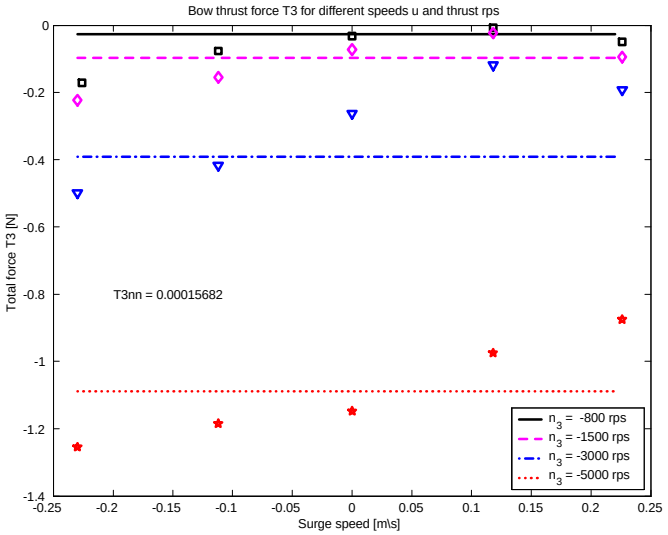

Figure B.11: Measured and interpolated bow thrust force T_3 for forward and backward motion of CyberShip II and different negative propeller revolutions.

is more intuitive since a control technician will himself be located in the body-frame when tuning the gains). The control law, the adaptive update law, and the maneuvering update law are given in Table B.3, where $\hat{\varphi}$ is the parameter estimate, $K_p = K_p^\top > 0$, $K_d = K_d^\top > 0$, and $\Gamma = \Gamma^\top > 0$ are controller gain matrices.

Finding the optimal actuator set-points (n, δ) for each commanded input f in (B.20) is termed control allocation. The simplest approach is to solve an unconstrained least-square optimization problem by using the generalized pseudo-inverse and the inverse functions (B.26), (B.28), and (B.34), that is,

$$(n, \delta) = f_{act}^{-1}\left(\nu, B^\dagger f\right)$$

where $B^\dagger = W^{-1}B^\top\left(BW^{-1}B^\top\right)^{-1}$ is the generalized pseudo-inverse with a weight matrix W (Fossen; 2002, Chapter 7.5). Experience has shown, though, that using the pseudo-inverse does not result in good control allocation when using varying control surfaces such as rudders. A more advanced method is to use constrained optimization techniques. For CS2 this has been developed and reported by Lindegaard and Fossen (2003); Johansen,

Table B.2: Experimentally identified parameters for CyberShip II

X_u	-0.72253	N_v	0.03130	$T^+_{\|n\|n}$	3.65034E-3
$X_{\|u\|u}$	-1.32742	$N_{\|v\|v}$	3.95645	$T^+_{\|n\|u}$	1.52468E-4
X_{uuu}	-5.86643	L^+_δ	6.43306	$T^-_{\|n\|n}$	5.10256E-3
Y_v	-0.88965	$L^+_{\|\delta\|\delta}$	5.83594	$T^-_{\|n\|u}$	4.55822E-2
$Y_{\|v\|v}$	-36.47287	L^-_δ	3.19573	$T_{\|n_3\|n_3}$	1.56822E-4
		$L^-_{\|\delta\|\delta}$	2.34356		

Table B.3: Maneuvering control and guidance system for CyberShip II

Control :

$$\dot{\hat{\varphi}} = \Gamma \Phi(\nu)^\top z_2$$
$$\dot{\theta} = \upsilon_s(\theta, t)$$
$$f = -z_1 - K_d z_2 - g(\nu) - \Phi(\nu)\hat{\varphi} + C(\nu)\alpha_1 + M\sigma_1 + M\alpha_1^\theta \upsilon_s(\theta, t)$$
$$\text{input} = \left\{ \begin{array}{l} (\eta, \nu)\,, \left(\eta_d(\theta), \eta_d^\theta(\theta), \eta_d^{\theta^2}(\theta)\right), \\ \left(\upsilon_s(\theta, t), \upsilon_s^\theta(\theta, t), \upsilon_s^t(\theta, t)\right) \end{array} \right\}$$
$$\text{output} = \{f, \theta\}$$

Guidance :

$$\text{input} = \{\theta, u_d(t), \dot{u}_d(t)\}$$
$$\text{output} = \left\{ \begin{array}{l} \left(\eta_d(\theta), \eta_d^\theta(\theta), \eta_d^{\theta^2}(\theta)\right), \\ \left(\upsilon_s(\theta, t), \upsilon_s^\theta(\theta, t), \upsilon_s^t(\theta, t)\right) \end{array} \right\}$$

Fuglseth, Tøndel and Fossen (2003), where the routine developed by the former authors has been used in these experiments.

For the experiment, the controller settings were $K_p = \text{diag}(0.5,\, 2.0,\, 1.5)$, $K_d = \text{diag}(8,\, 25,\, 18)$, and $\Gamma = \text{diag}(8, 4, 8, 8, 8, 4, 8, 8)$. The initial condition for the parameter update was $\hat{\varphi}(0) = 0$. The ship was first put to rest in dynamic positioning (zero speed) at $\eta_d(0)$, and then the ship was commanded online to move along the path with $u_{REF} = 0.15\,\text{m/s}$ for 22 rounds before we commanded it to come to a stop again. The experiment was conducted on calm water without environmental disturbances (sea state code 0) since we use and wish to estimate zero frequency hydrodynamic parameters.

Figure B.12 shows how CS2 accurately traced the path (in the time interval $t \in [808, 950]\,\text{s}$). In the experiment we experienced problems with

position measurement outages along the upper side of the path. This accounts for the transients at $t \approx 500\,\mathrm{s}$ in the surge speed response seen in Figure B.13. The way the maneuvering problem is posed, accurate path

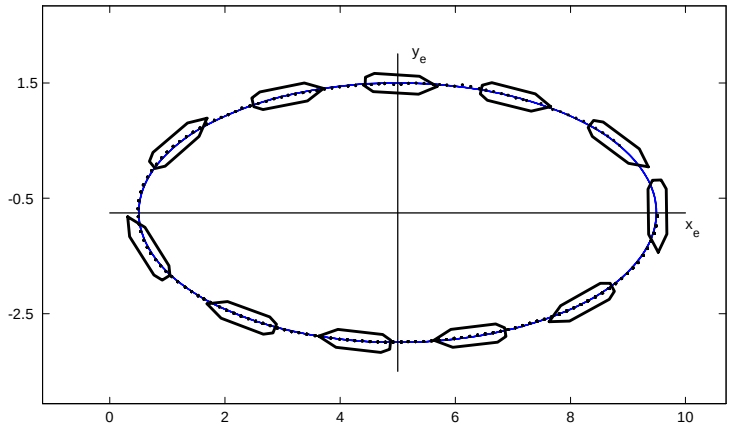

Figure B.12: CyberShip II tracing the desired path.

following has priority over accurate speed tracking. Nevertheless, it is seen in Figure B.13 that CS2 tracks the commanded speed quite well. Figure B.14 shows the adaptive parameter estimates of $\hat{\varphi}(t)$. We observe a rapid change and a subsequent slow convergence to new values. We believe those values are close to the true values for the nominal surge speed $u \approx 0.15\,\mathrm{m/s}$ and moving along this ellipsoidal path. It is likely that the parameter convergence will be different for different paths and speeds. Nonetheless, we adopt these values as approximate values for the remaining parameters in the maneuvering model for CS2; see Table B.4.

Table B.4: Adaptively estimated parameters for CyberShip II

$Y_{\|r\|v}$	-0.805	$N_{\|r\|v}$	0.130
Y_r	-7.250	N_r	-1.900
$Y_{\|v\|r}$	-0.845	$N_{\|v\|r}$	0.080
$Y_{\|r\|r}$	-3.450	$N_{\|r\|r}$	-0.750

This robust adaptive maneuvering design with experiments also illustrates that 100% numerically correct values for the hydrodynamic parameters are not necessary to achieve accurate tracing of the path. Table B.5

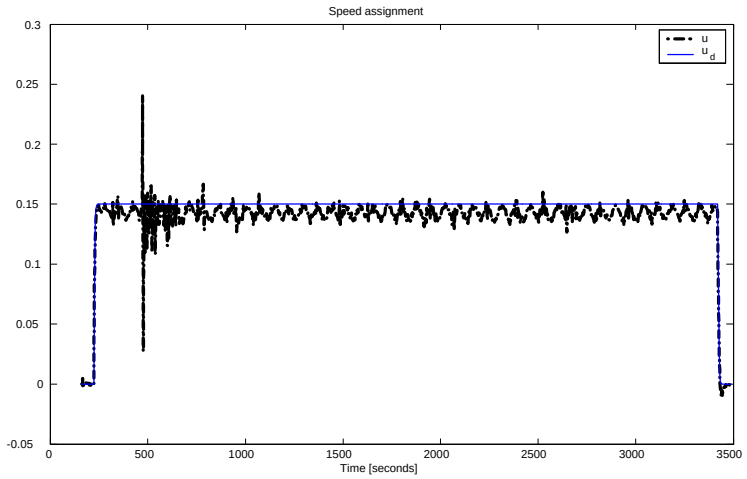

Figure B.13: The desired and actual surge speed of CyberShip II for the full experiment. Notice the discrepancies around $t \approx 500\,\mathrm{s}$ which resulted from position measurement outages.

shows the standard deviations of the error signals in z_1. The most important variable for path keeping is z_{12} since this is an approximate measure of the cross-track error (provided the ship is pointed along the path, $z_{13} \approx 0$). An accuracy of 2.26 cm is 7.8% of the ship breadth and acceptable. This corresponds to an accuracy of 1.58 m for the full scale ship having a breadth of 20.3 m.

Table B.5: Standard deviations for CyberShip II in the free-running maneuvering experiment.

$u_d[\,\mathrm{m/s}]$	$z_{11}[\,\mathrm{m}]$	$z_{12}[\,\mathrm{m}]$	$z_{13}[\mathrm{deg}]$	$u - u_d[\,\mathrm{m/s}]$
0.15	0.0350	0.0226	2.623	0.0080

B.4 Conclusion

We have presented a modeling, identification, and control design for the task of maneuvering a ship along desired paths. The identification and adaptive maneuvering procedure with experiments have provided numerical values

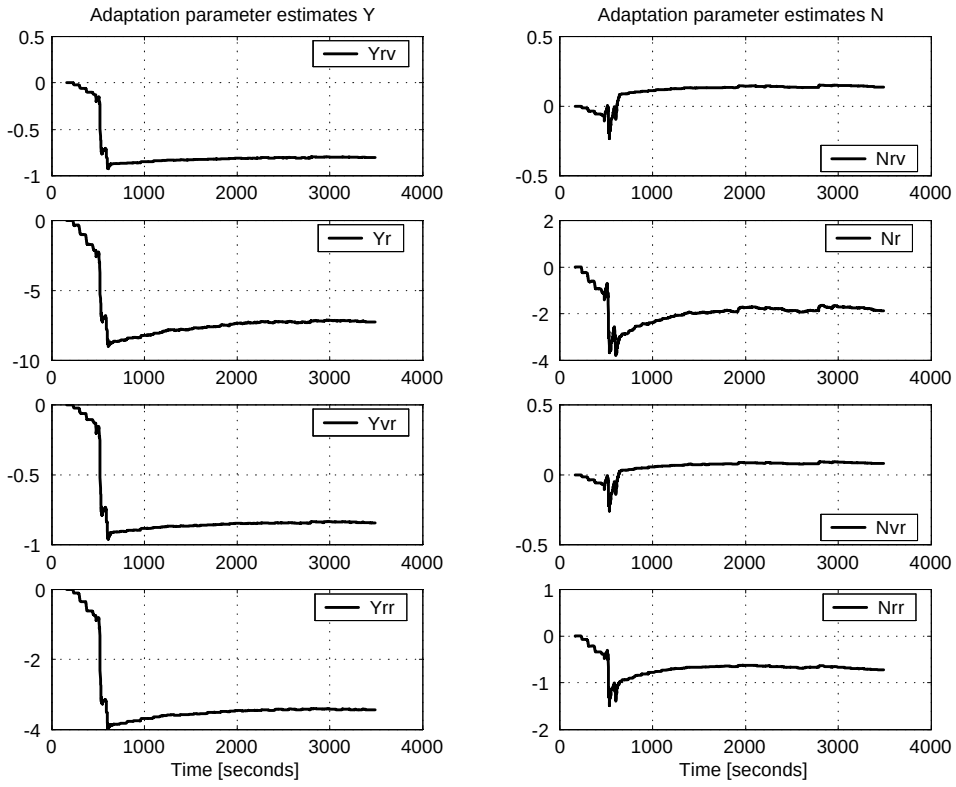

Figure B.14: Adaptive parameter estimates $\hat{\varphi}(t)$ in the free-running CyberShip II maneuvering experiment.

for all parameters in the nonlinear ship model for CyberShip II. It was the intention of the authors to quantify such a model and share it with the marine control research community for use in simulations and case studies. Material from a rich variety of references have been used to describe the model, its difficulties and possible simplifications.

System identification procedures, using a towing carriage in the Marine Cybernetics Laboratory in Trondheim, Norway, were performed where the model ship CyberShip II was towed at many different velocities and the average towing forces were recorded. For zero acceleration and zero input forces these measurements are directly related to the drag of the ship hull. These measurements were accurately fitted to a nonlinear damping model of the ship for pure surge and sway motions. Knowing these nominal mod-

els, the same towing tests were repeated, with the thrusters and rudders activated, to find the actuator models. After these tests, eight damping parameters related to the yaw rate of the ship were still unknown. To find these, an adaptive maneuvering control law was implemented and experimentally tested. The estimates of the unknown parameters in this experiment were assumed to be close to the true values and therefore adopted as the remaining numerical values.

In summary, this design with experimental testing has provided a complete maneuvering model with numerical values for CyberShip II. The accuracy of the obtained parameters are believed to be close to the true values (as far as this is possible to quantify for a nonlinear ship model that still is a mere simplification of the real world). Nonetheless, the free-running maneuvering experiment using a robust adaptive control law showed that accurate maneuvering along desired paths is very much achievable in presence of modeling uncertainties and exogenous disturbances.